UNIVERSITY OF MESSINA
Department of Chemical, Biological, Pharmaceutical and Environmental Sciences
Doctorate School in Chemical Sciences (*XXXII* cycle)
S.S.D. CHIM/08

Design, synthesis and biological evaluation of novel inhibitors of human and protozoan proteases

PhD Thesis of:
Santina Maiorana

Supervisor:
Prof. Maria ZAPPALÀ

Co-Supervisor:
Prof. Roberta ETTARI

PhD Coordinator:
Prof. Paola DUGO

2018/19 ACADEMIC YEAR

CONTENTS

1. AIM OF THE RESEARCH

1.1 The importance of proteases as drug targets

Proteases represent one of the most relevant group of enzymes. They catalyze the hydrolysis of peptide bonds and they are classified into endopeptidases, which cleave internal peptide bonds, and exopeptidases, which break terminal peptide bonds. Exopeptidases are further subclassified into aminopeptidases and carboxypeptidases. Based on the nature of their active sites, proteases are also divided in five main classes: aspartic, cysteine, serine and threonine proteases and metalloproteases.[1]

Proteases play many important roles in several key pathways, thus representing potential drug targets for the treatment of various diseases.

Many protease inhibitors for the treatment of several diseases are already commercially available. As a few examples, captopril (Capoten ®) targets the angiotensin-converting enzyme for the treatment of hypertension; saquanivir (Invirase ®) has been developed to act on the HIV proteases for the treatment of HIV; Bortezomib (Velcade ®) has been proven to be effective on multiple myeloma by inhibiting a proteolytic complex named proteasome; Denosumab (Prolia ®) targets the cathepsin K as therapeutic approach for the treatment of osteoporosis. Many other new protease inhibitors are in currently in the early stage of the clinical trials for the treatment of several diseases.

The key aspect of a protease is the ability to identify and to cleave its substrate in a specific way, thus also a protease inhibitor must possess specific structural features to accommodate into the protease binding pockets.

The challenge to develop novel drugs for new protease targets has revealed particular issues concerning the target selectivity, which is essential for the design of new inhibitors. The general approach to develop a specific inhibitor is to create a special motif to block the active site; generally a small molecule. Mostly, novel inhibitors have been discovered on the basis of the structure of known protease substrates. Many non-peptide or peptide-based inhibitors have been developed to date in literature, however a promising challenge is the development of peptidomimetics, which with respect to peptide-based inhibitors can lead an improvement of pharmacokinetic (i.e. metabolic stability) and pharmacodynamic properties (i.e. possibility to lock a defined conformation of the peptide, able to interact with the target enzyme in a specific way).

The design of novel protease inhibitors has made progress over the last years and currently, there are two major strategies to design new promising inhibitors. The first involves a fast screening (HTS, high-throughput screening) of libraries of small molecules already on hand or newly synthesized. Several interesting inhibitor structures have been discovered with this approach, but such screenings frequently reveals a number of uninteresting compounds that demonstrate to be nonspecific, thus being alkylating or oxidizing agents.

The second major approach to design novel inhibitors is the structure-based drug design made on the basis of X-ray crystallography.[2,3] Structural information are frequently used by medicinal chemists in order to improve their lead compounds.

A significant difference between inhibitors is also based on the mechanism of action.

An irreversible inhibition is normally desirable in the case of parasitic proteases, on the contrary in the case of human proteases it is more convenient to develop a reversible inhibitor to avoid undesidered or off-targets effects.

Selectively targeting critical protease of infectious organisms (e.g., viruses, bacteria and protozoa) is fundamental for the development of chemotherapeutic drugs as well as the selective inhibition of dysregulated human proteases can be fundamental in other disease.[4]

1.2 Development of immunoproteasome inhibitors

The development of immunoproteasome-selective inhibitors represents a promising strategy for the treatment of various diseases such as hematologic malignancies, autoimmune or inflammatory diseases; within this context, the main research goal of my PhD work was focused on the design, synthesis, and biological evaluation of a series of amide derivatives acting as immunoproteasome inhibitors. The compounds were designed to act as noncovalent inhibitors, thus being a promising therapeutic strategy because of the lack of all the drawbacks associated to the irreversible inhibition.

The 20S proteasome is the major non-lysosomal proteolytic system in eukaryotic cells that is involved in the degradation of many proteins. The 20S catalytic core of 26S proteasome shows a barrel-like structure, with the two outer and the two inner rings composed of seven different α and β subunits, respectively. The caspase-like (C-L),

trypsin-like (T-L) and chymotrypsin-like (ChT-L) activities of the proteasome are located into the catalytic subunits β1c, β2c and β5c, respectively.[5] In addition to the constitutive proteasome (cCP), vertebrates express a specialized form of proteasome, named immunoproteasome (iCP) which is mainly present in lymphocytes and monocytes. An increase of IFN-γ and TNF-α is reflected into the replacement of the β1c, β2c, and β5c subunits with the immuno-subunits β1i, β2i, and β5i, respectively (Fig.1).[6]

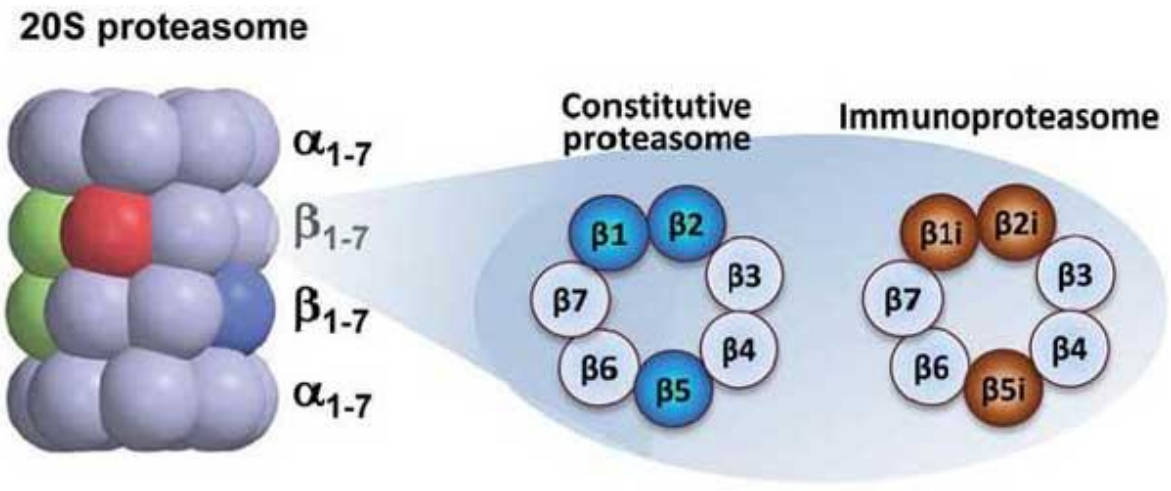

Figure 1. Structure of constitutive and immuno-proteasomes.

While the substrate preference of β5i and β2i subunits are comparable with their cCP analogues, the β1i subunit shows a remarkable chymotrypsin-like activity, while the caspase-like activity is reduced to background levels.[7] The expression of immunoproteasome is associated with a wide range of inflammatory diseases, such as Crohn's disease, inflammatory bowel and ulcerative diseases or autoimmune diseases like rheumatoid arthritis or systemic lupus erythematosus.[6]

The activity of immunoproteasome is also overexpressed in neoplastic diseases, including multiple myeloma (MM), hence targeting iCPs could be a very promising strategy for the treatment of these hematologic malignancies.[8-10]

Within this context, several efforts have been spent over the last decades to generate noncovalent proteasome/immunoproteasome inhibitors of β5i and/or β1i subunits.

In this scenario, the research group with whom I worked during my PhD has been actively involved in the development of novel 20S proteasome inhibitors; in particular, a series of amides[11-13] were identified, some of which inhibited the ChT-L activity of 20S

proteasome with K_i values in the submicromolar range. Docking studies allowed us to show the noncovalent binding mode of the most active inhibitors by simulations into the yeast 20S proteasome crystal structure.

In order to design novel immunoproteasome inhibitors, we decided to firstly screen several amide derivatives, already synthesized in our laboratories, against the three immuno-subunits, to identify active compounds. Among the tested compounds, *N*-benzyl-2-(2-oxopyridin-1(2*H*)-yl)acetamide (**1**) showed a relevant result, selectively inhibiting the β1i subunit with a K_i of 2.23 μM. Therefore, compound **1** was selected as hit compound to design a panel of derivatives characterized by structural variations at the *N*-substituent and at the methylene linker between the pyridone scaffold and the amide function (Fig. 2).[14]

Pyridones are often introduced as peptidomimetic scaffolds in the backbone of protease inhibitors, including cysteine or serine proteases, being a suitable surrogate for a portion of the peptide or a convenient strategy to lock a defined conformation of the peptide.[15-17]

The amide group was functionalized with hydrophobic aliphatic or aromatic substituents (compounds **2-5**), in agreement to the structural features required for the accommodation intothe S1 pockets of β1i and β5i subunits that are large and hydrophobic, whereas the 2-pyridone at the P3 site was kept unchanged due to the nature of S3 subsite that is small and polar.[9]

The glycine at P2 was replaced with a β-alanine homologue (compounds **6-11**), to evaluate if a longer distance between the amide portion and the pyridone scaffold could allow a better accommodation of these moieties into S1 and S3 pocket, respectively. The glycine residue at the P2 site was also replaced with a phenylalanine (Phe) (compounds **12-18**), or with the homologous homophenylalanine (HPhe) (compounds **19-25**), in order to explore the size of the S2 pocket of the catalytic site of the immuno-subunits.

With regard to the stereochemistry, precursors **12-25** have been developed in homochiral form with *S* absolute configuration, which appears to be the most suitable one. Noteworthy, the designed compounds lack of the electrophilic warhead and act as non-covalent proteasome inhibitors that, with respect to covalent inhibitors, might be a promising alternative to use in therapy, because of the lack of all drawbacks and side effects related to irreversible inhibition.[18]

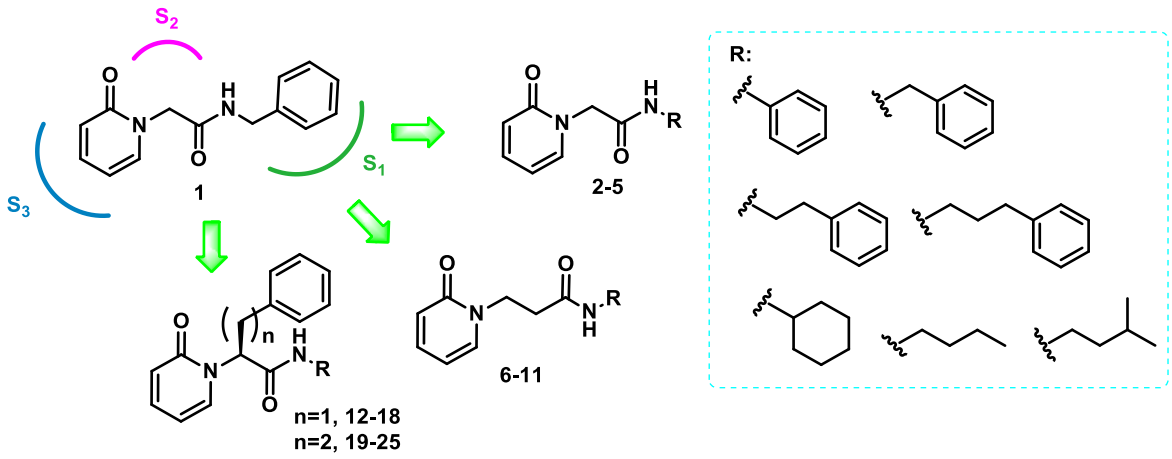

Figure 2. Design of novel immunoproteasome inhibitors.

Another compound (i.e. compounds **26**) was selected as lead compound to design a second series of amide derivatives as selective-immunoproteasome inhibitors The optimization of the lead compound **26**, inhibitor of the ChT-L (β5c, K_i=0.56 μM) proteasome activity, consisted in the replacement of the naphtyridinone scaffold at the P3 site with a 6,7-dimethoxyisoquinolin-1(2*H*)-one scaffold, chosen considering the strong preference of immunoproteasome core-particles for polar groups at the P3 site. Further modifications have been examined on the *N*-terminal group in terms of size with the aim to improve the binding affinity to the immune-core particles of the new inhibitors. On this regard, the amide group was *N*-alkyl or *N*-aryl substituted, in agreement to the strong preference of the immunoproteasome for bulky hydrophobic groups at the P1 site (compounds **27-33**).

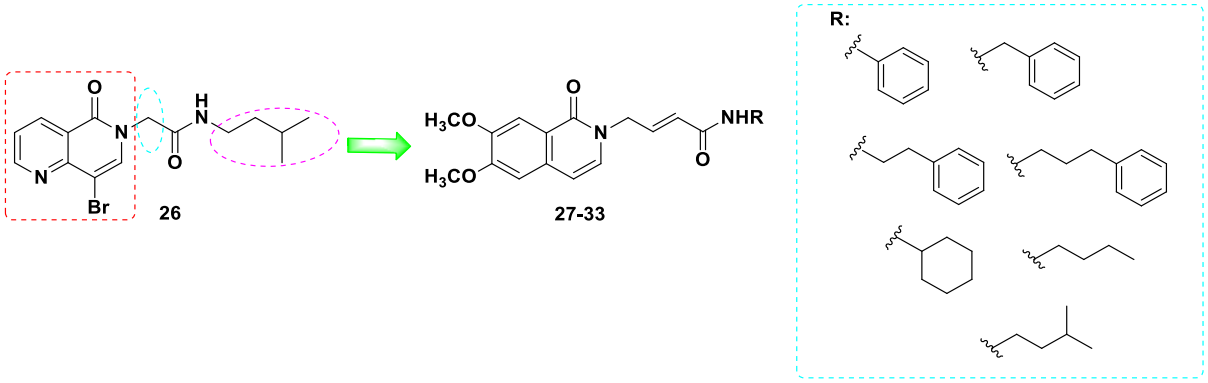

Figure 3. Design of novel immunoproteasome inhibitors.

An additional rigidification of the structure has been obtained by the introduction of an insaturated spacer that, could be responsible of an irreversible inhibition of the target, thus acting as Michael acceptor.

1.3 Development of rhodesain inhibitors

Human African Trypanosomiasis (HAT, also known as sleeping sickness) is an endemic parasitic disease, which affects more than 30 countries in sub-Saharan Africa, where it represents a significant cause of morbidity and mortality, mainly in the rural areas, despite the significant decrease in the number of new reported cases over the last years.[19]

HAT is caused by two species of *Trypanosoma*: *T. brucei gambiense*, widespread in central and western Africa, responsible for a chronic form of the disease, and *T. brucei rhodesiense,* the most common subspecies in southern and eastern Africa, which causes a rapid-onset acute form of HAT, with a higher mortality rate.[20]

The disease is spread by the bite of the tsetse flies of the *Glossina* genus and clinically developes in two main stages. The first stage, or hemolymphatic stage, is characterized by fever, shaking chills, muscle aches and fatigue and it persists for weeks or months; if untreated, can evolve into the second stage, during which the protozoan invades the central nervous system, inducing neurological symptoms, sleep disorders, coma and eventually death.[21]

Due to the turnover of the variant surface glycoproteins (VSGs) of the Trypanosoma coat,[22] which induces a high degree of antigenic variations, the preparation of an appropriate vaccine has not been possible yet. Therefore, chemotherapy is the only way

to control the infection; at the moment, there are five drugs available for HAT treatment: suramin and pentamidine, effective during the stage 1 since they are not able to cross the blood-brain barrier (BBB); melarsoprol, eflornithine and nifurtimox, which are active during the stage 2. However, melarsoprol causes encephalopathy in 5-10% of treated patients while eflornithine, although less toxic is effective only against *T. b. gambiense*.[23] The combination of eflornithine and nifurtimox, represents the first-line treatment of the second-stage of the *gambiense* trypanosomiasis.[24] More recently, in 2018, also fexinadazole, has been approved for the treatment of gambiense trypanosomiasis. As a consequence, there is an urgent need to identify new targets for HAT treatment.

Within this context, rhodesain, a Clan CA, family C1 (papain-family) cathepsin L-like cysteine protease of *T. brucei rhodesiense*, represents one of the most valuable targets for the development novel anti-HAT drugs.[25-26] The importance of rhodesain is due to its several functions: it is required to cross the BBB, thus inducing the neurological stage of HAT,[27] it is involved in the turnover of the trypanosome VSGs,[28] which form a densely packed coat surrounding the parasite. In addition, rhodesain causes the degradation of host anti-VSG immunoglobulins, which contributes to reducing the host immune system reaction.[29] Lastly, rhodesain also takes part in the degradation of protozoan proteins and intracellularly transported host proteins within the lysosomes.[30] All these functions clearly highlight the relevance of rhodesain both for *Trypanosoma* survival and at the same time for the progression of the disease in the patients.

During the last period of my PhD, I focused my research activity on the optimization of the high reactive vinyl ketone **3** which was previously identified as a potent rhodesain inhibitor of *T. b. rhodesiense*, with a k_{2nd} value of 67000·x 10^3 M^{-1} min^{-1} coupled with a potent binding affinity (K_i = 38 pM).[31]

Based on the structure of the lead compound **3**, we designed a new series of Michael acceptors (Fig. 4). Herein, the highly reactive vinyl ketone warhead and the HPhe at the P1 site were kept unchanged. The HPhe moiety at the P1 position assures resistance towards endopeptidases, leading to a greater stability *in vivo* with respect to the corresponding analogs bearing a natural amino acid side chain at P1.[32] We then decided to replace the Cbz group with some benzo-fused rings (i.e. **35-37**), one of which is the 2,3-dihydrobenzo[*b*][1,4]dioxine moiety, present in potent rhodesain inhibitors. A panel of aromatic moieties, variously decorated with halogen atoms (i.e. **38-45**), were also

introduced at the P3 site, in agreement to the structure of peptidic inhibitors bearing at the P3 site 3,5-difluoro- or 4-CF_3-phenyl moieties or taking into consideration non peptide rhodesain inhibitors based on a triazine nucleus variously decorated with halogen–substituted aromatic nuclei. This approach could also allow us to investigate the size of S3 pocket and to concurrently allow for the formation of halogen bonds and/or hydrophobic interactions. We also investigated the relevance of the L-Phe residue at the P2 site, by synthesizing the L-cyclohexylalanine, 4-F-L-phenylalanine and 4-methyl-L-phenylalanine derivatives. Cyclohexyl residues at the P2 position have been described in inhibitors of human protease that show some improvment of the binding or of metabolic stability;[33] 4-Me-L-Phe P2 substituent should afford highly rhodesain selective inhibitors according to a previous study [32] that suggest, moreover, that the introduction of small substituents on the phenyl ring of the P2 side chain could represent a good strategy for the design of novel rhodesain-selective inhibitors.

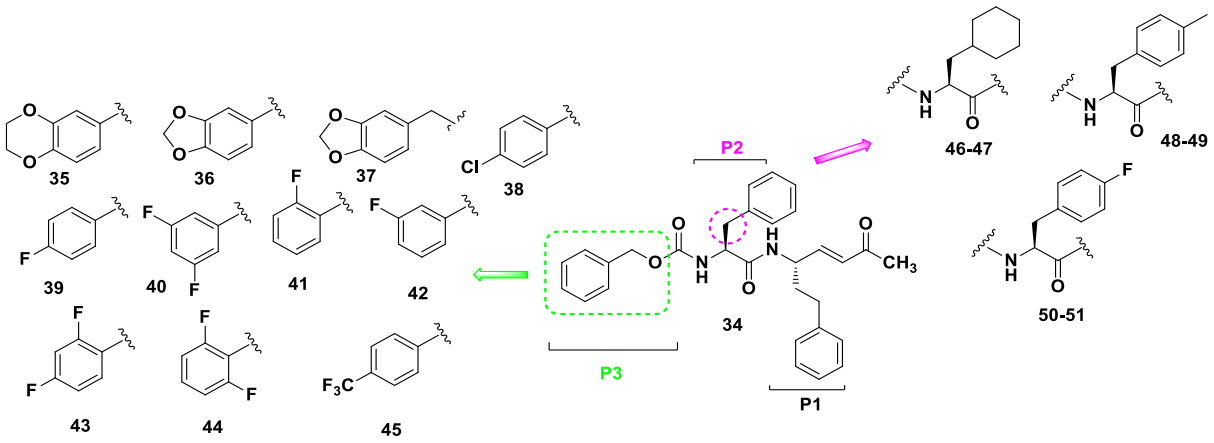

Figure 4. Design of novel rhodesain inhibitors.

2. DESIGN AND SYNTHESIS OF NOVEL AMIDES AS NONCOVALENT IMMUNOPROTEASOME INHIBITORS

2.1 Introduction

The ubiquitin-proteasome system (UPS) is the major non-lysosomal proteolytic pathway, which plays a fundamental role in the turnover of intracellular protein of eukaryotic cells, thus being responsible for cells' homeostasis. This role is absolved by the degradation of misfolded or aberrant proteins, which are no longer useful to the cells.[34-35] Proteolysis, mediated by the proteasome, is a complex process which includes several steps: in the first step, ATP-dependent, proteins are first targeted to be recognizable for the degradation by the addition of polyubiquitin chains to a residue of lysine of the substrate; in the second step, the polyubiquitinated proteins are processed by 26S proteasome into ubiquitin and short peptides (Fig. 5).[35-36] In particular, the ubiquitin-activating enzyme E1 catalyzes the activation of the ubiquitin through the formation of a thioester bond. This process needs the presence of ATP and occurs through the formation of ubiquitin-AMP intermediate and ubiquitin-E1 thiol ester is the final product.[37] After this, ubiquitin is transferred, via thioester bond, to the ubiquitin-conjugating enzyme E2, which adds ubiquitin to the lysine residue of either the target protein or the elongating polyubiquitin chain, with the help of the ubiquitin-ligase enzyme E3.

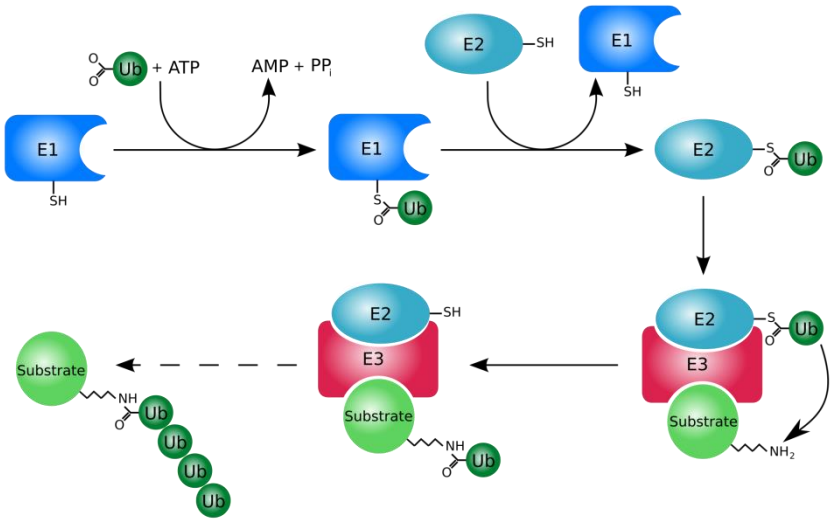

Figure 5. Schematic representation of the ubiquitination process.

In normal cells, the main function of the proteasome is to regulate different cellular functions, such as cell cycle regulation, cell differentiation and apoptosis, immune

surveillance.[38-39] In addition to the constitutive proteasome, eukaryotic cells express other two variants of proteasome: immunoproteasome, mainly expressed in monocytes and lymphocytes, and thymoproteasome, expressed by thymic cortical epithelial cells.[36,40]

2.2 Constitutive proteasome

The constitutive 26S proteasome (Fig. 6) is a multi-protease complex which includes a barrel-like 20S core particle (CP), covered by two 19S regulatory caps.[5] Each 19S cap is composed by a lid and a base: the lid is responsible for the recognition and the binding of the polyubiquitin chains, while the base includes ATPases that allow the entrance of substrates into the proteolytic 20S core.[41]

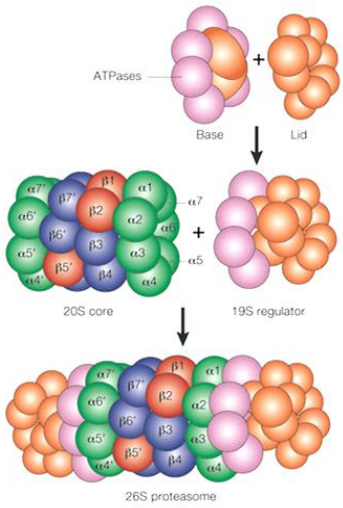

Figure 6. Proteasome structure

The central catalytic 20S CP is characterized by four stacked rings: two outer α-rings and two inner β-rings, which contain different α subunits (α1-α7) and different β subunits (β1-β7), respectively.[42] The β-rings contain the three proteolytic activity located in three subunits, endowed with different substrate specificities: the β1 subunit, also known as "post-glutamate peptide hydrolase" (PGPH) or "caspase-like" (C-L), which cleaves after acidic residues; the β2 subunit, which holds a "trypsin-like" (T-L) activity and cleaves after basic residues; lastly, the β5 subunit is responsible for the "chymotrypsin-like" (ChT-L) activity and cleaves after hydrophobic residues.[43-44]

S1 pockets, which are the closest ones to the active site, have the major influence upon the different substrate specificity of the proteasome catalytic subunits (Fig. 7).[5,45,46] The β1 subunit exhibits an Arg45 residue which preferably interacts with a Glu residue at P1 position of the protein substrate, thus conferring the post-glutamyl peptidyl hydrolase activity to this subunit. Similarly, the low steric hindrance of *β*2-Gly45 allows the formation of a large binding pocket with a Glu residue (Glu53) at the bottom, which accepts bulky basic P1 residues. Finally, the *β*5-Met45 generates a wide pocket which allows the accomodation of bulky hydrophobic P1 residues.

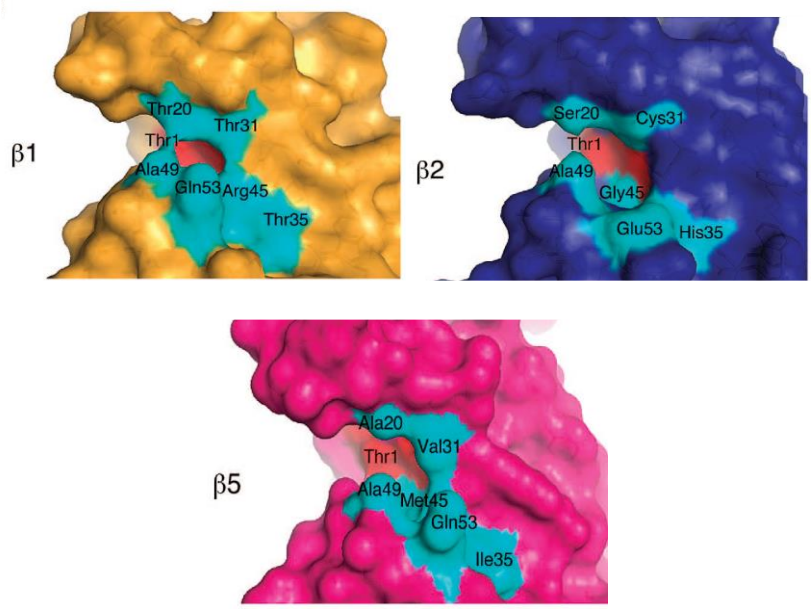

Figure 7. S1 pockets of the catalytic subunits binding sites.[5]

Each active site of the proteasome shows a γ-OH of a *N*-terminal threonine residue acting as nucleophile, crucial for the hydrolytic activity and peptide bond cleavage.[5,47] In particular, the β5 subunit is mainly involved in protein degradation and is thus considered a main target for the development of anticancer agents.

The immunoproteasome and the thymoproteasome originate by the replacement of the three constitutive catalytic subunits (β1c, β2c, β5c) with the three inducible low-molecular-mass protein (LMP) subunits (β1i; β2i; β5i/β5t) (Fig. 8).[40,48]

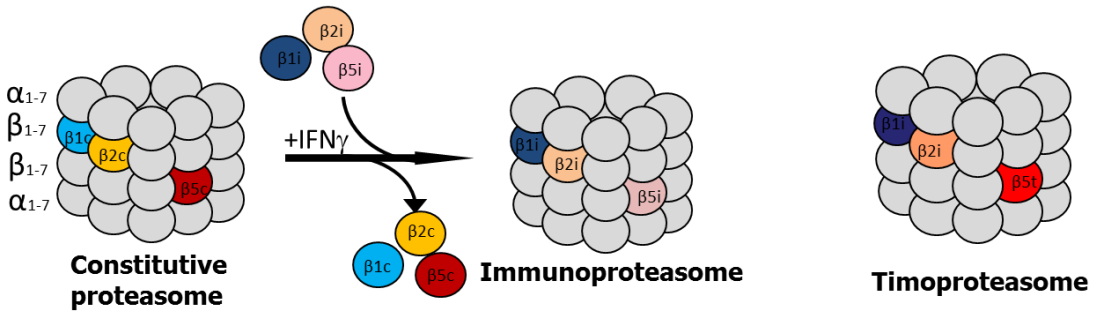

Figure 8. Different forms of proteasome.

2.3 Immunoproteasome

The immunoproteasome, mainly expressed by monocytes and lymphocytes, is responsible for cell-mediated immunity and for the generation of MHC (Major Histocompatibility Complex) class I ligands.[40,49] The thymoproteasome, expressed by thymic cortical epithelial cells, is instead involved in CD8+ T cells positive selection.[48,50] The expression of immunoproteasome is inducible in many tissues; in fact, it has been also detected in various cell types, not only in immune cells, under the stimuli of cytokines, such as INF-γ or TNF-α. The replacement of the catalytic subunits with the correspondent immune subunits leads to the formation of the 20S iCP. [51] The 20S iCP contains the LMP2/β1i and LMP7/β5i subunits, which are upregulated as a consequence to the IFN-γ,[52] and the MECL-1/β2i subunit, which is a multicatalytic endopeptidase complex.[53] While MECL-1 and LMP7 shows the same type of activities of their counterparts, the LMP2 subunit express a remarkable ChT-L activity, cleaving peptides after hydrophobic residues.

This change of activity is considered an essential requirement for the specific function of epitope generation for antigen presentation. In fact, peptides generated by the hydrolase activity of LMP2 are endowed with non-polar amino acids, which represents a perfect motif for binding to the MHC class I molecules.

A comparison between the S1 pockets of β5c and β5i subunits shows that the residues responsible for the ChT-L activity (Ala20, Met45, and Cys52) are maintained, while the amino acid 31 of β5i changes in terms of size (Met31 which replaces Val31), retaining the hydrophobic feature. However, a different conformation of Met45 allow the

formation of a larger S1 pocket, which is also stabilized by van der Waals interactions with the aliphatic side chains of the amino acid Gln53.[6]

In the end, the S1 pocket of β5c mainly accommodates peptides with small amino acids (Ala or Val), whereas the S1 pocket of β5i well accommodates large non-polar residues (Tyr, Trp, Phe). Therefore, β5c and β5i cleave different fluorogenic substrates Ac-WLA-AMC and Ac-ANW-AMC respectively.

Other differences were also observed between β1c and β1i: the substitutions T20V, T31F, R45L and T52A cause the enhancement of the hydrophobicity of β1i S1 pocket, but results in a reduction of dimension. Therefore, peptide hydrolysis occurs after small hydrophobic residues. On the contrary, in the S3 site of β1i subunit, the substitutions T22A and A27V generally downsize and polarize the S3 pocket. To summarize, a β5i-selective inhibitor requires bulky hydrophobic amino acids, like Trp or Phe, at the P1 site and small polar groups at the P3, while a β1i-selective inhibitor should be endowed with branched non-polar amino acids in P1 and small polar amino acids at the P3.[6,7]

Lastly subunit β2i is the only one not encoded on MHC cluster and it was found to be identical to β2c with the sole replacement of Asp53 (β2c) with Glu (β2i).

In spite of the presence of the *N*-terminal nucleophilic threonine residue in all the active sites, the preference cleavage for the various proteolytic subunits is due to the structure of substrate binding pockets. Based on the proximity to the active sites, the binding pockets are termed: nonprimed sites (S1, S2, S3,... Sn), located on the left of the scissile peptide bond; primed sites (S1', S2' S3',... Sn'), located on the right. As a consequence, substrate residues which interact with these binding pockets are named as P1, P2, P3,... Pn sites and P1', P2', P3',... Pn' sites, respectively (Figure 9).[34]

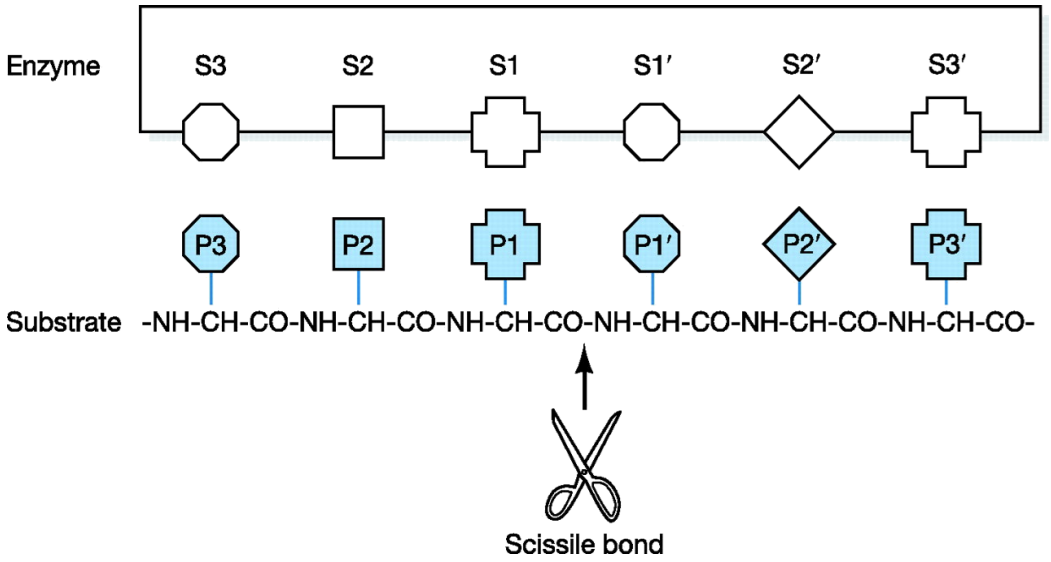

Figure 9. Peptide orientation (from *N*-terminus, to the *C*-terminus), in the active centre of β-subunits.

2.4 The role of immunoproteasome in human diseases

As stated before, under the stimuli of interferon-γ (IFN-γ), β1i/LMP2, β2i/MECL-1, and β5i/LMP7 are incorporated into the iCPs. Among the subunits, the β1i and β5i play a key role in antigen processing.[54] The immunoproteasome is also normally expressed in several non-immune tissues, thus his role is not only limited to MHC class I presentation.[55]

It was elucidated that the immunoproteasome is involved in protein homeostasis regulation, cell proliferation and differentiation, cytokine expression, being involved in many biological and pathological processes.[55]

The development of iCPs selective inhibitors is considered a valuable approach to investigate the biological role of each subunit and, at the same time, to treat the same pathologies in which the subunit is involved.

Immunoproteasome is mainly involved in inflammatory, autoimmune diseases and hematologic malignancies.

Since the inflammatory cytokines play a key role in the expression of the immunoproteasome, the role of the multicatalytic complex in inflammatory and autoimmune diseases has been widely explored.

High levels of immunoproteasomes were detected in a large number of autoimmune and inflammatory diseases such as Crohn's disease, [56] ulcerative colitis,[57] inflammatory bowel disease[58-59] and hepatitis. In Crohn's disease, an increased expression of the immunosubunits was observed; in particular, the replacement of the constitutive proteasome subunit β1 by the inducible immunosubunit β1i was noticed.[56] Also in the inflammatory bowel disease, an increased level of LMP2/β1i in the inflamed colon tissues, with respect to normal tissues, was detected.[59]

Many studies were also carried out on experimental models of colitis, thus assessing the involvement of both β1i and β5i subunits.

A murine model of dextran-sulfate sodium (DSS)-induced colitis showed an up-regulation of β1i subunit: as a result, transgenic mice lacking the β1i subunit did not suffer of this kind of inflammatory disease.[58] In another case of DSS-induced colitis, the inhibition of LMP7/β5i by ONX 0914, a β5i-selective inhibitor, strongly reduced the symptoms of experimental colitis and suppressed a number of cytokines in treated mice, resulting in the reduction of inflammation.[57] ONX-0914 proved to block, both in vitro and in vivo, the presentation of LMP7-specific MHC-I-restricted antigens, the production of interleukin-23 (IL-23), by activated monocytes, and of IFN-γ and IL-2 by T cells.

Regarding autoimmune diseases, proteasome inhibitors represents a promising strategy for the treatment of these kind of disorders. Rheumatoid arthritis (RA), one of the most important autoimmune disease, is characterized by synovial inflammation, auto-antibody production and cartilage and bone destruction. Muchamuel et al.[49] showed that the selective inhibition of immunoproteasome by ONX-0914 reduced the levels of auto-antibodies in mouse model of RA.

Always in mouse model was found that the inhibition of LMP7/β5i reduced Th1 differentiation, without affecting Th2 differentiation; the suppression of T cell activation seems to be beneficial for the treatment of RA.[60]

Other relevant studies suggested that the inhibition of the immunoproteasome is efficacious in preventing systemic lupus erythematosus (SLE), a complex autoimmune disease characterized by the production of auto-antibodies and IFN-α. The proteasome inhibitors Bortezomib and Carfilzomib, targeting both the constitutive and immuno-subunits, and the immunoproteasome-selective inhibitor ONX-0914 are effective in the

treatment of murine lupus through a dual inhibition of pathogenic IFN-α production and auto-reactive plasma cells. It was also demonstrated that the levels of auto-antibodies, produced by plasma cells, decreased with the reduction in plasma cell numbers in spleen and bone marrow.[61]

Cascio et al. [62] showed that protein synthesis moderates the responsiveness of differentiating and malignant plasma cells to proteasome inhibitors. It was suggested that protein synthesis could play a role in the proteasomal proteolytic burden and PIs sensitivity. The average proteolytic work accomplished by the proteasome can change by several orders of magnitude, both in MM cells and in differentiating plasma cells; it was suggested that the increased workload is associated with an enhanced sensitivity of PIs.

Another study concerning Multiple Sclerosis (MS), a chronic demyelinating immune-mediated disease of the central nervous system, investigated the potential function of ONX 0914. The β5i-selective inhibitor reduced the disease progression, by reducing levels of cytokine-producing CD4 (+) cells in treated mice, thus validating its potential applicability for the treatment of MS.[63] These findings highly clarified the importance of targeting LMP7 as a rational approach to treat inflammatory and autoimmune disorders.

A relevant implication of the immunoproteasome was confirmed also in rejection antibody-mediated. MECL-1 (β2i) increased in the graft and blood samples during chronic antibody-mediated rejection. In rat cardiac allografts, Bortezomib delayed acute rejection, attenuated the humoral response and strongly reduced the level of circulating donor-specific antibodies, in a dose-dependent manner.[64]

Immunoproteasome-inhibitors represent a promising strategy also in preventing transplant rejection.

Proteasome inhibition is an important strategy to treat hematologic malignancies; the nonspecific inhibitors cause side effects and toxicities that may let the therapy fail. Bortezomib (Velcade®) and Carfilzomib (Kyprolis®),also called conventional proteasome inhibitors, showed their effects on MM and other hematologic malignancies but they unfortunately are not selective, targeting both cCPs and iCPs indiscriminately.

Targeting the immunoproteasome is a valuable strategy against models of MM that does not respond to conventional drugs.[65]

The collateral effects of conventional proteasome inhibitors limit their applications; consequently, selectively targeting proteasome elements responsible for inflammatory pathways would increase the therapeutic index.[66-67]

The main collateral effect of Bortezomib is the peripheral neuropathy; however, it was also suggested that bortezomib-induced peripheral neuropathy (BIPN) occurs through a proteasome-independent mechanism.[68] The accumulation of Bortezomib in the dorsal root ganglia cells, mitochondria-mediated disregulation of Ca^{2+} homeostasis and disregulation of neurotrophins were suggested to be responsible of the pathogenesis of BIPN.[69] On the contrary, Carfilzomib showed a reduced peripheral neuropathy. In cellular lysates, Bortezomib, but not Carfilzomib, inhibited the serine proteases cathepsins G, A chymase, dipeptidyl peptidase-II and HtrA2/Omi, the latter being involved in neuronal survival.[68]

High levels of immunoproteasome were detected in MM cells, suggesting that immunospecific proteasome inhibitors could be a strategy to develop a potential treatment for hematological malignancies.[65]

Carlfilzomib, an α',β'-epoxyketone, showed a strong antitumor activity in MM cells but also an equal inhibition in normal cells was observed (80%), thus cells death was not selective.[70]

The immunoproteasome-specific inhibitor IPSI-001, a peptidyl aldehyde able to selectively target the β1i subunit of the immunoproteasome,[65] induces apoptosis in MM cells and other hematological malignancies, being able to overcome conventional drug resistance, also to Bortezomib; in addition also dexamethasone-resistant cells (MM1.R cells) showed comparable responses as dexamethasone-sensitive cells (MM1.S) to the inhibitor.

As a matter of fact, a non-covalent inhibition should be preferred in order to avoid the inhibition of other human proteases and reduce collateral effects.

Proteasome inhibition represents a valuable strategy for the treatment of Waldenström macroglobulinemia (WM), a kind of non-Hodgkin lymphoma (NHL).

It was proved that WM cells express higher level of iCPs in comparison with cCPs,[71] Oprozomib (ONX-0912), an orally active proteasome inhibitor with potent activity on both β5i and β5c subunits, demonstrated is responsible for the toxicity in WM cells and for the reduction of bone marrow (BM)–derived interleukin-6 and insulin-like growth

factor 1 (IGF-1) secretion, thus inhibiting BM-induced p-Akt and phosphorylated extracellular signal related kinase (p-ERK) activation in WM cells.[71]

2.5 Proteasome and immunoproteasome inhibitors

Many proteasome inhibitors targeting both the immuno- and constitutive proteasomes indiscriminately have been approved over the years.

Bortezomib (Velcade®, Fig. 2) represents the first proteasome inhibitor approved by the FDA in 2003 for the treatment of MM and later in 2006 for mantle cell lymphoma.[72-75]

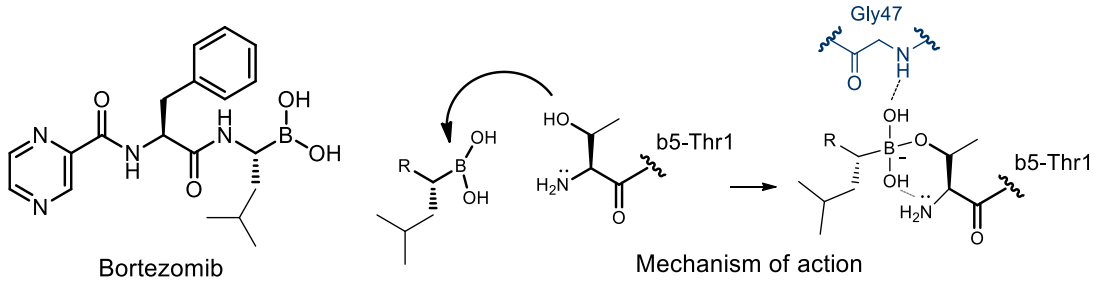

Figure 10. Bortezomib structure and mechanism of inhibition of the β5 subunit

Bortezomib is a dipeptidyl boronic acid able to inhibit all three catalytic activities of both the constitutive and immuno-proteasomes through the formation of a reversible tetrahedral adduct (Fig. 10), by reaction with the Thr1Oγ residue, as deduced from the crystal structure of 20S constitutive proteasome in complex with Bortezomib, reported by Groll and coworkers.[76]

Bortezomib showed similar potencies when evaluated against β1i, β5c and β5i subunits, with IC50 values of 5.5 nM, 7.0 nM, and 3.3 nM, respectively, all ChT-L activities.[77] The remaining catalytic sites are also inhibited by Bortezomib, but in particular the inhibition of the T-L activity of both isoforms was very poor. The most important side effect of Bortezomib is the peripheral neuropathy.[68] BIPN seemed, anyway, to be reversible in the most of of patients after dose reduction; although this side effect was more frequent in the presence of baseline neuropathy, the overall occurrence was independent of prior neurological disorders.[78]

Carfilzomib (Kyprolis®, Fig. 11) is a second-generation proteasome inhibitor approved by the FDA in 2012 for the treatment of refractory MM.

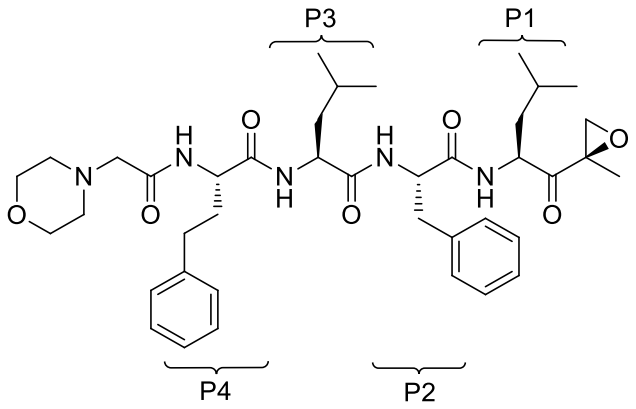

Figue 11. Carfilzomib structure

Carfilzomib is a tetrapeptide α',β'-epoxyketone with a *N*-acyl morpholine cap, obtained by optimization[79] of epoxomicin,[80] a natural and potent irreversible proteasome inhibitor.[81-82] The mechanism of action of epoxomicin, together with that of the related derivatives bearing an α',β'-epoxyketone warhead (Fig. 12), including Carfilzomib, was investigated by Groll and coworkers.[83]

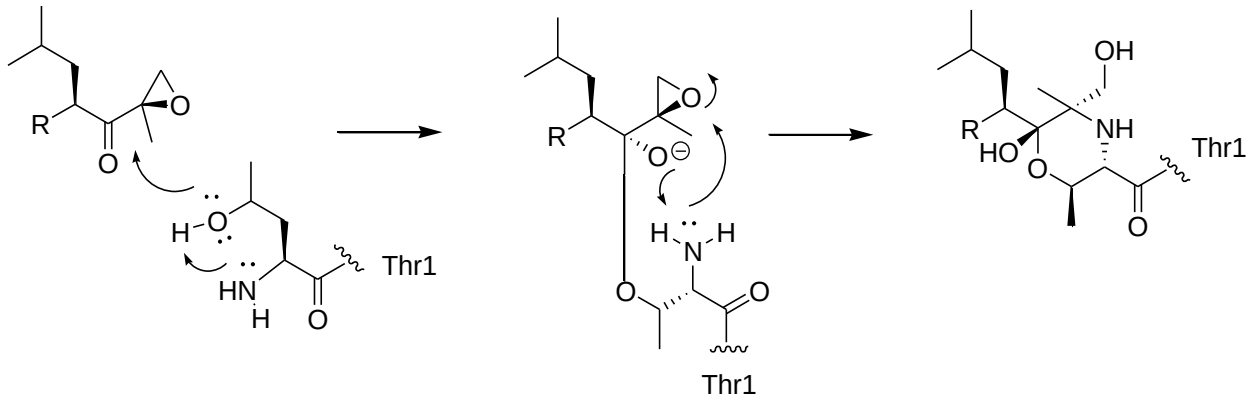

Figure 12. Mechanism of action of α',β'-epoxyketone inhibitors.

Both the hydroxyl and the amino groups of Thr1 are involved in a sequential double nucleophilic attack on the α',β'-epoxyketone warhead, leading to the formation of a stable morpholino ring. Given the key role in the mechanism of action of the free *N*-terminal amino group, it was suggested that the α',β'-epoxyketone derivatives are able to inhibit only the *N*-teminal nucleophile proteases, like the proteasome.

Studies carried out on both the constitutive and immuno-isoforms showed that Carfilzomib is a very potent proteasome inhibitor, able to inhibit both β5c and β5i

subunits at low nanomolar concentration, with a slight preference for the constitutive isoform (IC50 values of 6 nM and 33 nM, respectively).[84]

With regard to the other proteolytic subunits, Carfilzomib showed a lesser amount of activity, thus suggesting, as previously mentioned, that the selective inhibition of the ChT-L proteasome activities is sufficient to exert an antitumor response in hematological malignancies.[70]

Ixazomib or MLN9708, (Ninlaro®, Fig. 13) was approved by FDA in November 2015, in combination with lenalidomide and dexamethasone, for the treatment of patients with MM that received at least one prior therapy. It is an orally bioavailable prodrug of the boronic acid MLN2238, that overcomes the intravenous or subcutaneous routes of administration of Bortezomib and Carfilzomib. [85]

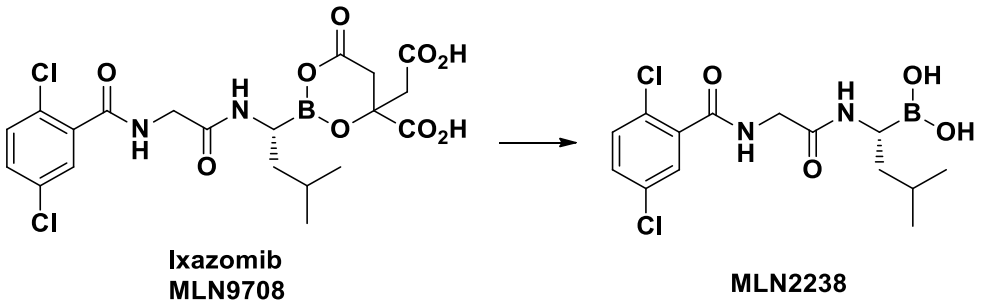

Figure 13. In vivo activation of Ixazomib to MLN2238

Ixazomib preferentially targets the β5c subunit with an IC_{50} value of 3.4 nM; however, it also shows a lower activity towards β1c and β2c with IC_{50} values of 31 nM and 3500 nM, respectively.[85] MLN9708 showed an improved pharmacokinetic, pharmacodynamic and antitumor activity with respect to Bortezomib. Like Bortezomib, Ixazomib targets both the immuno- and constitutive proteasomes,[8] however, no IC_{50} values have been reported in the literature.

More recently, considering the key role played by the immunoproteasome in various diseases, medicinal chemists focused their research on the discovery of potent selective inhibitors of this isoform. Many interesting inhibitors which show a high degree of selectivity towards the immunoproteasome have been developed.

UK-101 (Fig. 14) is a potent peptide inhibitor with a reactive epoxyketone warhead, which selectively targets β1i subunit.[86] A previous SAR study carried out on epoxomicin and eponemycin, two natural product able to inhibit the proteasome,[80,87] provided crucial

structural data. In detail, when tested in vitro, eponemycin showed remarkable inhibitory properties against the immunoproteasome compared to the constitutive isoform, in particular towards the β1i subunit.[88]

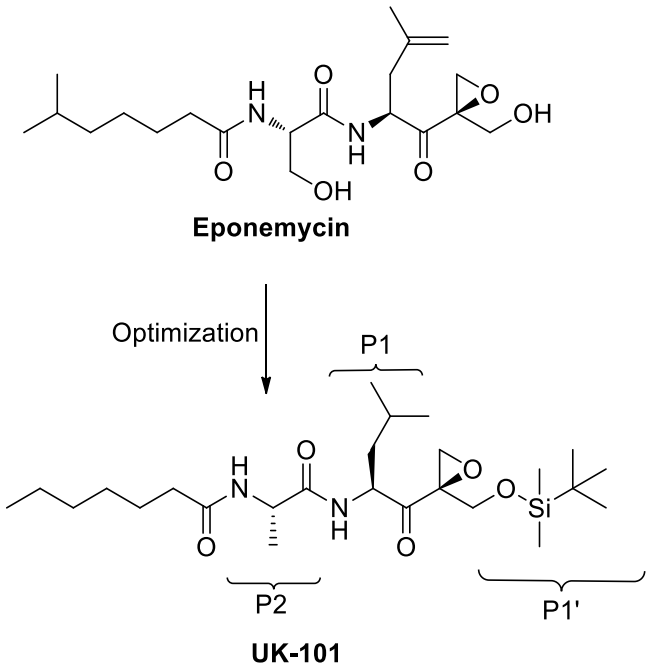

Figure 14. Development of UK-101 from eponemycin.

Based on these data, further SAR studies were carried out, starting from the idea to maintain the *N*-terminal hydrocarbon tail and the C-terminal hydroxyl group of eponemycin. This work resulted into a series of epoxyketone derivatives, including UK-101, which was identified as the most promising β1i-selective inhibitor.[86]

UK-101 contains a hydrophobic heptanoic tail at the *N*-terminal, an alanine residue at the P2 position and the hydroxyl group at the P1'site protected with a *tert*-butyldimethylsilyl (TBDMS) group at the *C*-terminal moiety, whereas the P1 leucine plays a key role for the inhibition of the ChT-L activity. In in vitro assays, UK-101 selectively inhibited β1i subunit with IC_{50} values in the range 100-500 nM. On the contrary, a lack of activity was noticed against the other proteolytic activities, with the only exception of the β5c subunit.[86]

Another interesting inhibitor with a good selectivity towards immmunoproteasome core particles β1i and β5i is represented by the dipeptidyl aldehyde IPSI-001 (Fig. 15).[65] As a matter of fact, when tested against the proteasome, IPSI-001 showed a great selectivity towards iCPs. More in detail, comparing the inhibitions of β1i *vs* β1c and β5i *vs* β5c, a

165- and 100-fold preference respectively for the iCPs β1i and β5i was observed, with an increased selectivity for LMP2/β1i subunit.

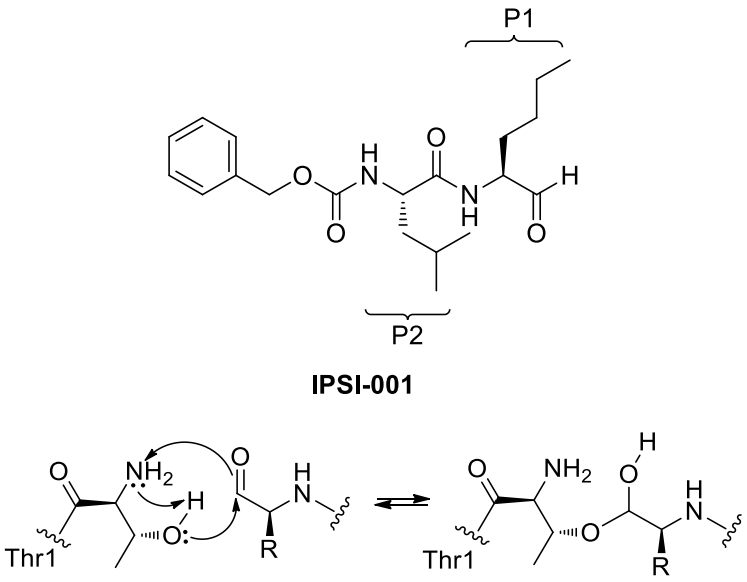

Figure 15. IPSI-001 structure and mechanism of action

The mechanism of action of IPSI-001 (Fig. 11) proceeds through the nucleophilic attack of the hydroxyl group of Thr1 on the carbonyl carbon, thus leading to the formation of a tetrahedral hemiacetal. Furthermore, this class of compounds binds to proteasome catalytic sites with a time-independent inhibition.[34] IPSI-001 is a dipeptide containing at the P1 site a norLeucine residue, at the P2 site a Leu residue, while at the *N*-terminal cap it bears a carbobenzyloxy (Cbz) protecting group.

Orlowski et al.[65] demonstrated that increasing the hydrophobic group of the P1 aminoacid determines a great selectivity towards the immunoproteasome, while the activity towards constitutive proteasome decreased.

ONX-0914 is a tripeptide epoxyketone (Fig. 16), reported as the first β5i-selective inhibitor[49,89] and actually in preclinical studies to evaluate the potential clinical application on autoimmune disorders such as RA, and SLE and for the inflammatory bowel disease.

X-ray structure of ONX-0914 covalently bound to the murine immuno- and constitutive proteasomes, suggested that the presence of a Phe residue at the P1 site induces a major conformational change in the S1 pocket of β5c, but only minor alterations in β5i.[7]

These results suggested also that the *N*-terminal morpholinyl acetyl cap does not interact with β5i subunit but, probably, is very important to enhance the solubility and to improve the physicochemical properties of ONX-0914.

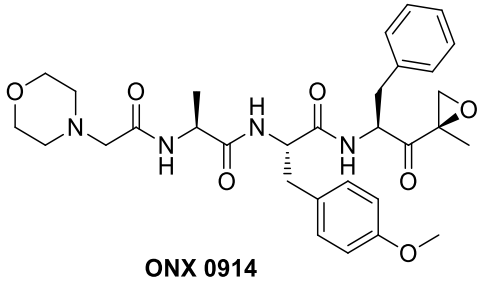

Figure 16. ONX 0914 structure

In Raji cell lysates, this inhibitor showed a great selectivity towards β5i subunit, with a 10-fold increased activity compared to β5c subunit. With regard to the remaining proteolytic sites, they were inhibited by ONX-0914 only at higher concentrations. Further investigations to verify the selectivity of this inhibitor for β5i were carried out: in β5i knockout mice, the inhibitory effect of ONX-0914 was not observed.[49] Furthermore, various studies have reported the promising potential of this compound in pathologies where immunoproteasome plays a key role, as inflammatory and autoimmune diseases (i. e. RA). ONX 0914 is able to inhibit the release of pro-inflammatory cytokines, IL-23 and TNF-α in activated monocytes and to block the disease progression, as well as to alleviate the severity of disease symptoms 49.

PR-924 (named also IPSI), currently in preclinical trial for the treatment of MM, is another β5i-selective inhibitor with a α',β'-epoxyketone warhead (Fig. 17) [88]. PR-924, when tested against Raji cell lysates [90] exhibited an IC_{50} value of 2.5 nM towards β5i, with a 100-fold lower activity against β5c. The remaining catalytic subunits were inhibited only at higher concentrations (i.e. β1i: IC_{50} value of 1.84 μM), or not inhibited at all.

PR-924 showed antileukemic activity, but only at the concentrations that inhibit both the constitutive (β5c) and immunoproteasome (β5i) subunits: the sole β5i inhibition is not sufficient to induce an anti-leukemia effect.

A recent study reported that PR-924 induces apoptotic cell death when tested in several MM cell lines.[91] No significant toxicities were observed in control cell lines when they were exposed at 20 μM concentration of PR-924.

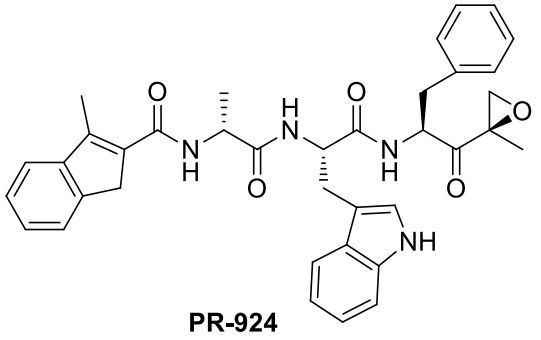

Figure 17. PR 924 structure

KZR-616 is a potent, selective dual immunoproteasome inhibitor of the subunits LMP7/LMP2 that shows IC50 of 39 nM/139 nM. KZR-616 was developed by Kezar Life Sciences and is presently in clinical trials for treatment of rheumatic disease.
KZR-616 (Fig. 18) acts as selective covalent inhibitor of the immunoproteasome that potently blocks inflammatory cytokine production *in vitro* and disease progression in mouse models of SLE. Durable disease remission in animals was achieved at well tolerated doses without affecting normal T-cell dependent immune responses.

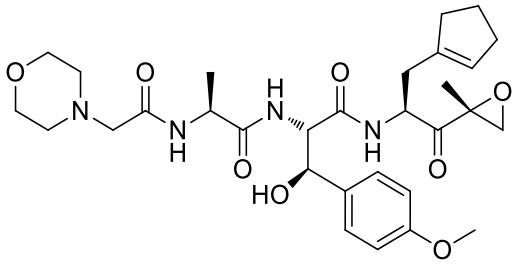

Figure 18. KZR-616 structure

Compared to ONX 0914, KZR-616 maintained LMP7 and LMP2 selective inhibition, a comparable cytokine inhibition profile and similar rapid pharmacokinetics. Moreover, efficacy of KZR-616 was comparable to ONX 0914 in the anticollagen antibody induced arthritis (CAIA) model at half the dosage while subcutaneous administration gave comparable results at similar dosages. KZR-616 showed no inhibition at 10 μM against a broad selectivity panel of 20 serine, metallo-, cysteine, and aspartyl proteases and 11

hydrolases. Based in part on these results, KZR-616 was selected as a clinical candidate for treatment of autoimmune disease.[92]

3. Results and discussion

3.1 Synthesis of amides 2-33

The synthesis of amides **2-11** was achieved according to a previously reported procedure,[11] starting from 2(1*H*)-pyridone **52** that was *N*-alkylated with ethyl bromoacetate or methyl 3-bromopropionate in the presence of NaH, to give esters **53-54**. These latter intermediates were converted into the corresponding carboxylic acids **55-56** by alkaline hydrolysis with LiOH. Coupling reactions between the carboxylic acids **55-56** and the suitable amines, in the presence of EDC·HCl, HOBt, as coupling reagents, and DIPEA as a base, gave the desired amides **2-5** and **6-11** in good yields (Scheme 1).

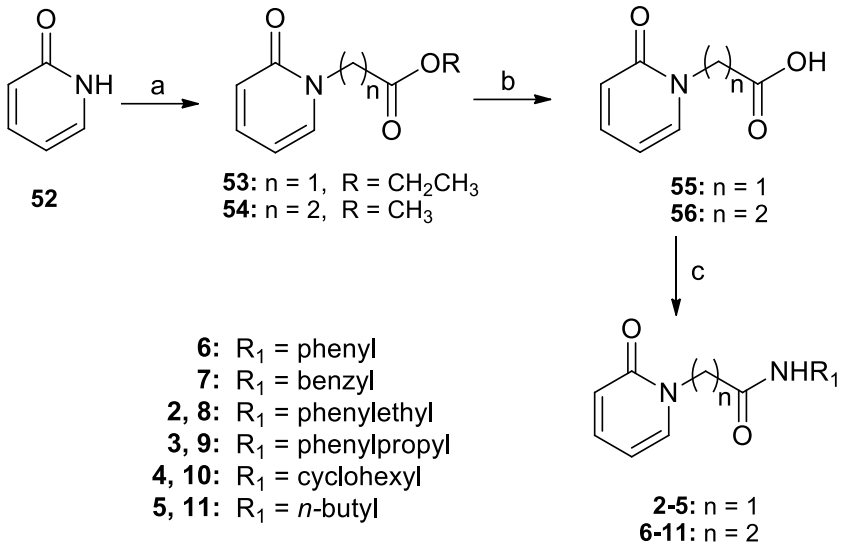

Scheme 1. Reagents and conditions**:** (a) NaH, DMF, 0°C, 1h, N_2; ethyl bromoacetate or methyl 3-bromopropionate, r.t. 12h; (b) LiOH, MeOH/H_2O/dioxane (1:1:1), 0°C-r.t., 6 h ; (c) DCM/DMF, 0°C, HOBt, EDC·HCl, 10 min, then DIPEA and a suitable amine, r.t., 12h.

The synthesis of the P2 fragments of compounds **12-25** was achieved starting from the commercially available (*R*)-2-hydroxy-3-phenyl propanoic acid methyl ester **57** and (*R*)-2-hydroxy-3-phenyl butanoic acid ethyl ester **58**, which were converted into the more reactive methanesulfonates **59-60,** by reaction with mesyl chloride in the presence of triethylamine (Scheme 2). Intermediates **59-60** were then condensed to the pyridone scaffold **52** to give the esters **61-62**, which were then converted into the corresponding carboxylic acids **63-64** by alkaline hydrolysis. Coupling reactions, carried out as reported in Scheme 1, between the carboxylic acids **63-64** and the suitable amines gave compounds **12-18** and **19-25** in high yields.

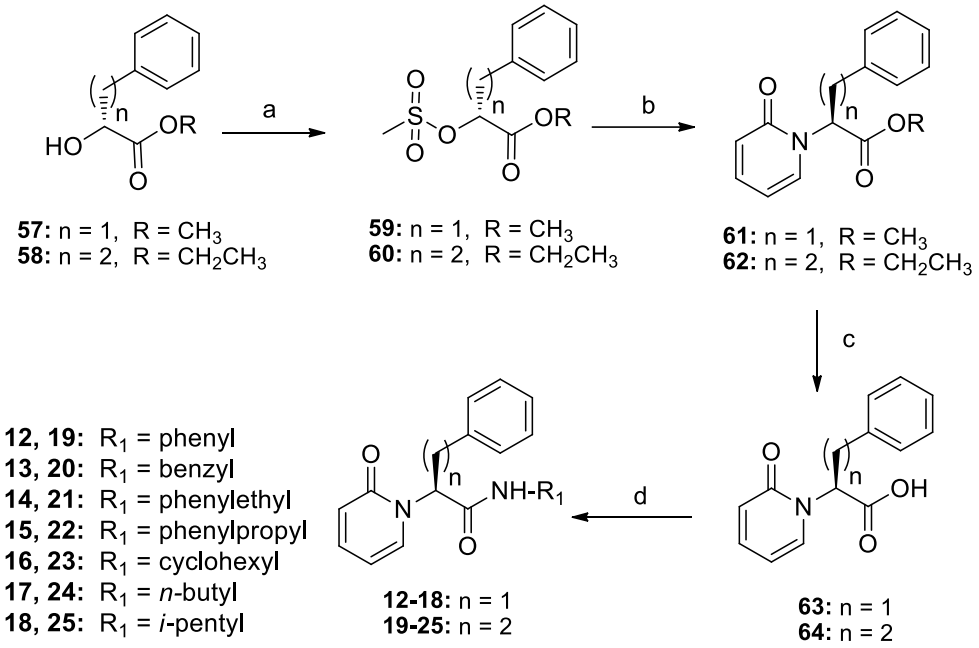

Scheme 2. Reagents and conditions**:** (a) MsCl, Et_3N, dry CH_2Cl_2, r.t., 2h, N_2; (b) compound **52**, NaH, dry DMF, 0°C-r.t., then **59** or **60**, 12h, N_2; (c) LiOH, MeOH/H_2O/dioxane (1:1:1), 0°C-r.t., 12h; (d) DMF, 0°C, HOBt, EDC·HCl, 10 min, then DIPEA and a suitable amine, 0°C-r.t., 12h

The synthesis of amides **27-33** (Scheme 3) was performed starting from commercial available 6,7-dimethoxyisoquinolin-1(2*H*)-one **65** that was *N*-alkylated with methyl 4-bromocrotonate in the presence of NaH, using dry DMF as solvent, under N_2 atmosphere, to give ester **66**. The latter intermediate was converted into the corresponding carboxylic acid **67** by alkaline hydrolysis with LiOH. Coupling reactions between the carboxylic acids **67** and the suitable amines, in the presence of HATU, an efficient coupling reagent, and DIPEA as a base, gave the peptides **27-33** in good yields.

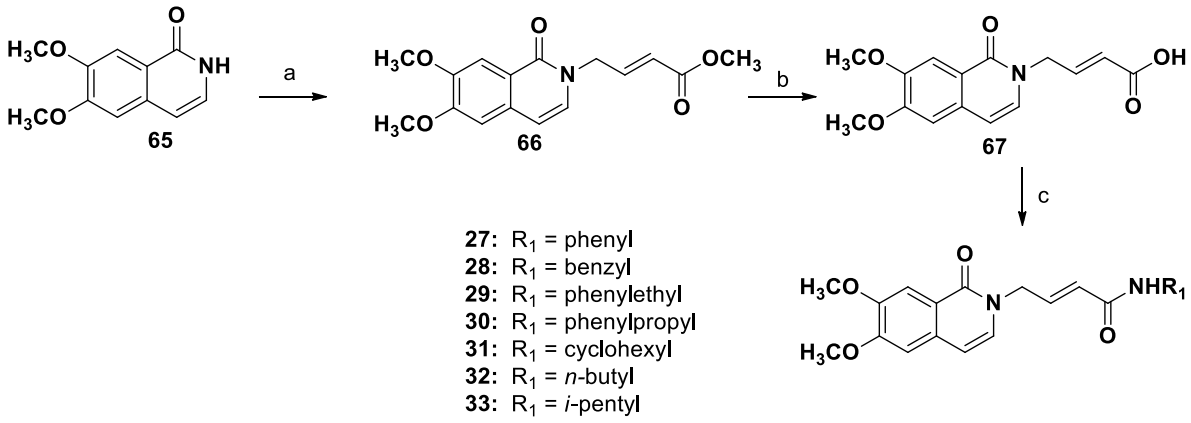

Scheme 3. Reagents and conditions: (a) NaH, DMF, 0°C, 1h, N_2; then methyl 4-bromocrotonate, rt, 12h ; (b) LiOH, MeOH, 0°C-rt, 12h; (c) DMF, 0°C, HATU, 10 min, then DIPEA, amines, rt, 12h.

3.2 Kinetic parameters calculated according to the binding mode of each inhibitor

Reversible inhibitors usually bind to the enzyme via non-covalent interactions, although exceptions are known in which covalently bound inhibitors result in reversible inhibition due to hydrolytically labile bonding (e.g., peptidyl aldehydes). Reversible inhibitors can act in a competitive or non-competitive manner. Competitive inhibitors compete with the substrate for access to the active site of the enzyme and can be displaced by increasing substrate concentrations. In contrast, in the case of non-competitive inhibitors, the substrate and inhibitor bind independently to the enzyme. The inhibitor promotes a conformational change within the catalytic site that does not prevent the binding of the substrate but that promotes the formation of a non-productive complex [E·S·I].

Irreversible inhibitors bind covalently to the enzyme, resulting in the permanent inactivation of the target protease. Consequently, these inhibitors cannot be displaced by increasing the substrate concentration.

For reversible inhibitors, IC_{50} values are typically used to describe inhibitory potency. However, for irreversible inhibitors, IC_{50} values are dependent on both the substrate concentration and the duration of the incubation of enzyme with inhibitor prior to the addition of substrate. Thus, irreversible inhibitors should be described by the following kinetic parameters: i) the dissociation constant (K_i) of the non-covalent enzyme-inhibitor complex [E·I], which is a measure of the binding affinity; ii) the inactivation rate constant, also called the first-order rate constant of inhibition (kinac min-1), which describes the rate of formation of the covalent enzyme-inhibitor complex E-I; and iii), the second-order rate constant of inhibition (k_{2nd} $M^{-1}min^{-1}$), which is calculated from the k_{inac}/K_i ratio, as a measure of inhibitor potency.

$$\text{Enz} + \text{I} \underset{}{\overset{\text{Ki}}{\rightleftharpoons}} [\text{Enz I}] \xrightarrow{\text{kinac}} \text{Enz-I}$$

3.3 Biological activity and docking studies

All the synthesized compounds were tested for their ability to inhibit each one of the catalytic subunits of c20S and i20S, by measuring the rate of hydrolysis of the appropriate fluorogenic substrate (Suc-Leu-Leu-Val-Tyr-AMC for β5i and β5c; Boc-Leu-Arg-Arg-AMC for β2i and β2c; Ac-Pro-Ala-Leu-AMC for β1i and Z-Leu-Leu-Glu-AMC for β1c). MG-132 (Z-Leu-Leu-Leu-al), a reversible inhibitor of both proteasome and immunoproteasome, was used as positive control.

First, compounds underwent a preliminary screening on each proteolytic subunit at 50 μM. Compounds able to inhibit the enzymatic activity by more than 60% were characterized in detail: continuous assays were thus performed (progress curve method, at seven different concentrations, ranging from those that minimally inhibited to those that fully inhibited the immunoproteasome or the proteasome subunit) to determine the K_i values reported in Table 1.

Among all the tested compounds, some of them (i.e. **1, 7, 10-13, 19** and **21**) turned to be active on the iCPs. Interestingly, compounds **1** and **7,** which were *N*-benzyl substituted amides selectively inhibited the β1i subunit, with a consistent improvement of activity observed for the *β*-alanine derivative with respect to the glycine derivative (K_i = 0.021 μM *vs* 2.23 μM).

The *β*-alanine derivatives **10** and **11**, bearing a cyclohexyl and an *n*-butyl substituent, on the contrary, targeted both the β1i and β5i subunits. When a Phe residue was introduced at P2 site (e.g. compounds **12** and **13**), the activity was switched on both the constitutive and immuno-core particles (β5i and β5c), with a strong preference for the constitutive core-particle (see e.g. compound **12,** K_i = 8.81 μM and 45.5 μM for β5c and β5i, respectively). It is worth noting that two the compounds bearing a HPhe residue at the P2 site turned to be active on both the ChT-L activities of i20S (i.e. **19**) or against the sole β5i (i.e. **21**).

Table 1. Activity on cCPs and iCPs of compounds **1-25**.

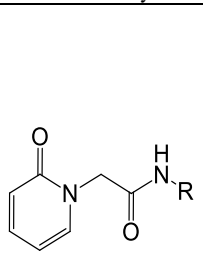

1-5

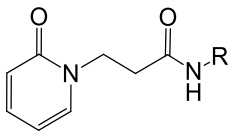

6-11

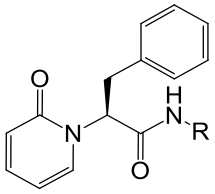

12-18

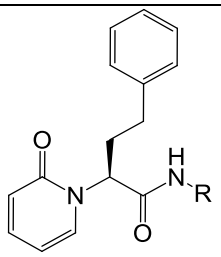

19-25

	% of inhibition at 50 μM or K_i (μM)						
Comp.	R	β1c	β2c	β5c	β1i	β2i	β5i
1	benzyl	32%	21%	n.i.	2.23±0.26	17%	n.i.
2	phenylethyl	24%	n.i.	n.i.	44%	n.i.	n.i.
3	phenylpropyl	32%	n.i.	n.i.	n.i.	11%	n.i.
4	cyclohexyl	36%	n.i.	n.i.	22%	10%	3%
5	*n*-butyl	36%	n.i.	n.i.	n.i.	5%	n.i.
6	phenyl	23%	1%	25%	n.i.	11%	25%
7	benzyl	37%	n.i.	n.i.	0.021±0.002	25%	17%
8	phenylethyl	24%	n.i.	3%	27%	n.i.	46%
9	phenylpropyl	22%	n.i.	18%	37%	n.i.	15.17±0.63
10	cyclohexyl	23%	n.i.	12%	2.92±0.87	n.i.	5.74±0.63
11	*n*-butyl	19%	n.i.	4%	3.09±1.06	n.i.	14.29±3.0
12	phenyl	15%	6%	8.81±1.11	23%	n.i.	45.5± 2.6
13	benzyl	14%	8%	3.02±0.29	19%	n.i.	7.77±1.51
14	phenylethyl	10%	13%	20.4±2.2	10%	n.i.	43%
15	phenylpropyl	15%	12%	50%	25%	n.i.	45%
16	cyclohexyl	5%	6%	45%	16%	n.i.	39%
17	*n*-butyl	n.i.	n.i.	48%	30%	9%	33%
18	*i*-pentyl	8%	n.i.	55%	23%	n.i.	30%
19	phenyl	n.i.	23%	n.i.	5.9± 0.16	n.i.	5.81±0.37
20	benzyl	n.i.	26%	n.i.	21%	n.i.	38%
21	phenylethyl	n.i.	31%	n.i.	48%	14%	3.85± 0.46
22	phenylpropyl	n.i.	33%	n.i.	36%	4%	34%
23	cyclohexyl	n.i	30%	n.i.	40%	6%	42%
24	*n*-butyl	n.i.	31%	n.i.	29%	n.i.	37%
25	*i*-pentyl	n.i.	30%	17%	18%	6%	39%

To help interpret the structure–activity relationship (SAR) data and elucidate the molecular mechanism of i20S inhibition of the most active compounds **1, 7, 13** and **21**, docking studies were carried out in collaboration with Prof. Lavecchia (Federico II University of Napoli), using the GOLD Suite docking package [93] with the X-ray crystal structure of the murine i20S in complex with the epoxyketone inhibitor PR-957 (PDB: 3UNF).[7] This structure was selected due to the high degree of amino acid sequence identity (>90%) between mouse and human i20S subunits around the respective catalytic sites. Moreover, the few non-identical residues are located at the interface with the concomitant adjacent subunits and are thus absent from the catalytic sites. Furthermore, the crystal structure of PR-957 bound to β1i reveals two well-defined water molecules within the S3 pocket, which coordinate a tight H-bond network between β1i-A50N, β2i-S118Oγ and the backbone amide nitrogen and carbonyl oxygen of the P3 alanine residue of PR-957. Accordingly, the intervening water molecules were included in the docking experiments.

Docking of the amide derivative **1** to the β1i subunit revealed a binding mode similar to that of PR-957 (Fig. 19a), with an almost identical positioning of the backbone amides, the P1 phenyl moieties adopting the same spatial arrangement and the P3 alanine residue of PR-957 nicely overlapped with the pyridone ring of **1** (Fig. 19b). The P1 benzyl substituent extends deeply into the S1 pocket, forming hydrophobic contacts with V20, F31, L45, A49 and A52. The **1** backbone amide is engaged in H-bonds with the NH group of S21 backbone and the carbonyl oxygen of G47 backbone, whereas the carbonyl oxygen of the pyridone ring accepts further H-bonds from A49N, S48Oγ and A50N, these last two through one of the two intervening water molecules located crystallographically in the PR-957 structure and included in our model. Moreover, the second water molecule forms a H-bond with the first one, while simultaneously engaging the β2i-S11833Oγ, which is at the bottom of the S3 pocket and contributes to a further stabilization of the ligand into the active site. Additional hydrophobic interactions occur between the pyridone ring and the V20 and V27 side chains located in proximity of S3 pocket of β1i subunit.

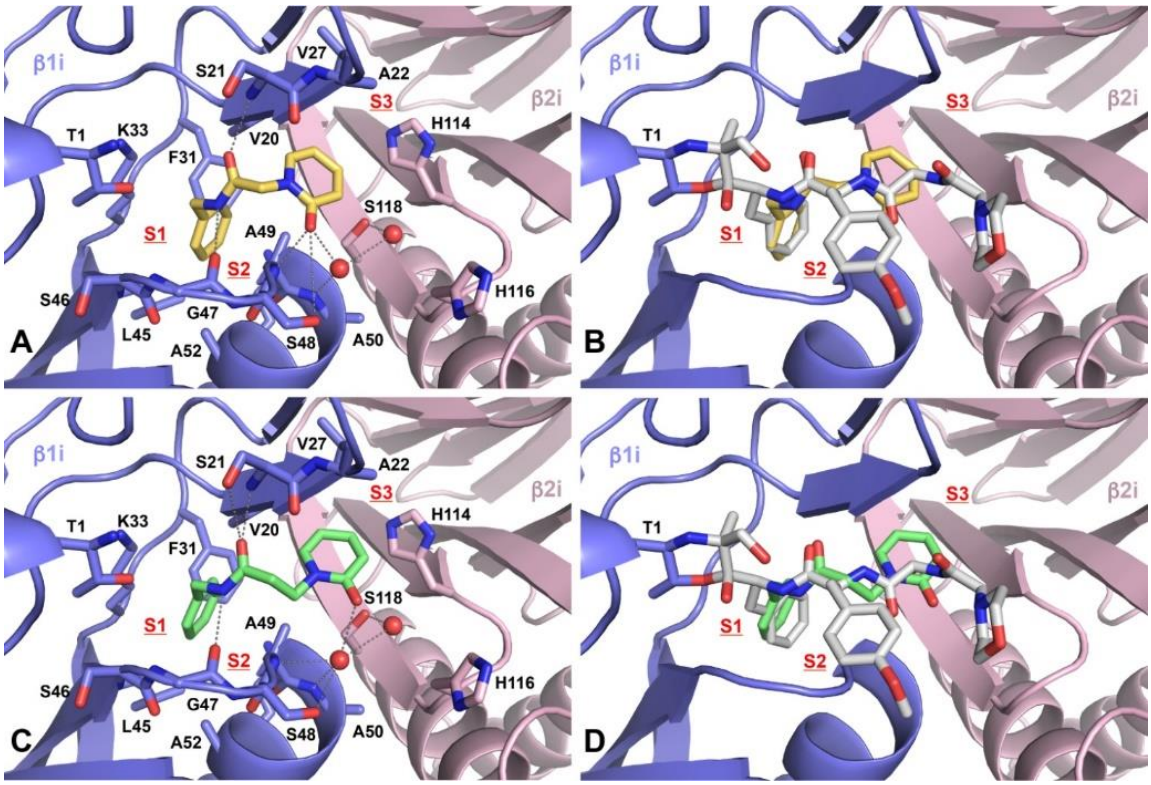

Figure 19. Binding modes of compounds **1** (A, yellow orange sticks) and **7** (C, lime green sticks) into the β1i (slate)/β2i (light pink) active site of mouse i20S, represented as a ribbon model. Only amino acids located within 4 Å of the bound ligand are displayed and labelled. H-bonds discussed in the text are depicted as dashed grey lines. The defined water molecules forming tight H-bonds to the protein are displayed as red spheres. S1-S3 specificity pockets are labeled. An overlay of **1** (B, docked pose) and **7** (D, docked pose) with PR-957 (white sticks, X-ray crystal pose) is shown in the β1i/β2i active site of mouse i20S.[14]

The β1i and β1c subunits strongly differ in their amino acid lining in the unprimed substrate binding channel. The hydrophobic active site surrounding of subunit β1i is replaced by a more polar one in subunit β1c. In particular, the amino acid substitutions V20T, F31T, L45R and A52T increase the polarity and the size of the β1c S1 pocket. Therefore, the more hydrophilic S1 pocket of subunit β1c opposes binding of the hydrophobic P1 substituents. These findings are in agreement with the poor inhibitory activity displayed by this series of derivatives towards β1c.

Elongation of the linker between the pyridone ring and the amide function from one to two methylene units yielded compound **7**, which showed the highest inhibitory potency and selectivity towards β1i (K_i = 0.021 μM). As a result of the docking of **7** into the β1i subunit, we obtained a complex showing an overall binding mode similar to that of **1** (Fig. 19c,d), with the ligand forming H-bonds with G47O, S21N and S21Oγ of β1i

through the amide group as well as the same pattern of hydrophobic interactions within the S1 pocket. These results are in consonance with the SAR data showing that compounds bearing a benzyl (**7**), cyclohexyl (**10**) or *n*-butyl (**11**) residue at P1 inhibit β1i much stronger than β1c, which confirms that the S1 pocket of β1i is more hydrophobic than that of β1c.[7] In addition, neither β1i nor β1c is inhibited by compounds featuring a bulky phenylethyl (**8**) or phenylpropyl (**9**) substituent at P1, an outcome that supports structural data displaying that β1i/c have a smaller S1 pocket than β5i/c.[7]

The pyridone moiety of **7** fits into the S3 pocket formed by S48, S118 and H114, which is beneficial for improving potency and selectivity for β1i subunit (Fig. 19c). In particular, the pyridone carbonyl oxygen forms a tight H-bond network with A49N, S48Oγ and A50N of β1i through one water molecule and with β2i-S118Oγ via the second water molecule. Additionally, the aromatic pyridone core makes an edge-to-face π-stacking interaction with the H114 imidazole ring in the subunit β2i. Compared to β1c, the S3 pocket of β1i is characterized by the amino acid replacements T22A, A27V as well as Y114H in the neighbouring subunit β2i. These differences lead to a more size-restricted and more hydrophilic S3 pocket in β1i compared to its counterpart β1c.

A second series of derivatives was designed, in which a residue of phenylalanine was used to replace the glycine P2 group. Among them, compound **13** was moderately active against β5i (K_i = 7.77 μM) and displayed a fairly good potency against β5c (K_i = 3.02 μM). As depicted in Fig. 20a,b, **13** exhibited a binding mode in β5i similar to that of derivatives **1**, **7** and PR-957. The P1 benzyl substituent fits into the S1 pocket, the backbone amide is stabilized by H-bonds with G47O, T21N and T21Oγ of β5i and the pyridone group protrudes into the S3 site with the carbonyl engaged in H-bonds with A49N and C48S. The P2 phenylalanine moiety projects into the central core of the 20S cavity, making little or no contacts with the β5i subunit. Docking of **13** to the human c20S crystal structure [94] elucidates that the P1 benzyl and the P3 pyridone ring fit into subunit β5c by interacting with T21, A27, A49, S129 and D144 of the neighbouring subunit β6 via an intervening water molecule. This latter interaction stabilizes the ligand into the S3 pocket and accounts for the enhanced potency of **13** for β5c.

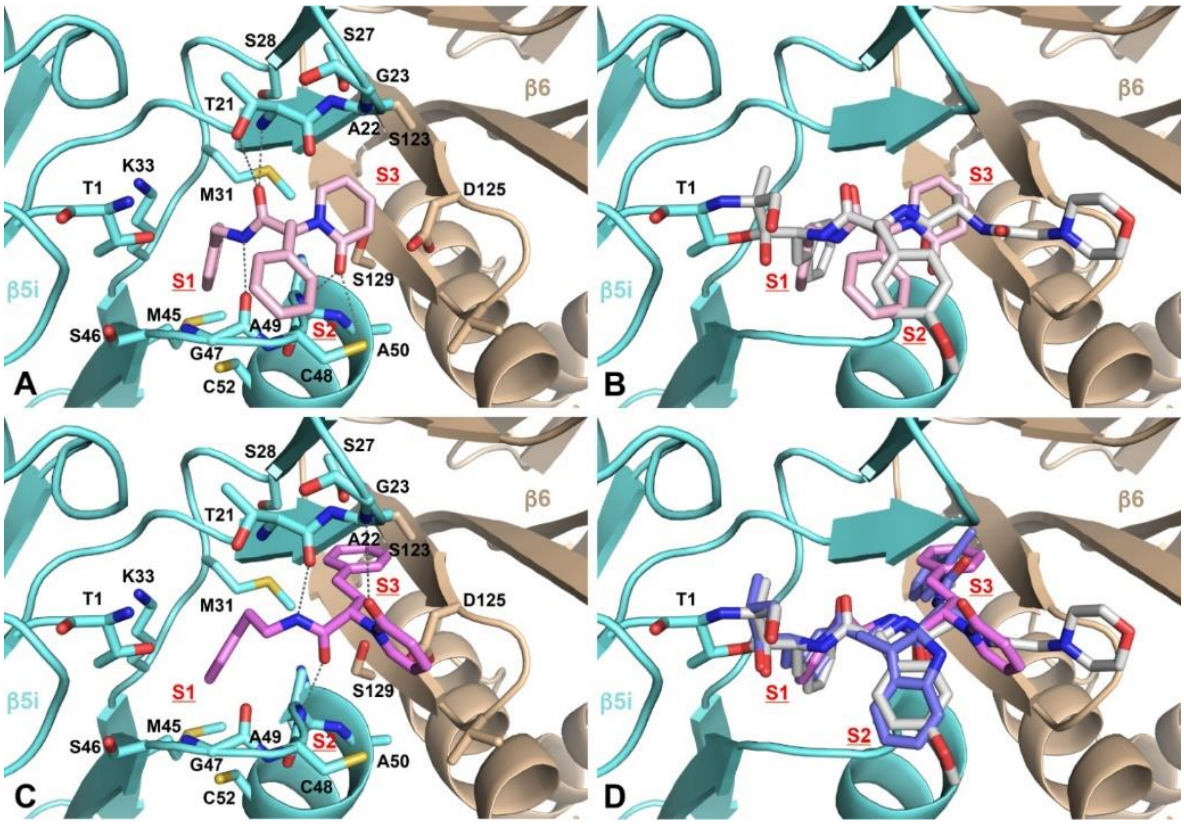

Figure20. Binding modes of compounds **13** (A, pink sticks) and **21** (C, violet) into the β5i (aquamarine)/β6 (wheat) active site of mouse i20S, represented as a ribbon model. Only amino acids located within 4 Å of the bound ligand are displayed and labelled. H-bonds discussed in the text are depicted as dashed grey lines. S1-S3 specificity pockets are labeled. An overlay of **13** (B, docked pose) and **21** (D, docked pose) with PR-957 (white sticks, X-ray crystal pose) is shown in the β5i/β6 active site of mouse immunoproteasome. Compound 21 overlaps with the X-ray crystal pose of PR-924 (slate sticks) bound to the humanized yeast i20S (PDB: 5L5H).[14]

Noteworthy, substitution of the glycine residue at P2 with a homophenylalanine residue yielded a series of derivatives in which the activity against c20S subunits β1 and β5 was completely lost. Among them, compound **21** showed selective inhibitory activity against β5i (K_i = 3.85 μM). Docking of **21** into the subunit β5i revealed a different binding mode in comparison to **1** and **7** derivatives, with the P2 substituent protruding into the S3 subsite instead of pointing toward the initially assumed S2 binding pocket (Fig. 20c). As a consequence, the pyridone scaffold assumes a folded conformation, engaging a very weak H-bond with β5i-G23N (distance of 4 Å).[95] The backbone amide establishes a H-bonding network involving T21O and A49N. The homophenylalanine residue deeply extends into the S3 subsite making O-H/π interactions with the hydroxyl groups of S27 from β5i and S129 from β6. The phenylethyl at P1 perfectly fits into the spacious S1

pocket of β5i and is stabilized by a cation- π contact with K33, a sulfur–arene interaction with M45[96-97] and by C-H/ π interactions with the side chains of M31, K33, and A49. Interestingly, the overlay of the docked pose of **21** with the β5i-specific inhibitors PR-957 (PDB ID: 3UNF) and PR-924 bound to the chimeric hβ5/hβ6 substrate binding channel (PDB ID: 5L5H)[98] reveals that 21 and PR-924 adopt a similar kinked binding mode, with an identical positioning of the amide scaffolds and a similar orientation of the P1 and P3 functions, whereas PR-957 adopts a linear orientation (Fig. 20d). The superior β5i-selectivity of **21** compared to ligands that target the strictly conserved peptide binding sites seems to result from its ability to exploit subpockets other than the substrate-binding channels. Moreover, insights into the selectivity of **21** towards i20S over c20S can be gained when considering amino acid compositions of β5c and β5i S1 pockets. Although the S1 specificity pockets of both β5c and β5i are formed by the same residues, the conformation of M45 in β5c is different from that in β5i, thus resulting in peculiarly sized S1 specificity pockets. [7] The observed selectivity of **21** can be rationalized by the impaired accommodation of the phenylethyl moiety into the smaller β5c S1 pocket because of the closed conformation of M45.

In conclusions, with this investigation we identified a series of amides with K_i values in the low micromolar or submicromalar range towards one or two chymotrypsin-like activities of immunoproteasome (β5i and β1i subunits). Amide **7** was identified as lead compound, due to the selective inhibition of β1i subunit in the submicromolar range (K_i = 21 nM). Docking studies allowed us to clarify the binding mode of the amides in the catalytic site of immunoproteasome proteolytic subunits, thus explaining the preferential inhibition of immunoproteasome with respect to proteasome.

Worthy of note, the noncovalent inhibition, characteristic of our amides, is strongly desirable, because free of drawbacks and side-effects related to covalent inhibition. Our future efforts will be devoted to optimize the identified lead compound **7** in terms of potency and selectivity and to check activity against a panel of hematological malignancies or against autoimmnune diseases in which immunoproteasome is overexpressed.

Also the second series of compounds was also evaluated by means of fluorimetric assays as described above. Interestingly, compound **33** revealed a high binding affinity for the

β1i subunit (0.27 μM) coupled with good inhibitory properties towards β5i and β5c subunits (Table 2).

Table 2. Activity of compounds **27-33** on cCPs and iCPs

% inhibition at 100 μM or K_i (μM)							
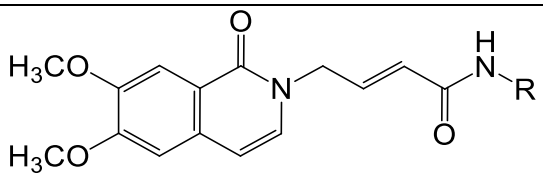 **27-33**							
Comp.	**R**	$\boldsymbol{\beta}_{1c}$	$\boldsymbol{\beta}_{2c}$	$\boldsymbol{\beta}_{5c}$	$\boldsymbol{\beta}_{1i}$	$\boldsymbol{\beta}_{2i}$	$\boldsymbol{\beta}_{5i}$
27	phenyl	17	15	49	10	12	50
28	benzyl	23	9	n.i.	3	n.i.	65
29	phenylethyl	n.i.	10	60	14	4	45
30	phenylpropyl	n.i.	5	10.61 ±0.25	50	3	64
31	cychlohexyl	n.i.	n.i.	23	n.i.	42	55
32	*n*-butyl	n.i.	10	19	n.i.	42	49
33	*i*-pentyl	n.i.	4	1.18±0.03	0.27±0.31	20	1.91±0.02

Preliminary docking studies of the most active inhibitor, **33**, into the β1i active site of mouse i20S show that the dimethoxy-isoquinolinonic portion is interposed between S2 and S3 pockets, orienting one of the methoxyl group towards Ser118 to form an H-bond, while the hydrocarbon chain is located into the S1' subpocket. Furthermore, the ligand forms H-bonds with Gly47 and Thr21 (Figure 21).

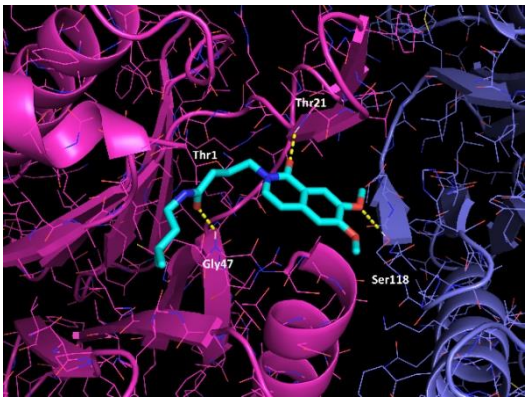

Figure 21. Binding modes of compounds **33** into the β1i active site of mouse i20S.

4. Experimental Section

4.1 Chemistry.

All reagents and solvents were purchased from commercial suppliers and used without any further purification. Elemental analyses were performed on a C. Erba Model 1106 Elemental Analyzer and the results are within ±0.4% of the theoretical values. Merck silica gel 60 F254 plates were used for analytical TLC; column chromatography was carried out on Merck silica gel (200–400 mesh). ^{1}H-NMR and ^{13}C-NMR spectra were recorded on a Varian 300 MHz NMR spectrometer operating at frequencies of 300.13 and 75.47 MHz, or on a Varian 500 MHz spectrometer operating at 499.74 and 125.73 MHz for ^{1}H-NMR and ^{13}C-NMR spectra, respectively. The residual signal of the deuterated solvent was used as internal standard. Chemical shifts are given in δ (ppm) and coupling constants (*J*) in Hz. Splitting patterns are described as singlet (s), broad singlet (bs), doublet (d), triplet (t), quartet (q), multiplet (m), doublet of doublet (dd), or triplet of doublets (td).

Ethyl (2-oxo-2*H*-pyridin-1-yl)-acetate (53).

A suspension of NaH (91 mg, 3.78 mmol) in dry DMF (10 mL) at 0 °C under N_2, was treated with a solution of pyridone **52** (300 mg, 3.15 mmol) in dry DMF (20 mL). After 1 h, ethyl bromoacetate (490 μL, 4.42 mmol) was added to the mixture and the reaction was stirred for a further 12 h at room temperature. The reaction was quenched with saturated NH_4Cl (5 mL) and the product was extracted with CH_2Cl_2 (3 × 70 mL). The combined organic phases were washed with water (3 × 100 mL), dried over Na_2SO_4, filtered and concentrated *in vacuo*. The crude was purified by column chromatography ($CHCl_3$/MeOH 95:5) to give compound **53** as a yellow oil (354 mg, 62%); R_f = 0.70 ($CHCl_3$/MeOH 9:1). ^{1}H NMR (300 MHz, $CDCl_3$) δ: 1.21 (t, *J* = 7.3 Hz 3H), 4.16-4.20 (m, 2H), 4.60 (s, 2H), 6.15-6.19 (m, 1H), 6.53-6.56 (m, 1H), 7.19-7.33 (m, 2H).

Methyl 3-(2-oxopyridin-1(2*H*)-yl)propanoate (54).

According to the same procedure described for compound **53**, compound **54** (300 mg, 3.15 mmol) was reacted with methyl 3-bromo-proprionate (481 μL, 4.41 mmol). Compound **54** was obtained as a yellow oil (474 mg, 83%), after purification by column chromatography ($CHCl_3$/MeOH 95:5); R_f = 0.70 ($CHCl_3$/MeOH 95:5). ^{1}H NMR (300

MHz, $CDCl_3$): δ: 2.33 (t, *J* = 6.5 Hz, 2H), 3.13 (s, 3H), 3.69 (t, *J* = 7.0 Hz, 2H), 5.67 (t, *J* = 7.0 Hz, 1H), 5.98 (d, *J* = 8.8 Hz, 1H), 6.82-6.88 (m, 1H), 7.05 (dd, *J* = 6.5, 1.8 Hz, 1H).

(2-Oxo-2*H*-pyridin-1-yl)-acetic acid (55).

A solution of ester **53** (354 mg, 1.95 mmol) in MeOH/H_2O/Dioxane (1:1:1, 30 mL) at 0 °C was treated with 1 N LiOH (4 mL) and stirred for 6 h at room temperature. The ethanol fraction was evaporated at reduced pressure and the residual aqueous solution was treated with 6 N HCl (pH ~ 3). The acqueous layer was extracted with EtOAc (50 mL x 3) and the organic phase was dried over Na_2SO_4, filtered and concentrated in vacuo to give compound **55** as a white powder, used without any further purification (233 mg, 78%); R_f = 0.27 (3% HCOOH in $CHCl_3$/MeOH 9:1). ^{1}H NMR (300 MHz, acetone-d_6) δ 4.60 (s, 2H), 6.16 (t, *J* = 5.9 Hz, 1H), 6.55 (dd, *J* = 7.4, 2.5 Hz, 1H), 7.20 (d, *J* = 5.9 Hz, 1H), 7.33 (t, *J* = 7.4 Hz, 1H).

3-(2-Oxopyridin-1(2*H*)-yl)propanoic acid (56).

Ester **54** (474 mg, 2.62 mmol) in MeOH/H_2O/Dioxane (1:1:1, 30 mL) was treated with 1 N LiOH (5 mL), according with the same procedure described for **55**, adjusting the residual aqueous solution to pH ~ 3. The title compound **56** was obtained as a white powder (416 mg, 95%) directly used without further purification; R_f = 0.33 (MeOH). ^{1}H NMR (300 MHz, DMSO-d_6): δ: 1.57-1.71 (m, 6H), 2.95-2.98 (m, 4H), 4.54 (s, 2H), 6.29 (t, *J* = 6.5 Hz, 1H), 6.91 (d, *J* = 6.5 Hz, 1H), 7.19 (d, *J* = 7.0 Hz, 1H).

General procedures for the synthesis of amides 2-5 and 6-11

The coupling reactions between the carboxylic acid (**55** or **56**) (1 equiv.) and the appropriate amines (1.5 equiv.) were carried out by dissolving compound **55** or **56** in dry DMF, then cooling to 0°C and adding HOBt (1.5 equiv.) and EDC·HCl (1.5 equiv.). After 10 minutes, DIPEA (2 equiv.) and the amine (1.5 equiv.) dissolved in DMF were added dropwise, and the mixture was stirred at room temperature overnight. The organic layer was washed with brine, dried over Na_2SO_4, filtered and concentrated under reduced pressure. The crude residue were purified by column chromatography, using $CHCl_3$/MeOH, 95:5 as eluent mixture.

2-(2-Oxopyridin-1(2*H*)-yl)-*N*-phenethylacetamide (2): yield: 90%. R_f = 0.32 ($CHCl_3$/MeOH, 95:5). ^1H NMR (300 MHz, $CDCl_3$): δ = 2.78 (t, *J* = 7. 1 Hz, 2H), 3.48 (q, *J* = 7.1 Hz, 2H), 4.49 (s, 2H), 6.25 (td, *J* = 6.6, 1.4 Hz, 1H), 6.60 (d, *J* = 9.1 Hz, 1H), 6.92 (bs, 1H), 7.12 (d, *J* = 7.1 Hz, 2H), 7.18-7.28 (m, 3H), 7.34-7.44 (m, 2H) ppm. ^{13}C NMR (75 MHz, $CDCl_3$): δ = 35.45, 40.80, 54.02, 107.02, 120.85, 126.42, 128.54, 128.66, 130.75, 137.98, 140.50, 162.81, 167.25 ppm. Elemental analysis: calcd for $C_{15}H_{16}N_2O_2$: C 70.29, H 6.29, N 10.93; found: C 70.11, H5.98, N 11.17.

2-(2-Oxopyridin-1(2*H*)-yl)-*N*-(3-phenylpropyl)acetamide (3): yield: 85%. R_f = 0.50 ($CHCl_3$/MeOH, 95:5). ^1H NMR (300 MHz, $CDCl_3$): δ = 1.76-1.86 (m, 2H), 2.59 (t, *J* = 7.6 Hz, 2H), 3.24 (q, *J* = 6.9 Hz, 2H), 4.52 (s, 2H), 6.27 (td, *J* = 6.6, 1.1 Hz, 1H), 6.63 (dd, *J* = 9.6, 1.1 Hz, 1H), 7.04 (bs, 1H), 7.1-7.31 (m, 5H), 7.38-7.45 (m, 2H) ppm. ^{13}C NMR (75 MHz, $CDCl_3$): δ = 30.85, 33.02, 39.14, 53.77, 106.99, 120.62, 125.91, 128.34, 138.37, 140.64, 141.30, 162.87, 167.10 ppm. Elemental analysis: calcd for $C_{16}H_{18}N_2O_2$: C 71.09, H 6.71, N 10.36; found: C 71.32, H 6.43, N 10.68.

***N*-Cyclohexyl-2-(2-oxopyridin-1(2*H*)-yl)acetamide (4):** yield: 65%. R_f = 0.60 ($CHCl_3$/MeOH, 95:5). ^1H NMR (300 MHz, $CDCl_3$): δ = 1.06-1.90 (m, 10H), 3.62-3.74 (m, 1H), 4.49 (s, 2H), 6.25 (td, *J* = 6.7, 1.3 Hz, 1H), 6.61 (d, *J* = 8.8 Hz, 1H), 6.81 (bs, 1H), 7.34-7.45 (m, 2H) ppm. ^{13}C NMR (75 MHz, $CDCl_3$): δ = 24.58, 25.40, 32.55, 48.45, 53.45, 106.76, 120.45, 138.55, 140.52, 162.80, 166.05 ppm. Elemental analysis: calcd for $C_{13}H_{18}N_2O_2$: C 66.64, H 7.74, N 11.96; found: C 66.89, H 7.86, N 11.74.

***N*-Butyl-2-(2-oxopyridin-1(2*H*)-yl)acetamide (5):** yield: 44%. R_f = 0.24 ($CHCl_3$/MeOH, 95:5). ^1H NMR (300 MHz, $CDCl_3$): δ = 0.89 (t, *J* = 7.2 Hz, 3H), 1.24-1.36 (m, 2H), 1.40-1.52 (m, 2H), 3.21 (q, *J* = 7.2, 2H), 4.53 (s, 2H), 6.25 (td, *J* = 6.7, 1.3 Hz, 1H), 6.63 (dd, *J* = 9.8, 1.3 Hz, 1H), 6.93 (bs, 1H), 7.36-7.45 (m, 2H) ppm. ^{13}C NMR (75 MHz, $CDCl_3$): δ = 13.67, 19.96, 31.25, 39.35, 53.59, 106.88, 120.56, 138.43, 140.56, 162.84, 166.99 ppm. Elemental analysis: calcd for $C_{11}H_{16}N_2O_2$: C 63.44, H 7.74, N13.45; found: C 63.61, H 7.53, N 13.64.

3-(2-Oxopyridin-1(2*H*)-yl)-*N*-phenylpropanamide (6): yield: 62%. R_f= 0.43 ($CHCl_3$/MeOH 95:5). ^{1}H NMR (300 MHz, $CDCl_3$): δ = 2.96 (t, *J* = 5.8 Hz, 2H), 4.34 (t, *J* = 5.8 Hz, 2H), 6.19 (td, *J* = 6.7, 1.2 Hz, 1H), 6.45 (d, *J* = 9.0 Hz, 1H), 7.07 (t, *J* = 7.4 Hz, 1H), 7.24-7.36 (m, 3H), 7.53-7.66 (m, 3H), 9.78 (bs, 1H) ppm.^{13}C NMR (75 MHz, $CDCl_3$): δ = 32.76, 45.21, 111.73, 118.92, 121.65, 124.45, 129.08, 134.52, 138.41, 138.87, 161.71, 173.73 ppm. Elemental analysis: calcd for $C_{14}H_{14}N_2O_2$, C 69.41, H 5.82, N 11.56; found. C 69.28, H 5.91, N 11.46.

***N*-Benzyl-3-(2-oxopyridin-1(2*H*)-yl)propanamide (7):** yield: 46%. R_f = 0.42 ($CHCl_3$/MeOH, 95:5). ^{1}H NMR (300 MHz, $CDCl_3$): δ = 2.74 (t, *J* = 6.1 Hz, 2H), 4.21 (t, *J* = 6.1 Hz, 2H), 4.38 (d, *J* = 5.8 Hz, 2H), 6.12 (td, *J* = 6.8, 1.2 Hz, 1H), 6.38 (d, *J* = 9.1 Hz, 1H), 6.81 (bs, 1H), 7.14 (d, *J* = 7.1 Hz, 2H), 7.22-7.32 (m, 4H), 7.43 (dd, *J* = 6.8, 1.6 Hz, 1H) ppm. ^{13}C NMR (125.73 MHz, $CDCl_3$): δ = 34.99, 43.49, 47.17, 106.13, 120.43, 127.35, 127.62, 128.56, 138.04, 139.10, 139.97, 162.77, 169.93 ppm. Elemental analysis: calcd for $C_{15}H_{16}N_2O_2$: C 70.29, H 6.29, N10.93; found: C 70.56, H 6.46, N 10.62.

3-(2-Oxopyridin-1(2*H*)-yl)-*N*-phenethylpropanamide (8): yield: 33%. R_f = 0.34 ($CHCl_3$/MeOH, 95:5). ^{1}H NMR (500 MHz, $CDCl_3$): δ = 2.66 (t, *J* = 6.4 Hz, 2H), 2.74 (t, *J* = 7.0 Hz, 2H), 3.47 (q, *J* = 7.0 Hz, 2H), 4.22 (t, *J* = 6.4 Hz, 2H), 5.81 (bs, 1H), 6.16 (t, *J* = 6.4 Hz, 1H), 6.55 (d, *J* =9.1 Hz, 1H), 7.11 (d, *J* = 7.1 Hz, 2H), 7.19-7.38 (m, 4H), 7.44 (dd, *J* = 6.4, 1.6 Hz, 1H) ppm. ^{13}C NMR (125.73 MHz, $CDCl_3$): δ = 35.14, 35.55, 40.73, 46.94, 105.98, 120.61, 126.50, 128.64, 128.61, 138.62, 139.01, 139.93, 162.75, 169.92 ppm. Elemental analysis: calcd for $C_{16}H_{18}N_2O_2$: C 71.09; H 6.71; N 10.36; found: C 71.39, H 6.56, N 6.96.

3-(2-Oxopyridin-1(2*H*)-yl)-*N*-(3-phenylpropyl)propanamide (9): yield: 33%. R_f =0.34 ($CHCl_3$/MeOH, 95:5). ^{1}H NMR (500 MHz, $CDCl_3$): δ = 1.72-1.78 (m, 2H,), 2.55 (t, *J* = 7.7 Hz, 2H), 2.67 (t, *J* = 6.1 Hz, 2H), 3.22 (q, *J* = 6.8 Hz, 2H), 4.21 (t, *J* = 6.1 Hz, 2H), 6.12 (td, *J* = 6.7, 0.8 Hz, 1H), 6.45 (bs, 1H), 6.49 (d, *J* = 9.1 Hz, 1H), 7.1-7.26 (m. 5H), 7.30 (ddd, J = 9.1, 6.7, 1.9 Hz, 1H), 7.43 (dd, *J* = 6.7, 1.5 Hz, 1H) ppm. ^{13}C NMR (125.73 MHz, $CDCl_3$): δ = 30.98, 33.14, 35.14, 39.18, 47.05, 106.11, 120.44, 125.94,

128.30, 128.39, 139.09, 140.05, 141.36, 162.79, 169.95 ppm. Elemental analysis: calcd for $C_{17}H_{20}N_2O_2$: C 71.81; H 7.09; N 9.85; found: C 71.45, H 7.21, N 9.73.

***N*-Cyclohexyl-3-(2-oxopyridin-1(2*H*)-yl)propanamide (10):** yield: 36%. R_f = 0.41 ($CHCl_3$/MeOH, 95:5). ^{1}H NMR (500 MHz, $CDCl_3$): δ = 0.98-1.83 (m, 10H), 2.67 (t, *J* = 6.1 Hz, 2H), 3.61-3.72 (m, 1H), 4.22 (t, *J* = 6.1 Hz, 2H), 6.07 (bs, 1H), 6.15 (td, *J* = 6.7, 1.2 Hz, 1H), 6.52 (d, *J* = 9.1 Hz, 1H), 7.34 (ddd, *J* = 9.1, 6.7, 2.0 Hz, 1H), 7.43 (dd, *J* = 6.7, 1.6 Hz, 1H) ppm. ^{13}C NMR (125.73 MHz, $CDCl_3$): δ = 24.78, 25.41, 32.89, 35.37, 47.19, 48.28, 105.97, 120.48, 139.08, 139.93, 162.78, 168.93 ppm. Elemental analysis: calcd for $C_{14}H_{20}N_2O_2$: C, 67.71; H, 8.12; N, 11.28; found: C 67.94, H 7.93, N 11.55.

***N*-Butyl-3-(2-oxopyridin-1(2*H*)-yl)propanamide (11):** yield: 57%. R_f = 0.37 ($CHCl_3$/MeOH, 95:5). ^{1}H NMR (500 MHz, $CDCl_3$): δ = 0.87 (t, *J* = 7.3 Hz, 3H), 1.21-1.30 (m, 2H), 1.37-1.44 (m, 2H), 2.70 (t, *J* = 6.1 Hz, 2H), 3.19 (q, *J* = 7.0, 2H), 4.23 (t, *J* = 6.1 Hz, 2H), 6.16 (td, *J* = 6.7, 1.1 Hz, 1H), 6.40 (bs, 1H), 6.50 (d, *J* = 9.1 Hz, 1H), 7.34 (ddd, *J* = 9.1, 6.7, 2.0 Hz, 1H), 7.45 (dd, *J* = 6.7, 1.6 Hz, 1H) ppm. ^{13}C NMR (125.73 MHz, $CDCl_3$): δ = 13.66, 19.93, 31.45, 35.14, 39.26, 47.10, 106.04, 120.43, 139.10, 139.97, 162.78, 169.87 ppm. Elemental analysis: calcd for $C_{12}H_{18}N_2O_2$: C 64.84; H 8.16; N 12.60; found: C 64.55, H 7.78, N 12.77.

Synthesis of carboxylic acids 63-64

(*R*)-1-(Methoxycarbonyl)-2-phenylethyl methanesulfonate (59) A solution of **57** (1.2 g, 6.6 mmol) in dry DCM was reacted with methanesulfonyl chloride (1.5 g, 13.2 mmol, 1.02 mL) and Et_3N (1.67 g, 16.5 mmol, 2.29 mL). The mixture was stirred at room temperature under nitrogen for 2 hours, then washed with water and dried (Na_2SO_4), filtered and evaporated under reduced pressure to afford **33** as a brown/yellow oil. Yield: 1.68 g (99%); R_f = 0.73 (light petroleum/EtOAc, 4:6). ^{1}H NMR (300 MHz, $CDCl_3$): δ = 2.77 (s, 3H), 3.12 (dd, *J* = 14.4, 8.8 Hz, 1H), 3.31 (dd, *J* = 14.4, 4.2 Hz, 1H), 3.80 (s, 3H), 5.18 (dd, *J* = 8.8, 4.2 Hz, 1H), 7.23-7.37 (m, 5H) ppm.

(*R*)-1-(Ethoxycarbonyl)-3-phenylpropyl methanesulfonate (60) According to the same procedure described for **59,** compound **58 (**1 g, 4.8 mmol, 0.930 mL) was reacted with methanesulfonyl chloride (1.01 g, 9.6 mmol, 0.74 mL) and Et_3N (1.21 g, 12 mmol, 1.67 mL) to give the title compound **60** as a brown/yellow oil. Yield: 1.4 g (99%); R_f = 0.77 (light petroleum/EtOAc, 4:6). ^{1}H NMR (300 MHz, $CDCl_3$): δ = 1.29 (t, *J* = 7.2 Hz, 3H), 2.18-2.30 (m, 2H), 2.75-2.83 (m, 2H) 3.17 (s, 3H), 4.23 (q, *J* = 7.2 Hz, 2H), 5.02 (dd, *J* = 7.8, 4.7 Hz, 1H), 7.17-7.35 (m, 5H) ppm.

(*S*)-Methyl 2-(2-oxopyridin-1(2*H*)-yl)-3-phenylpropanoate (61). To a suspension of NaH (311.7 mg, 7.8 mmol) in dry DMF, at 0 °C under N_2, a solution of pyridin-2(1*H*)-one **52** (741 mg, 7.8 mmol) in dry DMF was added via syringe. After stirring for 1h, (*R*)-1-(methoxycarbonyl)-2-phenylethyl methanesulfonate **59** (1.68 g, 6.5 mmol) was added to the mixture and the reaction was stirred overnight at room temperature. The reaction was then quenched with saturated NH_4Cl and the product was extracted with EtOAc. The combined organic layers were washed with brine, dried over Na_2SO_4, filtered and evaporated under reduced pressure. Column chromatography (light petroleum/EtOAc, 2:8) of the crude afforded compound **61** as white crystals. Yield**:** 869 mg (52%); R_f = 0.62 (light petroleum/EtOAc, 2:8). ^{1}H NMR (300 MHz, $CDCl_3$): δ = 3.33 (dd, *J* = 14.3, 10.0 Hz, 1H), 3.50 (dd, *J* = 14.3, 5.3 Hz, 1H), 3.73 (s, 3H), 5.29 (dd, *J* = 10.0, 5.3 Hz, 1H), 6.00 (td, *J* = 6.7, 1.3 Hz, 1H), 6.49 (dd, *J* = 9.4, 1.3 Hz, 1H), 6.95 (dd, *J* = 7.0, 1.8 Hz, 1H), 7.03-7.08 (m, 2H), 7.15-7.27 (m, 4H) ppm.

(*S*)-Ethyl 2-(2-oxopyridin-1(2*H*)-yl)-4-phenylbutanoate (62). The synthesis of ester **62** was carried out in agreement with the procedure described for compound **61**, by reacting pyridin-2(1*H*)-one **52** (799 mg, 8.4 mmol), NaH (336 mg, 8.4 mmol), and (*R*)-1-(ethoxycarbonyl)-3-phenylpropyl methanesulfonate **60** (2 g, 7 mmol). Consistency: yellow oil. Yield: 1.2 g (50%); R_f = 0.61 (light petroleum/EtOAc, 3:7). ^{1}H NMR (300 MHz, $CDCl_3$): δ = 1.24 (t, *J* = 7.1 Hz, 3H), 2.19-2.34 (m, 1H), 2.45-2.72 (m, 3H), 4.19 (q, *J* = 7.1 Hz, 2H), 5.50 (dd, *J* = 9.9, 4.5 Hz, 1H), 6.22 (td, *J* = 6.3, 1.3 Hz, 1H), 6.59 (dd, *J* = 9.1, 1.3 Hz, 1H), 7.10-7.39 (m, 7H) ppm.

(*S*)-2-(2-Oxopyridin-1(2*H*)-yl)-3-phenylpropanoic acid (63). A solution of ester **61** (275 mg, 1.07 mmol) in MeOH/H_2O/dioxane (1:1:1) at 0°C was treated with LiOH (128 mg, 5.34 mmol) and stirred for 12h. MeOH and dioxane was evaporated in vacuo and the aqueous solution was treated with 5% citric acid and extracted with EtOAc. The organic layer was dried over Na_2SO_4, filtered and concentrated to afford the acid **63** as a white powder. Yield: 240 mg (92%). ^{1}H NMR (300 MHz, CH_3OH-d_4): δ = 3.45 (dd, *J* = 14.2, 9.9 Hz, 1H), 3.59 (dd, *J* = 14.2, 5.2 Hz, 1H), 5.37 (dd, *J* = 9.9, 5.2 Hz, 1H), 6.18 (td, *J* = 6.6, 1.3 Hz, 1H), 6.45 (dd, *J* = 9.1, 1.3 Hz, 1H), 7.05-7.20 (m, 5H), 7.29-7.33 (m, 1H), 7.37-7.44 (m, 1H) ppm.

(*S*)-2-(2-Oxopyridin-1(2*H*)-yl)-4-phenylbutanoic acid (64). The synthesis of acid **64** was carried out in agreement with the procedure described for compound **63**, by reacting ester **62** (435 mg, 1.52 mmol) and LiOH (182 mg, 7.62 mmol). Consistency: white powder. Yield: 360 mg (89%). ^{1}H NMR (300 MHz, CH_3OH-d_4): δ = 2.35-2.48 (m, 1H), 2.49-2.64 (m, 3H), 5.30 (dd, *J* = 10.2, 4.1 Hz, 1H), 6.42 (td, *J* = 6.8, 1.3 Hz, 1H), 6.55 (dd, *J* = 8.7, 1.3 Hz, 1H), 7.11-7.29 (m, 5H), 7.53 (ddd, *J* = 8.9, 6.7, 2.0 Hz, 1H), 7.61 (dd, *J* = 6.8, 1.9 Hz, 1H) ppm.

General procedures for the synthesis of amides 12-18 and 19-25

The coupling reactions between the carboxylic acids **63-64** (1 equiv.) and the suitable amines (1.5 equiv.) were carried out as above described for compounds **2-11**. The final compounds were purified by column chromatography, using EtOAc/ light petroleum, 8:2 as eluent mixture.

(*S*)-2-(2-Oxopyridin-1(2*H*)-yl)-*N*,3-diphenylpropanamide (12): yield: 44%. R_f = 0.55 (EtOAc/light petroleum, 8:2). ^{1}H NMR (300 MHz, $CDCl_3$): δ = 3.19 (dd, *J* = 13.8, 7.5 Hz, 1H), 3.65 (dd, *J* = 13.8, 8.3 Hz, 1H), 6.04 (t, *J* = 7.8 Hz, 1H), 6.31 (td, *J* = 7.0, 1.3 Hz, 1H), 6.57 (dd, *J* = 9.1, 1.3 Hz, 1H), 7.02-7.50 (m, 11H), 7.71 (dd, *J* = 7.0, 1.5 Hz, 1H), 9.24 (bs, 1H) ppm. ^{13}C NMR: (75 MHz, $CDCl_3$): δ = 36.45, 63.76, 107.26, 119.95, 120.19, 124.45, 127.09, 128.69, 128.87, 129.12, 135.66, 137.63, 140.00, 142.78, 164.81, 166.72 ppm. Elemental analysis: calcd for $C_{20}H_{18}N_2O_2$: C 75.45; H 5.70; N 8.80; found: C 75.56, H 5.65, N 8.95.

(*S*)-*N*-Benzyl-2-(2-oxopyridin-1(2*H*)-yl)-3-phenylpropanamide (13): yield: 48%. R_f = 0.68 (EtOAc/ light petroleum, 9:1). ^{1}H NMR (300 MHz, $CDCl_3$): δ = 3.10 (dd, *J* = 13.5, 6.9 Hz, 1H), 3.52 (dd, *J* = 13.5, 9.1 Hz, 1H), 4.16 (dd, *J* = 15.0, 5.1 Hz, 1H), 4.48 (dd, *J* = 15.0, 6.6 Hz, 1H), 5.91 (t, *J* = 7.9 Hz, 1H), 6.25 (td, *J* = 7.0, 1.3 Hz, 1H), 6.33 (dd, *J* = 9.2, 1.3 Hz, 1H), 6.91-7.01 (m, 2H), 7.16-7.31 (m, 9H), 7.42 (bs, 1H), 7.76 (dd, *J* = 7.0, 1.3 Hz, 1H) ppm. ^{13}C NMR: (75 MHz, $CDCl_3$): δ = 37.03, 43.43, 53.79, 106.78, 120.02, 127.01, 127.26, 127.38, 128.51, 128.64, 129.24, 134.64, 137.53, 139.62, 141.70, 162.54, 168.51 ppm. Elemental analysis: calcd for $C_{21}H_{20}N_2O_2$: C 75.88; H 6.06; N 8.43; found: C 75.99, H 6.17, N 8.12.

(*S*)-2-(2-Oxopyridin-1(2*H*)-yl)-*N*-phenethyl-3-phenylpropanamide (14): yield: 92%. R_f = 0.63 (EtOAc/ light petroleum, 9:1). ^{1}H NMR (300 MHz, $CDCl_3$): δ = 2.54-2.73 (m, 2H), 3.06 (dd, *J* = 13.7, 7.2 Hz, 1H), 3.24-3.37 (m, 1H), 3.39-3.53 (m, 2H), 5.80 (t, *J* = 7.9 Hz, 1H), 6.22 (td, *J* = 7.0, 1.4 Hz, 1H), 6.39 (dd, *J* = 9.1, 0.8 Hz, 1H), 6.93-7.01 (m, 2H), 7.10 (bs, 1H), 7.13-7.35 (m, 9H), 7.69 (dd, *J* = 7.0, 1.8 Hz, 1H) ppm. ^{13}C NMR: (75 MHz, $CDCl_3$): δ = 35.37, 36.99, 40.92, 57.71, 106.68, 120.04, 126.34, 127.00, 128.48, 128.60, 128.64, 129.22, 134.67, 135.98, 138.66, 139.59, 162.45, 168.54 ppm. Elemental analysis: calcd for $C_{22}H_{22}N_2O_2$: C 76.28; H 6.40; N 8.09; found: C 76.20, H 6.12, N 8.29.

(*S*)-2-(2-Oxopyridin-1(2*H*)-yl)-3-phenyl-*N*-(3-phenylpropyl)propanamide (15): yield: 84%. R_f = 0.64 (EtOAc/ light petroleum, 9:1). ^{1}H NMR (300 MHz, $CDCl_3$): δ = 1.61-1.73 (m, 2H), 2.44 (t, *J* = 8.4 Hz, 2H), 3.02-3.14 (m, 2H), 3.17-3.29 (m, 1H), 3.50 (dd, *J* = 13.6, 8.8 Hz, 1H), 5.84 (dd, *J* = 8.4, 7.5 Hz, 1H), 6.24 (td, *J* = 7.0, 1.4 Hz, 1H), 6.47 (dd, *J* = 9.1, 0.8 Hz, 1H), 6.99-7.36 (m, 12H), 7.73 (dd, *J* = 7.0, 1.8 Hz, 1H) ppm. ^{13}C NMR: (75 MHz, $CDCl_3$): δ = 30.76, 32.88, 36.88, 39.06, 57.80, 106.76, 120.02, 125.90, 127.01, 128.35, 128.60, 129.16, 134.69, 135.92, 139.69, 141.30, 143.72, 162.57, 168.55 ppm. Elemental analysis: calcd for $C_{23}H_{24}N_2O_2$: C 76.64; H 6.71; N 7.77; found: C 76.50, H 6.83, N 7.40.

(*S*)-*N*-Cyclohexyl-2-(2-oxopyridin-1(2*H*)-yl)-3-phenylpropanamide (16): yield: 65%. R_f = 0.64 (EtOAc/ light petroleum, 9:1). ^{1}H NMR (300 MHz, $CDCl_3$): δ = 0.90-

1.79 (m, 10H), 3.09 (dd, *J* = 13.6, 7.0 Hz, 1H), 3.48 (dd, *J* = 13.6, 8.9 Hz, 1H), 3.55-3.71 (m, 1H), 5.78 (dd, *J* = 8.9, 7.0 Hz, 1H), 6.24 (td, *J* = 7.0, 1.4 Hz, 1H), 6.50 (dd, *J* = 9.1, 1.4 Hz, 1H), 6.66 (bs, 1H), 7.14-7.36 (m, 6H), 7.75 (dd, *J* = 7.0, 1.7 Hz, 1H) ppm. ^{13}C NMR: (75 MHz, $CDCl_3$): δ = 24.57, 25.36, 32.38, 32.52, 37.14, 48.40, 106.55, 119.98, 126.94, 128.55, 129.18, 134.73, 135.95, 139.54, 162.48, 167.54 ppm. Elemental analysis: calcd for $C_{20}H_{24}N_2O_2$: C 74.04; H 7.46; N 8.64; found: C 74.25, H 7.30, N 8.75.

(*S*)-*N*-Butyl-2-(2-oxopyridin-1(2*H*)-yl)-3-phenylpropanamide (17): yield: 47%. R_f = 0.60 (EtOAc/ light petroleum, 9:1). ^{1}H NMR (300 MHz, $CDCl_3$): δ = 0.82 (t, *J* = 7.3 Hz, 3H), 1.06-1.21 (m, 2H), 1.22-1.38 (m, 2H), 2.98-3.13 (m, 2H), 3.14-3.26 (m, 1H), 3.52 (dd, *J* = 13.6, 8.9 Hz, 1H), 5.78 (t, *J* = 7.9 Hz, 1H), 6.25 (td, *J* = 7.0, 1.2 Hz, 1H), 6.52 (dd, *J* = 9.1, 1.2 Hz, 1H), 6.67 (bs, 1H), 7.14-7.35 (m, 6H), 7.69 (dd, *J* = 7.0, 1.8 Hz, 1H) ppm. ^{13}C NMR: (75 MHz, $CDCl_3$): δ = 13.64, 19.77, 31.13, 36.70, 39.26, 57.83, 106.73, 120.07, 126.98, 128.60, 129.13, 134.54, 135.91, 139.62, 162.60, 168.38 ppm. Elemental analysis: calcd for $C_{18}H_{22}N_2O_2$: C 72.46; H 7.43; N 9.39; found: C 72.06, H 7.54, N 9.31.

(*S*)-*N*-Isopentyl-2-(2-oxopyridin-1(2*H*)-yl)-3-phenylpropanamide (18): yield: 69%. R_f = 0.57 (EtOAc/ light petroleum, 9:1). ^{1}H NMR (300 MHz, $CDCl_3$): δ = 0.80 (d, *J* = 6.5 Hz, 6H), 1.17-1.42 (m, 3H), 2.99-3.28 (m, 3H), 3.51 (dd, *J* = 13.6, 8.9 Hz, 1H), 5.78 (t, *J* = 7.9 Hz, 1H), 6.26 (td, *J* = 6.9, 1.2 Hz, 1H), 6.53 (dd, *J* = 9.1, 1.2 Hz, 1H), 6.78 (bs, 1H), 7.14-7.38 (m, 6H), 7.73 (dd, *J* = 6.9, 1.8 Hz, 1H) ppm. ^{13}C NMR: (75 MHz, $CDCl_3$): δ = 22.34, 25.50, 36.85, 37.86, 39.37, 51.45, 106.87, 120.02, 126.98, 128.58, 129.13, 134.63, 135.85, 139.69, 162.60, 168.34 ppm. Elemental analysis: calcd for $C_{19}H_{24}N_2O_2$: C 73.05; H 7.74; N 8.97; found: C 73.25, H 7.85, N 8.70.

(*S*)-2-(2-Oxopyridin-1(2*H*)-yl)-*N*,4-diphenylbutanamide (19): yield: 50%. R_f = 0.72 (EtOAc/ light petroleum, 8:2). ^{1}H NMR (300 MHz, $CDCl_3$): δ = 2.14-2.30 (m, 1H), 2.57-2.77 (m, 3H), 5.61 (t, *J* = 7.4 Hz, 1H), 6.31 (td, *J* = 6.8, 1.4 Hz, 1H), 6.66 (d, *J* = 9.2 Hz, 1H), 7.10 (t, *J* = 7.4 Hz, 1H), 7.13-7.24 (m, 3H), 7.25-7.35 (m, 4H), 7.39 (ddd, *J* = 8.9, 6.6, 2.0 Hz, 1H), 7.50-7.58 (m, 3H), 9.11 (bs, 1H) ppm. ^{13}C NMR: (75 MHz, $CDCl_3$): δ = 32.07, 44.13, 47.01, 101.50, 110.00, 119.90, 120.45, 121.81, 128.40, 128.63, 128.96,

136.31, 139.95, 140.07, 142.35, 165.12, 166.54 ppm. Elemental analysis: calcd for $C_{21}H_{20}N_2O_2$: C 75.88; H 6.06; N 8.43; found: C 75.56, H 6.016, N 8.58.

(*S*)-*N*-Benzyl-2-(2-oxopyridin-1(2*H*)-yl)-4-phenylbutanamide (20): yield: 95%. R_f = 0.63 (EtOAc/ light petroleum, 8:2). ^{1}H NMR (300 MHz, $CDCl_3$): δ = 2.07-2.24 (m, 1H), 2.43-2.71 (m, 3H), 4.30 (dd, *J* = 14.8, 5.3 Hz, 1H), 4.51 (dd, *J* = 14.8, 6.0 Hz, 1H), 5.60 (t, *J* = 7.7 Hz, 1H), 6.26 (td, *J* = 6.8, 1.4 Hz, 1H), 6.48 (d, *J* = 9.2 Hz, 1H), 7.08-7.36 (m, 11H), 7.43 (bs, 1H), 7.59 (dd, *J* = 6.8, 1.8 Hz, 1H) ppm. ^{13}C NMR: (75 MHz, $CDCl_3$): δ = 32.04, 32.42, 43.58, 56.29, 107.00, 120.14, 126.32, 127.42, 127.55, 128.35, 128.55, 128.64, 134.31, 137.77, 139.68, 140.24, 162.77, 168.92 ppm. Elemental analysis: calcd for $C_{22}H_{22}N_2O_2$: C 76.28; H 6.40; N 8.09; found: C 76.01, H 6.35, N 8.19.

(*S*)-2-(2-Oxopyridin-1(2*H*)-yl)-*N*-phenethyl-4-phenylbutanamide (21): yield: 92%. R_f = 0.56 (EtOAc/ light petroleum, 8:2). ^{1}H NMR (300 MHz, $CDCl_3$): δ = 1.98-2.15 (m, 1H), 2.39-2.66 (m, 3H), 2.68-2.85 (m, 2H), 3.38-3.56 (m, 2H), 5.43 (t, *J* = 7.8 Hz, 1H), 6.31 (td, *J* = 6.8, 1.4 Hz, 1H), 6.55 (dd, *J* = 9.2, 1.4 Hz, 1H), 6.84 (bs, 1H), 7.02-7.38 (m, 11H), 7.50 (dd, *J* = 6.8, 1.4 Hz, 1H) ppm.^{13}C NMR: (75 MHz, $CDCl_3$): δ = 32.00, 32.09, 35.48, 40.77, 56.63, 106.96, 120.27, 126.31, 126.45, 127.5, 128.34, 128.54, 128.64, 134.09, 138.52, 139.57, 140.27, 162.69, 168.81 ppm. Elemental analysis: calcd for $C_{23}H_{24}N_2O_2$: C 76.64; H 6.71; N 7.77; trov: C 76.34, H 6.81, N 7.50.

(*S*)-2-(2-Oxopyridin-1(2*H*)-yl)-4-phenyl-*N*-(3-phenylpropyl)butanamide (22): yield: 67%. R_f = 0.53 (EtOAc/ light petroleum, 8:2). ^{1}H NMR (300 MHz, $CDCl_3$): δ = 1.68-1.88 (m, 2H), 2.06-2.22 (m, 1H), 2.41-2.74 (m, 5H), 3.10-3.33 (m, 2H), 5.48 (t, *J* = 7.7 Hz, 1H), 6.26 (td, *J* = 6.8, 1.4 Hz, 1H), 6.58 (dd, *J* = 9.2, 1.4 Hz, 1H), 6.93 (bs, 1H), 7.03-7.41 (m, 11H), 7.55 (dd, *J* = 6.8, 2.1 Hz, 1H) ppm. ^{13}C NMR: (75 MHz, $CDCl_3$): δ = 31.98, 30.99, 32.04, 33.04, 39.12, 56.45, 107.08, 120.24, 125.97, 126.36, 128.37, 128.43, 128.57, 130.81, 134.14, 139.72, 140.26, 140.91, 165.48, 168.86 ppm. Elemental analysis: calcd for $C_{24}H_{26}N_2O_2$: C, 76.98; H, 7.00; N, 7.48; found: C 76.68, H 7.32, N 7.28.

(*S*)-*N*-Cyclohexyl-2-(2-oxopyridin-1(2*H*)-yl)-4-phenylbutanamide (23): yield: 89%. R_f = 0.56 (EtOAc/ light petroleum, 8:2). ^{1}H NMR (300 MHz, $CDCl_3$): δ = 0.97-

1.80 (m, 10H), 2.03-2.24 (m, 1H), 2.38-2.72 (m, 3H), 3.58-3.78 (m, 1H), 5.47 (t, *J* = 7.4 Hz, 1H), 6.24 (td, *J* = 6.8, 1.4 Hz, 1H), 6.58 (dd, *J* = 9.2, 1.4 Hz, 1H), 6.65 (bs, 1H), 7.09-7.41 (m, 6H), 7.57 (dd, *J* = 6.8, 1.8 Hz, 1H) ppm. ^{13}C NMR: (75 MHz, $CDCl_3$): δ = 24.70, 25.40, 32.06, 32.56, 32.81, 48.48, 56.35, 106.84, 120.07, 126.28, 128.34, 128.52, 134.38, 139.60, 140.36, 162.69, 167.91 ppm. Elemental analysis: calcd for $C_{21}H_{26}N_2O_2$: C 74.52; H 7.74; N 8.28; found: C 74.59, H 7.60, N 8.39.

(*S*)-*N*-Butyl-2-(2-oxopyridin-1(2*H*)-yl)-4-phenylbutanamide (24): yield: 51%. R_f = 0.57 (EtOAc/ light petroleum, 8:2). ^{1}H NMR (300 MHz, $CDCl_3$): δ = 0.87 (t, *J* = 7.2 Hz, 3H), 1.18-1.35 (m, 2H), 1.37-1.54 (m, 2H), 2.03-2.21 (m, 1H), 2.40-2.72 (m, 3H), 3.05-3.34 (m, 2H), 5.53 (t, *J* = 7.6 Hz, 1H), 6.26 (td, *J* = 6.7, 1.4 Hz, 1H), 6.57 (dd, *J* = 9.2, 1.4 Hz, 1H), 6.95 (bs, 1H), 7.07-7.41 (m, 6H), 7.59 (dd, *J* = 6.7, 1.8 Hz, 1H) ppm. ^{13}C NMR: (75 MHz, $CDCl_3$): δ =13.70, 19.97, 31.30, 32.06, 32.65, 39.34, 56.25, 106.88, 119.99, 126.26, 128.32, 128.51, 134.50, 139.68, 140.35, 162.72, 168.87 ppm. Elemental analysis: calcd for $C_{19}H_{24}N_2O_2$: C 73.05; H 7.74; N 8.97; found: C 72.95, H 7.85, N 8.81.

(*S*)-*N*-Isopentyl-2-(2-oxopyridin-1(2*H*)-yl)-4-phenylbutanamide (25): yield: 37%. R_f = 0.55 (EtOAc/ light petroleum, 8:2). ^{1}H NMR (300 MHz, $CDCl_3$): δ = 0.86 (d, *J* = 6.6 Hz, 6H), 1.16-1.46 (m, 3H), 2.04-2.25 (m, 1H), 2.40-2.73 (m, 3H), 3.09-3.35 (m, 2H), 5.44 (t, *J* = 7.6 Hz, 1H), 6.25 (td, *J* = 6.7, 1.3 Hz, 1H), 6.59 (dd, *J* = 9.2, 1.4 Hz, 1H), 6.76 (bs, 1H), 7.06-7.43 (m, 6H), 7.59 (dd, *J* = 6.7, 1.8 Hz, 1H) ppm. ^{13}C NMR: (75 MHz, $CDCl_3$): δ =22.35, 22.40, 25.77, 32.03, 32.27, 37.98, 38.04, 56.34, 107.08, 120.13, 126.31, 128.34, 128.54, 134.25, 139.72, 140.27, 162.80, 168.72 ppm. Elemental analysis: calcd for $C_{20}H_{26}N_2O_2$: C 73.59; H 8.03; N 8.58; found: C 73.79, H 8.24, N 8.41.

Synthesis of amides 27-33

(2*E*)-Methyl 4-(6,7-dimethoxy-1-oxoisoquinolin-2(1*H*)-yl)but-2-enoate (66)

A suspension of NaH (70.1mg, 2.92 mmol) in dry DMF, at 0 ºC under N_2, was treated with a solution of 6,7-dimethoxyisoquinolin-1(2*H*)-one **65** (500mg, 2.43 mmol) in dry DMF. After 1h, methyl 4-bromocrotonate (0.4 mL, 3.41 mmol) was added to the mixture and the reaction was stirred for 12h at room temperature. The reaction was then quenched with saturated NH_4Cl and the product was extracted with $CHCl_3$. The

combined organic layers were washed with water and NaCl, dried over Na_2SO_4, filtered and concentrated *in vacuo*. The crude was purified by column chromatography (light petroleum/EtOAc, 3:7), to give compound **66** as a yellow oil. Yield: 75 % (552 mg); R_f = 0.56 (EtOAc). ^{1}H NMR (300 MHz, $CDCl_3$): δ = 3.69 (s, 3H), 3.97 (s, 3H), 3.98 (s, 3H), 4.78 (dd, *J* = 4.7 Hz and 1.8 Hz, 2H), 5.78 (d, *J* = 15.8 Hz, 1H), 6.36-6.47 (m, 1H), 6.82-7.09 (m, 3H), 7.78 (s, 1H) ppm.

(2*E*)-4-(6,7-Dimethoxy-1-oxoisoquinolin-2(1*H*)-yl)but-2-enoic acid (67)

A solution of ester **66** (255 mg, 0.84 mmol) in MeOH/H_2O/Dioxane (1:1:1) at 0°C was treated with LiOH (60.4 mg, 2.52 mmol) and stirred overnight. The reaction was concentrated *in vacuo* and the residue was treated with 10% citric acid and extracted with EtOAc. The organic layer was dried over Na_2SO_4, filtered and concentrated to give the acid **67** as a white solid. Yield: 162.8 mg (67 %). ^{1}H NMR (500 MHz, acetone-d_6): δ = 3.93 (s, 3H), 3.94 (s, 3H), 4.86 (dd, *J* = 5.1 Hz and 1.7 Hz, 2H), 5.77 (d, *J* = 15.8 Hz, 1H), 6.35-6.46 (m, 1H), 6.80-7.07 (m, 3H), 7.80 (s, 1H) ppm.

General procedure for the synthesis of compounds 27-33

The coupling reactions between the carboxylic acid (**67**) (1 equiv.) and the suitable amines (1.5 equiv.) were carried out by dissolving compound **67** in dry DMF, then cooling to 0°C and adding HATU (1.5 equiv.). After 10 minutes, DIPEA (2 equiv.) and the suitable amine solubilized in DMF were added dropwise, and the mixture was stirred at room temperature overnight. The organic layer was washed with brine, dried over Na_2SO_4, filtered and concentrated under reduced pressure. The crude residue were purified by column chromatography, using appropriate eluent mixtures.

(2*E*)-4-(6,7-Dimethoxy-1-oxoisoquinolin-2(1*H*)-yl)-*N*-phenylbut-2-enamide (27)

Yield: 39 %. R_f = 0.34($CHCl_3$/Acetone, 9:1). ^{1}H NMR (300 MHz, $CDCl_3$): δ = 3.95 (s, 3H), 3.98 (s, 3H), 4.81 (dd, *J* = 4.7 Hz and 1.8 Hz, 2H), 5.92 (d, *J* = 15.2 Hz, 1H), 6.43-6.50 (m, 1H), 6.84 (bs, NH), 6.96 (d, *J* = 7.6 Hz, 1H), 7.02-7.12 (m, 2H), 7.24-7.33 (m, 3H), 7.49-7.56 (m, 2H), 7.70 (s, 1H) ppm. ^{13}C NMR (125.73 MHz, $CDCl_3$): δ = 46.6, 56.1, 111.5, 112.0, 112.5, 121.3, 121.8, 122.4, 123.9, 124.1, 128.7, 129.0, 135.7, 143.5,

149.1, 153.5, 156.2, 166.4 ppm. Elemental analysis: calcd for $C_{21}H_{20}N_2O_4$: C 69.22; H 5.53; N 7.69; found: C 69.32; H 5.20; N 7.80.

(2*E*)-*N*-Benzyl-4-(6,7-dimethoxy-1-oxoisoquinolin-2(1*H*)-yl)but-2-enamide (28)

Yield: 36 %. R_f = 0.38 (EtOAc). ^{1}H NMR (300 MHz, $CDCl_3$): δ = 3.95 (s, 3H), 3.96 (s, 3H), 4.45 (s, 2H), 4.72 (dd, *J* = 4.7 Hz and 1.8 Hz, 2H), 5.75 (d, *J* = 15.2 Hz, 1H), 6.08 (bs, NH), 6.40-6.46 (m,1H), 6.80-7.00 (m, 2H), 7.02-7.10 (m, 1H), 7.19-7.36 (m, 5H), 7.71 (s, 1H) ppm. ^{13}C NMR (125.73 MHz, $CDCl_3$): δ = 44.3, 46.2, 56.4, 111.9, 111.5, 112.3, 121.4, 122.8, 123.7, 126.5, 127.2, 128.5, 129.1, 141.7, 143.6, 149.5, 153.7, 156.1, 166.7 ppm. Elemental analysis: calcd for $C_{22}H_{22}N_2O_4$: C 69.83; H 5.86; N 7.40; found: C 69.71; H 5.99; N 7.20.

(2*E*)-4-(6,7-Dimethoxy-1-oxoisoquinolin-2(1*H*)-yl)-*N*-phenethylbut-2-enamide (29)

Yield: 35 %. R_f = 0.34 ($CHCl_3$/Acetone, 8:2). ^{1}H NMR (300 MHz, $CDCl_3$): δ = 2.80 (t, *J* = 7.0 Hz, 2H), 3.46-3.61 (m, 2H), 3.98 (s, 3H), 3.99 (s, 3H), 4.74 (dd, *J* = 4.7 Hz and 1.8 Hz, 2H), 5.71 (d, *J* = 15.2 Hz, 1H), 5.73 (bs, NH), 6.39-6.47 (m, 1H), 6.82-6.94 (m, 3 H), 7.11-7.32 (m, 5H), 7.73 (s, 1 H) ppm. ^{13}C NMR (125.73 MHz, $CDCl_3$): δ = 35.9, 40.2, 46.7, 56.5, 111.9, 111.8, 112.9, 121.2, 122.5, 123.7, 126.2, 127.8, 128.7, 128.9, 139.4, 143.1, 149.7, 153.1, 156.3, 166.5 ppm. Elemental analysis: calcd for $C_{23}H_{24}N_2O_4$: C 70.39; H 6.16; N 7.14; found: C 70.59; H 6.37; N 6.90.

(2*E*)-4-(6,7-Dimethoxy-1-oxoisoquinolin-2(1*H*)-yl)-*N*-(3-phenylpropyl)but-2-enamide (30)

Yield: 48 %. R_f = 0.43 ($CHCl_3$/Acetone, 8:2). ^{1}H NMR (300 MHz, $CDCl_3$): δ = 1.80 (t, *J* = 7.1 Hz, 2H), 2.61 (t, *J* = 7.5 Hz, 2H), 3.23-3.35 (m, 2 H), 3.95 (s, 3H), 3.97 (s, 3H), .4.73 (dd, *J* = 4.7 Hz and 1.8 Hz, 2H), 5.70 (d, *J* = 15.2 Hz, 1H), 5.83 (bs, NH), 6.39-6.46 (m, 1H), 6.80-6.94 (m, 3H), 7.07-7.28 (m, 5H), 7.72 (s, 1H) ppm. ^{13}C NMR (125.73 MHz, $CDCl_3$): δ = 29.3, 33.4, 40.2, 46.7, 56.2, 111.9, 112.1, 112.8, 121.0, 122.8, 123.9, 126.3, 128.4, 128.6, 128.9, 138.7, 143.6, 149.3, 153.4, 156.7, 166.6 ppm. Elemental analysis: calcd for $C_{24}H_{26}N_2O_4$: C, 70.92; H, 6.45; N, 6.89; found: C 70.63, H 6.62, N 6.70.

(2*E*)-*N*-Cyclohexyl-4-(6,7-dimethoxy-1-oxoisoquinolin-2(1*H*)-yl)but-2-enamide (31)

Yield: 36 %. R_f = 0.44 ($CHCl_3$/Acetone, 8:2). ^1H NMR (300 MHz, $CDCl_3$): δ = 0.98-1.20 (m, 5H), 1.53-1.77 (m, 5H), 3.64-3.83 (m, 1H), 3.98 (s, 3H), 3.99 (s, 3H), 4.75 (dd, *J* = 4.7 Hz and 1.8 Hz, 2H), 5.47 (d, *J* = 8.2 Hz, NH) 5.70 (d, *J* = 15.2, 1H), 6.39-6.47 (m, 1H), 6.81-6.96 (m, 3H), 7.76 (s, 1H) ppm. ^{13}C NMR (125.73 MHz, $CDCl_3$): δ = 22.9, 28.3, 33.4, 46.7, 47.9, 56.2, 111.7, 111.8, 112.8, 121.5, 122.9, 123.5, 129.1, 143.2, 149.2, 153.3, 156.6, 165.7 ppm. Elemental analysis: calcd for $C_{21}H_{26}N_2O_4$: C 68.09; H7.07; N 7.56; found: C 68.30; H 6.90; N 6.45.

(2*E*)-*N*-Butyl-4-(6,7-dimethoxy-1-oxoisoquinolin-2(1*H*)-yl)but-2-enamide (32)

Yield: 37 % R_f =0.38 ($CHCl_3$/Acetone, 8:2). ^1H NMR (300 MHz, $CDCl_3$): δ = 0.88 (t, *J* = 7.0 Hz, 3H), 1.16-1.37 (m, 2H), 1.38-1.55 (m, 2H), 3.15-3.33 (m, 2H), 3.98 (s, 3H), 3.99 (s, 3H), 4.75 (dd, *J* = 4.7 Hz and 1.8 Hz, 2H), 5.65 (bs, NH), 5.72 (d, *J* = 15.2 Hz, 1H), 6.40-6.47 (m, 1H), 6.82-6.96 (m, 3H), 7.76 (s, 1H) ppm. ^{13}C NMR (125.73 MHz, $CDCl_3$): δ = 13.5, 19.9, 32.5, 40.8, 46.6, 56.4, 111.7, 111.8, 112.8, 121.0, 122.9, 123.9, 128.9, 143.2, 149.4, 153.7, 156.4, 166.9 ppm. Elemental analysis: calcd for $C_{19}H_{24}N_2O_4$: C 66.26; H 7.02; N 8.13; found: C 68.40; H 7.41; N 8.01.

(2*E*)-*N*-Isopentyl-4-(6,7-dimethoxy-1-oxoisoquinolin-2(1*H*)-yl)but-2-enamide (33)

Yield: 34 %. R_f = 0.67 ($CHCl_3$/CH_3OH, 9:1). ^1H NMR (300 MHz, $CDCl_3$): δ = 0.91 (d, *J* = 6.6 Hz, 6H), 1.52-1.67 (m, 2H), 1.80-1.86 (m, 1H), 3.20-3.34 (m, 2H), 3.98 (s, 3H), 3.99 (s, 3H), 4.30 (dd, *J* = 8.5 Hz and 2.1 Hz, 2H), 5.36 (bs, NH), 5.71 (d, *J* = 15.2 Hz, 1H), 6.45-6.51 (m, 1H), 6.87 (s, 1H), 7.25-7.30 (m, 2H), 7.78 (s, 1H) ppm. ^{13}C NMR (125.73 MHz, $CDCl_3$): δ = 22.9, 25.7, 37.9, 39.7, 46.2, 56.2, 111.7, 111.8, 112.6, 121.6, 122.9, 123.5, 128.9, 143.7, 149.1, 153.8, 156.9, 166.4 ppm. Elemental analysis: calcd for $C_{20}H_{26}N_2O_4$: C, 67.02; H, 7.31; N, 7.82; found: C 66.80, H 7.10, N 8.03.

4.2 Biological activity

In vitro 20S immunoproteasome/proteasome inhibition assays

Human 20S immunoproteasome, obtained from human spleen, and human 20S proteasome, isolated from human erythrocytes, were purchased from Enzo Life Science. The hydrolysis of the appropriate peptidyl 7-amino-4-methyl-coumarin substrate was monitored to measure the different proteolytic activities of both proteasome and immunoproteasome. The substrates Suc-Leu-Leu-Val-Tyr-AMC (Bachem) for β5c-β5i, Boc-Leu-Arg-Arg-AMC (Bachem) for β2c-β2i, Z-Leu-Leu-Glu-AMC (Adipogen) for β1c and Ac-Pro-Ala-Leu-AMC (Biomol GmbH) for β1i subunits were employed at 50 μM, with the exception of Z-Leu-Leu-Glu-AMC (80 μM). Fluorescence of the product AMC of the substrate hydrolyses was measured at 30°C with a 380 nm excitation filter and a 460 nm emission filter, using an Infinite 200 PRO microplate reader (Tecan, Männedorf, Switzerland). A preliminary screening at 50 μM inhibitor concentrations was carried out on the three proteolytic activities of proteasome and immunoproteasome; an equivalent amount of DMSO as a negative control and MG-132, a reversible inhibitor of proteasome and immunoproteasome, as positive control were employed. Compounds showing at least 60% inhibition at the screening concentration were then progressed into detailed assays. Continuous assays were performed at seven different concentrations ranging from those that minimally inhibited to those that fully inhibited each proteolytic activity to calculate the dissociation constants K_i of the enzyme-inhibitor complex by means of the Cheng-Prusoff equation $K_i = IC_{50}/(1 + [S]\ K_m^{-1})$. Inhibitor solutions were prepared from stocks in DMSO. Each independent assay was performed in duplicate in 96-well-plates in a total volume of 200 μL. For the assay on β5i, β1i, β1c and β5c subunits, human 20S immunoproteasome or human 20S proteasome was incubated at 30°C obtaining a final concentration of 0.004 mg/mL with the inhibitor at seven different concentrations. The reaction buffer comprised: 50 mM Tris HCl, pH 7.4, 25 mM KCl, 10 mM NaCl, 1 mM $MgCl_2$, 0.03% SDS. AMC released from substrate hydrolysis was monitored in kinetic cycle over a period of 10 min. For the assay on β2i and β2c subunits, final concentration of immunoproteasome or proteasome was of 0.0025 mg/mL. The reaction buffer comprised: 50 mM Tris HCl, pH 7.4, 0.5 mM EDTA III, 50 mM NaCl, 0.03% SDS.

4.3 Docking studies

Protein and ligand preparation

Since the only available crystal structures of the human i20S are yeast chimera that incorporate key parts of human β5i and the neighboring β6 subunit but are devoid of the β1i subunit,[98] we employed the crystal structure of the murine i20S in complex with the inhibitor PR-957 (PDB ID: 3UNF)[7] for docking studies. Murine and human 20S subunits share a sequence identity of more than 90%, and the few non-identical residues are external to the active sites.

For docking purpose, we selected the catalytic subunits β1i (LMP2, *PSMB9*)/β2i (MECL-1, *PSMB10*) and β5i (LMP7, *PSMB8*)/β6i. The crystal structure of PR-957 bound to β1i revealed two well-defined water molecules within the S3 pocket, which coordinate a tight H-bond network between β1i-A50N, β2i-S118O$^{\gamma}$ and the carbonyl oxygen and the amide nitrogen of PR-957 P3 alanine, respectively. Accordingly, the intervening water molecules were included in the docking experiments. The protein setup was carried out using the Protein Preparation Wizard implemented in Maestro 11.3 (Schrödinger, LLC, New York, NY, 2018). Hydrogen atoms were added to the protein consistent with the neutral physiologic pH. Arginine and lysine side chains were considered as cationic at the guanidine and ammonium groups, and the aspartic and glutamic residues were considered as anionic at the carboxylate groups. The protonation and flip states of the imidazole rings of the histidine residues were adjusted together with the side chain amides of glutamine and asparagine residues in a H-bonding network optimization process. Successively, the protein hydrogen atoms only were minimized using the Impref module of Impact with the OPLS_2005 force field.

Initial coordinates of compounds **1**, **7**, **13** and **21** were constructed by using the Molecular Builder module in Maestro. The structures were energy-minimized using Macromodel 10.8 (Schrödinger, LLC, New York, NY, 2018) using the MMFF force field with the steepest descent (1000 steps) followed by truncated Newton conjugate gradient (500 steps) methods. Partial atomic charges were computed using the OPLS-AA force field.

Molecular docking

Docking of compounds **1**, **7**, **13** and **21** into the active site of β1i or β5i was performed with the genetic algorithm implemented in GOLD 5.5 (CCDC Software Limited:

Cambridge, U.K., 2008).[93] The coordinates of the cocrystallized ligand PR-957, in β1i and β5i respectively, were chosen as active-site origin. The active-site radius was set equal to 10 Å. Explicit water molecules were allowed to toggle on or off during the individual docking runs (i.e., these waters were not automatically present in the binding site, but were included if their presence strengthened the interaction of the ligand with the receptor, as determined by the scoring function).[99] Orientation mode of water hydrogen atoms was set to "spin". We adopted all the program default parameters: for each molecule tested the number of islands was set to 5, population size to 100, number of operations was 100,000 with a selective pressure of 1.1. For these experiments, the number of GA runs was set to 200 without the option of early termination, and scoring of the docked poses was performed with the original ChemPLP scoring function rescoring with ChemScore.[100] The final receptor-ligand complex for each ligand was chosen interactively by selecting the highest scoring pose that was consistent with the experimentally derived information about the binding mode of the ligand. Figures were prepared using Pymol (Schrödinger, LLC, New York, NY, 2018). All computations were performed on an E4 Computer Engineering E1080 workstation provided with an Intel Xeon processor.

5. DESIGN, SYNTHESIS AND BIOLOGICAL EVALUATION OF NOVEL RHODESAIN INHIBITORS FOR THE TREATMENT OF HUMAN AFRICAN TRYPANOSOMIASIS

5.1 Introduction

Human African Trypanosomiasis (HAT), commonly named sleeping sickness, is an endemic parasitic disease caused by two subspecies of *Trypanosoma*, *T. brucei gambiense* and *T. brucei rhodesiense.* It affects 36 countries of sub-Saharan Africa, where it represents an important cause of morbidity and mortality, especially in the rural areas, in spite of the significant decrease in the number of new reported cases over the last years by the World Health Organization.[19]

HAT is transmitted by the bite of the blood-feeding tsetse fly of '*Glossina*' genus; the disease mostly affects poor and rural areas of Africa, whereas travellers can also be infected when visiting regions in which the insect is spread. If left untreated, it is usually lethal.

Trypanosoma brucei gambiense and *rhodesiense* are both spread in Africa, according to the weather conditions: *T. b. gambiense* is spread in western and central Africa (24 countries), while *T. b. rhodesiense* is more diffused in eastern and southern Africa (13 countries). Both subspecies find a favourable weather in Uganda; both infect humans and animals but men are the main target of *T. b. gambiense*, while antelopes represent the main target of *T. b. rhodesiense.*[101]

T. b. gambiense, which cause 98% of deaths by sleeping sickness, is responsible for the chronic form of the disease, not easily detectible. Typically, the symptoms appear when the central nervous system has already been compromised and the stage of the disease is advanced. *T. b. rhodesiense* is responsible for the remaining 2% of deaths, it rapidly invades the central nervous system[102] causing the acute form of the disease whose symptoms can be observed in a few months or weeks.

5.2 The protozoan

The two subspecies of *T. brucei* share similar properties and structural features. They are unicellular eukaryotic organisms characterized by the presence of variant surface glycoproteins (VSGs) on the external cell membrane. The VSGs are dimeric proteins (60kD) with a density equal to 107 molecules per parasite, anchored to the plasma membrane by means of glycosylphosphatidylinositol (GPI).[103] The *C*-terminus is linked

to the cell membrane while the free *N*-terminus contains the variable regions responsible for the activation of the host's immune system, which result in the development of antibodies against the pathogen. In order to evade the immune system, the parasites have developed the ability to vary the antigenic portions of the surface, thus preventing the activation of the immune response.[104]

The protozoa protoplasm contains the nucleus, the endoplasmic reticulum, the deposit granules, contractile and digestive vacuoles, the mitochondria, the Golgi apparatus, the ribosomes and the kinetoplast, also called kDNA. The kinetoplast represents an additional genomic structure, consisting of several repeated copies of double-stranded mitochondrial DNA, smaller than the central karyosome and located within a large mitochondria in the posterior end of the body [105] (Figure 22). Parasites also display a flagellum, important for locomotion and reproductive cycles.

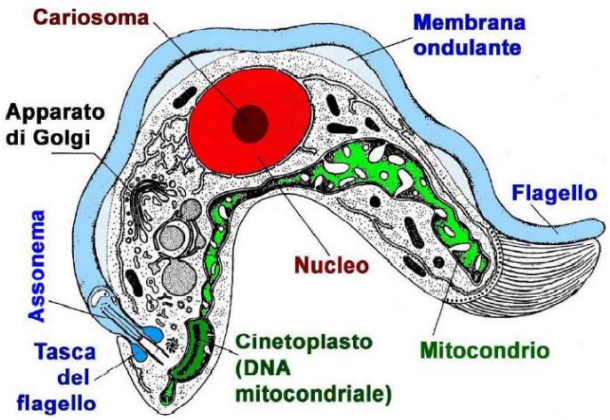

Figure 22. Main and peculiar structures present in *T.brucei*.

The protozoan does not have the ability to replicate independently and the reproductive cycle is completed thanks to the help of the tse-tse fly, intermediate host, and human, final host. The phases of the reproductive cycle are shown in Figure 23. The tse-tse fly transfers the parasite to humans through its bite. The trypanosome lies in the cutaneous tissue in a non-proliferative metacyclic trypomastigote stage and, from there, it reaches the blood stream where it turns into bloodstream form (BSF). At this level, it differs in the proliferative form (BSF-LS) which is responsible for maintaining the infection in the blood stream. The trypomastigote LS, if resists to antibodies, diffuses into the body through the blood and lymphatic pathways, colonizing the interstitial fluids of many

organs, including those of the myocardium and the central nervous system. The parasitic forms that invade intracellular fluids have been known for a long time, but not much is known about the forms of trypanosome that is present in the extravascular compartments. The multiplication of trypomastigoti is exhausted when specific host antibodies reduce its levels, but not all protozoa are familiar to the immune system and many elude the host's defences using different mechanisms:

• Antigenic mutation of surface glycoproteins (VSGs):[106] the VSGs do not provide the antigenic factor capable of triggering the body's immune response and therefore the host is totally exposed to the pathogenic action of the protozoan; [104, 107]

• Polyclonal and aspecific activation of B lymphocytes: acting as mitogens they stimulate the non-specific clonal expansion of B lymphocytes which results in the maximum production of non-specific IgM, autoantibodies against host proteins and nucleic acids. Spleen and lymph node hyperplasia are the side effects observed.

• Immunosuppression due to alteration of B and T cells functions and alteration in macrophage activation.

• Production of gp63-like protein. Trypanosomes possess genes coding for proteins similar to the gp63 present in Leishmania. Although their function has not been completely defined, it is believed to have a specific role in the evasion of complement-mediated lysis.

In the blood stream the trypomastigote LS is transformed into the short and stocky BSF-SS blood morphotype: this is the pre-adapted form for survival in the tse-tse fly.

At this point, the human colonization phase ends and the reproductive phase begins in the vector. The fly acquires the parasite in the short form when it feeds by the blood of an infected subject and here the trypomostigote differs into PCF (procyclic trypomastigotes). A long epimastigote (LE) and a short epimastigote (SE) are the two forms that originate when the PCF, through migration, reach the insect proventricles. The short-shaped epimastigote has the ability to associate with the glandular epithelium (AE) and then reach the salivary glands, where it continues to multiply to form non-proliferative methacyclic tripomastigotes. This form, inoculated in mammals, causes infection and is the only one able to survive in the vertebrate host.

The reproductive cycle takes approximately three weeks and is recurring when the tsetse fly bites a human or an infected animal.

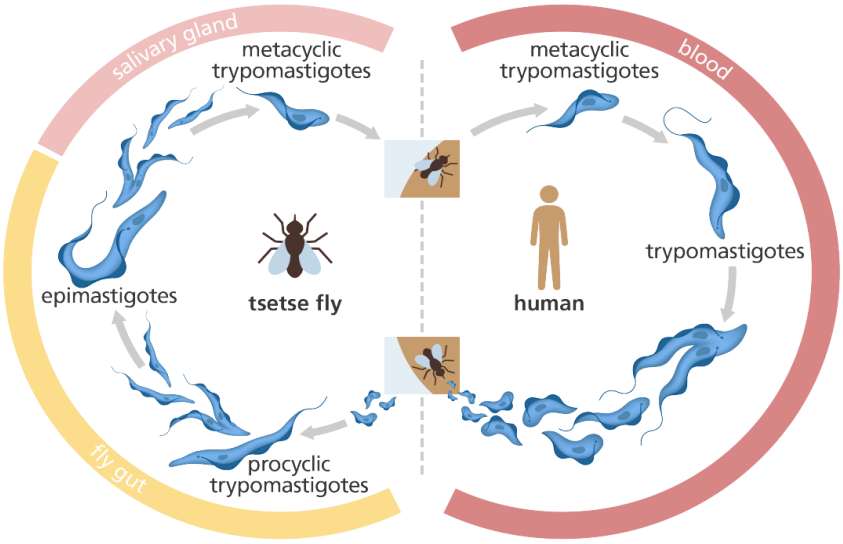

Figure 23. Life cycle of *Trypanosoma brucei.*

5.3. HAT stages and symptoms

The bite of the tsetse fly is followed by a period of incubation of the protozoan in the cutaneous tissue in the form of a metacyclic trypanosome that evolves into an inflammatory process. In particular, we observe the formation of a papule that rapidly turns into a dark, painful and hardened nodule called tripanosomal sifiloma, rarely observable in case of infection by *T. b. gambiense.*[108]

The invasion phase is followed by stage 1 or hemolymphatic phase, and stage 2, known as the neurological phase.

The hemolymphatic phase is characterized by the invasion of the blood stream and lymph nodes by the protozoan in the form of BSF-LS. The main source of energy of the protozoan is the glucose present in the blood, metabolized in glycosomes. The symptoms that characterize this phase are non-specific [109] and include intermittent fever and hepatosplenomegaly. Other side effects are headache, joint pain, weight loss, itching, myocarditis, lymphoadenomegaly, pericarditis, conjunctivitis, heart attacks, endocrine

dysfunction and fertility problems. The Winterbottom's signs (swollen lymph nodes in the posterior cervical triangle) is characteristic of HAT from *T. b. gambiense.*[106] The formation of antigen-antibody complexes is at the basis of organs damage and inflammation.[108] If not promptly treated, the hemolymphatic phase evolves into neurological phase. The BSF-LS trypomastigote is transformed into the short and stocky form that is able to colonize the blood, the lymph and the central nervous system. The protozoan, spreading in the brain, destroys large amounts of cells and others are destroyed by the body's immune reaction, in order to eliminate those attacked. [110] This phase is characterized by the persistence of sporadic fevers, mood alterations, motor disturbances, tremors, irritability, difficulty in articulating a speech, anxiety, confusion and alterations of the sleep-awake cycle, from which the pathology takes the name.[106] In the late phase of the disease, lymphocytes infiltrate the brain and phenomena of demyelination of central and peripheral nerves are also observed. In the most advanced stages of the pathology, there is a total dysfunction of the organism, which is not capable of eating and drinking, generating a weakness of the body's immune defences, now more vulnerable to the attack by pathogens. Without an appropriate pharmacological treatment, the pathogen induces the coma condition [111] and death occurs due to lack of feeding or secondary infections.[106]

In the case of infection by *T. b. gambiense*, the invasion of the CNS occurs within few months up to a year and death occurs between the 2nd and 3rd year after having contracted the infection. If the infection is due to the *T. b. rhodesiense*, the CNS is colonized in a few weeks and death occurs within few months. Severe pneumonia and inflammation of the heart are among the most infectious diseases that cause the deaths of HAT patients.[108]

5.4 Diagnosis

The diagnosis of the pathology is carried out by evaluating the presence of the protozoan in the host by direct and indirect analysis.

Direct qualitative and quantitative evaluations are carried out considering two parameters: the HAT stage and the agent that causes it. Diagnostic investigations are performed in silifoma fluid, lymph node aspirate and blood if the infection is at the first stage. The samples with the greatest diagnostic sensitivity are blood smears for *T. b.*

rhodesiense and lymph node aspirate for *T. b. gambiense.*[112] Diagnosis of late infection by both *T. b. rhodesiense* and *T. b. gambiense* is carried out in the cerebrospinal fluid, taken through lumbar puncture.[106] If the subject has contracted the disease, the pressure of the cerebrospinal fluid is increased and the liquid has an increased number of lymphocytes (≥ 5 cells / μL), total proteins and IgM. In addition to trypanosomes, the characteristic Mott cells may be present in the fluid: plasma cells with cytoplasmic vacuoles containing immunoglobulins (Russel bodies).

The analysis with indirect methods is carried out by evaluating the presence in the blood of specific antibodies against parasitic antigens. Differently from the direct analysis, indirect evaluations does not allow the identification of the pathogen species that causes trypanosomiasis.[113]

New diagnostic techniques will certainly have to be developed, taking into account the areas in which they will be used and the relative hospital infrastructures, they must be as simple, fast, reliable and inexpensive as possible.[114]

5.5 Pharmacological approaches

The ideal drug for HAT treatment should possess several features:[113]

- orally administrable and no more than seven days of administration;
- effective in both stages of the pathology;
- not necessarily effective against both forms of protozoa;
- safe even for children;
- low cost (no more than thirty euros per treatment).

Actually, it's not possible to design a vaccine capable of eradicating the disease due to the high variability of membrane glycoproteins.

The therapeutic approach that is employed for treating trypanosomiasis is chemotherapy and the choice of the appropriate drug is done accordingly to the stage of the disease. The four drugs available are:

- suramin and pentamidine in the first stage;
- melarsoprol and eflornithine in the second stage.

Other useful drugs for treating trypanosomiasis are: nifurtimox, benzoxaborol, fexinidazole and pafuramidine.

Suramin sodium is the drug of choice for the treatment of HAT, particularly in the case of infection by *T. brucei rhodesiense.*[115] It is a ureidic derivative with a symmetrical structure, with variously sulphated naphthylamine groups which account for the ionic nature of the molecule. The poor lipophilicity does not allow the crossing of the blood-brain barrier, making the drug useful only in the first stage of the pathology. The mechanism of action of suramin is not fully known.[115] It is believed that the drug inhibits dihydrofolate reductase, a key enzyme in the metabolism of folic acid, and thymidine kinase, an enzyme that catalyzes the nucleoside phosphorylation reaction to be inserted into DNA chains. The drug is administered exclusively in hospitals and an intravenous infusion is required every three to seven days for four weeks.[116] Among the most common adverse effects there are rash, pyrexia, nausea and reversible nephrotoxicity.[116]

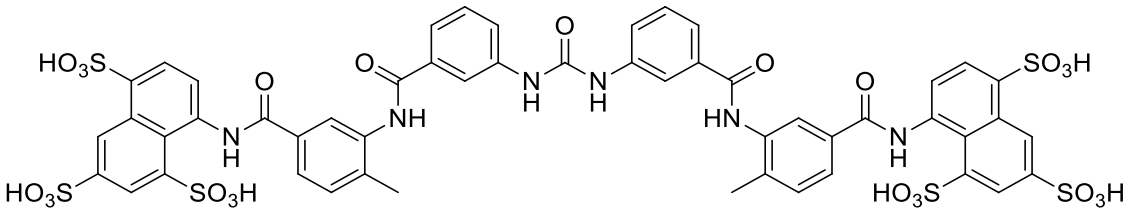

Figure 24. Chemical structure of suramin.

As well as suramin, also pentamidine isethionate, due to the high degree of ionization, is not able to cross the blood-brain barrier and is therefore effective only in the first stage of infection. Pentamidine is an aromatic diamidine (Figure 25) with trypanostatic rather than trypanocidal action.[117] The mechanism of action of the drug has not been clearly defined and it has been hypothesized that pentamidine accumulates in the parasite and binds to DNA through electrostatic interactions;[115] moreover, it seems to possess the ability to inhibit topoisomerase II, an enzyme capable of introducing negative supercoils during DNA replication. Administration is generally parenteral since the intramuscular route causes frequent pain at the injection site and possibility of developing febrile abscesses.[109] Side effects are observed in 50% of patients taking 4mg / kg / day and include severe hypotension, reversible nephrotoxicity, breathing difficulties, gastrointestinal disorders, liver dysfunction, fever, metallic taste and cardiac arrhythmias.[118] This molecule appears to be mainly active against *T. brucei rhodesiense.*

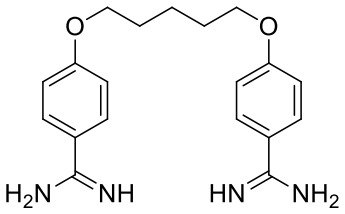

Figure 25. Chemical structure of pentamidine.

The treatment of the second stage, when the protozoan has already crossed the BBB, needs two other drugs, melarsoprol and eflornithine. Melarsoprol is a trivalent organic arsenical derivative available in therapy since 1949 and is the drug of choice for treating the second stage of trypanosomiasis. It is used against the *T. b. rhodesiense* and *gambiense* and it carries out its activity with a mechanism of action not entirely known that presupposes the in vivo bioconversion of the drug in the corresponding melarsen oxide (Mel Ox) (Figure 26) and its selective diffusion in the cells of the parasite, through the purine transporters. Mel Ox binds to the trypanothione and the resulting trypanothionate-adducted melarsen oxide inhibits the trypanothione reductase. The melarsen oxide-trypanothione adduct is formed by substituting the sulfhydryl groups of glutathione with those of the oxidized melarsen.

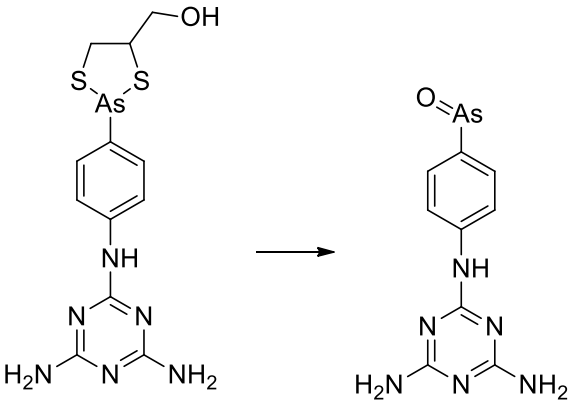

Figure 26. Melarsoprol and melarsen oxide after activation *in vivo*.

The exclusively hospital administration is necessary, due to several side effects such as encephalopathy and peripheral neuropathies, caused by the accumulation of the drug in the CNS. Other frequent side effects are agranulocytosis, skin rashes, cardiac arrhythmias and multifocal inflammatory disorders.[119] Encephalopathy remains the main side effect and has an incidence of 10% in patients treated with the drug, 50% of whom experience coma, epilepsy, cerebral oedema and finally death.[118]

Eflornithine is the second drug useful for the treatment of the neurological phase of the disease. It is a fluorinated analogue of ornithine that acts with a suicidal mechanism, inhibiting ornithine decarboxylase (ODC), a key enzyme for spermine and spermidine biosynthesis.

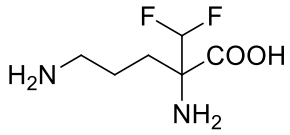

Figure 27. Chemical structure of eflornithine.

Eflornithine reacts with the cofactor PLP (pyridoxal-5'-phosphate) and the complex that forms undergoes a spontaneous decarboxylation which provides for the formation of an electrophilic carbon. The nucleophilic attack of the Cys-360 of the enzyme on the electrophilic carbon forms a stable and irreversible complex. The drug is the first choice for treating trypanosomiasis from *T. b.gambiense* in the late phase, but it is not active against *T.b. rhodesiense*. It turned out to be a drug with better performance than melarsoprol due to its lower toxicity and comparable pharmacological efficacy. Fever, migraine, alopecia, hypertension, rash, peripheral neuropathy, tremor and diarrhea are among the main side effects.[116] The drug is mainly administered parenterally. Due to the resistance, the nifurtimox-eflornithine combination therapy (NECT) [120] was introduced on the market, recommended for the treatment of melarsoprol-resistant *rhodesiense* trypanosomiasis and as a first choice for trypanosomiasis *gambiense*.

Nifurtimox (Figure 28) is an orally bioavailable 5-nitrofuran analogue[121] which is used for the treatment of Chagas disease, caused by *T. cruzi*: it generates a nitroanion radical causing damages to the parasite, unable to defend himself. The enzyme involved is the nitro reductase, which needs oxygen for its functions. The off-label use of nifurtimox associated to eflornithine improved the late stage HAT therapy,[24a] above all safety and patient compliance: monotherapy with eflornithine includes infusion every 6 h for 14 days, while in combination with nifurtimox one infusion every 12 h for 7 days.

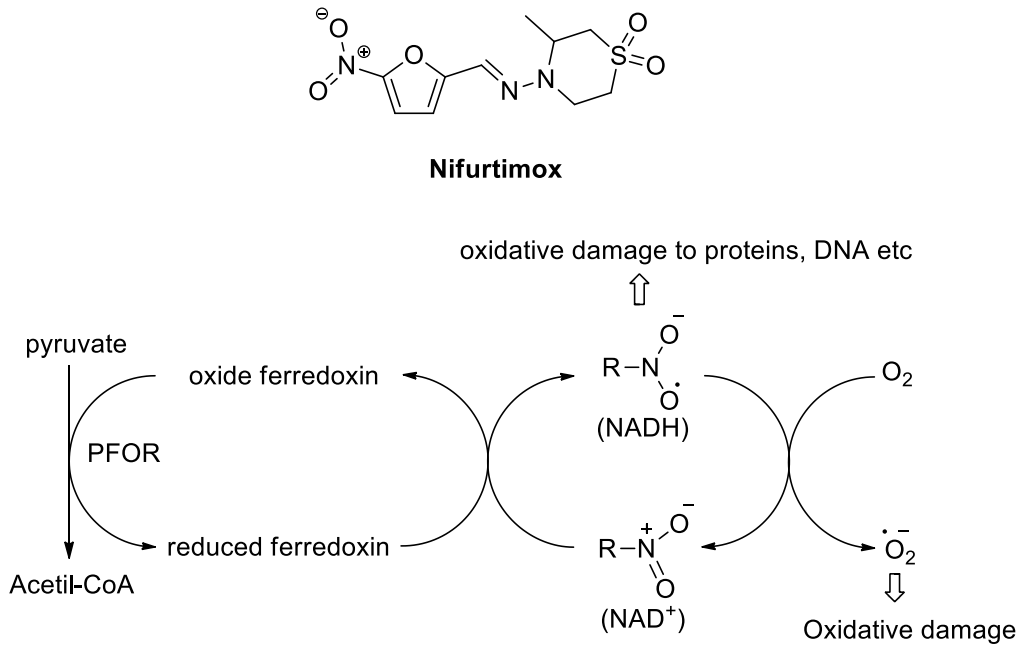

Figure 28. Chemical structure of nifurtimox and its mechanism of action.

The research developed two novel molecules as antitrypanosomal agents. The first is a diamine derivate, pafuramidine (DB289, Figure 29),[122] orally bioavailable and effective against the early-stage of HAT.

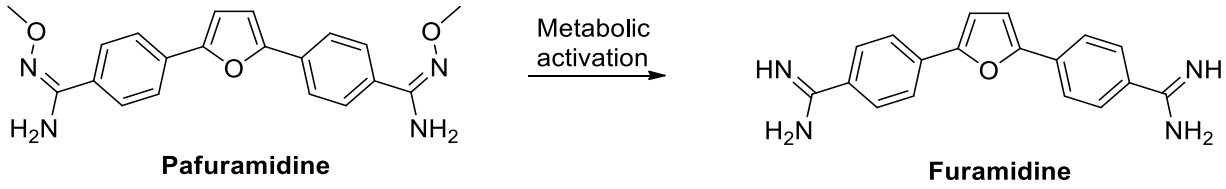

Figure 29. Pafuramidine and its active metabolite furamidine.

Fexinidazole is a DNA synthesis inhibitor that was developed by the Drugs for Neglected Diseases initiative (DNDi), in collaboration with Sanofi, for the oral treatment of HAT. It was identified by the DNDi in 2005 as a drug having activity against *Trypanosoma brucei gambiense* and *rhodesiense*. The Article 58 of Regulation (EC) no. 726/2004 evaluated fexinidazole with a positive opinion by the EMA for the treatment of both stages of HAT due to *T. b. gambiense* in adults and children with age more than 6 years and weighing more than 20 kg. This approval will improve the marketing authorization application in endemic countries in 2019; after appropriate registration, fexinidazole will be distributed by the WHO to endemic countries. Phase III evaluation of fexinidazole for *g*-HAT is ongoing in the Democratic Republic of the Congo and

Guinea and the drug is also in development for Chagas' disease, with a study currently ongoing in Spain.[123]Fexinidazole (Fig. 30) generates reactive amine species which are indirectly toxic and mutagenic to trypanosomes.[25a] Fexinidazole is active against *T. b. gambiense* and various other *T. b.* subspecies (including *T. b. rhodesiense* and *T. b. brucei*) in vitro, with its sulfoxide (M1) and sulfone (M2) metabolites demonstrating broadly similar trypanocidal activity.[124,102]

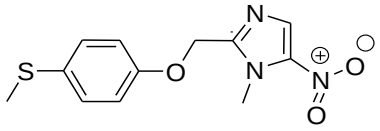

Figure 30. Fexinidaxole chemical structure.

In the present scenario, there is a clear need to find novel antitrypanosomal agents, with efficacy and safety properties, with the aim to provide new treatment for HAT.

5.6. New targets for the treatment of HAT

The several side effects of the classical drugs leads to an urgent need to develop novel drugs as well as discover new targets in addition to the traditional ones. The new targets must be investigated to overcome the problem of protozoan resistance to traditional drugs, which, over time, has proved to be an increasingly emerging problem. The new targets selected for HAT treatment have been identified by studying the morpho-functional characteristics of the protozoan, so that the selective action on the parasitic structures limits the side effects on humans.[125] Among the new targets [126] we must mention:

• acyl-carrier proteins: essential proteins for the biosynthesis of fatty acids;

• mitochondria: cytoplasmic organelles useful for glycolysis;

• tubulin multigene family: genes encoding essential proteins for the maintenance of the cytoskeleton;

• cysteine proteases: enzymes with proteolytic activity;

• plasma membrane proteins: useful for maintaining the cellular structure;

• cytosolic fraction: important for carrying out all the metabolic and biochemical processes that occur in the protozoan.

5.7 Cysteine proteases as promising targets

Cysteine proteases are enzymes that catalyse the peptide bond cleavage reaction using a cysteine residue as a nucleophile. Cysteine proteases can be classified into four clans [127] as highlighted in Figure 31.

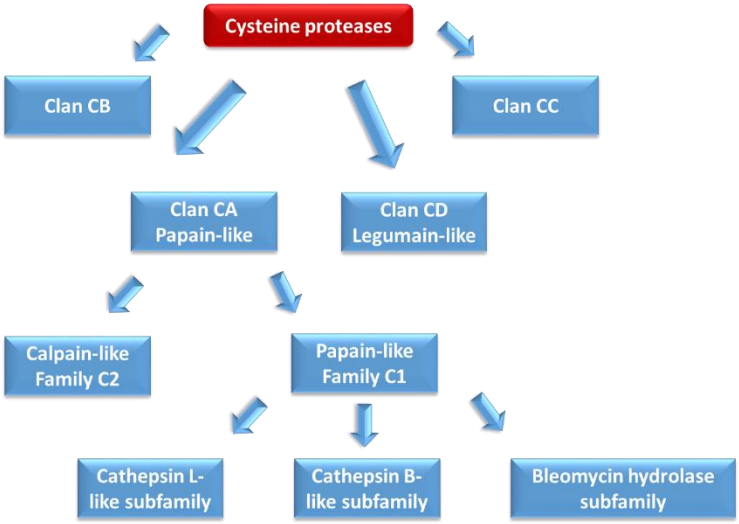

Figure 31. Schematic graphic of the cysteine proteases of parasitic organisms.

The cysteine proteases of the papain superfamily, widely expressed both in protozoa and in humans, have been recognized as ideal targets for the treatment of parasitic diseases. The key role that this class of enzymes plays in the parasitic infection has made the cysteines parasitic proteases interesting target for the design of new chemotherapeutic drugs.

A particular interest has recently been aroused by rhodesain (TbCatL) and by TbCatB the two most important cysteine proteasesof *T. brucei rhodesiense.*

Rodesain and TbCatB belong to the Clan CA, C1 family of proteases and they are similar to the cysteine human protease cathepsin L and cathepsin B, respectively. They are the only cysteines proteases produced by trypanosome during infection in the host and are crucial for the development of pathology. The two cathepsins differ structurally due to the presence of a highly conserved amino acid region called ERFNIN in cathepsin L and to the presence of a loop of 20 amino acids located on the surface of cathepsins B that give it an additional exopeptidase activity.[127]

Like all the enzymes, cysteine proteases show a substrate specificity due to the nature of the amino acid residues in the cleavage site. The nomenclature used to define the binding pockets[128] is relative to the cleavage site (Figure 32): Sn represents the enzyme pockets

which are numbered S1-S2-Sn from cleavage site toward *N*-terminus (non-primed pockets), whereas are indicated as S1'-S2'-Sn' toward *C*-terminus (primed pockets). At the same way, the number of substrate residues initiates from scissile bond and, in agreement with enzyme pocket numeration, they are numbered P1-P2-Pn, and P1'-P2'-Pn', toward *N*-terminus and *C*-terminus, respectively.

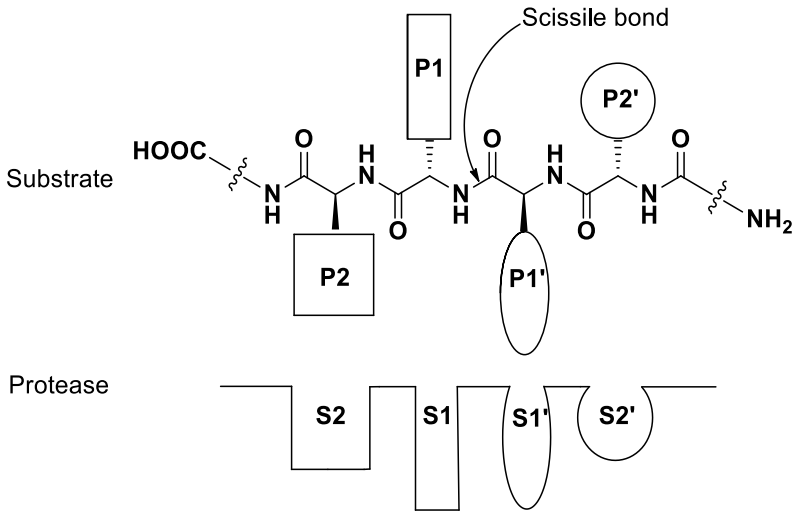

Figure 32. Nomenclature of the substrate specificity of protease.

5.8 Rhodesain: structure and functions

Rhodesain (TbCatL) is a protease belonging to the C1 family of Clan CA. It is an enzyme consisting of 215 amino acids, presenting a right (R) and left (L) domains, connected by the catalytic triad (Cys25/His162/Asn182).[129] Figure 13 shows the secondary structures of rhodesain that displays the amino-terminal end in the right domain, in grey, and the carboxiterminal end in the left domain, in green.

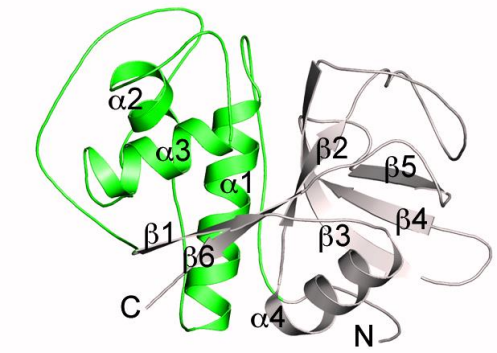

Figure 33. The figure shows the secondary structure of rhodesain, with two domains left (green) and right (grey).

Cys25/His162/Asn182 represent the amino acids that characterize the catalytic site and, as every cysteine proteases, the –SH group of Cys in the form of a thiolate anion attacks the peptide bond in order to cleave it. The other two amino acids of the catalytic site act as acid-base catalysts. The hydrolysis mechanism is depicted in Figure 34.

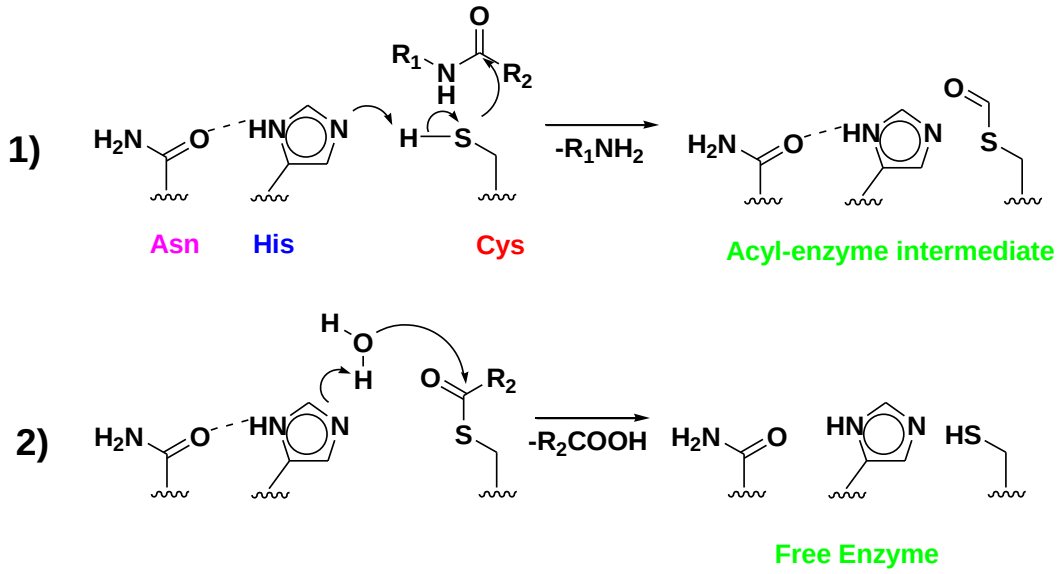

Figure 34. Mechanism of hydrolysis mediated by cysteine proteases.

Rhodesain has a high degree of structural homology with cruzain, cysteine proteases expressed by *T. cruzi*, and a minor homology with falcipain-2 (FP-2) and falcipaina-3 (FP-3), cysteine proteases expressed by Plasmodium falciparum.

Rhodesain performs numerous functions:

• it allows the protozoan crossing through the hematoencephalic barrier and therefore the colonization of the CNS which causes disease progression from stage 1 to stage 2.[130a, b] When rhodesain interacts with PAR (protease activated receptors) receptors, Gq protein-coupled receptors, we are observing the formation of IP3 (inositol-1,4,5-triphosphate) and DAG (diaglycerol). The binding of IP3 to its own receptor causes the mobilization of Ca^{2+} contained in the endoplasmic reticulum and a considerable increase in intracellular Ca^{2+}.This results in structural changes of the cytoskeleton of endothelial cells and dysfunctions of the blood-brain barrier.[27] The Ras protein mediates another independent Ca^{2+} mechanism.[27]

• it allows the mutation of VSG proteins, giving the pathogen the ability to evade the host's immune system. VSG protein variability is guaranteed through genetic

recombination processes. Normally only one gene in a thousand is expressed and the recombination processes lead to the genesis of proteins, towards which the host does not have antibodies. [131] In addition, there is the ability of rhodesain, as observed for the congopaine protease of *T. Congolese*, to internalize and degrade membrane-exposed VSGs so to be able to use the amino acids derived from it for the synthesis of new VSG proteins. [29a, 13]

• it carries out intense proteolytic activity by degrading both the protozoan and the host proteins transported in the lysosomal districts through active transport. [30] Proteolytic activity is also carried out against host immunoglobulins [29]. The ability to catalyse the hydrolysis reactions of IgG immunoglobulins has been shown by pre-treating the trypanosome with the two potent cysteine protease inhibitors, K11777 and E-64.[133] the IgG concentration does not decrease but remains constant.[29b]

5.9 Comparative studies on Rhodesain and TbCatB

In order to understand the main role of rhodesain and TbCatB, several studies were conducted using molecules that inhibit the expression of mRNA sequences that translate for these two proteases. The investigations were performed *in vivo* with mice infected by *T. b. brucei* and *in vitro* with models of the blood–brain barrier; doxycycline was used to inhibit the transcription of TbCatB and rhodesain. The mice that does not express TbCatB when the protozoan is in the blood form heals from the lethal infection, while death from infection occurs after 13 days if the mouse expresses the enzyme. Mice that do not express TbCatL fail to eradicate the infection but 50% of them survive 60 days longer. These results suggest that TbCatB could be the ideal target for HAT treatment but the abundance and the role of rhodesain in facilitating the entrance of the parasite in the brain justifies the use of this target for the development of new drugs for HAT. [130b] TbCatB and TbCatL inhibitors are both valuable drugs for the treatment of African trypanosomiasis. The functions and consequences of activity and inactivity of the two proteases have been highlighted in Table 3.

Table 3. Properties of rhodesain and TbCatB.

Enzyme	Functions	Consequences of the activity	Consequences of the inactivity
Rhodesain	Distruption of BBB of the host	Progression of the disease from stage 1 to 2.	Inability to develop the pathology and lengthening of the life of the host by about half time
Rhodesain	Mutation of VSGs	Evasion of recognition by the host's immune system.	
Rhodesain	Proteolytic activity	Degradation of protozoan and host proteins, including immunoglobulins.	
TbCatB	Acquisition of host transferrin	Vitality of the parasite and correct development of metabolic reactions.	Regression of the pathology

From the structural point of view, important differences between the two enzymes have been highlighted, emerging through X-ray crystallography of the rodesain-K11002 and TbCatB-CA074 complexes [129] (Figure 35, 36).

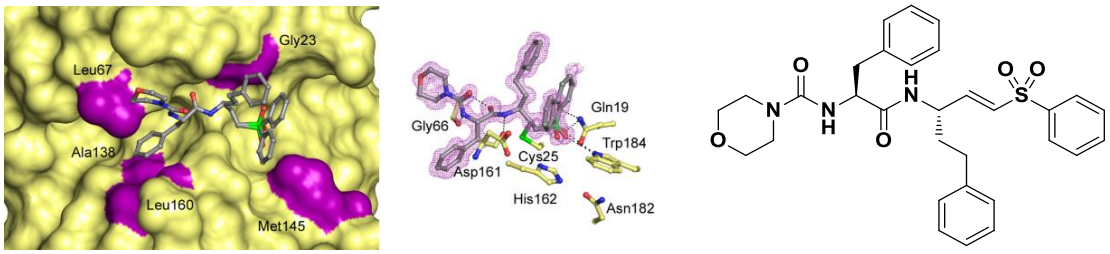

Figure 35. Crystal structure of rhodesain in complex with K11002.

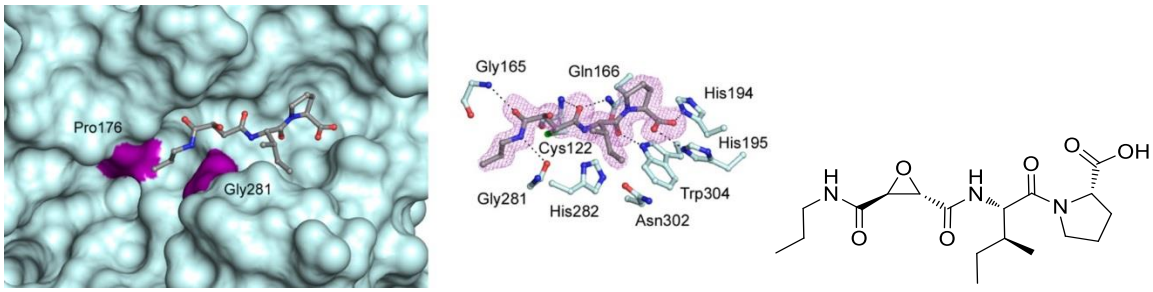

Figure 36. Co-crystal structure TbCatB-CA074.

The mature domain of our TbCat-CA074 structure includes an elongated *N*-terminus with additional 16 residues preceding the maturation cleavage site. *N*-terminal Edman

sequencing showed a longer extension than observed in the crystal structure. The TbCat-CA074 structure reveals that the occluding loop, which is a fundamental portion of the substrate-binding site, generates a larger pocket in the active site. Experimental data further highlight a higher flexibility in the occluding loop main chain and structural differences from mammalian cathepsin B enzymes that can influence the design of novel inhibitors. Considering the rhodesain-K11002 complex, the dual conformation of the phenylsulfone moiety at the $P1^1$ position of the inhibitor is worth noting (Figure 35).

The complex of rhodesain-K11002 is comparable to the rhodesain-K11777 (PDB ID 2P7U) [133] complex with differences only at the P3 position (*N*-methyl piperazine (*N*-Mpip) in K11777 vs. morpholino urea (Mu) in K11002). Many hydrogen bonds are formed between residues of the substrate-binding site and the inhibitor backbone, while a number of hydrophobic residues are also relevant at the S2 subsite (Figure 35), which confers selectivity for this class of protease. Instead, in the case of the TbCatB-CA074 complex hydrogen bonding between the enzyme and inhibitor overcome the hydrophobic interactions. The phenylsulfone moiety at P1' is a common motif of many protozoan cysteine protease-vinylsulfone complexes. The dual conformation of this portion in the rhodesain-K11002 structure is exceptional for a protozoan cysteine protease-vinylsulfone complex. Superimposition of TbCatB-CA074 and rhodesain-K11002 show structural variations that highlight how rhodesain is more sterically restricted at the S2 subsite. First of all, Asp16675 in TbCatB is replaced with a Leu in rhodesain (Leu67); Leu67 interacts more favourably against the hydrophobic environment of the rhodesain S2 subsite with the large hydrophobic phenylalanyl at the P2 position of K11002. Moreover, rhodesain has the larger Ala208 (Gly328245 in TbCatB) at the bottom of the S2 subsite, making the pocket thinner.

The main differences between the two enzymes, summarized in Table 4, were highlighted in the S2 site and in the immediately adjacent regions. The presence of the amino acid loop present in TbCatB also justifies the additional interactions of enzyme-inhibitor hydrogen bonding.

Table 4. Structural differences of the S2 site and of the adjacent regions of the rhodesain and TbCatB enzymes.

Enzyme	S2	Regions adjacent to S2
Rhodesain	Ala208	Leu67 (hydrophobic region)
TbCatB	Gly328	Asp166 (hydrophilic region)

The crystal structure of rhodesain-K11777 was also reported in literature.[133]

The active site of rhodesain displays a wide number of residues that are able to interact, through non-polar contacts, with the inhibitor that is endowed with hydrophobic substituents (Fig. 37).

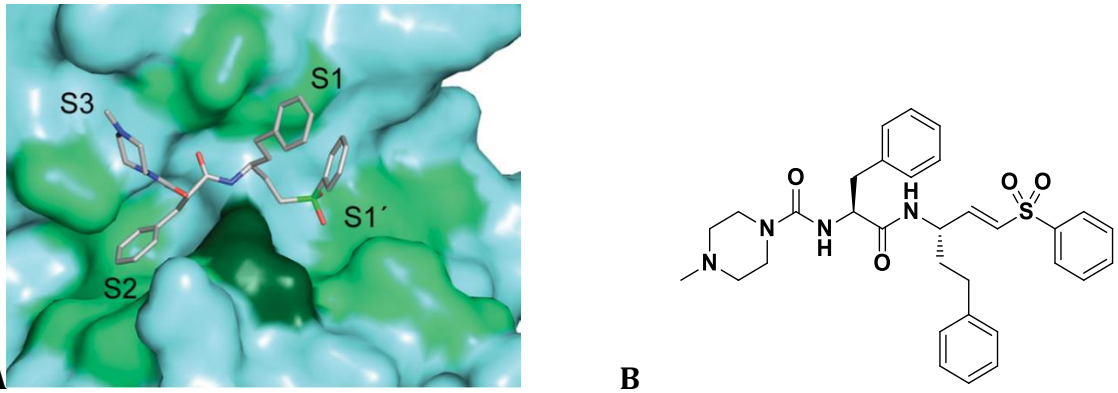

Figure 37. A. Hydrophobic environment of the active sites. Hydrophobic residues are colored light green, and polar residues that interact with the ligand through their non-polar C–C bonds are colored dark green. B. Structure of K11777

Interestingly, flipping of the phenyl sulfone at the P1 position seems to be a consistent structural feature in rhodesain. The high resolution crystal structure of rhodesain in complex with the vinyl sulfone K11002 reveals that this flipping may be transient.

Rhodesain reveals a strong preference for large and hydrophobic residues at the P2 position of substrates. A more remarkable difference regards the P3 position.

The P3 substituent of the vinyl sulfones has recently been a point of interest because a modification of this position proved to influence many properties, as hepatotoxicity and pharmacokinetics. Superimposition of the rhodesain-K11002 and rhodesain-K11777 structures shows that the residue equivalent to Ser-61 in rhodesain (Phe-61) is able to exclude the solvent that would otherwise be available to allow Mu to interact with S3 residues. Meanwhile, in the rhodesain-K11777 complex, Phe-61 makes torsional re-adjustments out of the S3 subsite and provide space for the branched *N*-Mpip (Fig. 38).

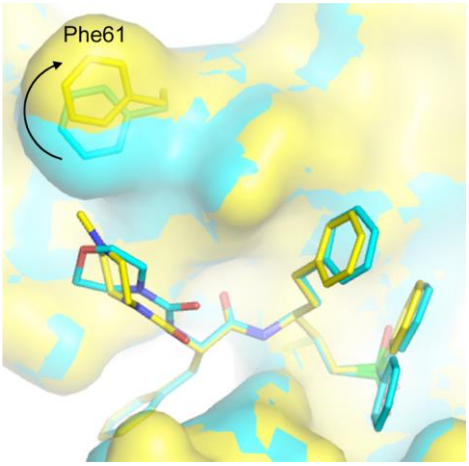

Figure 38. P3 substituent in the S3 subsite of rhodesain. Surface and stick representations, showing Phe61 swinging out of the S3 subsite during binding of K11777.

Thus, although rhodesain is unable to form any specific polar interactions with Mu, this moiety may nonetheless be preferred to the slightly larger *N*-Mpip.

Cysteine proteases are, thus, very promising drug targets and the overall structural features could better allow the design of new inhibitors for HAT treatment.

6. Results and discussion

6.1 Synthesis of compounds 35-40

The synthetic strategy used to obtain peptidyl vinylketones involves coupling of a P1 HPhe synthon to P2 fragment which afforded a dipeptide functionalized at the *N*-terminus in such a way to span into P3 region, and bearing at the *C*-terminus the required terminal olefin handle in readiness for further functionalization via cross metathesis methodology to introduce the α,β-unsaturated ketone moiety.

The synthesis of P1 HPhe synthon **74** (Scheme 4) has been accomplished in agreement with a previously reported procedure.[134] L-hPhe **68** was treated with $SOCl_2$ in presence of ethanol for 48h, to afford the corresponding ester as hydrochloride **69**, which was reacted with trityl chloride, in presence of Et_3N, to provide intermediate **70**. The reduction with $LiAlH_4$ gave the alcohol **71** which was in turn oxidized by Swern reaction to give the corresponding aldehyde **72**. The subsequent Wittig reaction gave olefin **73**, which finally gave amine **74** by treatment with TFA.

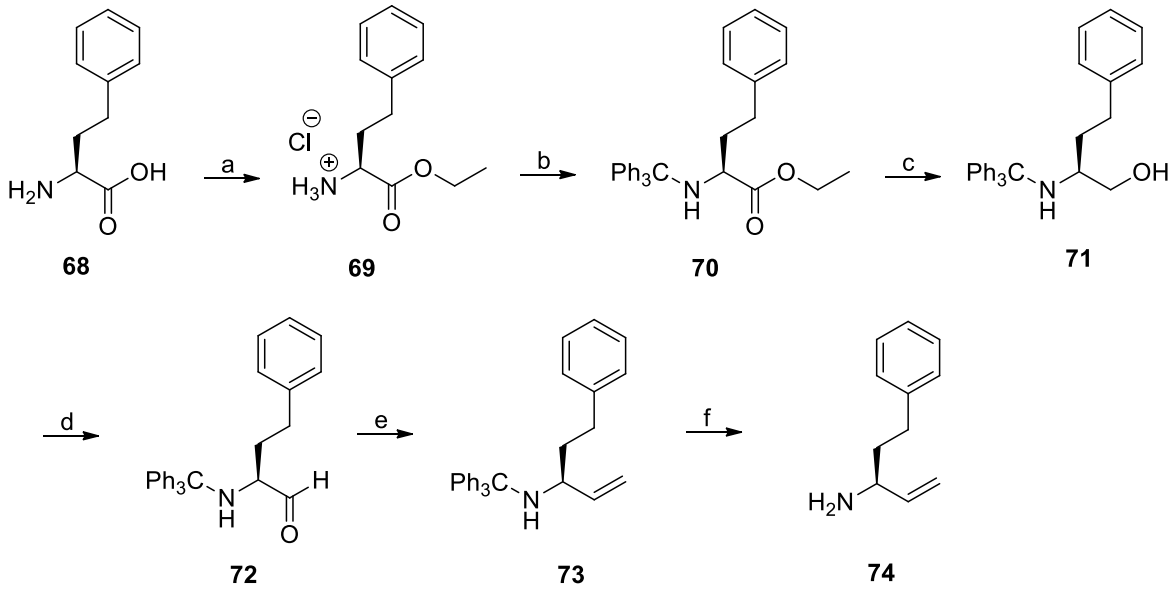

Scheme 4. Reagents and conditions: a) ethanol, $SOCl_2$, 0° C, then rt, 48 h; b) Ph_3CCl, Et_3N, CH_2Cl_2, rt., 12 h; c) $LiAlH_4$, dry THF, N_2, 0° C, then rt, 6h; d) oxalyl chloride/DMSO, -78° C, 30 min, then Et_3N, -23°C, 40 min; e) $Ph_3PCH_3^+I^-$, *n*-BuLi, dry THF, 0° C then rt, 5 h; f) 2% TFA in CH_2Cl_2, rt, 4 h.

On the other hand, the synthesis of the P2-P3 fragment was carried out by functionalization of the amino group of Phe methyl ester **81** with different acids **75-80** (Scheme 5) to obtain the esters **82-87**, spanning into P3-P2 regions, which were then

converted in the corresponding carboxylic acids **88-93** *via* hydrolysis in alkaline conditions. Subsequently, coupling reactions with amine **74** provided intermediates **94-99**, which by treatment with methyl vinyl ketone **100**, in presence of 2nd generation Hoveyda-Grubbs catalyst and under microwave irradiation at 100° for 2h, allowed us to obtain the CM products **35-40**.

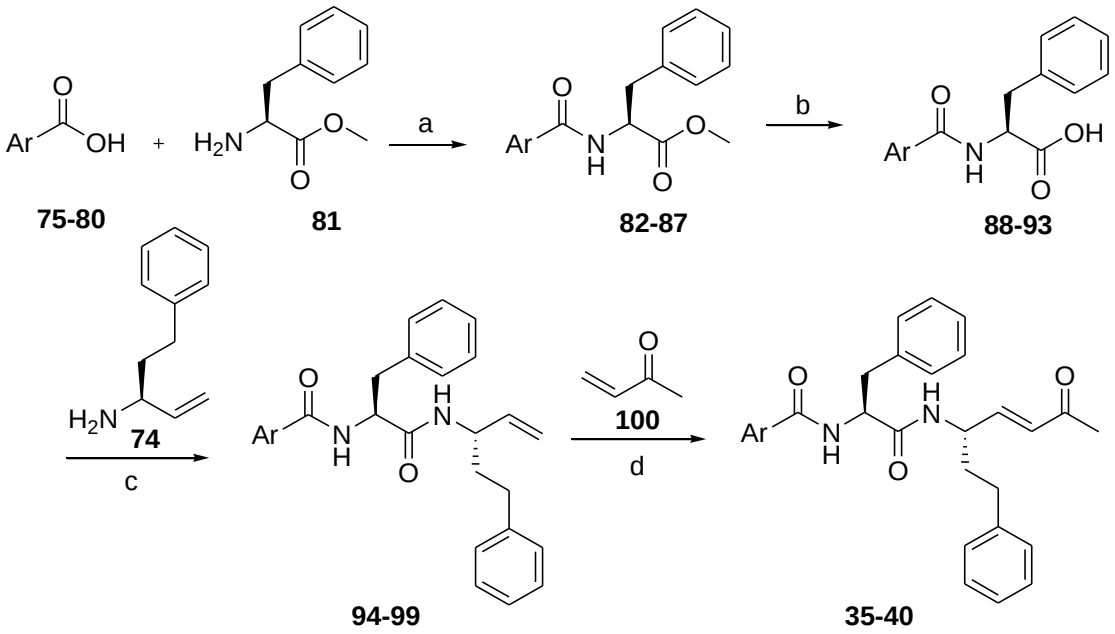

75, 82, 88, 94	76, 83, 89, 95	77, 84, 90, 96	78, 85, 91, 97	79, 86, 92, 98	80, 87, 93, 99
35	**36**	**37**	**38**	**39**	**40**
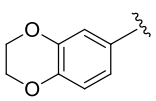	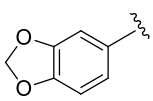	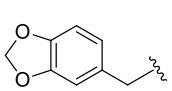	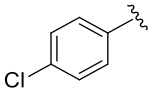	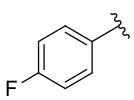	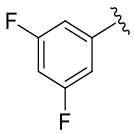

Scheme 5. Reagents and conditions: a) HOBt, EDCI, dry DMF/CH_2Cl_2 (1:1), 0°C, 10 min, then DIPEA, **5**, rt, 12h; b) LiOH, MeOH/H_2O/dioxane (1:1:1), 0° C, 10 min, then rt, 12h; c) HOBt, EDCI, dry DMF/CH_2Cl_2, 0°C, 10 min, then DIPEA, **74**, rt, 12h; d) 2nd generation Hoveyda-Grubbs catalyst, dry CH_2Cl_2, 100 °C, MW, 2 h.

6.2 Biological activity and docking studies

All compounds **35-40** were tested against recombinant rhodesain by using Cbz-Phe-Arg-AMC as a fluorogenic substrate.[135] First, a preliminary screening at a fixed inhibitor concentration of 50 μM was performed. An equivalent volume of DMSO was used as the negative control, and E-64,[136] the irreversible standard inhibitor of clan CA family C1 cysteine proteases (papain family), was used as the positive control. All compounds inhibited the enzyme activity by 85%-100%.

Continuous assays were then performed at seven different concentrations ranging from minimally inhibitory to fully inhibitory concentrations, to determine the first-order rate constants of inhibition k_{inac} (min^{-1}), the dissociation constants K_i (nM), and the second-order rate constants of inhibition k_{2nd} (M^{-1} min^{-1}), as $k_{2nd} = k_{inac}/K_i$ (Table 5).

All compounds inhibited rhodesain in an irreversible manner, as demonstrated by analysis of the progress curves at seven different concentrations (see e.g. **39**, Figure 37) and in agreement with literature data of related compounds containing the same warheads.[135]

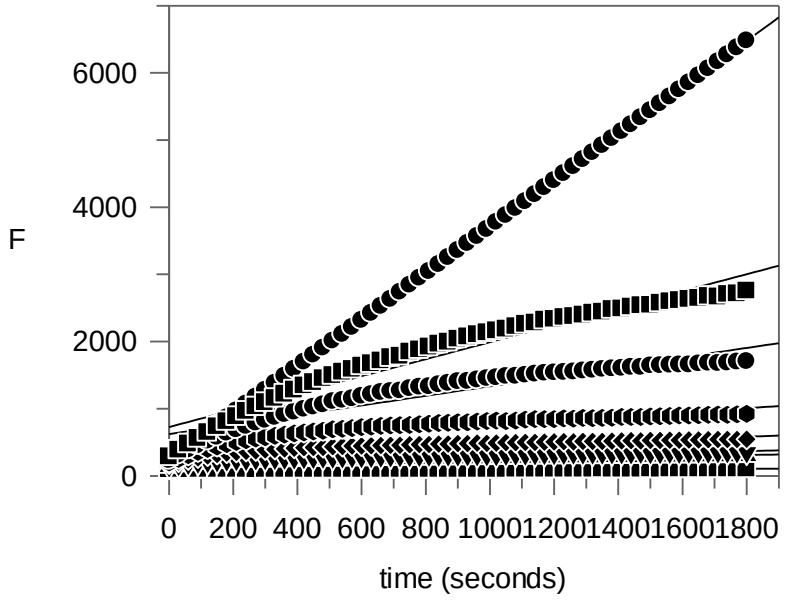

Figure 37. Progress curves of substrate hydrolysis in the presence of the inhibitor **39**. Inhibitor concentrations (from top to bottom): 0, 0.005, 0.010, 0.025, 0.050, 0.075, 0.1, 0.5 nM.

A survey of the data reported in Table 5 shows that a slight reduction in activity was observed in the case of compounds **35** and **36**, which bear a 2,3-dihydrobenzo[*b*][1,4]dioxine and a benzo[*d*][1,3]dioxole group, respectively at the P3 site.

It is worth noting that when the benzo-fused nucleus at the P3 site is directly linked to the amide portion, the inhibitory properties are enhanced. In contrast, compound **37**, with a methylene spacer between the amide moiety and the benzo[*d*][1,3]dioxole nucleus, showed a k_{2nd} value between one and two orders of magnitude lower with respect to compound **36** (i.e. k_{2nd} 15300 x $10^3 M^{-1}$ $min^{-1}$and 435 x 10^3 M^{-1} $min^{-1}$for **36** and **37**, respectively).

The most promising results were obtained with compounds containing a halogenated aromatic nucleus at the P3 site. The 4-fluoroderivative **39** proved to be the most potent derivative of the series with an impressive k_{2nd} value of 881100 x 10^3 M^{-1} min^{-1} with respect to the chlorine **38** derivative that showed a potency between one and two orders of magnitude lower (i.e. k_{2nd} value of 29300 x 10^3 M^{-1} min^{-1}). Moreover, the 3,5-difluoroderivative (i.e. **40**) showed a slight decrease in activity (k_{2nd} 112600 x 10^3 M^{-1} min^{-1}) with respect to compound **39**, thus suggesting the relevance of the fluorine atom at the position 4 of the aromatic nucleus.

Interestingly, the structural modifications realized on the *lead compound* **34** allowed to improve its potency, as shown by the vinyl ketones **39-40**. It is worth noting that the most active compound **39** showed a k_{2nd} value one order of magnitude higher with respect to that of the lead compound **34**, coupled with a consistent improvement of binding affinity (i.e. K_i value 1.1 pM *vs* 38 pM).

The most potent rhodesain inhibitors were tested for their activity against cultured *T. b. brucei*. Compounds **36** and **38-40** were used in concentrations from 16.7 μM to 32.5 nM in consecutive dilutions in two independent triplicates at two timepoints (24 h and 48 h). EC_{50} values of all four compounds are in a low micromolar range from 3.2 ± 0.5 μM to 5.1 ± 1.0 μM (Table 7).

Table 5. Activity of the Michael acceptors 35-40 towards rhodesain.

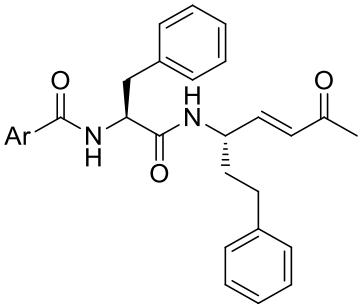

Comp	Ar	Rhodesain		
		k_{inac} (min^{-1})	K_i (nM)	k_{2nd} (x 10^3 M^{-1} min^{-1})
35	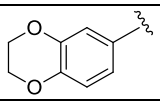	0.0043±0.0032	0.74±0.62	7200±1800
36	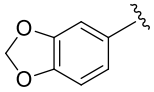	0.0005±0.0001	0.034±0.011	15300±2200
37	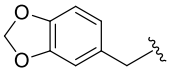	0.00085±0.00025	2.10±0.98	435±83
38	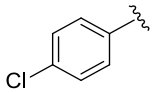	0.0008±0.0001	0.029±0.002	29300±6300
39	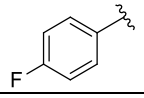	0.0009±0.00002	0.0011±0.0002	881100±102450
40	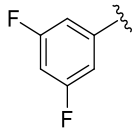	0.0016±0.0006	0.015±0.008	112600±18600
34[31]	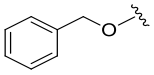	0.00255 ± 0.00075	0.038 ± 0.011	67000 ± 432
E-64[31]		0.009 ± 0.0004	35 ± 5	261 ± 27

Selectivity assays were also performed by testing the active inhibitors towards cathepsin L, a papain-family human cysteine protease, on the basis of the high structural homology with rhodesain. An equivalent volume of DMSO as negative control, and E-64 as positive control were used. The results of the evaluation indicated that all tested compounds inhibited cathepsin L to a lower extent with respect to rhodesain (Table 6). The best selectivity was generally shown by vinyl ketones **39** and **40**; in these cases, in fact, the second-order rate constants of inhibition for cathepsin L are almost 3 orders of magnitude lower than those observed for rhodesain inhibition.

Table 6. Activity of the Michael acceptors 35-40 towards human cathepsin-L

Comp	Human Cathepsin L		
	k_{inac} (min^{-1})	K_i(nM)	k_{2nd} (x 10^3 M^{-1} min^{-1})
35	0.0076±0.0010	78.2±20.9	102±14
36	0.0016±0.0001	10.2±0.2	157±3
37	0.0053 ±0.0002	90.3±6.8	59±2
38	0.0018±0.0001	0.60±0.06	3030 ±303
39	0.0018±0.0001	1.5±0.2	1228±136
40	0.0022±0.0001	14.8±3.3	156±34
34[31]	0.002±0.0004	0.4±0.1	5754±523
E-64[31]	0.0032±0.0001	30±3	110±6

Table 7. Antitrypanosomal activity of the four most potent rhodesain inhibitors

Comp	*T. brucei brucei* EC_{50} (μM)	
	24 h	48 h
36	5.0 ± 0.9	3.7 ± 0.4
38	4.8 ± 0.5	3.2 ± 0.5
39	5.1 ± 1.0	3.6 ± 0.2
40	4.0 ± 0.8	3.4 ± 0.9
34[31]	3.2 ± 2.2	3.0 ± 1.2

The lack of a perfect correlation between inhibitory properties and antitrypanosomal activity is a problem that often occurs in medicinal chemistry field, reported in literature also in the case of the most promising rhodesain inhibitors.[25a] In the case of peptidyl inhibitors, the absence of a clear correlation between enzymatic and cellular activity

might be due to the proteolytic instability of the inhibitor, which can be increased, for instance, by inserting D-amino acids into the peptide scaffold or by prodrug approaches or by emerging technologies such as the incorporation of drugs into liposomes or nanocarriers that might offer new opportunities to develop potent enzymatic inhibitors into efficacious antitrypanosomal agents.

To elucidate the structural basis of inhibition of the novel compounds, docking studies were performed in collaboration with Prof. Cosconati (University of Campania Luigi Vanvitelli, Caserta). For these *in silico* experiments, the AutoDock4.2 (AD4) covalent docking protocol was employed.[137-139, 31]The compounds **35-40** were all covalently docked into the crystal structure of rhodesain (PDB code 2P86)[129] through residue C25. The binding pose of the most active inhibitor **39** in the active site of rhodesain is shown in Figure 38.

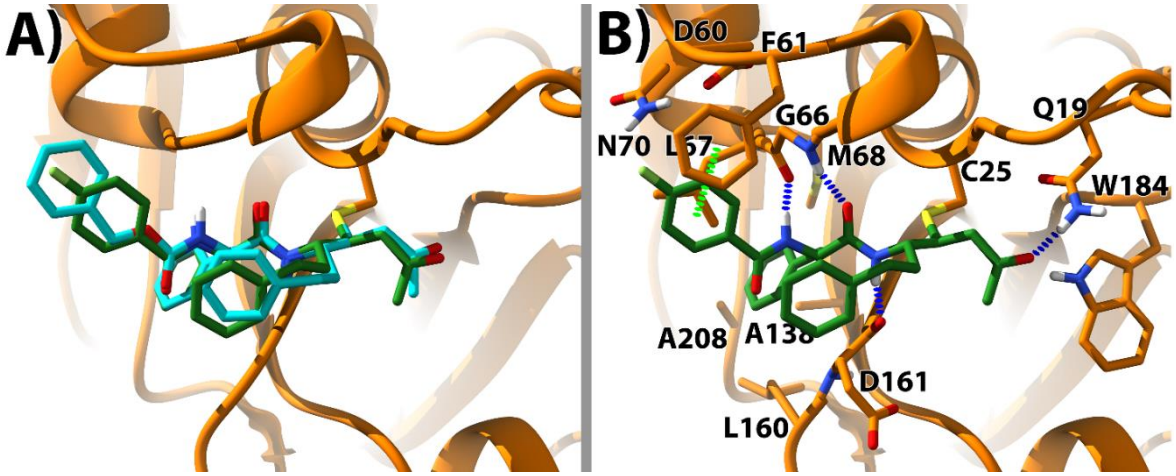

Figure 38. a) Superimposition of compounds **34**[31] (cyan sticks) and **39** (green sticks) docked conformations in rhodesain (orange ribbons). b) Rhodesain/**39** theoretical complex. The enzyme is depicted as orange ribbons and sticks, while the ligand as green sticks. Important residues are labelled. H-bonds are shown in blue dashed lines. The π-stacking interaction is shown in light green dashed lines. The rhodesain 3D structure was extracted from the PDB 2P86.[129]

The achieved docked conformation for the compounds is in accordance with the previous study.[31] In particular, the ligands establish a tight network of H-bonds within the active site. The backbone atoms of G66 engage in a double-bridged H-bond interaction with the ligand P2 CO and NH atoms. The backbone NH of P1 is involved in a H-bond with the backbone CO of D161. Furthermore, the ketone warhead is well

positioned to accept two H-bonds from Q19 and W184 sidechains. The Phe P2 moiety is favorably lodged in the hydrophobic S2 gorge lined by M68, A138, L160, and A208 residues. As for the P3 moieties, they generally fit in the S3 cleft lined by residues D60, F61, L67, and N70. According to our docking study, the sole exception to this trend is represented by compound **37**, whose bulky P3 portion was found to be lodged in the S2 region of the active site, with the Phe P2 placed in the S3 cleft. Possibly, this switch between S2 and S3 of the P2 and P3 residues could be energetically disfavored, causing a decrease in affinity. Interestingly, in the case of the P3 aromatic substituents of **38-40**, a parallel-displaced π-stacking interaction can be observed with F61. Such an interaction should be enhanced in compounds **38-40**, featuring substituents with electron-withdrawing groups. It is also worth noting that in compounds **38-40** the aromatic ring is directly connected to an amide portion. This latter portion engages in a H-bond with G66, as we mentioned before. Therefore, it could be postulated that, given the overall electronic conjugation, electron-withdrawing groups on the aromatic substituents (**38-40**), especially in a *para* position, would enhance the strength of the H-bond to G66.[140] Additionally, the *para*-fluorine in **39** is also situated in a H-bonding position with N70. Thus, **39** seems to feature the best decoration pattern to yield high inhibitory potency at rhodesain.

The drug-likeness of compounds **34, 36, 38** and **39** was in silico assessed through the QikProp tool, part of the Schrödinger suite (Schrödinger Release 2019-1: QikProp, Schrödinger, LLC, New York, NY, 2019). The latter is useful to predict several physicochemical and pharmacokinetic parameters of a given compound, and the results are compared to the values obtained for the 95% of marketed drugs. The summary of the calculated values are reported in Table 8.

Table 8. Calculated Physicochemical and Pharmacokinetic Properties of Compounds **34**, **36**, **38** and **39**.

Parameter	**34**	**36**	**38**	**39**	**Range of recommended values**[a]
#rotor[b]	12	11	11	11	0 – 15
#rtvFG[c]	1	2	1	1	0 – 2
Lipinski Rule of 5 violations[d]	1	1	1	1	N.A.
mol_MW[e]	484.59	498.58	489.01	472.56	130.0 – 725.0
dipole[f]	8.67	3.05	3.19	3.35	1.0 – 12.5
SASA[g]	936.81	813.33	835.12	820.54	300.0–1000.0
donorHB[h]	1.25	1.25	1.25	1.25	0.0 – 6.0
accptHB[i]	6.25	7.75	6.25	6.25	2.0 – 20.0
QPlogPo/w[j]	6.34	5.03	6.05	5.80	-2.0 – 6.5
QPlogS[k]	-8.19	-5.74	-6.87	-6.50	–6.5 – 0.5
QPPCaco[l]	492.04	1014.04	1077.76	1067.54	<25 poor, >500 great
QPlogBB[m]	-1.64	-1.04	-0.83	-0.89	-3.0 – 1.2
QPPMDCK[n]	369.83	721.38	2073.99	1500.74	<25 poor, >500 great
Jorgensen Rule of 3 violations[o]	1	1	1	1	N.A.
#metab[p]	5	4	4	4	1 – 8
Human Oral Absorption[q]	100	100	100	100	<25% poor, >80% high

[a]For 95% of known drugs. [b]Number of non-trivial (not CX3), non-hindered (not alkene, amide, small ring) rotatable bonds. [c]Number of reactive functional groups. [d]Predicted numbers of violations of Lipinski's rule of five. [e]Molecular weight of the molecule. [f]Computed dipole moment of the molecule. [g]Total solvent accessible surface area (SASA) in square angstroms using a probe with a 1.4 Å radius. [h]Estimated number of hydrogen bonds that would be donated by the solute to water molecules in an aqueous solution. [i]Estimated number of hydrogen bonds that would be accepted by the solute from water molecules in an aqueous solution. [j]Predicted octanol/water partition coefficient. [k]Predicted aqueous solubility, log S. S in mol dm^{-3} is the concentration of the solute in a saturated solution that is in equilibrium with the crystalline solid. [l]Predicted apparent Caco-2 cell permeability in nm/sec. Caco-2 cells are a model for the gut-blood barrier. [m]Predicted brain/blood partition coefficient for orally delivered drugs. [n]Predicted apparent MDCK cell permeability in nm/sec. MDCK cells are considered to be a good mimic for the blood-brain barrier. [o]Predicted numbers of violations of Jorgensen rule of three. [p]Number of likely metabolic reactions. [q]Predicted qualitative human oral absorption percentage.

Indeed, all the compounds showed good drug-like properties with 100% oral absorption, one violation of the Lipinski rule, one violation of the Jorgensen rule, and good lipophilic features. A marked improvement with respect to the lead compound **34** was recorded for the predicted apparent MDCK and Caco-2 cell permeability, and the predicted brain/blood partition coefficient, especially for compounds **38** and **39**. These data represent key features for an effective antitrypanosomal agent. Moreover, a prospective increase in the solubility is also reported for **39** and **36**, which fall within the suggested range of values. Thus, compound **39** should meet the necessary requirements to be a good lead compound for new antitrypanosomal agents design and discovery.

6.3 Synthesis and biological activity of compounds 41-51

In the light of the obtained data, compounds **41-45** variously decorated with fluorine atoms in different positions of the aromatic nucleus were synthesized to further investigate the role of the fluorine at the P3 position.

The synthesis of compounds **41-45** was carried out in a similar way as described for derivatives **35-40** and is reported in Scheme 6.

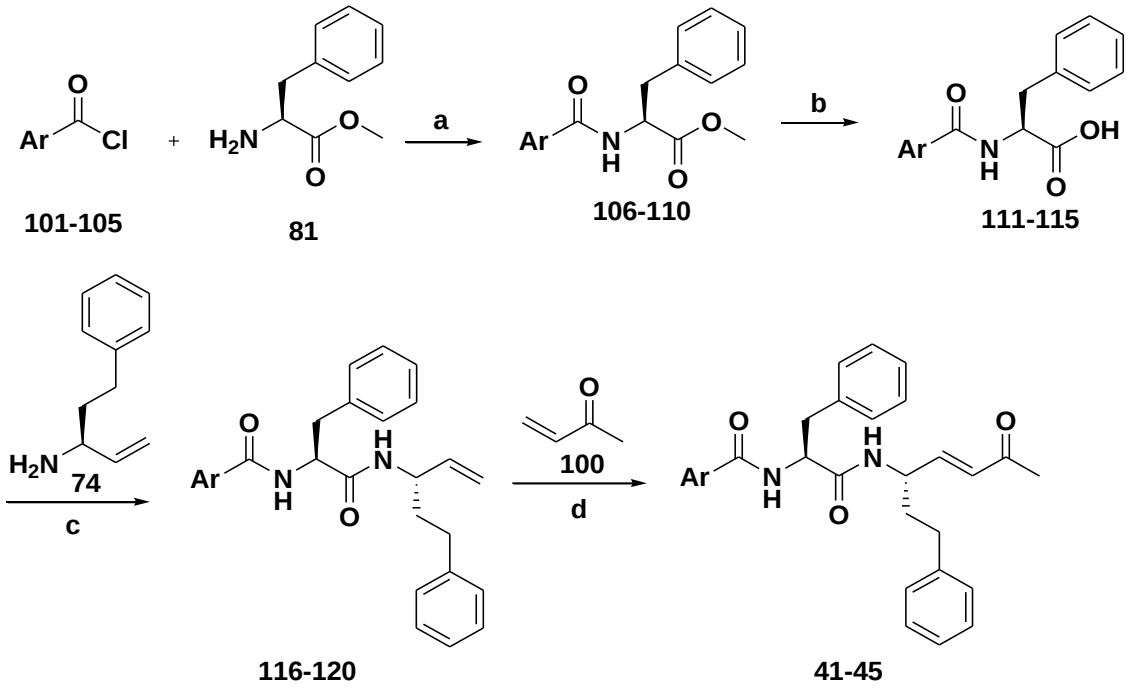

101, 106, 111, 116	102, 107, 112, 117	103, 108, 113, 118	104, 109, 114, 119	105, 110, 115, 120
41	42	43	44	45
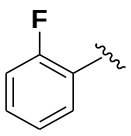	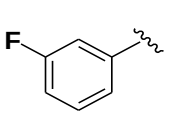	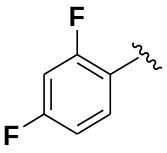	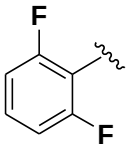	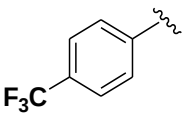

Scheme 6. Reagents and conditions: a) Appropriate acyl chloride, dry DCM, DIPEA, MW, 10 min, 50 °C, 200 W; b) LiOH, MeOH/H_2O/dioxane (1:1:1), 0° C, 10 min, then rt, 12h; c) HOBt, EDCI, dry DMF/CH_2Cl_2, 0°C, 10 min, then DIPEA, rt, 12h; e) 2nd generation Hoveyda-Grubbs catalyst, dry CH_2Cl_2, 100 °C, MW, 100 W, 2 h.

At the same time, I synthesized derivatives **46-51** characterized by the presence of different non-natural amino acids at P2 site, i.e. L-cyclohexylalanine, 4-F-L-Phe and 4-methyl-L-Phe, whose amino group was functionalized as 4-fluorobenzoyl or 3,5-difluorobenzoyl amide. The synthesis of compound **46-51** is reported in Schemes 7 and 8.

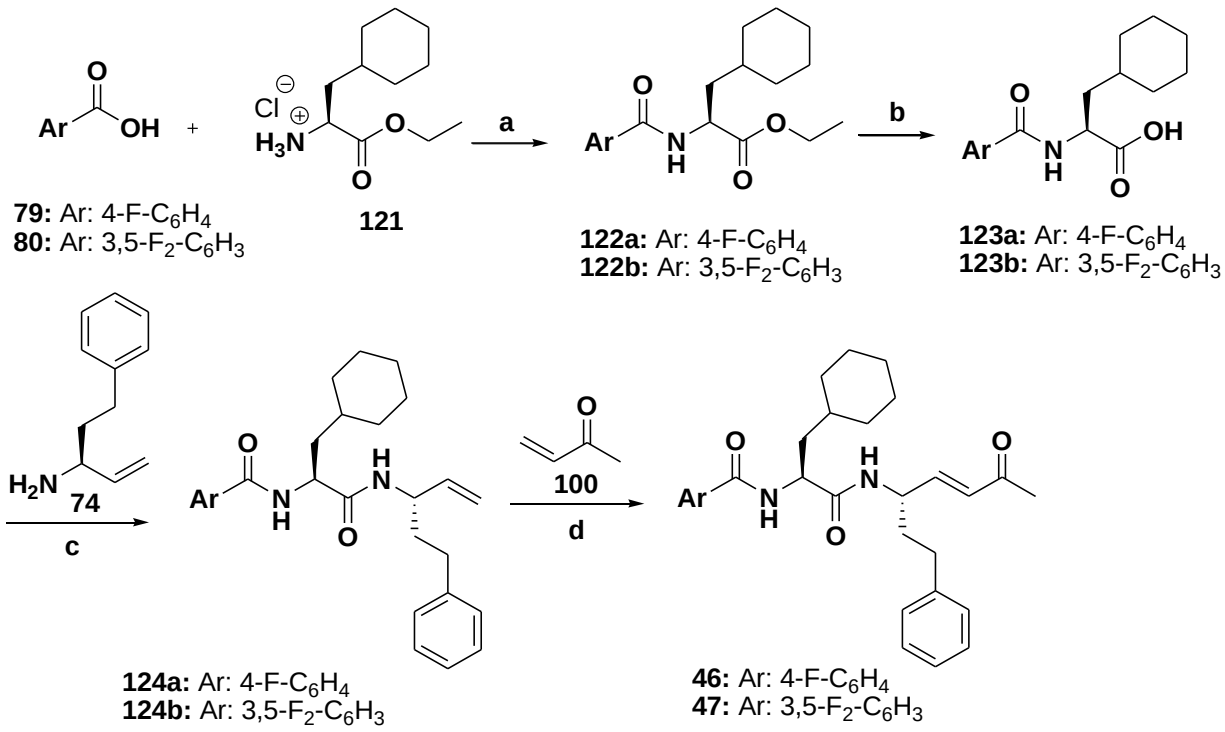

Scheme 7. Reagents and conditions: a) HOBt, EDCI, dry DMF/CH_2Cl_2, 0°C, 10 min, then DIPEA, rt, 12h; b) LiOH, MeOH/H_2O/dioxane (1:1:1), 0° C, 10 min, then 12h; c) HOBt, EDCI, dry DMF/CH_2Cl_2, 0°C, 10 min, then DIPEA, rt, 12h; e) 2nd generation Hoveyda-Grubbs catalyst, dry CH_2Cl_2, 100 °C, MW, 2 h.

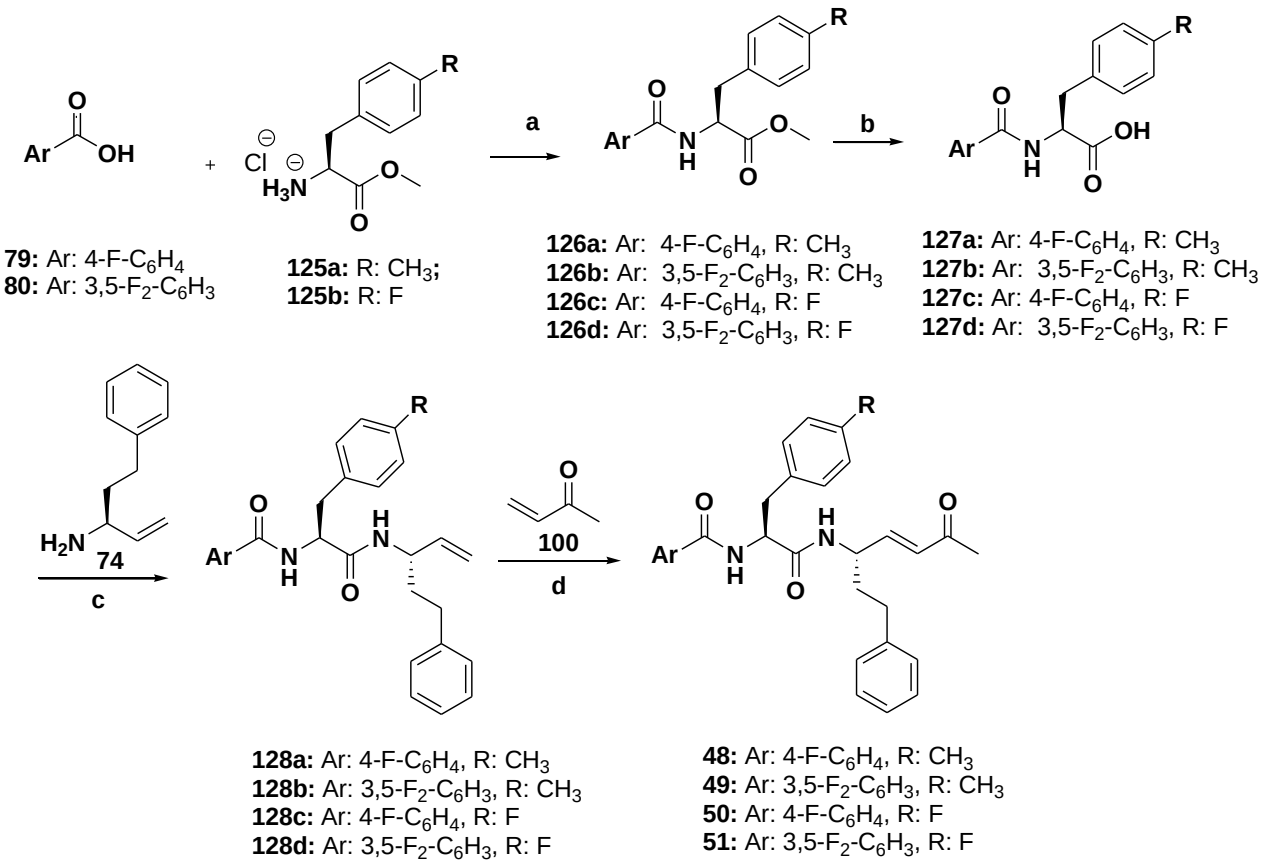

Scheme 8. Reagents and conditions: a) HOBt, EDCI, dry DMF/CH_2Cl_2, 0°C, 10 min, then DIPEA, rt, 12h; b) LiOH, MeOH/H_2O/dioxane (1:1:1), 0° C, 10 min, then 12h; c) HOBt, EDCI, dry DMF/CH_2Cl_2, 0°C, 10 min, then DIPEA, rt, 12h; e) 2nd generation Hoveyda-Grubbs catalyst, dry CH_2Cl_2, 100 °C, MW, 2 h.

Also in this case, compounds **41-51** were tested to evaluate their activity against rhodesain by fluorimetric assays. A survey of the results of rhodesain inhibition of compounds **41-45** (Table 9), in comparison with those obtained for compounds **39-40**, put in evidence that the substitution pattern on the phenyl at the P3 position has a remarkable impact on the inhibition of the target protease. If we consider the K_i values, which express the affinity of the inhibitor for the enzyme, the 2,4-difluoro substituted derivative **43**, with its subpicomolar K_i (K_i = 0.6 pM) gave the best results. However, being irreversible inhibitors, the rate of the formation of the covalent adduct (i.e. k_{inac}) should also be considered. Thus, based on both values of K_i and k_{2nd}, we can conclude that the optimal substitution pattern on the phenyl is represented by the presence of

electronwithdrawing fluorine atom or CF_3 group located at 2 or 4 position. In difluoro-derivatives, the best results have been achieved with 2,6-F_2-substituted compound **44**.

Table 9. Activity of the Michael acceptors **41-45** towards rhodesain**.**

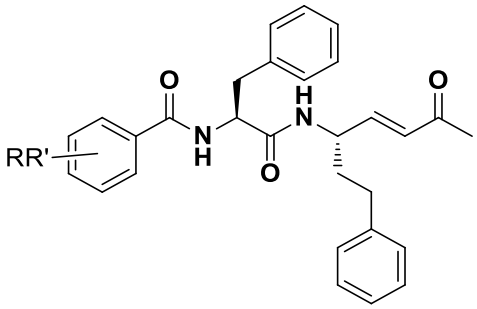

Comp	R	R'	Rhodesain		
			k_{inac} (min^{-1})	K_i (nM)	k_{2nd} (x 10^3 M^{-1} min^{-1})
41	2-F	H	0.0006±0.0001	0.003±0.001	230300±86200
42	3-F	H	0.0032±0.0005	0.023±0.008	149200±27900
43	2-F	4-F	0.00007±0.00003	0.0006±0.0003	107100±2200
44	2-F	6-F	0.0012±0.0001	0.0076±0.001	150800±6500
45	4-CF_3	H	0.00075±0.00005	0.0044±0.0005	174700±31400
39	4-F	H	0.0009±0.00002	0.0011±0.0002	881100±102450
40	3-F	5-F	0.0016±0.0006	0.015±0.008	112600±18600

With the synthesis of derivatives **46-51**, we wanted to investigate the relevance of the L-Phe residue at the P2 site: data reported in Table 9 indicate that the substitution of Phe residue with the L-cyclohexylalanine, 4-F-L-phenylalanine and 4-methyl-L-phenylalanine causes a significant reduction of the inhibitory properties. However, since literature data suggest that these residues at P2 position could influence the metabolic stability or selectivity, these compounds could represent a good starting point to develop novel inhibitors with improved pharmacokineticand selectivity properties. A better rationalization of the obtained data will require molecular modeling studies as well as the evaluation of the inhibition profile of the most interesting derivatives against other cysteine proteases and an evaluation of the assessment of the pharmacokinetic properties. These studies are currently in progress.

Table 10. Activity of the Michael acceptors **46-51** towards rhodesain**.**

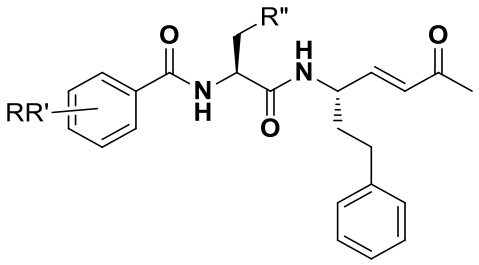

Comp	R	R'	R''	Rhodesain		
				k_{inac} (min^{-1})	K_i (nM)	k_{2nd} (x 10^3 M^{-1} min^{-1})
46	4-F	H	C_6H_{11}	0.0013±0.0001	1.10±0.15	1110±80
47	3-F	5-F	C_6H_{11}	0.0005±0.0002	0.04±0.03	18200±8000
48	4-F	H	4-Me-C_6H_4	0.00037±0.00003	0.027±0.004	14200±1100
49	3-F	5-F	4-Me-C_6H_4	0.0022±0.0003	0.20±0.04	11200±800
50	4-F	H	4-F-C_6H_4	0.0005±0.0002	0.046±0.008	10500±2600
51	3-F	5-F	4-F-C_6H_4	0.0006±0.0001	0.015±0.008	52500±26200
39	4-F	H	C_6H_5	0.0009±0.00002	0.0011±0.0002	881100±102450
40	3-F	5-F	C_6H_5	0.0016±0.0006	0.015±0.008	112600±18600

In conclusion, we designed and synthesized novel peptide-based vinyl ketones, some of which were shown to be nanomolar/picomolar irreversible inhibitors of rhodesain, with an antitrypanosomal activity in a low micromolar range. The vinyl ketone **39**, with a picomolar binding affinity and impressive potency towards rhodesain, coupled to its good antiparasitic activity, could represent a new lead compound for the development of novel antitrypanosomal agents.

7. Experimental Section

7.1 Chemistry.

All reagents and solvents were purchased from commercial suppliers and used without any further purification. Elemental analyses were performed on a C. Erba Model 1106 Elemental Analyzer and the results are within ±0.4% of the theoretical values. Merck silica gel 60 F254 plates were used for analytical TLC; column chromatography was carried out on Merck silica gel (200–400 mesh). ^{1}H-NMR and ^{13}C-NMR spectra were recorded on a Varian 300 MHz NMR spectrometer operating at frequencies of 300.13 and 75.47 MHz, or on a Varian 500 MHz spectrometer operating at 499.74 and 125.73 MHz for ^{1}H-NMR and ^{13}C-NMR spectra, respectively. The residual signal of the deuterated solvent was used as internal standard. Chemical shifts are given in δ (ppm) and coupling constants (*J*) in Hz. Splitting patterns are described as singlet (s), broad singlet (bs), doublet (d), triplet (t), quartet (q), multiplet (m), doublet of doublet (dd), or triplet of doublets (td).

_(S)_-2-Amino-4-phenylbutyric acid ethyl ester hydrochloride (69).

To a solution of ethanol (17 mL) at 0°C, $SOCl_2$ (2.1 mL, 29 mmol) was added dropwise. Compound **68** (4g, 22.3 mmol) was then added while stirring. The reaction was allowed to stirr for 48 h at room temperature. Solvent was removed *in vacuo* to afford compound **69** as white crystals**.** Yield = 99%. R_f = 0.66 (CH_2Cl_2/CH_3OH 9:1); ^{1}H NMR (300 MHz, $CDCl_3$): δ= 1.32 (t, J = 7.6 Hz, 3H) 1.65-1.84 (m, 1H), 1.85-2.04 (m, 1H), 2.49-2.70 (m, 2H), 3.24-3.39 (m, 1H), 3.56 (s, 3H), 6.94-7.20 (m, 5H) ppm.

_(S)_-4-Phenyl-2-(tritylamino)-butyric acid ethyl ester (70).

A mixture of *(S)*-2-amino-4-phenylbutyric acid ethyl ester hydrochloride **69** (5 g, 20 mmol), triphenylmethyl chloride (6.1 g, 22 mmol) and Et_3N (6.13 mL, 44 mmol) in dry CH_2Cl_2 (200 mL) was stirred at room temperature under nitrogen atmosphere for 12 h. After this time the mixture was washed with citric acid and water. The organic phase was dried over Na_2SO_4 and the solvent was removed under reduced pressure. The residue was purified by flash chromatography using as eluent petroleum ether/EtOAc (95/5) to afford title compound **70** (7.9 g, 89%). $[\alpha]^{20}_D$: +62,06 (c= 1.7, $CHCl_3$). RP-HPLC-MS: gradient D, retention time 5.95 min. MS (ESI$^+$) m/z 450.0 $[M + H]^+$ (100%). ^{1}H NMR

(300 MHz, $CDCl_3$): δ = 1.04 (t, J = 7.1 Hz, 3H), 2.01-2.17 (m, 2H), 2.55-2.79 (m, 2H), 3.35-3.55 (m, 2H), 3.63 (m, 1H), 7.14-7.29 (m, 15H), 7.49 (d, J = 8.0 Hz, 5H). ^{13}C NMR (75 MHz, $CDCl_3$): 14.15, 30.64, 33.58, 55.79, 61.33, 67.56, 126.18, 126.34, 128.34, 128.93, 129.38, 138.13, 145.01, 171.66.

***(S)*-4-Phenyl-2-(tritylamino)-butan-1-ol (71).**

To a solution of *(S)*-4-phenyl-2-(tritylamino)-butyric acid ethyl ester **70** (7.9 g, 17.8 mmol) in dry THF (90 mL) at 0 °C, under nitrogen atmosphere, $LiAlH_4$ was added (1.7 g, 44.5 mmol). After 6 h the mixture was quenched with NH_4Cl (20 mL) followed by evaporation of the solvent. The solide was removed by filtration while the residue was extracted with EtOAc. The organic layer was dried (Na_2SO_4) and the solvent was removed under reduced pressure. The title compound **71** (7.2 g, 99%) was used directly in the following step. $[\alpha]^{20}_D$: +47,40 (c= 0.27, $CHCl_3$). RP-HPLC-MS: gradient D, retention time 3.14 min. MS (ESI$^+$) m/z 408.0 $[M + H]^+$ (100%). ^{1}H NMR (300 MHz, $CDCl_3$): δ = 1.43-1.63 (m, 2H), 1.85 (bs, 1H), 2.21-2.49 (m, 2H), 2.67 (m, 1H), 3.15 (dd, J = 10.8, 4.2 Hz, 1H), 3.32 (dd, J = 10.8, 2.9 Hz, 1H), 7.12 (d, J = 6.9 Hz, 2H), 7.36-7.53 (m, 13H), 7.52 (d, J = 7.5 Hz, 5H). ^{13}C NMR (75 MHz, $CDCl_3$): 31.25, 33.19, 51.92, 67.30, 68.23, 126.09, 126.35, 128.25, 128.36, 128.62, 129.36, 138.73, 145.01.

***(S)*-4-Phenyl-2-(tritylamino)-butyraldehyde (72).**

To a 2M solution of oxalyl chloride in CH_2Cl_2 (15 mL, 30 mmol) at -78 °C under nitrogen atmosphere was added a solution of DMSO (5 mL, 71.2 mmol) in CH_2Cl_2 (6 mL) dropwise over a period of 10 min. A solution of alcohol **71** (7.2 g, 17.8 mmol) in CH_2Cl_2 (10 mL) was added dropwise over 20 min. The reaction mixture was stirred at -65 °C for 45 min, then Et_3N (16 mL, 115.7 mmol) was added dropwise over a period of 10 min and the mixture was stirred at -23 °C for further 40 min. The solvent was then evaporated under reduced pressure and the residue was taken up into diethyl ether (200 mL) and 0.5 N $KHSO_4$ solution (200 mL). The organic layer was separated, washed with water (200 mL) and brine (200 mL), dried (Na_2SO_4), filtered and concentrated under reduced pressure. The crude aldehyde **72** (7.2 g, 99%) was used for the next step without any further purification. $[\alpha]^{20}_D$: +100,22 (c= 0.45, $CHCl_3$).RP-HPLC-MS: gradient D, retention time 5.20 min. MS (ESI$^+$) m/z 406.0 $[M + H]^+$ (100%). ^{1}H NMR (300 MHz,

$CDCl_3$): δ = 1.73-1.82 (m, 2H), 2.50 (m, 1H), 2.71 (m, 1H), 3.43 (m, 1H), 7.09-7.31 (m, 15H), 7.45-7.58 (m, 5H), 9.01 (s, 1H). ^{13}C NMR (75 MHz, $CDCl_3$): 30.62, 30.73, 66.06, 67.63, 126.18, 126.34, 128.25, 128.32, 128.99, 129.32, 138.15, 145.02, 200.20.

***(S)*-(1-Phenethylallyl)-tritylamine (73).**

To a suspension of triphenylphosphonium iodide (14.39 g, 35.6 mmol) in dry THF (360 mL), at 0 °C under nitrogen atmosphere, was added BuLi (1.6 M solution in THF, 22.2 mL, 35 mmol) dropwise over 10 min. The resulting clear orange solution was stirred at 0°C for 10 min before adding aldehyde **72** (7.20 g, 17.8 mmol) as a solution in dry THF (20 mL). The resulting mixture was allowed to warm to room temperature over a period of 3 h, when hexane (200 mL) was added. The resulting precipitate was filtered off and the filtrate was washed with water (2 x 200 mL). The organic phase was separated, dried (Na_2SO_4), and concentrated under reduced pressure. The residue was purified by flash chromatography eluting with petroleum ether/EtOAc (1/1) to give compound **34** (6.45 g, 90%) as a yellow oil. $[\alpha]^{20}_D$: +12,31 (c= 0.65, $CHCl_3$). RP-HPLC-MS: gradient D, retention time 5.75 min. MS (ESI^+) m/z 404.0 $[M + H]^+$ (100%). ^1H NMR (300 MHz, $CDCl_3$): δ = 0.83-0.90 (m, 2H), 2.23 (m, 1H), 2.41 (m, 1H), 3.04 (q, J = 6.6 Hz, 1H), 4.88-4.94 (m, 2H), 5.61 (m, 1H), 6.91 (d, J = 7.1 Hz, 2H), 7.09-7.32 (m, 12H), 7.52 (d, J = 7.1 Hz, 6H). ^{13}C NMR (75 MHz, $CDCl_3$): 31.32, 38.13, 51.96, 68.24, 115.87, 126.18, 126.34, 128.22, 128.38, 128.94, 129.35, 135.21, 138.11, 145.06.

***(S)*-1-Phenethylallylamine (74).**

To a solution *(S)*-(1-phenethylallyl)-tritylamine **73** (6.45 g 16 mmol) in dichlorometane (261 mL) was added TFA (5 mL, 2%) dropwise over 5 min and the resulting mixture was stirred for 4 h. The solvent was then evaporated under reduced pressure, the residue was taken up in Et_2O (200 mL) and water. The acqueous phase was brought to pH = 12 by additon of solid Na_2CO_3 and extracted with CH_2Cl_2 (2 x 200 mL). The organic phase was dried (Na_2SO_4), filtered, and concentrated under reduced pressure to give amine **74** (2.26 g, 88%). $[\alpha]^{20}_D$: +5,05 (c= 0.43, $CHCl_3$). RP-HPLC-MS: gradient D, retention time 1.53 min. MS (ESI^+) m/z 162.0 $[M + H]^+$ (100%). ^1H NMR (300 MHz, $CDCl_3$): δ = 1.92-1.99 (m, 2H), 2.57-2.70 (m, 2H), 3.94 (q, J = 6.5 Hz, 1H), 5.01-5-07 (m, 2H), 5.79

(m, 1H), 7.15-7.21 (m, 3H), 7.25-7.29 (m, 2H). ^{13}C NMR (75 MHz, $CDCl_3$): 31.01, 39.75, 54.04, 115.87, 126.15, 128.27, 128.93, 135.27, 138.15.

(*S*)-Methyl 2-(2,3-dihydrobenzo[*b*][1,4]dioxine-6-carboxamido)-3-phenylpropanoate (82)

To a solution of acid **75** (200 mg, 1.1 mmol, 1 equiv.) in dry DMF/CH_2Cl_2 (1:1), HOBt (179 mg, 1.33 mmol, 1.2 equiv.) and EDCI (276 mg, 1.33, 1.2 equiv.) were added at 0° C. After 10 min, the amine **81** (255 mg, 1.33 mmol, 1.2 equiv.) and DIPEA (279 μL, 1.6 mmol, 1.5 equiv.) were added and the reaction mixture was stirred at rt for 12 h. After this time, the mixture was washed with brine (5 x 30 mL), dried over Na_2SO_4, filtered and concentrated *in vacuo*. The crude residue was purified by column chromatography using light petroleum/EtOAc (9:1) as eluent mixture, to obtain compound **82**. Yield*:* 81%; Consistency: white solid; R_f = 0.37 (light petroleum/EtOAc, 7:3); ^{1}H NMR (300 MHz, $CDCl_3$) = *δ*: 3.11 (dd, *J* = 12.4, 7.3 Hz, 1H), 3.35 (dd, *J* = 12.4, 7.3 Hz, 1H), 3.78 (s, 3H), 4.20-4.39 (m, 4H), 4.93-5.06 (m, 1H), 6.99 (d, *J* = 1.4 Hz, 1H), 7.10-7.20 (m, 4H), 7.24-7.31 (m, 2H), 7.58 (d, *J* = 1.4 Hz, 1H); ^{13}C (75 MHz, $CDCl_3$) = *δ*: 37.90, 53.18, 53.98, 64.16, 64.53, 116.42, 116.83, 120.66, 127.37, 128.39, 129.13, 129.52, 135.96, 143.37, 146.73, 166.19, 172.17.

(*S*)-Methyl 2-(benzo[*d*][1,3]dioxole-5-carboxamido)-3-phenylpropanoate (83)

Synthesis of product **83** was carried out following the procedure described for compound **82**, using **76** as acid. Yield: 91%; Consistency*:* brown oil; R_f = 0.70 (light petroleum/EtOAc, 5:5); ^{1}H NMR (300 MHz, $CDCl_3$) = δ: 3.20 (qd, *J* = 13.8, 5.9 Hz, 2H), 3.71 (s, 3H), 4.94-5.10 (m, 1H), 5.93 (s, 2H), 6.73 (d, *J* = 7.9 Hz, 2H), 7.06-7.35 (m, 7H) ppm.

(*S*)-Methyl 2-(2-(benzo[*d*][1,3]dioxol-5-yl)acetamido)-3-phenylpropanoate (84)

Synthesis of product **84** was carried out following the procedure described for compound **82**, using **77** as acid. Yield: 77%; Consistency: white solid; R_f = 0.44 (light petroleum/EtOAc, 1:1); ^{1}H NMR (300 MHz, $CDCl_3$) = *δ*: 2.90-3.14 (m, 2H), 3.42 (s, 2H), 3.69 (s, 3H), 4.73-4.91 (m, 1H), 5.85-6.03 (bs, 1H), 5.93 (s, 2H) 6.57-6.77 (m, 3H), 6.88-6.98 (m, 2H), 7.13-7.29 (m, 3H); ^{13}C (75 MHz, $CDCl_3$) = *δ*: 35.57, 43.12, 52.31,

52.93, 101.09, 108.56, 109.72, 122.57, 127.06, 127.97, 128.48, 129.15, 135.58, 146.86, 147.98, 170.56, 171.82.

(*S*)-Methyl 2-(4-chlorobenzamido)-3-phenylpropanoate (85)

Synthesis of product **85** was carried out following the procedure described for compound **82**, using **78** as acid. Yield*:* 74%; Consistency: white crystals; R_f = 0.35 (light petroleum/EtOAc, 8:2); ^{1}H NMR (300 MHz, $CDCl_3$) = δ: 3.12-3.35 (m, 2H), 3.77 (s, 3H), 4.99-5.13 (m, 1H), 6.53 (bs, 1H), 7.07-7.16 (m, 2H), 7.22-7.34 (m, 3H), 7.35-7.44 (m, 2 H), 7.61-7.70 (m, 2H) ppm.

(*S*)-Methyl 2-(4-fluorobenzamido)-3-phenylpropanoate (86)

Synthesis of product **86** was carried out following the procedure described for compound **82**, using **79** as acid. Yield*:* 78%; Consistency: clear oil; R_f = 0.64 (light petroleum/EtOAc, 7:3); ^{1}H NMR (300 MHz, $CDCl_3$) = δ: 3.24 (qd, *J* = 13.8, 5.7 Hz, 2H), 3.76 (s, 3H), 5.01-5.11 (m, 1H), 6.63 (d, *J* = 7.4 Hz, 1H), 7.02-7.17 (m, 4H), 7.22-7.34 (m, 3H), 7.68-7.76 (m, 2 H) ppm.

(*S*)-Methyl 2-(3,5-difluorobenzamido)-3-phenylpropanoate (87)

Synthesis of product **87** was carried out following the procedure described for compound **82**, using **80** as acid. Yield: 77%; Consistency*:* white solid*;* R_f = 0.22 (light petroleum/EtOAc, 9:1); ^{1}H NMR (300 MHz, $CDCl_3$) = *δ*: 3.16 (qd, *J* = 13.9, 5.7 Hz, 2H), 3.70 (s, 3H), 4.90-5.02 (m, 1H), 6.60 (d, *J* = 7.1 Hz, 1H), 6.85 (t, *J* = 8.5 Hz, 1H), 7.00-7.27 (m, 7H); ^{13}C (75 MHz, $CDCl_3$) = *δ*: 37.71, 52.60, 53.71, 107.15 (t, *J* = 25.4 Hz), 110.35 (q, *J* = 26.2, Hz), 127.37, 128.73, 129.25, 135.59, 137.16, 151.29, 162.92 (dd, *J* = 250.8, 12.0 Hz), 171.88.

(*S*)-2-(2,3-Dihydrobenzo[*b*][1,4]dioxine-6-carboxamido)-3-phenylpropanoic acid (88)

To a solution of the **82** (360 mg, 1.05 mmol, 1 equiv.) in a mixture methanol/water/dioxane (1:1:1), LiOH as powder (75 mg, 3.16 mmol, 3 equiv.) was added at 0° C. The reaction mixture was then stirred at rt for 12h. After this time, the solvents were evaporated *in vacuo*. The residue was treated with 10% solution citric acid

(2 x 20 mL), and the organic phase was extracted with EtOAc (3 x 30 mL), dried over Na_2SO_4 and concentrated to afford the pure carboxylic acid **88**. Yield: 93%; Consistency: white solid; R_f = 0.04 (light petroleum/EtOAc, 7:3); ^{1}H NMR (300 MHz, MeOD) = δ: 3.19 (dd, J = 12.4, 7.3 Hz, 1H), 3.39 (dd, J = 12.4, 7.3 Hz, 1H), 4.26-4.43 (m, 4H), 4.98-5.11 (m, 1H), 7.03 (d, J = 1.5 Hz, 1H), 7.12-7.22 (m, 4H), 7.25-7.34 (m, 2H), 7.63 (d, J = 1.5 Hz, 1H); ^{13}C (75 MHz, MeOD) = δ: 37.22, 53.68, 64.11, 64.47, 116.39, 116.77, 120.52, 127.48, 128.69, 129.52, 129.83, 136.03, 143.52, 146.87, 165.94, 171.87.

(*S*)-2-(Benzo[*d*][1,3]dioxole-5-carboxamido)-3-phenylpropanoic acid (89)

Synthesis of product **89** was carried out following the procedure described for compound **88**. Yield*:* 87%; Consistency*:* white crystals*;* R_f = 0.02 (light petroleum/EtOAc, 9:1); ^{1}H NMR (300 MHz, MeOH-d_4) = δ: 3.02-3.16 (m, 1H), 3.25-3.31 (m, 1H), 4.83 (dd, J = 9.4, 5.0 Hz, 1H), 5.95 (s, 2H), 6.78 (d, J = 8.1 Hz, 1H), 7.12 – 7.34 (m, 8H) ppm.

(*S*)-2-(2-(Benzo[*d*][1,3]dioxol-5-yl)acetamido)-3-phenylpropanoic acid (90)

Synthesis of product **90** was carried out following the procedure described for compound **88**. Yield: 94%; Consistency: white solid; R_f = 0.04 (light petroleum/EtOAc, 1:1); ^{1}H NMR (300 MHz, MeOD) = δ: 2.86 (dd, J = 13.8, 5.9 Hz, 1H), 3.17 (dd, J = 13.8, 5.9 Hz, 1H), 3.39 (s, 2H), 4.66 (dd, J = 13.8, 5.9 Hz, 1H), 5.91 (s, 2H), 6.58-6.74 (m, 3H), 7.08-7.24 (m, 5H); ^{13}C (75 MHz, MeOD) = δ: 36.80, 41.72, 53.51, 100.85, 107.66, 109.05, 121.95, 126.38, 128.01, 128.69, 128.86, 136.77, 146.54, 147.68, 172.47, 173.22.

(*S*)-2-(4-Chlorobenzamido)-3-phenylpropanoic acid (91)

Synthesis of product **91** was carried out following the procedure described for compound **88** Yield: 94%; Consistency: white crystals; ^{1}H NMR (300 MHz, $CDCl_3$) = δ : 3.25 (dd, J = 14.0, 5.7 Hz, 1H), 3.29-3.36 (dd, J = 13.9, 5.4 Hz, 1H), 5.02-5.12 (m, 1H), 6.63 (d, J = 7.6 Hz), 7.13-7.22 (m, 2H), 7.23-7.33 (m, 3H), 7.34-7.40 (m, 2 H), 7.56-7.65 (m, 2H) ppm.

(*S*)-2-(4-Fluorobenzamido)-3-phenylpropanoic acid (92)

Synthesis of product **92** was carried out following the procedure described for compound **88**. Yield: 96%; Consistency: white crystals; ^{1}H NMR (300 MHz, MeOH-d_4) = δ : 3.10 (dd, *J* = 13.9, 9.7 Hz, 1H), 3.29-3.31 (m, 1H), 4.81-4.86 (m, 1H), 7.09-7.33 (m, 7H), 7.72-7.84 (m, 2H) ppm.

(*S*)-2-(3,5-Difluorobenzamido)-3-phenylpropanoic acid (93)

Synthesis of product **93** was carried out following the procedure described for compound **88**. Yield*:* 96%; Consistency*:* white solid*;* R_f = 0.02 (light petroleum/EtOAc, 9:1); ^{1}H NMR (300 MHz, MeOD) = *δ*: 3.07 (dd, *J* = 13.9, 10.1 Hz, 1H), 3.35 (dd, *J* = 13.9, 4.9 Hz, 1H), 4.84 (dd, *J* = 10.1, 4.9 Hz, 1H), 7.06-7.37 (m, 8H); ^{13}C (75 MHz, MeOD) = *δ*: 37.23, 53.61, 107.22 (t, *J* = 24.3 Hz), 107.22 (q, *J* = 24.3 Hz), 127.52, 128.84, 129.31, 135.32, 136.74, 151.04, 162.77 (dd, *J* = 251.0, 12.1 Hz), 170.36.

***N*-((*S*)-1-Oxo-3-phenyl-1-((*S*)-5-phenylpent-1-en-3-ylamino)propan-2-yl)-2,3-dihydrobenzo[*b*][1,4]dioxine-6-carboxamide (94)**

To a solution of acid **88** (58 mg, 0.18 mmol, 1.2 equiv.) in dry DMF/CH_2Cl_2 (1:1), HOBt (24 mg, 1.2 equiv.) and EDCI (34 mg, 1.2 equiv.) were added at 0° C. After 10 min, the amine **74** (25 mg, 0.15 mmol, 1 equiv.) and DIPEA (41 μL, 0.23 mmol, 1.5 equiv.) were added and the reaction mixture was stirred at rt for 12 h. After this time, the mixture was washed with brine (5 x 40 mL), dried over Na_2SO_4, filtered and concentrated *in vacuo*. The crude residue was purified by flash column chromatography using cyclohexane/EtOAc (6:4) as eluent mixture, to obtain terminal olefin **94**. Yield*:* 80%; Consistency: white solid; R_f = 0.31 (light petroleum/EtOAc, 1:1); ^{1}H NMR (300 MHz, $CDCl_3$) = *δ*: 1.68-1.94 (m, 2H), 2.52 (t, *J* = 7.6 Hz, 2H), 3.00-3.19 (m, 2H), 4.18-4.42 (m, 5H), 4.67-4.81 (m, 1H), 4.88-5.09 (m, 2H), 5.27 (d, *J* = 6.7 Hz, 1H), 5.58-5.70 (m, 1H), 5.88 (d, *J* = 7.3 Hz, 1H), 7.03 (d, *J* = 1.5 Hz, 1H), 7.12-7.22 (m, 7H), 7.25-7.34 (m, 4H), 7.63 (d, *J* = 1.5 Hz, 1H); ^{13}C (75 MHz, $CDCl_3$) = *δ*: 31.84, 36.32, 38.59, 51.84, 56.02, 64.17, 64.51, 115.61, 116.44, 116.80, 120.74, 126.23, 126.78, 127.63, 128.01, 128.21, 128.63, 128.86, 136.74, 137.55, 141.20, 146.59, 147.73, 166.87, 170.38.

***N*-((*S*)-1-Oxo-3-phenyl-1-(((*S*)-5-phenylpent-1-en-3-yl)amino)propan-2-yl)benzo[*d*][1,3]dioxole-5-carboxamide (95).**

Synthesis of product **95** was carried out following the procedure described for compound **94**, using **89** as acid. Yield: 70%; R_f = 0.49 (cyclohexane/EtOAc, 7:3). Consistency*:* white solid. ^{1}H NMR (300 MHz, $CDCl_3$) =δ: 1.55-1.83 (m, 2H), 2.48 (t, *J* = 8.2 Hz, 2H), 3.02-3.30 (m, 2H), 4.33-4.47 (m, 1H), 4.79-4.89 (m, 1H), 4.90-5.15 (m, 2H), 5.54-5.74 (m, 1H), 6.01 (s, 2H), 6.08-6.23 (m, 1H), 6.79 (d, *J* = 7.6 Hz, 1H), 6.88-7.02 (m, 1H), 7.04- 7.32 (m, 12 H).

(*S*)-2-(2-(benzo[*d*][1,3]dioxol-5-yl)acetamido)-3-phenyl-*N*-((*S*)-5-phenylpent-1-en-3-yl)propanamide (96)

Synthesis of product **96** was carried out following the procedure described for compound **94**, using **90** as acid. Yield*:* 83%; Consistency: white solid*;* R_f = 0.33 (light petroleum/EtOAc, 1:1); ^{1}H NMR (300 MHz, CDCl3) = δ: 1.59-1.81 (m, 2H), 2.51 (t, *J* = 7.6 Hz, 2H), 3.01-3.16 (m, 2H), 3.41 (s, 2H), 4.20-4.29 (m, 1H), 4.64-4.76 (m, 1H), 4.90-5.09 (m, 2H),5.44 (d, *J* = 6.8 Hz, 1H), 5.55-5.71 (m, 1H), 5.80 (d, *J* = 7.4 Hz, 1H),5.94 (s, 2H), 6.58-6.74 (m, 3H), 7.07-7.32 (m, 10H); ^{13}C (75 MHz, $CDCl_3$) = δ: 31.97, 36.38, 38.15, 43.11, 51.42, 54.33, 101.09, 108.38, 109.43, 115.36, 122.67, 125.76, 126.16, 128.20, 128.38, 128.55, 128.79, 129.58, 136.42, 137.58, 141.40, 146.88, 148.13, 170.23, 171.31.

4-Chloro-*N*-((*S*)-1-oxo-3-phenyl-1-(((*S*)-5-phenylpent-1-en-3-yl)amino)propan-2-yl)benzamide (97).

Synthesis of **97** was carried out following the procedure described for compound **94**, using **91** as acid. Yield: 68%; R_f = 0.42 (light petroleum /EtOAc, 3:2). Consistency: white solid. ^{1}H NMR (300 MHz, $CDCl_3$) = δ: 1.64-1.86 (m, 3H), 2.50 (t, *J* = 7.9 Hz, 2H), 3.03-3.15 (m 1H), 3.17-3.29 (m, 1H), 4.33-4.48 (m, 1H), 4.71-4.87 (m, 1H), 4.89-5.16 (m, 1H), 5.51-5.88 (m, 2H), 6.93 (d, *J* = 7.0 Hz, 1H), 7.04-7.13 (m, 2H), 7.18-7.34 (m, 8H), 7.36-7.43 (m, 2H), 7.65-7.73 (m, 2H).

4-Fluoro-*N*-((*S*)-1-oxo-3-phenyl-1-(((*S*)-5-phenylpent-1-en-3-yl)amino)propan-2-yl)benzamide (98).

Synthesis of terminal olefin **98** was carried out following the procedure described for compound **94**, using **92** as acid. Yield*:* 65%; R_f = 0.62 (cyclohexane/EtOAc, 3:2).

Consistency: white solid. ^{1}H NMR (300 MHz, $CDCl_3$) = δ: 1.57-1.89 (m, 3H), 2.49 (t, *J* = 7.9 Hz, 2H), 3.03-3.28 (m 2H), 4.34-4.48 (m, 1H), 4.84-5.22 (m, 3H), 5.52-5.78 (m, 1H), 6.97-7.35 (m, 13 H), 7.75 (dd, *J* = 8.6, 5.3 Hz, 2H).

3,5-Difluoro-*N*-((*S*)-1-oxo-3-phenyl-1-((*S*)-5-phenylpent-1-en-3-ylamino)propan-2-yl)benzamide (99)

Synthesis of product **99** was carried out following the procedure described for compound **94**, using **93** as acid. Yield: 74%; Consistency*:* white solid; R_f = 0.43 (light petroleum/EtOAc, 4:1); ^{1}H NMR (300 MHz, $CDCl_3$) = *δ*: 1.88-1.98 (m, 2H); 2.58 (t, *J* = 7.6 Hz, 2H), 2.99-3.18 (m, 2H), 4.18-4.27 (m, 1H), 4.60-4.72 (m, 1H), 4.96-5.12 (m, 2H), 5.42 (d, *J* = 6.7 Hz, 1H), 5.57-5.70 (m, 1H), 5.86 (d, *J* = 8.3 Hz, 1H),6.98-7.09, (m, 1H), 7.18-7.34 (m, 8H), 7.40-7.51 (m, 4H); ^{13}C (75 MHz, $CDCl_3$) = *δ*: 31.93, 36.22, 38.64, 51.74, 55.84, 107.16 (q, *J* = 25.7 Hz), 110.53 (t, *J* = 28.1 Hz), 115.69, 125.80, 126.21, 128.23, 128.51, 129.20, 129.60, 136.38, 137.15, 137.40, 141.21, 162.88 (dd, *J* = 251.5, 10.0 Hz), 164.81, 170.11.

***N*-((*S*)-1-oxo-1-(((*S*,*E*)-6-oxo-1-phenylhept-4-en-3-yl)amino)-3-phenylpropan-2-yl)-2,3-dihydrobenzo[*b*][1,4]dioxine-6-carboxamide (35)**

A solution of terminal olefin **94** (1 equiv.) in dry CH_2Cl_2 (3 mL), in a 10 mL microwave tube equipped with a magnetic stirrer, was treated with methyl vinyl ketone **100** (10 equiv.) and 2nd generation Hoveyda–Grubbs catalyst [(1,3-bis-(2,4,6-trimethylphenyl)-2-imidazolidinylidene)-dichloro-(*o*-isopropoxyphenylmethylene) ruthenium] (0.1 equiv.) under microwave irradiation at 100°C for 2h. Subsequently, the solvent was removed under reduced pressure and the residue was purified by column chromatography using light petroleum/EtOAc, 2:3 as eluent mixture, to obtain Michael acceptor **35**. Yield: 87%; Consistency: white solid; R_f = 0.17 (light petroleum/EtOAc, 1:1); ^{1}H NMR (300 MHz, $CDCl_3$) = *δ*: 1.69-1.98 (m, 2H), 2.27 (s, 3H), 2.50 (t, *J* = 7.6 Hz, 2H), 2.96-3.17 (m, 2H), 4.22-4.46 (m, 5H), 4.59-4.71 (m, 1H), 5.39 (d, *J* = 6.4 Hz, 1H), 5.88 (d, *J* = 7.3 Hz, 1H),6.04 (d, *J* = 15.2 Hz, 1H), 6.67 (dd, *J* = 15.2, 6.0 Hz, 1H),7.06 (d, *J* = 1.6 Hz, 1H), 7.11-7.39 (m, 11H), 7.63 (d, *J* = 1.6 Hz, 1H);); ^{13}C (75 MHz, $CDCl_3$) = *δ*: 26.83, 31.93, 36.41, 38.67, 51.94, 56.17, 64.20, 64.56, 116.52, 116.84, 120.89, 126.34, 126.74, 127.76, 128.07, 128.27, 128.69, 128.93, 130.77, 136.81, 141.35, 146.62, 147.86, 149.16,

166.90, 170.43, 197.65; Elemental analysis: calcd for $C_{31}H_{32}N_2O_5$: C 72.64; H 6.29; N 5.47; found: C 72.47, H 5.96, N 5.71.

_N_-((_S_)-1-Oxo-1-(((_S,E_)-6-oxo-1-phenylhept-4-en-3-yl)amino)-3-phenylpropan-2-yl)benzo[_d_][1,3]dioxole-5-carboxamide (36).

Synthesis of product **36** was carried out following the procedure described for compound **35**, using **95** as terminal olefin. Yield: 86%; R_f = 0.70 (light petroleum/EtOAc, 2:3). Consistency: white powder. ^{1}H NMR (300 MHz, $CDCl_3$) = δ: 1.62-1.89 (m, 2H), 2.20 (s, 3H), 2.56 (t, J = 7.6 Hz, 2H), 3.07-3.32 (m, 2H), 4.49-4.65 (m, 1H), 4.74-4.89 (m, 1H), 5.93 (d, J = 15.8 Hz, 1H), 6.02 (s, 2H), 6.23 (d, J = 7.6 Hz, 1H), 6.46 (dd, J = 15.8, 5.6 Hz, 1H), 6.69 (d, J = 6.4 Hz, 1H), 7.05 (d, J = 7.5 Hz, 2H), 7.13-7.38 (m, 11H). ^{13}C (125MHz, $CDCl_3$) = 27.70, 31.81, 35.74, 38.04, 50.03, 55.19, 101.81, 107.59, 108.10, 121.86, 127.27, 127.60, 128.30, 128.52, 128.87, 129.25, 129.28, 129.30, 129.94, 136.46, 140.51, 145.27, 148.09, 166.77, 170.45, 197.87.Elemental analysis calcd for $C_{30}H_{30}N_2O_5$: C 72.27; H 6.06; N 5.62. Found: C 72.38; H 6.29; N 5.40.

(_S_)-2-(2-(Benzo[_d_][1,3]dioxol-5-yl)acetamido)-_N_-((_S,E_)-6-oxo-1-phenylhept-4-en-3-yl)-3-phenylpropanamide (37)

Synthesis of product **37** was carried out following the procedure described for compound **35**, using **96** as terminal olefin. Yield: 81%; Consistency: white solid; R_f = 0.18 (light petroleum/EtOAc, 1:1); ^{1}H NMR (300 MHz, $CDCl_3$) = δ: 1.66-1.92 (m, 2H), 2.24 (s, 3H), 2.54 (t, J = 7.8 Hz, 2H), 2.96-3.11 (m, 2H), 3.39 (s, 2H), 4.17-4.28 (m, 1H), 4.59-4.67 (m, 1H), 5.55 (d, J = 6.6 Hz, 1H), 5.89 (d, J = 7.3 Hz, 1H), 5.96 (s, 2H), 6.14 (d, J = 15.1 Hz, 1H), 6.69 (dd, J = 15.1, 6.1 Hz, 1H),6.58-6.74 (m, 3H), 7.07-7.32 (m, 10H); ^{13}C (75 MHz, $CDCl_3$) = δ: 27.51, 32.04, 38.21, 43.16, 51.54, 54.43, 101.17, 108.42, 109.49, 122.74, 125.80, 126.19, 128.29, 128.43, 128.62, 128.84, 129.66, 130.81, 136.42, 141.53, 146.95, 148.17, 149.24, 170.29, 171.33, 197.57; Elemental analysis: calcd for $C_{31}H_{32}N_2O_5$: C 72.64; H 6.29; N 5.47; found: C 72.40, H 6.55, 5.19.

4-Chloro-_N_-((_S_)-1-oxo-1-(((_S,E_)-6-oxo-1-phenylhept-4-en-3-yl)amino)-3-phenylpropan-2-yl)benzamide (38).

Synthesis of Michael acceptor **38** was carried out following the procedure described for compound **35**, starting from terminal olefin **97** under microwave irradiation for 2 h. Yield*:* 82%; R_f = 0.79 (light petroleum/EtOAc, 2:3). Consistency: white powder. ^{1}H NMR (300 MHz, $CDCl_3$) **=** *δ*: 1.62-1.92 (m, 2H), 2.20 (s, 3H), 2.52 (t, *J* = 7.6 Hz, 2H), 3.06-3.26 (m, 2H), 4.49-4.61 (m, 1H), 4.84-4.98 (m, 1H), 6.10 (d, *J* = 15.8 Hz, 1H), 6.45 (dd, *J* = 15.8 Hz, 5.4, 1H),6.53-6.66 (m, 1H), 6.99-7.12 (m, 2H), 7.13-7.42 (m, 11H), 7.60-7.75 (m, 2H). ^{13}C (125MHz, $CDCl_3$) = *δ*: 27.68, 31.84, 35.72, 38.35, 50.07, 55.23, 126.24, 127.31, 128.25, 128.50, 128.53, 128.84, 128.94, 129.29, 130.01, 131.85, 136.23, 138.35, 140.49, 145.15, 166.37, 170.34, 197.77. Elemental analysis calcd for $C_{29}H_{29}ClN_2O_3$: C 71.23; H 5.98; N 5.73. Found: C 71.65; H 5.82; N 5.60.

4-Fluoro-*N*-((*S*)-1-oxo-1-(((*S,E*)-6-oxo-1-phenylhept-4-en-3-yl)amino)-3-phenylpropan-2-yl)benzamide (39).

Synthesis of Michael acceptor **39** was carried out following the procedure described for compound **35**, starting from terminal olefin **98**. Yield: 84%; R_f = 0.77(light petroleum/EtOAc, 2:3). Consistency: white powder. ^{1}H NMR (300 MHz, $CDCl_3$) = *δ*: 1.62-1.91 (m, 2H), 2.19 (s, 3H), 2.52 (t, *J* = 7.6 Hz, 2H), 3.06-3.27 (m, 2H), 4.49-4.63 (m, 1H), 4.85-4.99 (m, 1H), 6.10 (d, *J* = 15.8 Hz, 1H), 6.46 (dd, *J* = 15.8 Hz, 5.9, 1H), 6.51-6.71 (m, 1H), 6.99-7.37 (m, 13H), 7.67-7.81 (m, 2H). ^{13}C (125MHz, $CDCl_3$) = *δ*: 27.67, 31.84, 35.47, 38.34, 50.05, 55.21, 115.76 (d, *J* = 21.9) 126.23, 127.29, 128.25, 128.52, 128.83, 129.29, 129.45 (d, *J* = 9.1), 129.67, 129.99, 136.30, 140.52, 145.20, 165.00 (d, J = 252.4), 166.42, 170.40, 197.57.Elemental analysis calcd for $C_{29}H_{29}FN_2O_3$: C 73.71; H 6.19; N 5.93. Found: C 73.65; H 6.32; N 5.61.

3,5-Difluoro-*N*-((*S*)-1-oxo-1-(((*S,E*)-6-oxo-1-phenylhept-4-en-3-yl)amino)-3-phenylpropan-2-yl)benzamide (40).

Synthesis of product **40** was carried out following the procedure described for compound **35**, using **99** as terminal olefin. Yield*:* 83%; Consistency: white solid*;* R_f = 0.27 (light petroleum/EtOAc, 4:1); ^{1}H NMR (300 MHz, $CDCl_3$) = *δ*: 1.86-1.97 (m, 2H), 2.23 (s, 3H) 2.55 (t, *J* = 7.8 Hz, 2H), 3.01-3.22 (m, 2H), 4.16-4.29 (m, 1H), 4.51-4.60 (m, 1H), 5.36 (bs, 1H), 5.94 (d, *J* = 8.3 Hz, 1H), 6.01 (d, *J* = 15.2 Hz, 1H), 6.54 (dd, *J* = 15.2, 6.1 Hz, 1H), 7.02-7.11, (m, 1H), 7.16-7.32 (m, 8H), 7.44-7.57 (m, 4H); ^{13}C (75 MHz,

$CDCl_3$) = *δ*: 26.54, 32.14, 36.86, 38.41, 51.18, 56.67, 107.22 (q, *J* = 25.9 Hz), 110.59 (t, *J* = 28.0 Hz), 126.24, 126.97, 128.54, 128.79, 129.04, 129.51, 130.83, 136.78, 137.12, 141.29, 149.39, 163.51 (dd, *J* = 251.2, 9.8 Hz), 164.94, 170.22, 197.58; Elemental analysis: calcd for $C_{29}H_{28}F_2N_2O_3$: C 71.01; H 5.75; N 5.71; found: C 70.86, H 5.97, N 5.93.

(*S*)-Methyl 2-(2-fluorobenzamido)-3-phenylpropanoate (106)

To a solution of **81** (50 mg, 0.32 mmol) in dry CH_2Cl_2 (1 mL), DIPEA (112 μL, 0.64 mmol) and the suitable benzoyl chloride **101** (37.6 μL, 0.32 mmol) was added. The reaction was stirred under microwave irradiation for 10 min at 50 °C. After the reaction was stopped by the addition of CH_3OH (1 mL), water was added, and the mixture was extracted with CH_2Cl_2. The obtained organic phase was washed many times with brine and dried with anhydrous Na_2SO_4. Subsequently, the solvent was removed under reduced pressure and the product was used for the next step without further purification. Yield: 92%; Consistency*:* white solid*;* R_f = 0.86 (light petroleum/EtOAc, 5:5); ^{1}H NMR (300 MHz, $CDCl_3$) = *δ*: 3.23 (dd, *J* = 13.9, 5.9 Hz, 1H), 3.25 (dd, *J* = 13.9, 5.9 Hz, 1H), 3.78 (s, 3H), 5.02–5.16 (m, 1H), 7.05–8.114 (m, 10H) ppm.

(*S*)-Methyl 2-(3-fluorobenzamido)-3-phenylpropanoate (107)

Synthesis of product **107** was carried out following the procedure described for compound **106,** using **81** (50 mg, 0.32 mmol), DIPEA (112 μL, 0.64 mmol) and the suitable benzoyl chloride **102** (38.4 μL, 0.32 mmol). Yield: 85%; Consistency*:* white solid*;* R_f = 0.50 (light petroleum/EtOAc, 8:2); ^{1}H NMR (300 MHz, $CDCl_3$) = *δ*: 3.23 (dd, *J* = 13.9, 5.6 Hz, 1H), 3.28 (dd, *J* = 13.9, 5.6 Hz, 1H), 3.75 (s, 3H), 5.09 (ddd, *J* = 7.6, 5.6, 5.6 Hz, 1H), 6.53 (d, *J* = 7.6 Hz, 1H) 7.15–7.79 (m, 9H) ppm.

(*S*)-Methyl 2-(2,4-difluorobenzamido)-3-phenylpropanoate (108)

Synthesis of product **108** was carried out following the procedure described for compound **106,** using **81** (50 mg, 0.32 mmol), DIPEA (112 μL, 0.64 mmol) and the suitable benzoyl chloride **103** (38.8 μL, 0.32 mmol). Yield: 53 %; Consistency*:* white solid*;* R_f = 0.35 (light petroleum/EtOAc, 8:2); ^{1}H NMR (300 MHz, $CDCl_3$) = *δ*: 3.22 (dd, *J* = 13.9, 5.9 Hz, 1H), 3.25 (dd, *J* = 13.9, 5.9 Hz, 1H), 3.77 (s, 3H), 5.10 (dddd, *J* = 7.6, 5.9,

5.9, 2.0 Hz, 1H), 6.83 (ddd, *J* = 12.0, 8.5, 2.4 Hz, 1H), 6.94–7.09 (m, 1H), 7.03–7.19 (m, 1H) 7.13–7.34 (m, 5H), 8.05–8.19 (dt, *J* = 9.0, 6.6 Hz, 1H) ppm.

(*S*)-Methyl 2-(2,6-difluorobenzamido)-3-phenylpropanoate (109)

Synthesis of product **109** was carried out following the procedure described for compound **106,** using **81** (50 mg, 0.32 mmol), DIPEA (112 μL, 0.64 mmol) and the suitable benzoyl chloride **104** (39.6 μL, 0.32 mmol). Yield: 66 %; Consistency*:* white solid*;* R_f = 0.31 (light petroleum/EtOAc, 8:2); ^{1}H NMR (500 MHz, $CDCl_3$) = *δ*: 3.23 (dd, *J* = 13.9, 5.3 Hz, 1H), 3.32 (dd, *J* = 13.9, 5.7 Hz, 1H), 3.77 (s, 3H), 5.12 (dt, *J* = 7.6, 5.5 Hz, 1H), 6.49 (bd, *J* = 6.6 Hz, 1H), 6.91 – 6.97 (m, 2H), 7.14 – 7.19 (m, 2H), 7.22 – 7.31 (m, 3H), 7.36 (tt, *J* = 8.5, 6.3 Hz, 1H) ppm.

(*S*)-Methyl 2-(4-(trifluoromethyl)benzamido)-3-phenylpropanoate (110)

Synthesis of product **110** was carried out following the procedure described for compound **106,** using **81** (50 mg, 0.32 mmol), DIPEA (112 μL, 0.64 mmol) and the suitable benzoyl chloride **105** (46.9 μL, 0.32 mmol). Yield: 97%; Consistency*:* white crystals*;* R_f = 0.35 (light petroleum/EtOAc, 8:2); ^{1}H NMR (500 MHz, $CDCl_3$) = *δ*: 3.23 (dd, *J* = 13.9, 5.5 Hz, 1H), 3.31 (dd, *J* = 13.9, 5.8 Hz, 1H), 3.79 (s, 3H), 5.09 (dd, *J* = 13.2, 5.7 Hz, 1H), 6.68 (bd, *J* = 7.2 Hz, 1H), 7.13 (d, *J* = 6.7 Hz, 2H), 7.24 – 7.33 (m, 3H), 7.68 (d, *J* = 8.2 Hz, 2H), 7.82 (d, *J* = 8.1 Hz, 2H) ppm.

(*S*)-2-(2-Fluorobenzamido)-3-phenylpropanoic acid (111)

Synthesis of product **111** was carried out following the procedure described for compound **88.** Yield: 94%; Consistency*:* white solid; ^{1}H NMR (300 MHz, DMSO-*d*6) = *δ*: 3.05 (dd, *J* = 13.8, 9.8 Hz, 1H), 3.19 (dd, *J* = 13.8, 4.7 Hz, 1H), 4.59 (ddd, *J* = 9.8, 7.9,4.7 Hz, 1H), 7.18-7.40 (m, 7H), 7.42-7.68 (m, 2H), 8.47 (dd, *J* = 7.9, 2.8 Hz, 1H) ppm.

(*S*)-2-(3-Fluorobenzamido)-3-phenylpropanoic acid (112)

Synthesis of product **112** was carried out following the procedure described for compound **88**. Yield*:* 99%; Consistency: white solid*;* ^{1}H NMR (500 MHz, $CDCl_3$) = *δ*:

3.26 (dd, *J* = 14.0, 5.8 Hz, 1H), 3.36 (dd, *J* = 14.0, 5.6 Hz, 1H), 5.08 (dd, *J* = 13.1, 5.8 Hz, 1H), 6.61 (d, *J* = 7.3 Hz, 1H), 7. 18 – 7.47 (m, 9H) ppm.

(*S*)-2-(2,4-Difluorobenzamido)-3-phenylpropanoic acid (113)

Synthesis of product **113** was carried out following the procedure described for compound **88**. Yield: 98 %; Consistency*:* white solid; ^{1}H NMR (500 MHz, $CDCl_3$) = *δ*: 3.23 (dd, *J* = 14.0, 6.3 Hz, 1H), 3.34 (dd, *J* = 14.0, 5.4 Hz, 1H), 5.06 – 5.11 (m, 1H), 6.87 – 6.79 (m, 1H), 6.97 (dt, *J* = 16.5, 4.8 Hz, 1H), 7.10 (dd, *J* = 12.2, 7.2 Hz, 1H), 7.18 – 7.34 (m, 5H), 8.04 – 8.11 (m, 1H) ppm.

(*S*)-2-(2,6-Difluorobenzamido)-3-phenylpropanoic acid (114)

Synthesis of product **114** was carried out following the procedure described for compound **88**. Yield: 99 %; Consistency: white solid; ^{1}H NMR (500 MHz, $CDCl_3$) = *δ*: 3.26 (dd, *J* = 14.1, 5.4 Hz, 1H), 3.38 (dd, *J* = 14.3, 5.7 Hz, 1H), 5.08 – 5.21 (m, 1H), 6.49 (bd, *J* = 6.7 Hz, 1H), 6.93 (t, *J* = 8.2 Hz, 2H), 7.19 – 7.42 (m, 6H) ppm.

(*S*)-2-(4-(Trifluoromethyl)benzamido)-3-phenylpropanoic acid (115)

Synthesis of product **115** was carried out following the procedure described for compound **88**. Yield: 85%; Consistency*:* white solid; ^{1}H NMR (300 MHz, DMSO-*d6*) = 3.09 (dd, *J* = 13.7, 10.6 Hz, 1H). 3.26 (dd, *J* = 13.7, 4.5 Hz, 1H), 4.66 (ddd, *J* = 10.6, 8.1, 4.5 Hz, 1H), 7.15-7.25 (m, 1H), 7.23- 7.36 (m, 4H), 7.85 (d, *J* = 8.2 Hz, 2H), 7.99 (d, *J* = 8.2 Hz, 2H), *δ*: 8.97 (d, *J* = 8.1 Hz, 1H) ppm.

2-Fluoro-*N*-((*S*)-1-oxo-3-phenyl-1-(((*S*)-5-phenylpent-1-en-3-yl)amino)propan-2-yl)benzamide (116)

Synthesis of product **116** was carried out following the procedure described for compound **94.** Yield: 36%; Consistency*:* white crystals; R_f = 0.31 (light petroleum /EtOAc, 8:2); ^{1}H NMR (500 MHz, $CDCl_3$) = δ:1.67-1.83 (m, 2H), 2.54 (t, *J* = 7.8 Hz, 2H), 3.13 (dd, *J* = 13.7, 8.0 Hz, 1H), 3.25 (dd, *J* = 13.7, 6.2 Hz, 1H), 4.40 – 4.50 (m, 1H), 4.81 (ddd, *J* = 9.4, 8.0, 1.9 Hz, 1H), 4.93 – 5.08 (m, 2H), 5.61 (ddd, *J* = 17.1, 10.5, 5.8

Hz, 1H), 5.74 (d, *J* = 8.4 Hz, 1H), 7.06– 7.17 (m, 4H), 7.18 – 7.34 (m, 9H), 7.44-7.51 (m, 1H), 8.03 (td, *J* = 7.8, 1.9 Hz, 1H) ppm.

3-Fluoro-*N*-((*S*)-1-oxo-3-phenyl-1-(((S)-5-phenylpent-1-en-3-yl)amino)propan-2-yl)benzamide (117)

Synthesis of product **117** was carried out following the procedure described for compound **94**. Yield: 70%; Consistency*:* white crystals; *Rf* = 0.27 (light petroleum /EtOAc, 8:2); ^{1}H NMR (500 MHz, $CDCl_3$) = δ: 1.65-1.84 (m, 2H), 2.49 (t, *J* = 7.8 Hz, 2H), 3.09 (dd, *J* = 13.6, 8.7, 1H), 3.22 (dd, *J* = 13.7, 5.8 Hz, 1H), 4.34 – 4.48 (m, 1H), 4.73-4.85 (m, 1H), 4.94 (d, *J* = 17.2 Hz, 1H), 5.08 (m, 1H), 5.58 (ddd, *J* = 17.1, 10.5, 5.8 Hz, 1H), 5.72 (d, *J* = 8.3 Hz, 1H), 6.94 (d, *J* = 7.4 Hz, 1H), 7.02– 7.17 (m, 3H), 7.18 – 7.33 (m, 8H), 7.35-7.42 (m, 1H), 7.45-7.54 (m, 2H) ppm.

2,4-Difluoro-*N*-((*S*)-1-oxo-3-phenyl-1-((*S*)-5-phenylpent-1-en-3-ylamino)propan-2-yl)benzamide (118)

Synthesis of product **118** was carried out following the procedure described for compound **94**. Yield: 72%; Consistency*:* white powder; *Rf* = 0.28 (cyclohexane/EtOAc, 8:2); ^{1}H NMR (500 MHz, $CDCl_3$) = δ: 1.65-1.83 (m, 2H), 2.49 (t, *J* = 8.1 Hz, 2H), 3.11 (dd, *J* = 13.6, 8.2, 1H), 3.24 (dd, *J* = 13.7, 6.0 Hz, 1H), 4.43 (ddd, *J* = 13.7, 7.6, 6.2 Hz, 1H), 4.74-4.89 (m, 1H), 4.93-5.13 (m, 2H), 5.59 (ddd, *J* = 17.1, 10.4, 5.9 Hz, 1H), 5.72-5.90 (m, 1H), 6.84-6.90 (m, 1H), 6.94-6.99 (m, 1H), 7.05-7.17 (m, 3H), 7.18-7.33 (m, 8H), 8.00-8.09 (m, 1H) ppm.

2,6-Difluoro-*N*-((*S*)-1-oxo-3-phenyl-1-((*S*)-5-phenylpent-1-en-3-ylamino)propan-2-yl)benzamide (119)

Synthesis of product **119** was carried out following the procedure described for compound **94.** Yield: 78%; Consistency*:* white powder; *Rf* = 0.57 (cyclohexane/EtOAc, 7:3); ^{1}H NMR (500 MHz, $CDCl_3$) = δ: 1.68-1.88 (m, 2H), 2.49 (t, *J* = 7.8 Hz, 2H), 3.12 (dd, *J* = 13.7, 8.1, 1H), 3.18 (dd, *J* = 13.7, 8.1 Hz, 1H), 4.35-4.48 (m, 1H), 4.85 (dd, *J* = 14.0, 7.9 Hz, 1H), 4.89-5.13 (m, 2H), 5.59 (ddd, *J* = 17.1, 10.7, 6.0 Hz, 1H), 5.80 (d, *J* = 8.5 Hz, 1H), 6.66 (d, *J* = 7.6 Hz, 1H), 6.93 (t, *J* = 8.1 Hz, 2H), 7.06-7.42 (m, 11H) ppm.

_N_-((_S_)-1-Oxo-3-phenyl-1-(((_S_)-5-phenylpent-1-en-3-yl)amino)propan-2-yl)-4-trifluoromethylbenzamide (120)

Synthesis of product **120** was carried out following the procedure described for compound **94**. Yield: 55%; Consistency*:* white solid; *Rf* = 0.55 (light petroleum /EtOAc, 8:2); ^{1}H NMR (500 MHz, $CDCl_3$) = δ: 1.66-1.85 (m, 2H), 2.50 (t, *J* = 8.1 Hz, 2H), 3.09 (dd, *J* = 13.8, 8.7 Hz, 1H), 3.24 (dd, *J* = 13.6, 5.8 Hz, 1H), 4.35–4.46 (m, 1H), 4.72-4.89 (m, 1H), 4.89-5.15 (m, 2H), 5.58 (ddd, *J* = 17.1, 10.5, 5.8 Hz, 1H), 5.64-5.86 (m, 2H), 7.04-7.34 (m, 11 H), 7.67 (d, *J* = 8.1 Hz, 2H), 7.85 (d, *J* = 8.1 Hz, 2H) ppm.

2-Fluoro-_N_-((_S_)-1-oxo-1-(((_S,E_)-6-oxo-1-phenylhept-4-en-3-yl)amino)-3-phenylpropan-2-yl)benzamide (41)

Synthesis of product **41** was carried out following the procedure described for compound **35**, using **116** (13 mg, 0.031 mmol) as terminal olefin. Yield*:* 60 %; Consistency: white powder*;* R_f = 0.15 (cyclohexane /EtOAc, 7:3); ^{1}H NMR (500 MHz, $CDCl_3$) = δ: 1.73-1.92 (m, 2H), 2.21 (s, 3H), 2.51-2.60 (m, 2H), 3.16 (dd, *J* = 13.7, 8.0 Hz, 1H), 3.23 (dd, *J* = 13.8, 6.5 Hz, 1H), 4.55-4.62 (m, 1H), 4.80-4.86 (m, 1H), 5.96 (dd, *J* = 16.0, 1.4 Hz, 1H), 6.07 (d, *J* = 8.3 Hz, 1H), 6.49 (dd, *J* = 16.0, 5.6 Hz, 1H), 7.05 (d, *J* = 7.1 Hz, 2H), 7.09-7.18 (m, 2H), 7.17-7.36 (m, 9H), 7.44-7.54 (m, 1H), 8.03 (td, *J* = 7.8, 1.7 Hz, 1H) ppm. ^{13}C NMR (125.73 MHz, $CDCl_3$) = δ: 27.75. 31.85, 35.75, 37.80, 50.00, 55.47, 116.23 (d, *J* = 24.5 Hz), 120.23, 124.89 (d, *J* = 3.3 Hz), 126.19, 127.26, 128.28, 128.50, 128.86, 129.32, 129.90, 131.85 (d, *J* = 1.8 Hz), 133.89 (d, *J* = 9.4 Hz), 136.35, 140.61, 145.31, 160.72 (d, *J* = 248.7 Hz), 163.53, 170.10, 197.88. Elemental analysis: calcd for $C_{29}H_{29}FN_2O_3$: C 73.71; H 6.19; N 5.93; found: C 71.60, H 6.22, N 5.92.

3-Fluoro-_N_-((_S_)-1-oxo-1-(((_S,E_)-6-oxo-1-phenylhept-4-en-3-yl)amino)-3-phenylpropan-2-yl)benzamide (42)

Synthesis of product **42** was carried out following the procedure described for compound **35**, using **117** (19 mg, 0.045 mmol) as terminal olefin. Yield*:* 64 %; Consistency: white powder*;* Rf = 0.21 (cyclohexane /EtOAc, 7:3); ^{1}H NMR (500 MHz, $CDCl_3$) = δ: 1.72-1.82 (m, 2H), 2.20 (s, 3H), 2.48 (d, *J* = 7.8 Hz, 2H), 3.11 (dd, *J* = 13.5, 8.5 Hz, 1H), 3.21 (dd, *J* = 13.6, 6.2 Hz, 1H), 4.49-4.60 (m, 1H), 4.82-4.93 (m, 1H), 5.91

(d, *J* = 16.0 Hz, 1H), 6.35 (d, *J* = 8.3 Hz, 1H), 6.45 (dd, *J* = 16.0, 5.8 Hz, 1H), 7.05 (dd, *J* = 15.6, 7.3 Hz, 2H), 7.10-7.31 (m, 10H), 7.33-7.41 (m, 1H), 7.42-7.52 (m, 2H) ppm. ^{13}C NMR (125.73 MHz, $CDCl_3$) = δ: 27.65, 31.84, 35.71, 38.36, 50.08, 55.25, 114.53 (d, *J* = 22.5 Hz), 119.03 (d, *J* = 21.2 Hz), 122.52 (d, *J* = 2.7 Hz), 126.22, 127.31, 128.25, 128.52, 128.84, 129.29, 130.01, 130.36 (d, *J* = 7.7 Hz), 135.72 (d, *J* = 6.9 Hz), 136.23, 140.50, 145.16, 163.73, 166.08, 170.32, 197.77 ppm. Elemental analysis: calcd for $C_{29}H_{29}FN_2O_3$: C 73.71; H 6.19; N 5.93; found: C 71.59, H 6.29, N 5.95.

2,4-Difluoro-*N*-((*S*)-1-oxo-1-(((*S,E*)-6-oxo-1-phenylhept-4-en-3-yl)amino)-3-phenylpropan-2-yl)benzamide (43)

Synthesis of product **43** was carried out following the procedure described for compound **35**, using **118** (22 mg, 0.049 mmol) as terminal olefin. Yield*:* 65 %; Consistency: white powder*;* R_f = 0.40 (cyclohexane /EtOAc, 6:4); ^{1}H NMR (300 MHz, $CDCl_3$) = δ: 1.71-1.92 (m, 2H), 2.21 (s, 3H), 2.50 (d, *J* = 7.8 Hz, 2H), 3.13 (dd, *J* = 13.5, 8.2 Hz, 1H), 3.22 (dd, *J* = 13.6, 6.2 Hz, 1H), 4.52-4.64 (m, 1H), 4.78-4.91 (m, 1H), 5.95 (d, *J* = 15.9 Hz, 1H), 6.09-6.17 (m, 1H), 6.42-6.52 (m, 1H), 6.82-6.93 (m, 1H), 6.94-7.01 (m, 1H), 7.02-7.11 (m, 2H), 7.12-7.35 (m, 8H), 8.03 (dd, *J* = 8.4, 6.5 Hz, 1H) ppm. ^{13}C NMR (125.73 MHz, $CDCl_3$) = δ: 27.71, 31.84, 35.74, 38.10, 50.03, 55.50, 112.38, 104.50 (dd, *J* = 28.2, 25.7 Hz), 112.48 (dd, *J* = 20.9, 3.1 Hz), 126.21, 127.29, 128.25, 128.51, 128.84, 129.30, 129.96, 136.23, 137.8, 140.57, 145.25, 162.53, 166.16, 166.93, 170.06, 197.80 ppm. Elemental analysis: calcd for $C_{29}H_{28}F_2N_2O_3$: C 71.01; H 5.75; N 5.71; found: C 71.21, H 5.54, N 5.50.

2,6-Difluoro-*N*-((*S*)-1-oxo-1-(((*S,E*)-6-oxo-1-phenylhept-4-en-3-yl)amino)-3-phenylpropan-2-yl)benzamide (44)

Synthesis of product **44** was carried out following the procedure described for compound **35**, using **119** (24 mg, 0.054 mmol) as terminal olefin. Yield*:* 66%; Consistency: white powder*;* R_f = 0.39 (cyclohexane /EtOAc, 6:4); ^{1}H NMR (500 MHz, $CDCl_3$) = δ:1.73-1.90 (m, 2H), 2.18 (s, 3H), 2.52-2.64 (m, 2H), 3.15 (dd, *J* = 13.7, 8.0 Hz, 1H), 3.23 (dd, *J* = 13.7, 6.4 Hz, 1H), 4.53-4.63 (m, 1H), 4.93 (dd, *J* = 14.4, 7.8 Hz, 1H), 5.91 (dd, *J* = 16.0, 1.4 Hz, 1H), 6.27 (d, *J* = 8.4 Hz, 1H), 6.46 (dd, *J* = 16.0, 5.6 Hz, 1H), 6.68 (d, *J* = 7.8 Hz, 1H), 6.88-6.97 (m, 2H), 7.07 (d, *J* = 8.0 Hz, 2H), 7.13 (dd, *J* =

10.6, 4.1 Hz, 1H), 7.18-7.32 (m, 7H), 7.32-7.42 (m, 1H) ppm. ^{13}C NMR (125.73 MHz, $CDCl_3$) = δ: 27.73, 31.82, 35.61, 38.03, 49.99, 55.14, 112.09 (dd, *J* = 21.1, 4.4 Hz), 113.36 (d, *J* = 19.5 Hz), 126.11, 127.24, 128.33, 128.48, 128.77, 129.35, 129.79, 132.18 (t, *J* = 10.4 Hz), 136.06, 140.72, 145.24, 159.93 (dd, *J* = 253.1, 6.5 Hz), 160.42, 169.67, 197.84 ppm. Elemental analysis: calcd for $C_{29}H_{28}F_2N_2O_3$: C 71.01; H 5.75; N 5.71; found: C 71.25, H 5.56, N 5.52.

_N_-((_S_)-1-Oxo-1-(((_S,E_)-6-oxo-1-phenylhept-4-en-3-yl)amino)-3-phenylpropan-2-yl)-4-trifluoromethylbenzamide (45)

Synthesis of product **45** was carried out following the procedure described for compound **35**, using **120** (15 mg, 0.032 mmol) as terminal olefin. Yield: 78 %; Consistency: white powder*;* R_f = 0.22 (cyclohexane/EtOAc, 7:3); ^{1}H NMR (500 MHz, $CDCl_3$) = δ: 1.76-1.93 (m, 2H), 2.21 (s, 3H), 2.50 (d, *J* = 7.8 Hz, 2H), 3.11 (dd, *J* = 13.4, 8.4 Hz, 1H), 3.23 (dd, *J* = 13.5, 6.3 Hz, 1H), 4.51-4.62 (m, 1H), 4.79-4.90 (m, 1H), 5.92 (d, *J* = 16.0 Hz, 1H), 6.24 (d, *J* = 8.1 Hz, 1H), 6.45 (dd, *J* = 16.0, 5.8 Hz, 1H), 7.01-7.10 (m, 2H), 7.11-7.33 (m, 9H), 7.67 (d, *J* = 7.9 Hz, 2H), 7.83 (d, *J* = 7.7 Hz, 2H) ppm. ^{13}C NMR (125.73 MHz, $CDCl_3$) = δ: 27.70, 31.83, 35.70, 38.38, 50.14, 55.31, 123.57 (q, *J* = 272.7 Hz), 125.66 (q, *J* = 3.7 Hz), 126.27, 127.39, 127.55, 128.54, 128.89, 129.07, 128.89, 129.27, 130.06, 133.46 (q, *J* = 32.6 Hz), 136.13, 140.43, 145.24, 166.05, 170.14, 197.78. Elemental analysis: calcd for $C_{30}H_{29}F_3N_2O_3$: C 68.95; H 5.59; N 5.36; found: C 68.99, H 5.46, N 5.52.

(_S_)-Ethyl 2-amino-3-cyclohexylpropanoate hydrochloride 121

To a flask containing anhydrous methanol (5.0 mL) at 0°C was added thionylchloride (0.74 mL, 10.22 mmol, 3.5 equiv). (*S*)-2-amino-3-cyclohexylpropanoic acid (0.50 g, 2.92 mmol) was added and the reaction mixture was stirred for 48 hours. The solvent was evaporated and the residue was used without further purification (Yield: 96%). ^{1}H NMR (500 MHz, D_2O) = *δ*: 0.86 – 1.27 (m, 5H) 1.30 (t, *J* = 7.1 Hz, 3H), 1.34 – 1.44 (m, 1H), 1.62 – 1.88 (m, 7H), 4.22 (q, *J* = 7.1 Hz, 2H), 4.84 (m, 1H) ppm.

(_S_)-Ethyl 2-(4-fluorobenzamido)-3-cyclohexylpropanoate 122a

To a solution of acid **79** (71 mg, 0.5 mmol, 1.2 equiv.) in CH_2Cl_2 at 0° C, HOBt (69 mg, 0.5 mmol, 1.2 equiv.) and EDCI (98 mg, 0,5 mmol, 1.2 equiv.) were added. After 10 min, the amine **121** (100 mg, 0.4 mmol, 1 equiv.) and DIPEA (108 mg, 149 μL, 0.8 mmol, 2 equiv.) were added and the reaction mixture was stirred at rt for 12 h. After this time, the residue was washed with brine (x 3), dried over Na_2SO_4, filtered and concentrated in *vacuo*. The crude residue was purified by column chromatography using light petroleum/EtOAc (8:2) as eluent mixture, to obtain **122a** as white crystals. Yield: 74%; R_f = 0.45 (light petroleum/EtOAc, 8:2); ^{1}H NMR (500 MHz, $CDCl_3$) = δ: 0.86 – 1.27 (m, 5H) 1.30 (t, J = 7.1 Hz, 3H), 1.34 – 1.44 (m, 1H), 1.62 – 1.88 (m, 7H), 4.22 (q, , J = 7.1 Hz, 2H), 4.84 (td, J = 8.5, 5.6 Hz, 1H), 6.61 (d, J = 8.0 Hz, 1H), 7.06 – 7.16 (m, 2H), 7.75 – 7.87 (m, 2H) ppm.

(*S*)-Ethyl 2-(3,5-difluorobenzamido)-3-cyclohexylpropanoate (122b)

Synthesis of product **122b** was carried out following the procedure described for compound **122a**, using **80** as acid.. Yield: 83%; R_f = 0.33 (light petroleum/EtOAc, 9:1); ^{1}H NMR (500 MHz, $CDCl_3$) = δ: 0.83 – 1.27 (m, 5H), 1.31 (t, J = 7.1 Hz, 3H), 1.34 – 1.44 (m, 1H), 1.60 – 1.88 (m, 7H), 4.24 (q, J = 7.0 Hz, 2H), 4.82 (td, J = 8.5, 5.5 Hz, 1H), 6.71 (d, J = 7.9 Hz, 1H), 6.94 (dd, J = 11.7, 5.3 Hz, 1H), 7.30 (d, J = 5.6 Hz, 2H) ppm.

(*S*)-2-(4-Fluorobenzamido)-3-cyclohexylpropanoic acid (123a)

Synthesis of product **123a** was carried out following the procedure described for compound **88**. Yield: 99 %; Consistency*:* white crystals*;* ^{1}H NMR (500 MHz, DMSO-*d6*) = δ: 0.86 (d, J = 9.78 Hz, 1H), 0.94 (d, J = 10.76 Hz, 1H), 1.07 - 1.25 (m, 4H), 1.33 - 1.46 (m, 1H), 1.59 (bs, 1H), 1.60 - 1.67 (m, 4H), 1.69 - 1.79 (m, 2H), 4.38 - 4.61 (m, 1H), 7.31 (t, J = 8.80 Hz, 2H), 7.93 (dd, J = 5.62, 8.07 Hz, 2H), 8.62 (d, J = 7.83 Hz, 1H) ppm.

(*S*)-2-(3,5-Difluorobenzamido)-3-cyclohexylpropanoic acid (123b)

Synthesis of product **123b** was carried out following the procedure described for compound **88**. Yield: 91 %; Consistency: clear oil; ^{1}H NMR (500 MHz, $CDCl_3$) = δ:

0.81-1.06 (m, 5H), 1.38-1.48 (m, 1H), 1.63-1.89 (m, 7H), 4.83 (td, *J* = 8.6, 5.3 Hz, 1H), 6.54 (d, *J* = 7.9 Hz, 1H), 6.97 (tt, *J* = 8.3, 2.2 Hz, 1H), 7.29 – 7.34 (m, 2H) ppm.

_N_-((_S_)-1-((_S_)-5-Phenylpent-1-en-3-ylcarbamoyl)-2-cyclohexylethyl)-4-fluorobenzamide (124a)

Synthesis of product **124a** was carried out following the procedure described for compound **94**, using **123a** as acid. Yield: 39%; Consistency*:* white powder; R_f = 0.71 (light petroleum /EtOAc, 7:3); ^{1}H NMR (500 MHz, $CDCl_3$) = δ: 0.79-1.41 (m, 7H), 1.48-2.04 (m, 8H), 2.64 (d, *J* = 8.1 Hz, 2H), 4.44-4.54 (m, 1H), 4.61-4.70 (m, 1H), 5.05-5.24 (m, 2H), 5.82 (ddd, *J* = 17.1, 10.5, 5.5 Hz, 1H), 6.24 (d, *J* = 8.5 Hz, 1H), 6.65 (d, *J* = 8.2 Hz, 1H), 7.07-7.32 (m, 7H), 7.77-7.83 (m, 2H) ppm.

_N_-((_S_)-1-((_S_)-5-Phenylpent-1-en-3-ylcarbamoyl)-2-cyclohexylethyl)-3,5-difluorobenzamide (124b)

Synthesis of product **124b** was carried out following the procedure described for compound **94**, using **123b** as acid. Yield: 47%; Consistency*:* white powder; R_f = 0.54 (light petroleum /EtOAc, 8:2); ^{1}H NMR (500 MHz, $CDCl_3$) = δ: 0.74-1.41 (m, 7H), 1.45-2.06 (m, 8H), 2.61 (d, *J* = 8.1 Hz, 2H), 4.45-4.59 (m, 1H), 4.60-4.73 (m, 1H), 5.06-5.22 (m, 2H), 5.79 (ddd, *J* = 17.1, 11.4, 5.7 Hz, 1H), 6.30 (d, *J* = 8.5 Hz, 1H), 6.90 – 6.98 (m, 1H), 7.04-7.12 (m, 2H), 7.13-7.42 (m, 6H) ppm.

_N_-((_S_)-1-((_S,E_)-6-Oxo-1-phenylhept-4-en-3-ylcarbamoyl)-2-cyclohexylethyl)-4-fluorobenzamide (46)

Synthesis of product **46** was carried out following the procedure described for compound **35**, using **124a** (15 mg, 0.033 mmol) as terminal olefin. Yield*:* 60 %; Consistency: white powder*;* R_f = 0.21 (light petroleum/EtOAc, 7:3); ^{1}H NMR (500 MHz, $CDCl_3$) = δ: 0.65-1.95 (m, 13H), 2.22 (s, 3H), 2.49-2.66 (m, 2H), 3.61-3.72 (m, 2H), 4.18-4.26 (m, 1H), 4.54-4.66 (m, 1H), 4.71 (d, *J* = 7.1 Hz, 1H), 6.15 (d, *J* = 15.7 Hz, 1H), 6.65 (dd, *J* = 15.9, 4.7 Hz, 1H), 6.80-6.96 (m, 2H), 6.97-7.33 (m, 6H), 7.72-7.84 (m, 2H). ^{13}C NMR (126 MHz, $CDCl_3$) = δ: 26.03, 26.13, 26.28, 27.46, 31.92, 32.96, 33.48, 34.30, 35.85, 39.27, 49.97, 51.72, 63.03, 115.74 (d, *J* = 22 Hz), 126.18, 128.31, 128.49, 129.53 (d, *J* = 9.2), 129.63, 129.94, 140.60, 145.93, 164.99 (d, *J* = 253.1 Hz), 166.73,

171.89, 198.04. Elemental analysis: calcd for $C_{29}H_{35}FN_2O_3$: C 72.78; H 7.37; N 5.85; found: C 72.68, H 7.21, N 5.91.

_N_-((_S_)-1-((_S,E_)-6-Oxo-1-phenylhept-4-en-3-ylcarbamoyl)-2-cyclohexylethyl)-3,5-difluorobenzamide (47)

Synthesis of product **47** was carried out following the procedure described for compound **35**, using **124b** as terminal olefin. Yield*:* 50 %; Consistency: white powder*;* R_f = 0.27 (light petroleum/EtOAc, 7:3); ^{1}H NMR (500 MHz, $CDCl_3$) = δ: 0.71-1.36 (m, 7H), 1.54-2.01 (m, 8H), 2.24 (s, 3H), 2.54-2.77 (m, 2H), 4.57-4.73 (m, 2H), 6.14 (d, *J* = 16.0, 1H), 6.61-6.70 (m, 2H), 6.91-6.99 (m, 1H), 7.02 (d, *J* = 8.0 Hz, 1H), 7.05 – 7.09 (m, 1H), 7.14 – 7.19 (m, 1H), 7.19 – 7.30 (m, 3H), 7.31 – 7.39 (m, 2H). ^{13}C NMR (126 MHz, $CDCl_3$) δ 25.98, 26.09, 26.24, 27.49, 31.94, 32.94, 33.47, 34.26, 35.87, 39.28, 50.07, 51.91, 107.31 (t, *J* = 25 Hz), 110.47 (dd, *J* = 26.8, 3.7 Hz), 126.28, 128.29, 128.56, 128.65, 130.01, 136.77 (t, *J* =7.6 Hz), 140.51, 145.64, 162.95 (dd, *J* = 250.9, 12.2 Hz), 165.22, 171.49, 197.86. Elemental analysis: calcd for $C_{29}H_{34}F_2N_2O_3$: C 70.14; H 6.90; N 5.64; found: C 70.28, H 7.21, N 5.50.

(_S_)-Methyl 2-amino-3-(p-tolyl)propanoate hydrochloride (125a)

To a flask containing anhydrous methanol (5.0 mL) at 0°C was added thionylchloride (0.71 mL, 9.77 mmol, 3.5 equiv). (2*S*)-2-amino-3-(4-methylphenyl)propanoic acid (0.50 g, 2.79 mmol) was added and the reaction mixture was stirred for 48 hours. The solvent was evaporated and the residue was used without further purification (Yield: 95%). ^{1}H NMR (500 MHz, D_2O) = δ: 2.31 (s, 3 H), 3.19 (dd, *J* = 14.47, 7.33 Hz, 1 H), 3.28 (dd, *J* = 14.56, 5.95 Hz, 1 H), 3.82 (s, 3 H), 4.39 (dd, *J* = 7.33, 6.04 Hz, 1 H), 7.11–7.21 (m, 2 H), 7.21–7.30 (m, 2 H).

(_S_)-Methyl 2-amino-3-(4-fluorophenyl)propanoate hydrochloride (125b)

To a flask containing anhydrous methanol (5.0 mL) at 0°C was added thionylchloride (0.71 mL, 9.55 mmol, 3.5 equiv). (S)-2-amino-3-(4-fluorophenyl)propanoic acid (0.50 g, 2.73 mmol) was added and the reaction mixture was stirred for 48 hours. The solvent was evaporated and the residue was used without further purification (Yield: 94%). ^{1}H

NMR (500 MHz, D_2O) = δ: 3.18 (dd, *J* = 14.3, 5.6 Hz, 1 H), 3.27 (dd, *J* = 14.5, 5.8 Hz, 1 H), 3.80 (s, 3 H), 4.20 (m, 1 H), 6.90–7.20 (m, 4 H).

(S)-Methyl 2-(4-fluorobenzamido)-3-(p-tolyl)propanoate (126a)

To a solution of acid **79** (73 mg, 0.5 mmol, 1.2 equiv.) in CH_2Cl_2 at 0° C, HOBt (70 mg, 0.5 mmol, 1.2 equiv.) and EDCI (99 mg, 0,5 mmol, 1.2 equiv.) were added. After 10 min, the amine **125a** (100 mg, 0.4 mmol, 1 equiv.) and DIPEA (112 mg, 154 μL, 0.8 mmol, 2 equiv.) were added and the reaction mixture was stirred at rt for 12 h. After this time, the residue was washed with brine (x 3), dried over Na_2SO_4, filtered and concentrated in *vacuo*. The crude residue was purified by column chromatography using light petroleum/EtOAc (8:2) as eluent mixture, to obtain **126a** as white crystals. Yield: 66%; R_f = 0.59 (light petroleum/EtOAc, 7:3); ^{1}H NMR (500 MHz, $CDCl_3$) = δ: 2.30 (s, 3H), 3.16 (dd, *J* = 13.9, 5.7 Hz, 1H), 3.23 (dd, *J* = 13.9, 5.7 Hz, 1H), 3.76 (s, 3H), 5.03 (dd, *J* = 13.2, 5.7 Hz, 1H), 6.67 (d, *J* = 7.3 Hz, 1H), 6.99 – 7.11 (m, 6H), 7.72 (dd, *J* = 8.6, 5.3 Hz, 2H) ppm.

(S)-Methyl 2-(3,5-difluorobenzamido)-3-(p-tolyl)propanoate (126b)

Synthesis of product **126b** was carried out following the procedure described for compound **126a**, using acid **80** (83 mg, 0.5 mmol, 1.2 equiv.). Yield: 79 %; R_f = 0.40 (light petroleum/EtOAc, 8:2); ^{1}H NMR (500 MHz, $CDCl_3$) = δ: 2.32 (s, 1H), 3.17 (dd, *J* = 14.0, 5.4 Hz, 1H), 3.24 (dd, *J* = 14.0, 5.7 Hz, 1H), 3.79 (s, 1H), 5.02 (dd, *J* = 13.0, 5.6 Hz, 1H), 6.51 (d, *J* = 7.1 Hz, 1H), 6.90-7.02 (m, 3H), 7.08-7.28 (m, 5H) ppm.

(S)-Methyl 2-(4-fluorobenzamido)-3-(4-fluorophenyl)propanoate (126c)

To a solution of acid **79** (72 mg, 0.5 mmol, 1.2 equiv.) in CH_2Cl_2 at 0° C, HOBt (70 mg, 0.5 mmol, 1.2 equiv.) and EDCI (99 mg, 0,5 mmol, 1.2 equiv.) were added. After 10 min, the amine **125b** (100 mg, 0.4 mmol, 1 equiv.) and DIPEA (111 mg, 152 μL, 0.8 mmol, 2 equiv.) were added and the reaction mixture was stirred at rt for 12 h. After this time, the residue was washed with brine (x 3), dried over Na_2SO_4, filtered and concentrated in *vacuo*. The crude residue was purified by column chromatography using light petroleum/EtOAc (7:3) as eluent mixture, to obtain **126c** as white crystals. Yield: 67%; R_f = 0.51 (light petroleum/EtOAc, 7:3); ^{1}H NMR (500 MHz, $CDCl_3$) = δ: 3.17 (dd, *J* =

14.0, 5.7 Hz, 1H), 3.26 (dd, *J* = 14.0, 5.8 Hz, 1H), 3.76 (s, 3H), 5.03 (dd, *J* = 13.1, 5.8 Hz, 1H), 6.71 (d, *J* = 7.2 Hz, 1H), 6.97 (t, *J* = 8.6 Hz, 2H), 7.09 (dd, *J* = 16.2, 7.9 Hz, 4H), 7.73 (dd, *J* = 8.6, 5.3 Hz, 2H) ppm.

(S)-Methyl 2-(3,5-difluorobenzamido)-3-(4-fluorophenyl)propanoate (126d)

Synthesis of product **126d** was carried out following the procedure described for compound **126c**, using acid **80** (81 mg, 0.5 mmol, 1.2 equiv.). Yield: 67 %; R_f = 0.30 (light petroleum/EtOAc, 8:2); ^{1}H NMR (500 MHz, $CDCl_3$) = δ: 3.18 (dd, *J* = 14.0, 5.4 Hz, 1H), 3.27 (dd, *J* = 14.0, 5.8 Hz, 1H), 3.79 (s, 3H), 5.02 (dd, *J* = 13.0, 5.7 Hz, 1H), 6.56 (d, *J* = 6.8 Hz, 1H), 6.92– 7.32 (m, 8H) ppm.

(*S*)-2-(4-Fluorobenzamido)-3-(p-tolyl)propanoic acid (127a)

Synthesis of product **127a** was carried out following the procedure described for compound **88.** Yield: 99 %; ^{1}H NMR (500 MHz, $CDCl_3$) = δ: 2.32 (s, 3H), 3.23 (dd, *J* = 14.1, 5.8 Hz, 1H), 3.31 (dd, *J* = 14.1, 5.6 Hz, 1H), 5.04 (dd, *J* = 13.0, 5.7 Hz, 1H), 6.51 (d, *J* = 7.3 Hz, 1H), 7.04– 7.15 (m, 6H), 7.66 –7.74 (m, 2H) ppm.

(*S*)-2-(3,5-Difluorobenzamido)-3-(p-tolyl)propanoic acid (127b)

Synthesis of product **127b** was carried out following the procedure described for compound **88.** Yield: 98 %; ^{1}H NMR (500 MHz, $CDCl_3$) = δ: 2.32 (s, 3H), 3.21 (dd, *J* = 13.8, 5.3 Hz, 1H), 3.30 (dd, *J* = 13.8, 4.9 Hz, 1H), 4.99-5.08 (m, 1H), 6.59 (d, *J* = 6.8 Hz, 1H), 6.94 (t, *J* = 8.1 Hz, 1H), 7.01-7.30 (m, 6H) ppm.

(S)-2-(4-Fluorobenzamido)-3-(4-fluorophenyl)propanoic acid (127c)

Synthesis of product **127c** was carried out following the procedure described for compound **88**. Yield: 99 %; ^{1}H NMR (500 MHz, $CDCl_3$) = δ: 3.22 (dd, *J* = 14.2, 5.7 Hz, 1H), 3.34 (dd, *J* = 14.2, 5.6 Hz, 1H), 5.04 (dd, *J* = 12.7, 5.9 Hz, 1H), 6.59 (d, *J* = 7.2 Hz, 1H), 6.98 (t, *J* = 8.5 Hz, 2H), 7.06 – 7.19 (m, 4H), 7.71 (dd, *J* = 8.5, 5.3 Hz, 2H) ppm.

(*S*)-2-(3,5-Difluorobenzamido)-3-(4-fluorophenyl)propanoic acid (127d)

Synthesis of product **127d** was carried out following the procedure described for compound **88**. Yield: 97 %; ^{1}H NMR (500 MHz, $CDCl_3$) = δ: 3.21 (dd, *J* = 13.7, 5.5 Hz,

1H), 3.32 (dd, *J* = 13.7, 5.0 Hz, 1H), 4.95-5.11 (m, 1H), 6.48 (d, *J* = 6.6 Hz, 1H), 6.88-7.30 (m, 7H) ppm.

4-Fluoro-*N*-((*S*)-1-oxo-1-(((*S*)-5-phenylpent-1-en-3-yl)amino)-3-(p-tolyl)propan-2-yl)benzamide (128a)

Synthesis of product **128a** was carried out following the procedure described for compound **94.** Yield: 59%; Consistency*:* white powder; R_f = 0.36 (light petroleum /EtOAc, 8:2); ^{1}H NMR (500 MHz, $CDCl_3$) = δ: 1.66-1.86 (m, 2H), 2.27 (s, 3H), 2.53 (t, *J* = 8.0 Hz, 2H), 3.06 (dd, *J* = 13.5, 8.3 Hz, 1H), 3.16 (dd, *J* = 13.6, 8.0 Hz, 1H), 4.35-4.47 (m, 1H), 4.80-4.90 (m, 1H), 4.91-5.16 (m, 2H), 5.61 (ddd, *J* = 17.1, 10.7, 5.9 Hz, 1H), 6.28 (d, *J* = 8.3 Hz, 1H), 6.96-7.31 (m, 12H), 7.69-7.80 (m, 2H) ppm.

3,5-Difluoro-*N*-((*S*)-1-oxo-1-(((*S*)-5-phenylpent-1-en-3-yl)amino)-3-(p-tolyl)propan-2-yl)benzamide (128b)

Synthesis of product **128b** was carried out following the procedure described for compound **94.** Yield: 72%; Consistency*:* white powder; R_f = 0.63 (light petroleum /EtOAc, 8:2); ^{1}H NMR (500 MHz, $CDCl_3$) = δ: 1.66 – 1.83 (m, 2H), 2.28 (s, 3H), 2.54 (t, *J* = 8.0 Hz, 2H), 3.04 (dd, *J* = 13.6, 8.2 Hz, 1H), 3.15 (dd, *J* = 13.7, 6.4 Hz, 1H), 4.37 – 4.47 (m, 1H), 4.81 (dd, *J* = 14.3, 7.8 Hz, 1H), 4.93– 5.10 (m, 2H), 5.61 (ddd, *J* = 16.7, 10.4, 6.0 Hz, 1H), 6.14 (d, *J* = 8.3 Hz, 1H), 6.88– 7.32 (m, 12H), 7.36 (d, *J* = 7.6 Hz, 1H) ppm.

4-Fluoro-*N*-((*S*)-3-(4-fluorophenyl)-1-oxo-1-(((*S*)-5-phenylpent-1-en-3-yl)amino)propan-2-yl)benzamide (128c)

Synthesis of product **128c** was carried out following the procedure described for compound **94.** Yield: 78 %; Consistency*:* white powder; *Rf* = 0.23 (light petroleum /EtOAc, 8:2); ^{1}H NMR (500 MHz, $CDCl_3$) = δ: 1.63-1.81 (m, 2H), 2.55 (t, *J* = 8.0 Hz, 2H), 3.07 – 3.14 (m, 2H), 4.34-4.4 (m, 1H), 4.89 – 4.99 (m, 1H), 5.04 – 5.17 (m, 1H), 5.62 (ddd, *J* = 16.8, 10.4, 6.0 Hz, 1H), 6.64 (d, *J* = 8.4 Hz, 1H), 6.79– 7.30 (m, 11H), 7.37 (d, *J* = 8.0 Hz, 1H), 7.70 – 7.80 (m, 2H) ppm.

3,5-Difluoro-*N*-((*S*)-3-(4-fluorophenyl)-1-oxo-1-(((*S*)-5-phenylpent-1-en-3-yl)amino)propan-2-yl)benzamide (128d)

Synthesis of product **128d** was carried out following the procedure described for compound **94**. Yield: 39%; Consistency*:* white powder; R_f = 0.44 (light petroleum /EtOAc, 8:2); ^{1}H NMR (500 MHz, $CDCl_3$) = δ: 1.68 – 1.87 (m, 2H), 2.56 (t, *J* = 7.7 Hz, 1H), 2.99-3.17 (m 2H), 4.36-4.46 (m, 1H), 4.73-4.86 (m, 1H), 4.94-5.18 (m, 2H), 5.62 (ddd, *J* = 16.7, 10.5, 6.0 Hz, 1H), 6.18 (d, *J* = 7.9 Hz, 1H), 6.84– 7.34 (m, 12H), 7.40 (d, *J* = 7.0 Hz, 1H) ppm.

4-Fluoro-*N*-((*S*)-1-oxo-1-(((*S,E*)-6-oxo-1-phenylhept-4-en-3-yl)amino)-3-(p-tolyl)propan-2-yl)benzamide (48)

Synthesis of product **48** was carried out following the procedure described for compound **35** using **128a** (33 mg, 0.073 mmol) as terminal olefin. Yield*:* 70%; Consistency: white powder*;* R_f = 0.13 (light petroleum/EtOAc, 7:3); ^{1}H NMR (500 MHz, $CDCl_3$) = δ: 1.76 (td, *J* = 14.7, 8.6 Hz, 1H), 1.86 (td, *J* = 14.3, 6.6 Hz, 1H), 2.20 (s, 3H), 2.30 (s, 3H), 2.48-2.64 (m, 2H), 3.08 (dd, *J* = 13.5, 8.5 Hz, 1H), 3.18 (dd, *J* = 13.7, 6.1 Hz, 1H), 4.53-4.60 (m, 1H), 4.81 (dd, *J* = 14.4, 7.9 Hz, 1H), 5.94 (d, *J* = 16.0 Hz, 1H), 6.23 (d, *J* = 8.2 Hz, 1H), 6.47 (dd, *J* = 16.0, 5.7 Hz, 1H), 6.86 (d, *J* = 7.5 Hz, 1H), 6.98-7.31 (m, 11H), 7.74 (dd, *J* = 8.6, 5.3 Hz, 2H). ^{13}C NMR (126 MHz, $CDCl_3$) δ: 21.01, 27.50, 31.90, 35.73, 37.89, 50.07, 55.28, 115.75 (d, *J* = 21.8 Hz), 126.23, 128.26, 128.52, 129.39, 129.42, 129.55, 129.71 (d, *J* = 4.3 Hz), 130.0, 133.13, 136.93, 140.53, 145.31, 165.21 (d, *J* = 262.3 Hz), 166.01, 170.45, 197.77. Elemental analysis: calcd for $C_{30}H_{31}FN_2O_3$: C 74.05; H 6.42; N 5.76; found: C 73.98, H 6.69, N 5.61.

3,5-Difluoro-*N*-((*S*)-1-oxo-1-(((*S,E*)-6-oxo-1-phenylhept-4-en-3-yl)amino)-3-(p-tolyl)propan-2-yl)benzamide (49)

Synthesis of product **49** was carried out following the procedure described for compound **35** using **128b** (30 mg, 0.064 mmol) as terminal olefin. Yield:78 %; Consistency: white powder*;* R_f = 0.27 (light petroleum/EtOAc, 7:3); ^{1}H NMR (500 MHz, $CDCl_3$) = δ: 1.72-1.96 (m, 2H), 2.20 (s, 3H), 2.33 (s, 3H), 2.57 (t, *J* = 7.3 Hz, 2H), 3.04 (dd, *J* = 13.6, 8.7 Hz, 1H), 3.19 (dd, *J* = 13.5, 5.6 Hz, 1H), 4.50-4.61 (m, 1H), 4.65-4.75 (m, 1H), 5.73 (d, *J* = 8.1 Hz, 1H), 5.92 (d, *J* = 16.0 Hz, 1H), 6.45 (dd, *J* = 16.0, 5.7

Hz, 1H), 6.81 (d, *J* = 7.0 Hz, 1H), 6.97 (d, *J* = 8.5 Hz, 1H), 7.05-7.30 (m, 11H) ppm. ^{13}C NMR (126 MHz, $CDCl_3$) δ: 21.33, 27.32, 31.74, 36.79, 38.01, 50.55, 56.40, 107.34 (t, *J* = 25.1 Hz), 110.38 (dd, *J* = 20.7, 7.4 Hz), 126.29, 128.24, 128.56, 129.14, 129.63, 130.08, 132.91, 136.85(t, *J* = 7.1 Hz), 138.48, 140.46, 145.02, 163.78 (dd, *J* = 262.5, 7.1 Hz), 168.29 (t, *J* = 3.5 Hz), 170.78, 198.91 ppm. Elemental analysis: calcd for $C_{30}H_{30}F_2N_2O_3$: C 71.41; H 5.99; N 5.55; found: C 71.68, H 6.18, N 5.42.

4-Fluoro-*N*-((*S*)-3-(4-fluorophenyl)-1-oxo-1-(((*S,E*)-6-oxo-1-phenylhept-4-en-3-yl)amino)propan-2-yl)benzamide (50)

Synthesis of product **50** was carried out following the procedure described for compound **35** using **128c** (44 mg, 0.097 mmol) as terminal olefin. Yield: 79%; Consistency: white powder*;* R_f = 0.07 (light petroleum/EtOAc, 7:3); ^{1}H NMR (500 MHz, $CDCl_3$) = δ: 1.72-1.92 (m, 2H), 2.21 (s, 3H), 2.53-2.63 (m, 2H), 3.07-3.18 (m, 2H), 4.52-4.61 (m, 1H), 4.79 (dd, *J* = 14.6, 7.7 Hz, 1H), 5.93 (d, *J* = 16.0 Hz, 1H), 6.29 (d, *J* = 8.3 Hz, 1H), 6.49 (dd, *J* = 16.0, 5.7 Hz, 1H), 6.81 (d, *J* = 7.8 Hz, 1H), 6.89-7.32 (m, 11H), 7.69-7.79 (m, 2H). ^{13}C NMR (126 MHz, $CDCl_3$) δ: 27.64, 31.86, 35.74, 37.42, 50.08, 55.26, 115.78 (dd, *J* = 21.6, 17.0 Hz), 126.31, 128.25, 128.56, 129.78 (d, *J* = 6.7 Hz), 130.68, 130.78 (d, *J* = 1.5 Hz), 131.32 (d, *J* = 4.6 Hz), 140.45, 145.53, 161.79 (d, *J* = 261.7 Hz), 164.58 (d, *J* = 262.5 Hz), 166.37, 170.26, 197.72. Elemental analysis: calcd for $C_{29}H_{28}F_2N_2O_3$: C 71.01; H 5.75; N 5.71; found: C 71.23, H 5.97, N 5.60.

3,5-Difluoro-*N*-((*S*)-3-(4-fluorophenyl)-1-oxo-1-(((*S,E*)-6-oxo-1-phenylhept-4-en-3-yl)amino)propan-2-yl)benzamide (51)

Synthesis of product **51** was carried out following the procedure described for compound **35** using **128d** (21 mg, 0.045 mmol) as terminal olefin. Yield*:* 87%; Consistency: white powder*;* R_f = 0.15 (light petroleum/EtOAc, 7:3); ^{1}H NMR (500 MHz, $CDCl_3$) = δ: 1.74-1.97 (m, 2H), 2.22 (s, 3H), 2.59 (t, *J* = 7.5 Hz, 2H), 3.01-3.23 (m, 2H), 4.53-4.62 (m, 1H), 4.68 (dd, *J* = 14.4, 7.9 Hz, 1H), 5.82 (d, *J* = 8.1 Hz, 1H), 5.91 (d, *J* = 16.0 Hz, 1H), 6.46 (dd, *J* = 15.8, 6.1 Hz, 1H), 6.79 (d, *J* = 7.3 Hz, 1H), 6.94-7.31 (m, 12 H) ppm. ^{13}C NMR (126 MHz, $CDCl_3$) δ: 27.68, 31.65, 36.82, 38.51, 50.89, 56.27, 108.69 (t, *J* = 26.9 Hz), 113.72 (dd, *J* = 26.9, 7.5 Hz), 115.75 (d, *J* = 26.8 Hz), 126.82, 128.56, 128.82, 130.09, 130.78 (d, *J* = 6.8 Hz), 133.45 (d, *J* = 3.8 Hz), 136.89(t, *J* = 7.2

Hz), 140.56, 145.22, 161.78 (d, *J* = 261.4Hz), 164.58 (dd, *J* = 261.4, 7.2 Hz), 168.197(t, *J* = 3.2 Hz), 171.58, 199.41 ppm. Elemental analysis: calcd for $C_{29}H_{27}F_3N_2O_3$: C 68.49; H 5.35; N 5.51; found: C 68.72, H 5.24, N 5.55.

7.2 Biological activity

Enzyme assays against rhodesain.

Preliminary screening with rhodesain was performed with 50 μM inhibitor concentrations using an equivalent amount of DMSO as negative control. The enzyme was recombinantly expressed as previously described.[30,135,141-142] Product release from substrate hydrolysis (Cbz-Phe-Arg-AMC, 10 μM) was determined continuously over a period of 30 min. Compounds showing at least 85% inhibition at 50 μM were subjected to detailed assays. Second-order rate constants of inhibition were determined with 7 different inhibitor concentrations ranging from those that minimally inhibited to those that fully inhibited the enzyme. The assay buffer contains: 50 mM sodium acetate, pH = 5.5, 5 mM EDTA, 200 mM NaCl and 0.005 % Brij 35 to avoid aggregation and wrong-positive results. Enzyme buffer contains 5 mM DTT rather than Brij 35. Product formation was monitored continuously for 30 min at room temperature. To determine the first-order inactivation rate constants (k_{obs}) for the irreversible inhibition, progress curves (fluorescence (F) versus time) were analyzed by non-linear regression analysis using the equation F = A (1-exp (-k_{obs}t)) +B.[143] Fitting of the k_{obs} values against the inhibitor concentrations to the hyperbolic equation $k_{obs} = k_{inac}$ [I]/(K_{iapp}+[I]) gave the individual values of K_{iapp} and k_{inac}.[143] The K_{iapp} values were corrected to zero substrate concentration by the term (1+[S]/K_m) in equation $K_i = K_{iapp}$/(1+[S]/K_m). The second-order rate constants $k_{2nd} = k_{inac}/K_i$ were directly calculated from the individual constants. K_i and k_{inac} values were calculated by non-linear regression analyses using the program GraFit.[144] The K_m value used to correct K_{iapp} values was determined to 0.9 μM.[145] Inhibitor solutions were prepared from stocks in DMSO. Each independent assay was performed twice in duplicate in 96-well-plates in a total volume of 200 μL. Fluorescence of the product AMC of the substrate hydrolyses was measured using an Infinite 200 PRO microplate reader (Tecan, Männedorf, Switzerland) at room temperature with a 380 nm excitation filter and a 460 nm emission filter.

Enzyme assays against hCatL[145]

Assays with hCatL was performed as described for rhodesain, using fluorogenic substrate Cbz-Phe-Arg-AMC (5 μM) and K_m value of 6.5 μM.

Drug screening on *T. b. brucei* cultures.

The antitrypanosomal activity was determined using the ATPlite assay[146] as described previously.[141] This assay is based on the adenosine triphosphate (ATP) dependent light emitting reaction catalyzed by firefly luciferase. In the presence of ATP and Mg ions, the enzyme transforms D-luciferine into D-luciferine adenylate which then turns into the excited keto form of oxyluciferin. ATP can be used as a marker for cell viability. All experiments were performed in white 96-well microplates (PerkinElmer). Each well was filled with 90 μL of medium containing 2500 cells/mL. The BS parasites used in this work were of the *T. brucei brucei* 449 cell line, which is a descendant of the Lister 427 strain.[147] Each tested compound (5 mM stock solutions) was then diluted in HMI-9 medium: firstly 1:3, then 1:10 and subsequently in ten 1:2 dilution steps using separate microplates. Of the final ten 1:2 dilutions, 10 μL each were then added to the 90 μL cell suspension, leading to an additional final 1:10 dilution for all compounds.[141] Addition of 10 μL DMSO corresponding to 10% DMSO, was used as a positive control. For drug addition, highest concentration of DMSO added was 0.3% DMSO. Addition of 0.3% DMSO served as a negative control. The plates were incubated at 37 °C for 24 h and 48 h in two separate triplicates. 50 μL of ATPlite 1 step solution (PerkinElmer) was added to each well of the microplate, providing luciferin and luciferase as well as initiating cell lysis, and luminescence was measured in a Infinite® M200 PRO plate reader (Tecan Trading AG) at room temperature. A dose-response curve was obtained by plotting the measured values against the compound concentrations and the EC_{50} values were calculated using GraFitVs. 5.013, Erithacus Software Ltd.

7.3 Docking studies

Covalent docking calculations.

AD4[137-138] was employed for the docking calculations. In this case, as the ligands covalently bind to the enzyme, it was necessary to employ a specific docking protocol devised by Bianco et al.,[139] namely the "flexible side chain method". The latter requires to modify the residue which takes part in the covalent bond and to attach it to the ligand; during the docking calculation this modified residue is treated as flexible. To this end, using the Maestro suite,[148] we modeled ligands **35-40** with two extra atoms where the

alkylation would take place. Specifically a sulphur and a carbon atom, in order to match the corresponding atoms in the C25. The crystal structure of rhodesain from the Protein Data Bank (PDB code 2P86).[129] was downloaded and prepared for docking using the Protein Preparation Wizard tool in Maestro. Then, with the help of the scripts provided by the AD4 website,[149] it was possible to overlap the ligand with the C25 residue. Then, the receptor grid was calculated with the AutoGrid4 software, mapping the interaction energies of the receptor using the ligand atom types as probes. The grid of 60 Å × 60 Å × 60 Å with 0.375 Å spacing was centered on the coordinates of the ligand originally present in the 2P86 crystal. Finally, the actual docking was run for each compound separately, keeping the remodeled residue as flexible. This allowed sampling the torsional degrees of freedom of the ligands in order to optimize the interactions of the bound ligand with the surrounding residues. For the simulations the Lamarckian Genetic Algorithm (LGA) was employed. Given the complexity of the ligands and their high number of torsional degrees of freedom, 200 runs of LGA were executed for each compound. Each docking run consisted of 20 million energy evaluations using the Lamarckian genetic algorithm local search (GALS) method. The GALS method evaluates a population of possible docking solutions and propagates the most successful individuals from each generation into the subsequent generation of possible solutions. A low-frequency local search according to the method of Solis and Wets is applied to docking trials to ensure that the final solution represents a local minimum. All dockings described in this paper were performed with a population size of 150, and 300 rounds of Solis and Wets local search were applied with a probability of 0.06. A mutation rate of 0.02 and a crossover rate of 0.8 were used to generate new docking trials for subsequent generations, and the best individual from each generation was propagated over the next generation. All the other settings were left at their default value. The docking results from each calculation were clustered on the basis of root-mean square deviation (rmsd) (solutions differing by less than 2.0 Å) between the Cartesian coordinates of the atoms and were ranked on the basis of free energy of binding (ΔG_{AD4}). All the images were rendered using the UCSF Chimera Molecular Modeling Software.[150]

8. SUPPLEMENT

Synthesis and biological evaluation of an immunoproteasome inhibitor-doxorubicin conjugate with different linkers

8.1 Aim of the research

During my first year of PhD, I spent a period at the Bioorganic Synthesis group of the "Leiden Institute of Chemistry", in the Netherlands, under the supervision of Prof. H. Overkleeft. In this chapter, I will briefly describe the aim of my research project and the obtained results.

The main topic of my research project was the development of new classes of proteasome inhibitors as a potential new therapeutic strategy for the treatment of multiple myeloma (MM). MM is the second most common hematologic malignancy, which develops in the plasma cells, situated at the centre of the bone marrow. Plasma cells normally produce antibodies, which play a fundamental role in our immune system; healthy plasma cells could turn into malignant myeloma cells, under certain conditions. As a result, abnormal antibodies, or M proteins, are produced, offering no benefit to the body, thus causing MM symptoms.[10,151-152]

Although MM is considered an incurable disease, treatment options have increased over the last decade and today they include various proteasome inhibitors, immunomodulatory drugs, DNA damaging drugs including doxorubicin, radiotherapy, monoclonal antibodies, heat shock protein inhibitors and steroids.[10,152]

With respect to proteasome inhibition as a therapeutic strategy, it has recently come to the fore that inhibition of immunoproteasome activities selectively with respect to their constitutive proteasome counterparts could be an attractive alternative to the proteasome inhibitors currently applied in the clinic.[6,65] These inhibitors, bortezomib and carfilzomib, target both the constitutive proteasome and immuno-proteasome, indiscriminately. This lack of specificity may explain the side effects of these drugs, such as peripheral neuropathy and gastrointestinal effects. By selectively inhibiting the immunoproteasome catalytic subunits, it may be possible to maintain the antimyeloma and antilymphoma efficacy while reducing the toxicity, thereby increasing the therapeutic index.[6] Immunoproteasomes are predominantly expressed in monocytes and

lymphocytes and are responsible for the generation of antigenic peptides for cell-mediated immunity; the expression of constitutive subunits of the proteasome is replaced by the synthesis of the immune counterparts upon the exposure of specific stimuli such as the inflammatory cytokines IFN-γ and TNF-α and a preferential expression of the immunoproteasome was observed in MM cells. As a consequence, immunoproteasome-selective inhibitors are currently the focus of antimyeloma drug design.[10]

Classic chemotherapy strategies include the administration of doxorubicin, one of the most widely applied agents of all FDA approved chemotherapeutic agents in the past decades. The advantages of this drug, with its ability to target rapidly dividing cells and slow down the progression of the disease, are unfortunately combined with various drawbacks derived by toxicity on healthy cells in the human body. Doxorubicin belongs to the nonselective class I family of the anthracyclines. The aglycon in doxorubicin consists of a tetracyclic ring and the sugar, daunosamine, is attached to one of the rings through a glycosidic bond.[153] As stated before, the main collateral effect of anthracycline drugs is the multidirectional cytotoxic effect, with cardiotoxicity as the most frequent collateral effect together with brain, kidneys and liver toxicity. As a result, various efforts have been spent in order to develop specific drug delivery systems capable of controlling the drug's toxicity. Current drug delivery systems include the enclosing of drugs into polymeric drug carriers, such as liposomes, hydrogels, and nanoparticles. [153]

To conclude, MM is not completely treatable; for that reason, creating novel therapies is necessary in order to overcome drug resistance and increase life survival. In particular, targeting proteasome components responsible for inflammatory pathways would increase efficacy and reduce side effects of non-selective inhibitors. [10]

In this scenario, the aim of my project was to create a new therapeutic strategy bringing different classes of drugs with complementary properties together, creating a highly selective and cytotoxic conjugate for cancer treatment (Fig.39). The strategy involves the conjugation of an immunoproteasome inhibitor that guarantees the selectivity towards MM cells to a cytotoxic drug through cleavable linkers.

Figure 39. Cytotoxic drug delivery system

The mentioned linker should be in possession of certain features, which allow the selective release of the cytotoxic drug into the malignant cells under particular stimuli. The cleavage of a protecting group under certain conditions allows an accurate control over drug activity. The availability of specific PPG (photocleavable protecting group) allow to cage a functional group in a molecule and to release it through the advantages offered by light. In particular, the introduction of PPGs that can be uncaged with longer wavelengths of light made possible to control biological process with no side effects. One of the most studied classes of photocleavable protecting groups is represented by the ortho-nitrobenzyl derivatives. The mechanism concerning the uncaging of the PPG is based on the photochemically-induced photoisomerisation of o-nitrobenzyl alcohol derivatives into o-nitrosobenzaldehyde as reported in Scheme 9.[154-155]

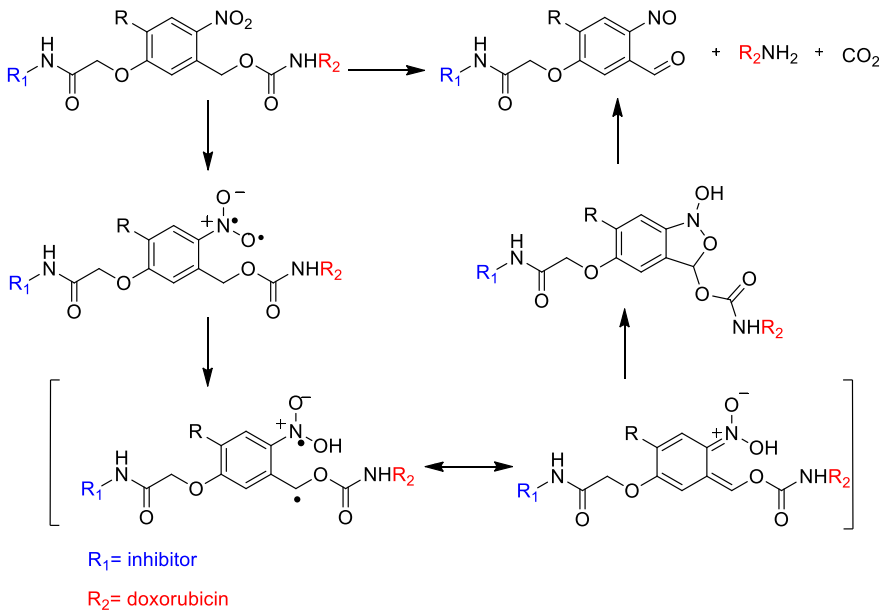

Scheme 9. Mechanism of photocleavage for o-nitro benzyl derivatives.

In the case of molecules that contain alcoholic functions, vinyl ethers protecting groups can be employed as reagents to assess biorthogonal reactions. This type of bioorthogonal reaction reveals a wide range of applicability because it proceeds under biocompatible conditions with good yields and may be appropriate for in vivo applications (Scheme 10). The reaction in discussion is the inverse electron demand Diels–Alder (iEDDA) which occurs between a tetrazine derivative and olefins containing a caged doxorubicin. The release of the cytotoxic drug into the site of interest is the purpose of the reaction. [156-157]

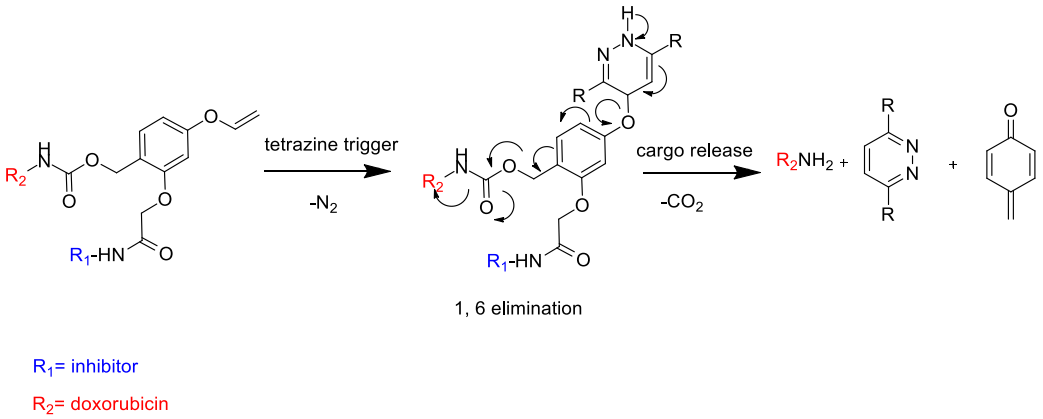

Scheme 10. Tetrazine-mediated decaging for vinyl ether

The conjugated compounds, which were designed (Fig. 40), are characterized by the β5i immunoproteasome inhibitor LU-035i, synthesised by the Biosyn group and already reported in literature, [90] connected through different linkers to the doxorubicin.

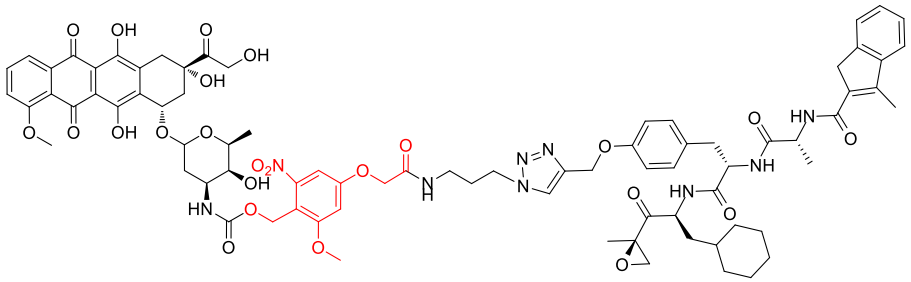

142

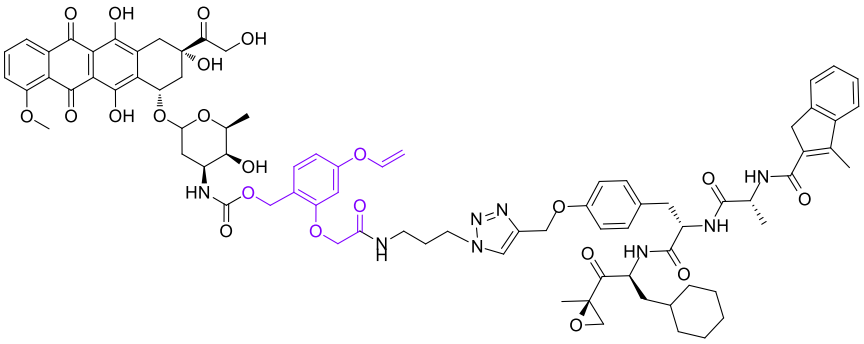

143

Figure 40. Target compounds **142-143**

8.2 Results and discussions

The synthesis of compound **142** is reported in Scheme 11. The synthesis was performed starting from compound **129** which was first alkylated with *tert*-butyl 2-bromoacetate and K_2CO_3 as a base to give compound **130**. The resulting product was then converted into the more reactive *p*-nitrophenylcarbonate derivative **131** using *p*-nitrophenyl chloroformate and pyridine as a base. The *tert*-butyl ester was deprotected in the presence of TFA giving compound **132,** which reacted with doxorubicin hydrochloride and TEA as a base for 3 days to afford compound **133**. Finally, the acid **133** was coupled with the β5i inhibitor, in the presence of HCTU and DIPEA, to give final compound **142**. All the reactions were performed covered from light.

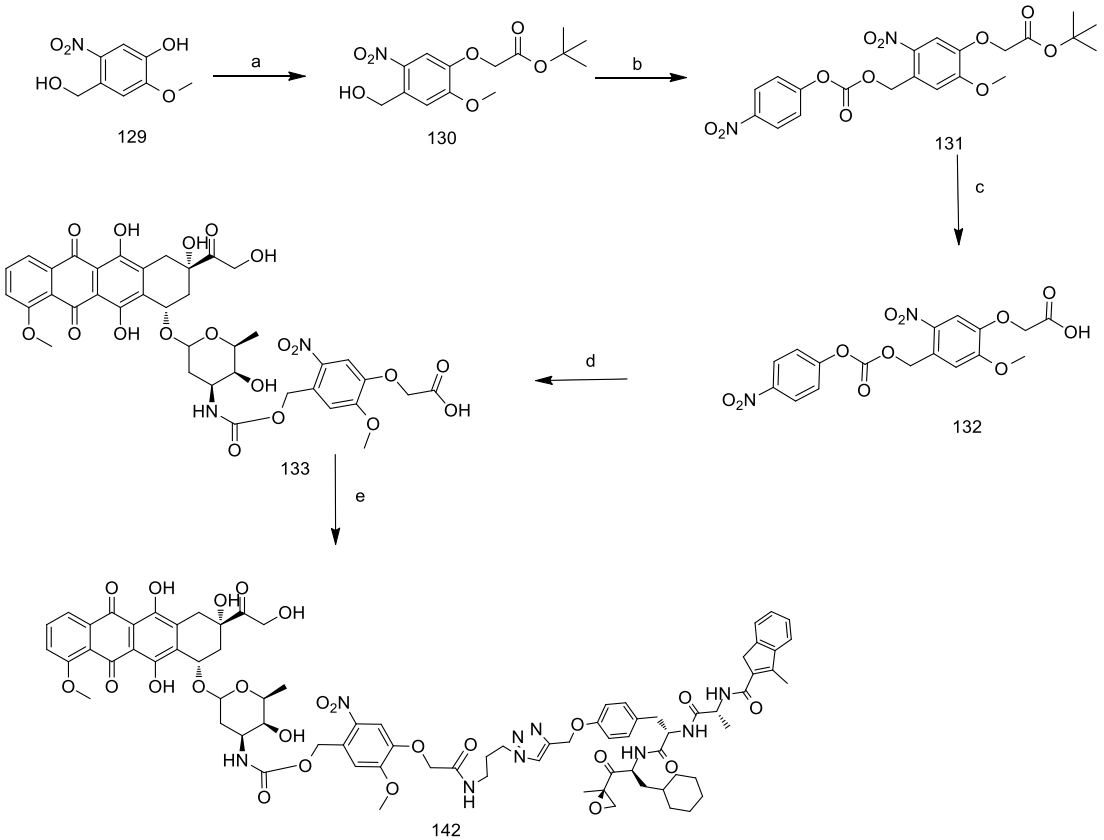

Scheme 11. Reagents and conditions: a) *tert*-butyl 2-bromoacetate, K_2CO_3, 90°C, DMF, 2h; b) *p*-nitrophenylcholoroformate, ACN, pyridine, N_2, 0°C-rt, 18h; c) TFA/DCM (1:1), 2h, rt; d) Doxorubicin, TEA, NMP, 0°C-rt, 3 days; e) HCTU, β5i inhibitor, DIPEA, DMF, 0°C-rt,18 h.

The synthesis of compound **143** is reported in Scheme 12**.** Compound **134** was first protected with 3,4-dihydro-2*H*-pyran to give compound **135**, which reacted then with *tert*-butyl 2-bromoacetate and K_2CO_3 as a base to give compound **136.** Compound **136** was dissolved in a mixture of acetic acid/water (4:1) to give compound **137** which reacted with 2,4,6-Trivinylcyclotriboroxane pyridine complex, in the presence of copper acetate and pyridine to give compound **138.** The aldehyde group was reduced using $NaBH_4$ to give compound **139**, which was converted into the more reactive *p*-nitrophenylcarbonate derivative **140** using *p*-nitrophenyl chloroformate and pyridine. The subsequent reactions to obtain compound **143** were not performed yet.

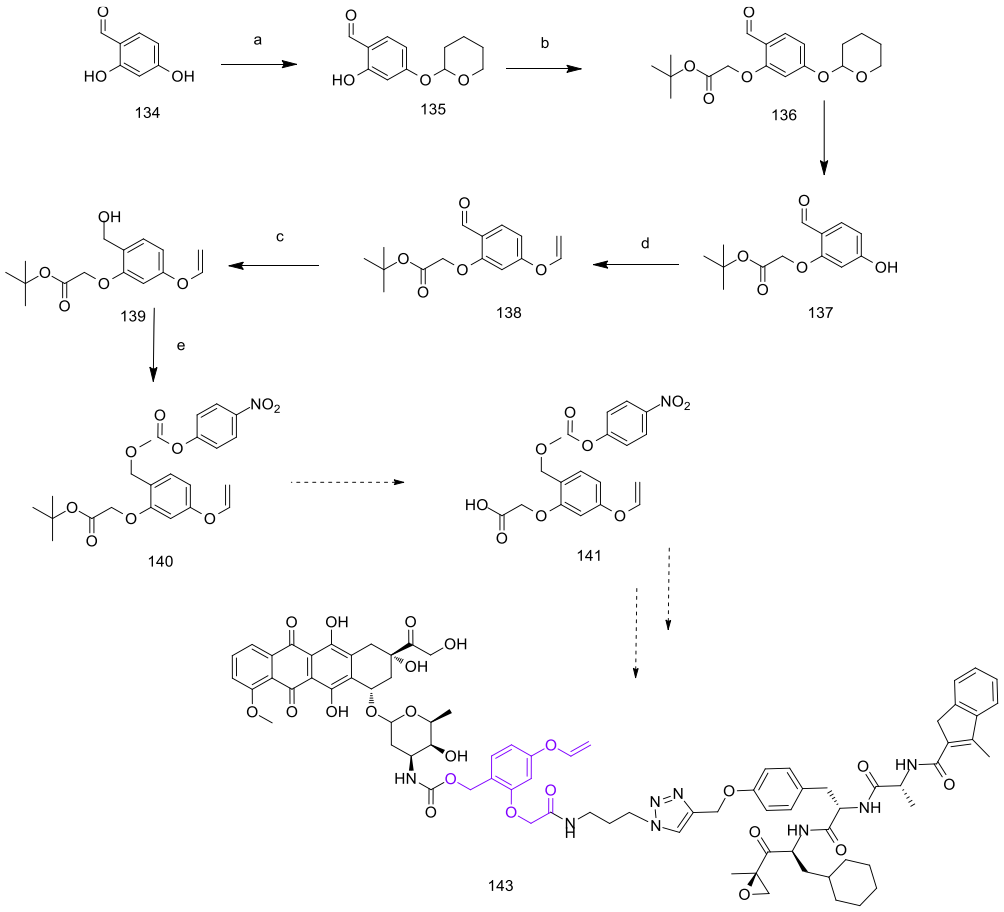

Scheme 12. Reagents and conditions: a) DHP, PPTS, dry DCM, 4h, rt; b) *tert*-butyl 2-bromoacetate, K_2CO_3, 90°C, DMF, 7h; c) $AcOH/H_2O$ (4:1), 3h, rt; d) 2,4,6-Trivinylcyclotriboroxane, copper acetate, pyridine, dry DCM, 24h, rt; e) $NaBH_4$, MeOH, 0°C, 2h; f) *p*-nitrophenylcholoroformate, dry DCM, pyridine, N_2, 0°C-rt, 24h.

Compound **52** was first evaluated on its selective immunoproteasome inhibition profile applying an established ABPP assay, on a lysate from Raji cells (a human B-cell lymphoma cell line that expresses both cCPs and iCPs), in order to evaluate whether the compound was still selective for the β5i subunit despite of the big moiety (doxorubicin) which was attached to it. Treatment of Raji cells lysate with the ABP cocktail results in six well-resolved bands, the two top bands labelled in green corresponding to β2c and β2i subunits, the two middle bands in blue to β1c and β1i subunits and the two bottom bands in red to β5i and β5c subunits. The ABP cocktail is composed of different probes which bind covalently to the active site residue of the different subunit of the cCPs and the iCPs. The probes are endowed with a fluorescent group, allowing us to detect the full resolution of all the six subunits by SDS-PAGE and in-gel fluorescent detection. [158] Compound **142** has been tested at 100, 10, 1, 0.1, 0.01, 0.001 μM final concentrations. The lysate was first incubated with compound **142** for one hour after which the ABP cocktail was added. As depicted in Figure 41, the compound is still selective in a range from 0.1 μM to 10 μM**.** We can notice that only the band corresponding to the β5i subunit is not detectable, meaning that compound **142** targeted this subunit and that the corresponding probe could not bind to the same subunit.

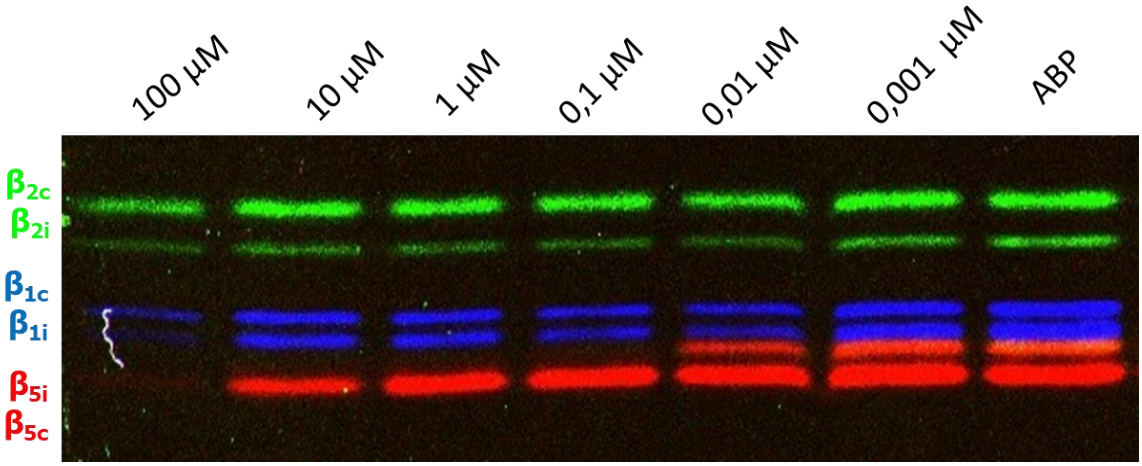

Figure 41. ABP cocktail allows the detection of the inhibition profile of the cCP and iCP subunits on SDS-PAGE.

In order to establish the range of time which was required to photocleave compound **142** or, in other words, for the release of the doxorubicin from the conjugated, an experiment was assessed using an UV irradiator at 350 nm. A 10 μM solution in DMSO

of the compound **142**was collected in a 96 well plate. The plate was irradiated and, at different range of time, a sample was taken out of the well and analysed by LC-MS. The area of the peaks corresponding to the doxorubicin and compound **1** detected by LC-MS over the time was plotted in the graphic in Figure 42 where we can notice that the release of the doxorubicin appears already after 30 seconds of irradiations and it reaches a maximum in 4 minutes while the opposite occurs for compound **142**.

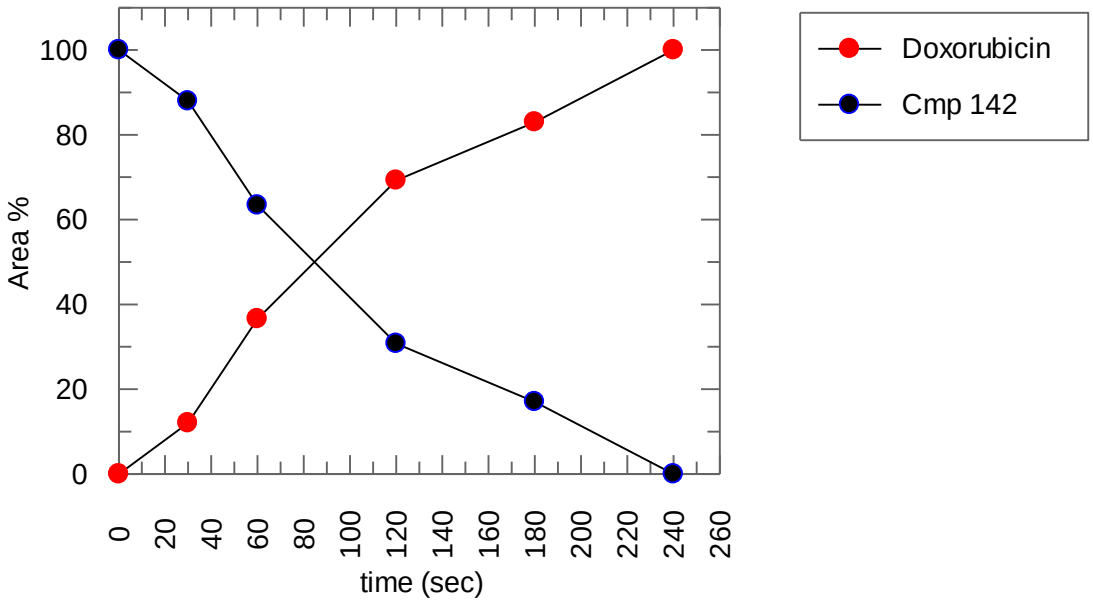

Figure 42. Release of doxorubicin under UV irradiation over the time.

At the same time, another important experiment was performed to evaluate the survival of the living cells to the UV light exposure. UV light is in fact known to be highly dangerous to normal cells due to the interaction with DNA. A long time of exposure to UV light leads to the formation of thymine dimers causing a damage that produces cancerous or precancerous cells; otherwise, in the worst case, the cells will die. A particular gene, called p53, is responsible for prevent cancer formation and mutations. If the damage is reparable, p53 activates the DNA repair. If the damage is irreparable, it leads the cell to apoptosis, or programmed cell death.

A 96 well plate filled with AMO-1 cells (multiple myeloma cell line) was irradiated at 350 nM and at different range of time (from 0 to 20 minutes) a line was transferred to another plate. The cells viability was then measured incubating the cells with the reagent alamarBlue. The experiment was performed twice, in the first experiment the cells

viability was measured without incubation time after the UV light exposure (Fig. 43) and the second time the cells viability was measured after an incubation time of three days (Fig. 44). As we can notice in the two figures, the DNA damage, thus the cells death appears after an UV exposure of 5 minutes and after an incubation time of three days.

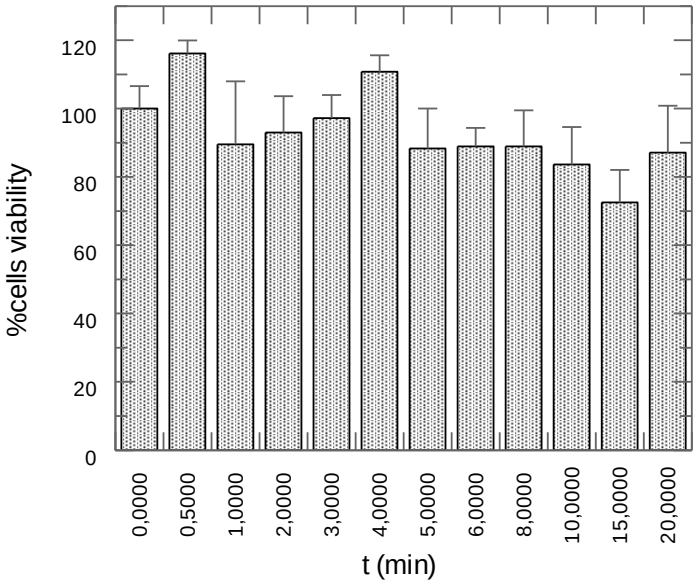

Figure 43. Cells viability after exposition to UV light for different range of time (0-20 min) and no incubation time.

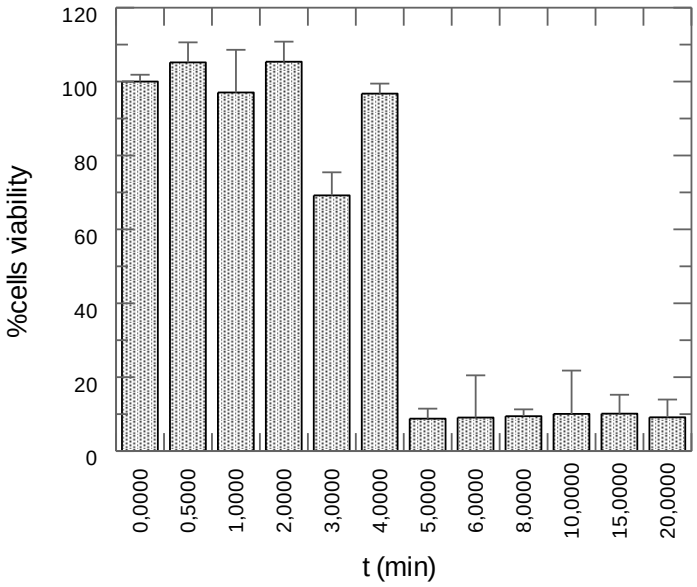

.

Figure 44. Cells viability after exposition to UV light for different range of time (0-20 min) and three days of incubation.

With the obtained data, it was possible to assess the experiment for testing compound **142** directly on living cells. The time of irradiation for the experiment was then set to 4

minutes because, with this range of exposure, we guarantee the release of the doxorubicin from the conjugated and avoid cells death due to a longer exposure to UV light, thus evading false positive results. The AMO-1 cells ($2x10^6$ cells/mL) were incubated with different concentrations of compound **142** (10, 5, 2.5, 0.5, 0.05, 0 μM) for 18 h. After this period, the cells were washed and then collected in two 96 well plates. One of this plate was treated with UV light for 4 minutes while the other plate was used as a control. Both plates were incubated then for 3 days to allow the doxorubicin to interact with the DNA and cause cells death. The viability of the cells was then measured using alamarBlue. The graphic shows that only in the plate which was exposed to UV light we had a significant cells death proportional to the concentration of compound **142** while the cells which were not exposed to UV light doesn't show any cells death (Fig. 45).

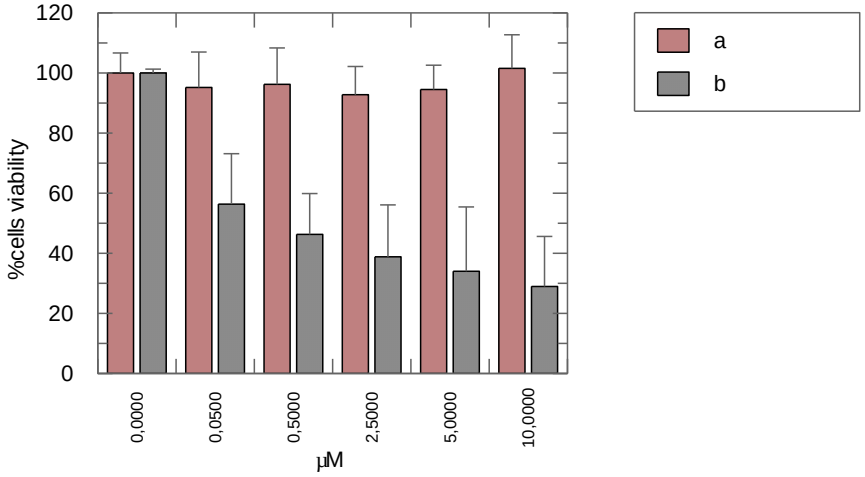

Figure 45. a) Cells viability of AMO-1 cells after the incubation with compound **142**; **b)** Cells viability of AMO-1 cells after the incubation with compound **142** and exposure to UV light.

In conclusion, this chapter describes the design, synthesis and preliminary assays of a novel doxorubicin-immunoproteasome inhibitor conjugated, which was evaluated by biological studies, proving its therapeutic potential; further investigations could allow a better examination about this type of drug delivery. A great advantage of this conjugated is definitely the selectivity due to the limited effect that the doxorubicin exerts only to

the targeted cells. Other experiments on different cells' lines expressing the constitutive proteasome could be performed to confirm this hypothesis.

A new linker has been also developed in order to connect doxorubicin and the proteasome inhibitor. In this case, the click reaction called iEDDA will be employed to allow the release of the doxorubicin.

8.3 Experimental section

Synthesis

All reagents and solvents were obtained from commercial suppliers and were used without further purification. Anhydrous solvents were prepared with activated 3 Å or 4 Å molecular sieves. ^{1}H-NMR and ^{13}C- NMR spectra were recorded on Bruker AV-400 (400 MHz). Chemical shifts are given in ppm (δ) relative to tetramethylsilane as an internal standard. Coupling constants are given in Hz. Merck silica gel 60 F254 plates were used for analytical TLC and UV visualization (λ = 254 nm) followed by $KMnO_4$ spray staining were used to record reaction progress. All column chromatography purifications were performed using solvents as received and silica gel. LC-MS analysis was performed on a Finnigan Surveyor HPLC system (detection at 200-600 nm) with an analytical C18 column (Gemini, 50 x 4.6 mm, 3 μm particle size, Phenomenex) coupled to a Finnigan LCQ Advantage MAX ion-trap mass spectrometer (ESI+). LC-MS samples were prepared by dissolving compounds in a tBuOH:ACN:H_2O mixture (1:1:1 by volume).

***Tert*-butyl 2-(4-(hydroxymethyl)-2-methoxy-5-nitrophenoxy)acetate (130)**

Compound **129** (1.03 g, 5 mmol) was dissolved in DMF (50 mL) and K_2CO_3 (700 mg, 5 mmol) was then added. *Tert*-butyl 2-bromoacetate (1.07 g, 0.81 mL, 5.5 mmol) was added and the reaction mixture was stirred at 90°C for 2 hour. The mixture was extracted with diethyl ether and washed with HCl 1M. The organic layer was finally washed with brine and then dried over Na_2SO_4 to give **130** as yellow crystals in a quantitative yield (1.5 g, 95%). ^{1}H NMR (400 MHz, MeOD): δ = 1.52 (s, 9H), 4.01 (s, 3H), 4.72 (s, 2H), 4.98 (s, 2H), 7.48 (s, 1H), 7.71 (s, 1H) ppm.

4-((*Tert*-butoxycarbonyl)methoxy)-5-methoxy-2-nitrobenzyl 4-nitrophenyl carbonate (131)

Compound **130** (50 mg, 0.16 mmol) was dissolved in ACN and pyridine (63 mg, 64.7 μL, 0.8 mmol) was then added dropwise while stirring under N_2. 4-Nitrophenyl chloroformate (32.25 mg, 0.16 mmol) was added at 0°C and the solution was stirred for 3 hours. The mixture was extracted with DCM and washed with brine. The organic layer was dried over Na_2SO_4 and the crude product was purified by column chromatography

(EtOAc/light petroleum, 3:7) to give **131** as a yellow solid. Yield: 40 % ^{1}H NMR (400 MHz, $CDCl_3$): δ = 1.51 (s, 9H), 4.02 (s, 3H), 4.69 (s, 2H), 5.72 (s, 2H), 7.15 (s, 1H), 7.42 (dd, *J* = 9.2 Hz, 2H), 7.69 (s, 1H), 8.31 (dd, *J* = 9.2 Hz, 2H) ppm.

2-(2-Methoxy-5-nitro-4-((((4-nitrophenoxy)carbonyl)oxy)methyl)phenoxy)acetic acid (132)

Compound **131** (27 mg, 0.056 mmol) was dissolved in a mixture of DCM/TFA, 1:1. The reaction mixture was stirred at room temperature for 2 hours. After completion of the reaction monitored by TLC analysis, the solvent was removed under reduced pressure followed by co-evaporation with toluene to give compound **132** as a yellow solid in a quantitative yield (97 %). ^{1}H NMR (400 MHz, CD_3CN): δ = 3.99 (s, 3H), 4.78 (s, 2H), 5.64 (s, 2H), 7.23 (s, 1H), 7.49 (d, *J* = 9.2 Hz, 2H), 7.70 (s, 1H), 8.31 (d, *J* = 9.1 Hz, 2H) ppm.

Compound 133

Compound 132 (19 mg, 0.047 mmol) was dissolved in NMP and doxorubicin hydrochloride (27 mg, 0.047 mmol) and TEA (6.5 μL, 0.047 mmol) were added under N_2. The mixture was stirred for 3 days at room temperature, covered from light. The solvent was removed and the crude product was purified by column chromatography (DCM/MeOH, 98:2) to give **133** as a red-purple powder (Yield: 40%, 15 mg). LC−MS (linear gradient 10% → 90% MeCN, 0.1% TFA, 12.5 min), t_R (min): 6.16. ESI-MS (m/z), 844.0 ($M + H_3O^+$).

Compound 142

Compound **133** (5 mg, 0.006 mmol) was dissolved in DMF and HCTU (8.68 mg, 0.021 mmol) was added. The β5i inhibitor (4.9 mg, 0.007 mmol) and DIPEA (3.66 μL, 0.021 mmol) were then added and the mixture was stirred overnight covered from light. The solvent was removed under reduced pressure and the crude was purified by column chromatography (DCM:MeOH, 98:2) to give **52** as a red powder. (5 mg, 54 % yield). LC−MS (linear gradient 10% → 90% MeCN, 0.1% TFA, 12.5 min), t_R (min): 8.33. (ESI-MS (m/z), 1548.0 (M + H+)).

2-Hydroxy-4-(tetrahydro-2*H*-pyran-2-yloxy)benzaldehyde (135)

Compound **135** was synthesised following a literature procedure.[157] 2,4-Dihydroxybenzaldehyde (1g, 7 mmol) and 3,4-dihydro-2*H*-pyran (1.17 g, 1.27 mL, 14 mmol) were dissolved in anhydrous CH_2Cl_2 and pyridinium p-toluenesulfonate (1.75 g, 7 mmol) was added. The reaction mixture was stirred at room temperature for 4 hours; the solution was washed with saturated $NaHCO_3$ solution and the organic layer was finally washed with brine and then dried over Na_2SO_4. The crude product was purified by column chromatography (Pentane/EtOAc 9:1) to give **135** as a clear oil. Analytical data were in accordance with the literature. R_f : 0.76 (Pentane/EtOAc, 7:3). Yield: 770 mg, 50 %. ^{1}H NMR (400 MHz, $CDCl_3$): δ = 1.60-1.79 (m, 4H), 1.83-1.92 (m, 2H), 3.57-3.67 (m, 1H), 3.60-3.75 (m, 1H), 5.51 (t, *J* = 3.1 Hz, 1H), 6.63 (d, *J* = 2.2 Hz, 1H), 6.66 (dd, *J* = 8.6, 2.2 Hz, 1H), 7.44 (d, *J* = 8.6 Hz, 1H), 9.73 (s, 1H), 11.37 (s, 1H) ppm. ^{13}C NMR (101 MHz, $CDCl_3$): δ = 18.5, 25.0, 30.0, 62.2, 96.3, 103.7, 109.5, 115.8, 135.4, 164.2, 164.4, 194.7 ppm.

***Tert*-butyl 2-(2-formyl-5-(tetrahydro-2*H*-pyran-2-yloxy)phenoxy)acetate (136)**

Compound **135** (240 mg, 1.1 mmol) was dissolved in DMF and K_2CO_3 (151 mg, 1.1 mmol) was added. *Tert*-butyl 2-bromoacetate (232 mg, 1.2 mmol) was added and the reaction mixture was stirred at 90°C for 7 hours. Water was added and the mixture was extracted with EtOAc. The organic layer was finally washed with brine and then dried over Na_2SO_4. The crude was purified by column chromatography (Pentane/EtOAc 9:1) to give **136** as a pale yellow oil. R_f: 0.60 (Pentane/EtOAc, 8:2). Yield: 290 mg, 80%. ^{1}H NMR (400 MHz, $CDCl_3$): δ = 1.49 (s, 9H), 1.56-1.76 (m, 4H) 1.81-1.90 (m, 2H), 3.57-3.66 (m, 1H), 3.77-3.86 (m, 1H), 4.61 (s, 2H), 5.48 (t, *J* = 2.9 Hz, 1H), 6.51 (d, *J* = 2.1 Hz, 1H), 6.74 (dd, *J* = 8.7, 1.5 Hz, 1H), 7.82 (d, *J* = 8.7 Hz, 1H), 10.41 (s, 1H) ppm. ^{13}C NMR (101 MHz, $CDCl_3$): δ = 18.4, 25.0, 28.1, 30.0, 62.01, 66.0, 82.9, 96.3, 100.4, 109.6, 119.7, 130.3, 162.0, 163.6, 167.2, 188.43 ppm. LC−MS (linear gradient 10% → 90% MeCN, 0.1% TFA, 12.5 min), t_R (min): 8.08. (ESI-MS (m/z), 336.9 (M + H+)).

***Tert*-butyl 2-(2-formyl-5-hydroxyphenoxy)acetate (137)**

Compound **136** (70 mg, 0.21 mmol) was dissolved in a mixture of acetic acid/water (4:1) and it was stirred at room temperature for 3 hours. Upon completion, the solvent was

removed *in vacuo* and the residue was diluted with EtOAc and washed with saturated $NaHCO_3$ solution. The organic layer was dried over Na_2SO_4, filtered and concentrated to give **137** as a white solid in a quantitative yield (52 mg, 98 %). R_f: 0.30 (Pentane/EtOAc,7:3).^{1}H NMR (400 MHz, $CDCl_3$): δ = 1.49 (s, 9H), 4.60 (s, 2H), 6.32 (d, *J* = 2.0 Hz, 1H), 6.54 (dd, *J* = 8.6, 1.6 Hz, 1H), 7.72 (d, *J* = 8.6 Hz, 1H), 10.27 (s, 1H) ppm. ^{13}C NMR (101 MHz, $CDCl_3$): δ = 28.1, 65.9, 83.4, 99.7, 109.7, 118.6, 131.1, 162.7, 164.3, 167.6, 189.2 ppm. LC−MS (linear gradient 10% → 90% MeCN, 0.1% TFA, 12.5 min), t_R (min): 6.21. (ESI-MS (m/z), 252.8 (M + H+)).

***Tert*-butyl 2-(2-formyl-5-(vinyloxy)phenoxy)acetate (138)**

Compound **137** (639 mg, 2.5 mmol) was dissolved in dry DCM and 2,4,6-Trivinylcyclotriboroxane pyridine complex (400 mg, 1.67 mmol), copper acetate (460 mg, 2.5 mmol) and pyridine (2 mL, 25.3 mmol) were added to the solution. The reaction mixture was exposed to ambient air through a calcium chloride drying tube and stirred at room temperature for 24 h. The solvent was removed *in vacuo* and the crude product purified by column chromatography (Pentane/EtOAc 9:1) to give **138** as white crystals. R_f: 0.56 (Pentane/EtOAc, 9:1), Yield: 550 mg, 80 %.^{1}H NMR (400 MHz, $CDCl_3$): δ = 1.47 (s, 9H), 4.58-4.63 (m, 3H), 4.91 (dd, *J* = 13.6, 1.9 Hz, 1H), 6.40 (d, *J* = 2.1 Hz, 1H), 6.58-6.68 (m, 2H), 7.86 (d, *J* = 8.6 Hz, 1H), 10.40 (s, 1H) ppm. ^{13}C NMR (101 MHz, $CDCl_3$): δ = 28.1, 65.9, 83.1, 98.5, 100.9, 109.3, 120.8, 130.6, 146.1, 161.9, 162.8, 166.9, 188.3 ppm. LC−MS (linear gradient 10% → 90% MeCN, 0.1% TFA, 12.5 min), t_R (min): 8.13. (ESI-MS (m/z), 278.8 (M + H+)).

***Tert*-butyl 2-(2-(hydroxymethyl)-5-(vinyloxy)phenoxy)acetate (139)**

Compound **138** (300 mg, 1.1 mmol) was dissolved in MeOH at 0°C. $NaBH_4$ (118 mg, 3 mmol) was added and the solution was stirred for two hours. The reaction was quenched with cold water and the solvent was removed in *vacuo*. The residue was extracted with DCM. The product was obtained as a colourless oil in a quantitative yield (305 mg, 99%). R_f: 0.23 (Pentane/EtOAc, 9:1).^{1}H NMR (400 MHz, $CDCl_3$): δ = 1.45 (s, 9H), 4.41 (dd, *J* = 6.1, 1.7 Hz, 1H), 4.52 (s, 2H), 4.62 (s, 2H), 4.73 (dd, *J* = 13.6, 1.7 Hz, 1H), 6.42 (d, *J* = 2.1 Hz, 1H), 6.53-6.59 (m, 2H), 7.19 (d, *J* = 8.2 Hz, 1H) ppm. ^{13}C NMR (101 MHz,

$CDCl_3$) δ = 28.1, 61.3, 65.9, 83.1, 95.6, 102.2, 109.5, 125.3, 130.3, 148.1, 157.0, 157.4, 168.2 ppm.

2-((*tert*-butoxycarbonyl)methoxy)-4-(vinyloxy)benzyl 4-nitrophenyl carbonate (140)

To compound **139** (73 mg, 0.26 mmol) in anhydrous DCM, 4-nitrophenyl chloroformate (105 mg, 0.52 mmol) and pyridine (63.18 μL, 0.78 mmol) were added and the mixture was stirred overnight under N_2. After 24 hours DCM was added and the organic layer was washed with water and then brine. The organic layer was dried over Na_2SO_4, filtered and concentrated and the crude was purified by column chromatography (Pentane/EtOAc, 7:3) to give **140** as a white solid. Yield: 60%. R_f: 0.9 (Pentane/EtOAc, 7:3). ^{1}H NMR (400 MHz, $CDCl_3$): δ = 1.45 (s, 9H), 4.46 (dd, *J* = 6.0, 1.7 Hz, 1H), 4.55 (s, 2H), 4.77 (dd, *J* = 13.6, 1.7 Hz, 1H), 5.35 (s, 2H), 6.43 (d, *J* = 2.2 Hz, 1H), 6.54-6.61 (m, 2H), 7.31-7.38 (m, 3H), 8.21 (d, *J* = 9.2 Hz, 2H) ppm. 13C NMR (101 MHz, $CDCl_3$) δ = 28.03, 65.99, 66.32, 82.81, 96.44, 101.75, 109.13, 118.10, 121.33, 121.76, 125.26, 125.56, 132.18, 145.27, 145.87, 147.41, 154.89, 155.75, 157.57, 158.73 ppm.

General methods

Competition experiments in cell lysate

Lysates of Raji cells were prepared by sonication in 3 volumes of lysis buffer containing 50 mM Tris pH 7.5, 1 mM DTT, 5 mM $MgCl_2$, 250 mM sucrose, 2 mM ATP, and 0.05% (w/v) digitonin. Protein concentration was determined by the Bradford assay. Cell lysates (diluted to 5 μg of total protein in buffer containing 50 mM Tris pH 7.5, 2 mM DTT, 5 mM $MgCl_2$, 10% (v/v) glycerol, 2 mM ATP) were exposed to the inhibitors for 1 h at 37 °C prior to incubation with cocktail ABPs for another 1 h, followed by 3 min boiling with a reducing gel-loading buffer and fractionation on 12.5% SDS PAGE. In-gel detection of residual proteasome activity was performed in the wet gel slabs directly on a ChemiDoc™ MP system using Cy2 settings to detect BODIPY(FL)-LU-112, Cy3 settings to detect BODIPY(TMR)-NC-005-VS and Cy5 settings to detect Cy5-NC-001. Intensities of bands were measured by fluorescent densitometry and normalized to the intensity of bands in mock-treated extracts.

Assay on living cells. AMO-1 cell line was cultured in RPMI-1640 media (Sigma-Aldrich, USA) supplemented with 10% (v/v) fetal calf serum (Sigma-Aldrich, USA), penicillin/streptomycin (Gibco/ThermoFisher Scientific, USA) in a 5% CO_2 humidified incubator. An amount of 2 x10^6 cells/mL cells was exposed to indicated concentrations of proteasome inhibitor for 18 h at 37°C. Cells were washed and collected in two 96-well plates. One of this plate was irradiated with a CAPRI box irradiator at 350 nm for 4 minutes. Both plates were incubated for three nights. Cell viability was measured using the Alamar Blue mitochondrial dye conversion assay. First, 33 µL of 50mM alamar blue solution was pipetted into each well and then incubated for 4 h at 37 °C in a humidified, 5% CO_2 atmosphere. The optical density was determined at 490 nm (background subtraction at 690 nm) using a TECAN plate reader.

9. Abbreviations

Ac: acetyl

ACN: acetonitrile

ABPP: activity-based protein profiling

Ala (or A): alanine

AMC: 7-amino-methyl-coumarin

Arg (or R): arginine

Asn (or N): Asparagine

ATP: Adenosine triphosphate

BBB: Blood-Brain Barrier

BIPN: bortezomib-induced peripheral neuropathy

BSF: Bloodstream form

Cbz (or Z): Carbobenzyloxy

cCP: constitutive core-particle

ChT-L: chymotrypsin-like

C-L: caspase-like

CM: Cross-Methatesis

CNS: Central Nervous System

Cys (or C): Cysteine

DAG: diacylglycerol

DCM: Dichloromethane

DIPEA: N,N'-Diisopropylethilamine

DMF: N,N'-Dimethylformamide

DNDi: Drug for Neglected Diseases initiative

EDCI: N-Ethyl-N'-(3-dimethylaminopropyl)carbodiimide hydrochloride

ETOAC: Ethyl acetate

ET_2O: Diethyl ether

EC_{50}: Half maximal effective concentration

EDCI: 1-Ethyl-3-(3-dimethylaminopropyl)carbodiimide

EWG: Electron-Withdrawing Group

FP-2: falcipain-2

Gln (or Q): Glutamine

GLU (OR E): GLUTAMIC ACID

GLY (OR G): GLYCINE

GPI: GLYCOSYLPHOSPHATIDYLINOSITOL

HAT: HUMAN AFRICAN TRYPANOSOMIASIS

HATU: N-[(DIMETHYLAMINO)-1H-1,2,3-TRIAZOLO-[4,5-B]PYRIDIN-1-YLMETHYLENE]-N-METHYLMETHANAMINIUM HEXAFLUOROPHOSPHATE N-OXIDE

HCTU: N,N,N',N'-TETRAMETHYL-O-(6-CHLORO-1H-BENZOTRIAZOL-1-YL)URONIUM HEXAFLUOROPHOSPHATE

IEDDA: INVERSE ELECTRON DEMAND DIELS–ALDER

HIS (OR H): HISTIDINE

HOBT: HYDROXYBENZOTRIAZOLE

HPHE: HOMOPHENYLALANINE

IC_{50}: HALF MAXIMAL INHIBITORY CONCENTRATION

ICP: IMMUNO-CORE PARTICLE

IFN-Γ: INTERFERON-GAMMA

IL-2: INTERLEUKIN-2

IP3: INOSITOL-1,4,5-TRIPHOSPHATE

K_I: DISSOCIATION CONSTANT

K_{2ND}: SECOND ORDER RATE CONSTANT

LE: LONG EPIMASTIGOTE

LEU (OR L): LEUCINE

LMP: LOW-MOLECULAR WEIGHT PROTEIN

MECL-1: MULTICATALYTIC ENDOPEPTIDASE COMPLEX

MEL OX: MELARSEN OXIDE

MEL T: MELARSEN OXIDE-TRYPANOTHIONE

MET (OR M): METHIONINE

MHC: MAJOR HISTOCOMPATIBILITY COMPLEX

MM: MULTIPLE MYELOMA

MS: MULTIPLE SCLEROSIS

MU: MORPHOLINO UREA

MW: MICROWAVE

NECT: NIFURTIMOX-EFLORNITHINE COMBINATION THERAPY

NHL: NON-HODGKIN LYMPHOMA

N-MPIP: N-METHYL PIPERAZINE

NTDS: NEGLECTED TROPICAL DISEASES

ODC: ORNITHINE DECARBOXYLASE

PARS: PROTEASE ACTIVATED RECEPTORS

PCF: PROCYCLIC TRYPOMASTIGOTES FORM

PDB: PROTEIN DATA BANK

PGPH: POST-GLUTAMATE PEPTIDE HYDROLASE

PIS: PROTEASOME INHIBITORS

PLP: PYRIDOXAL 5'-PHOSPHATE

PHE (OR F): PHENYLALANINE

PPG: PHOTOLABILE PROTECTING GROUP

PRO (OR P): PROLINE

RA: RHEUMATOID ARTHRITIS

SAR: STRUCTURE-ACTIVITY RELATIONSHIP

SE: SHORT EPIMASTIGOTE

SD: STANDARD DEVIATION

SLE: SYSTEMIC LUPUS ERYTHEMATOSUS

TBCATB: TRYPANOSOMA BRUCEI CATHEPSIN B

TBCATL: TRYPANOSOMA BRUCEI CATHEPSIN L

TC_{50}: TOXIC CONCENTRATION IN 50% OF THE CELL POPULATION

TFA: TRIFLUOROACETIC ACID

THR (OR T): THREONINE

T-L: TRYPSIN-LIKE

TNF-A: TUMOUR NECROSIS FACTOR

TRP (OR W): TRYPTOPHAN

TYR (OR Y): TYROSINE

UPS: UBIQUITIN-PROTEASOME SYSTEM

VAL (OR V): VALINE

VSGS: VARIANT SURFACE GLYCOPROTEINS

WHO: WORLD HEALTH ORGANIZATION

10. REFERENCES

1. Powers, J. C.; Asgian, J. L.; Ekici, Ö. D.; James, K. E. Irreversible Inhibitors of Serine, Cysteine, and Threonine Proteases. *Chem. Rev.* **2002**, *102 (12)*, 4639-4750
2. Whittle, P. J.; Blundell, T. L. Protein structure-based drug design. *Annu. Rev. Biophys. Biomol. Struct.* **1994**, *23*, 349-75.
3. Kuntz, I. D.; Meng, E. C.; Shoichet, B. K. Structure-Based Molecular Design. *Acc. Chem. Res.* **1994**, *27*, 117-123.
4. Copeland, R.A. Evaluation of Enzyme Inhibitors in Drug Discovery: A Guide for medicinal Chemists and Pharmacologists. **2005,** *1st ed.*; Wiley-Interscience: Weinheim.
5. Groll, M.; Ditzel, L.; Lowe, J.; Bochtler M.; Bartunik, H. D.; Huber, R. Structure of 20S proteasome from yeast at 2.4°A resolution. *Nature.* **1997**, *386*, 463-471.
6. Ettari, R.; Previti, S.; Bitto, A.; Grasso, S.; Zappalà, M. Immunoproteasome-selective inhibitors: a promising strategy to treat hematologic malignancies, autoimmune and inflammatory diseases. *Curr. Med. Chem* **2016**, *23*, 1217-1238.
7. Huber, E. M.; Basler, M.; Schwab, R.; Heinemeyer, W.; Kirk, C. J.; Groettrup, M.; Groll, M. Immuno- and constitutive proteasome crystal structures reveal differences in substrate and inhibitor specificity. *Cell,* **2012**, *148*, 727-738.
8. Kuhn, D.J.; Orlowski, R.Z. The immunoproteasome as a target in hematologic malignancies. *Semin. Hematol.* **2012**, *49*, 258–262.
9. Huber E.M.; Groll M. Inhibitors for the immuno- and constitutive proteasome: Current and future trends in drug development. *Angew. Chem. Int. Ed. Engl.* **2012**, *51*, 8708–8720.
10. Ettari, R.; Zappalà, M.; Grasso, S.; Musolino, C.; Innao, V.; Allegra, A. Immunoproteasome-selective and non-selective inhibitors: a promising approach for the treatment of multiple myeloma. *Pharmacol. Ther.* **2018**, *182*, 176-192.
11. Scarbaci, K.; Troiano, V.; Micale, N.; Ettari, R.; Tamborini, L.; Di Giovanni, C.; Cerchia, C.; Grasso, S.; Novellino, E.; Schirmeister, T.; Lavecchia, A.; Zappalà, M. Identification of a new series of amides as non-covalent proteasome inhibitors. *European Journal of Medicinal Chemistry* **2014**, *76*, 1-9.

12. Troiano, V.; Scarbaci, K.; Ettari, R.; Micale, N.; Cerchia, C.; Pinto, A.; Schirmeister, T.; Novellino, E.; Grasso, S.; Lavecchia, A.; Zappalà, M. Optimization of peptidomimetic boronates bearing a P3 bicyclic scaffold as proteasome inhibitors. *Eur. J. Med. Chem.* **2014**, *83*, 1–14.
13. Scarbaci, K.; Troiano, V.; Ettari, R.; Pinto, A.; Micale, N.; Di Giovanni, C.; Cerchia, C.; Schirmeister, T.; Novellino, E.; Lavecchia, A.; Zappalà, M.; Grasso, S. Development of novel selective peptidomimetics containing a boronic acid moiety, targeting the 20S proteasome as anticancer agents. *Chem. Med. Chem*. **2014**, *9*, 1801-16.
14. Ettari, R.; Cerchia, C.; Maiorana, S.; Guccione M.; Novellino E.; Bitto A.; Grasso S.; Lavecchia A.; Zappalà M. Development of novel amides as non-covalent inhibitors of immunoproteasome *ChemMedChem*. **2019**, *14*(8), 842-852.
15. Dragovich, PS.; Prins, TJ.; Zhou, R.; Johnson, TO.; Hua, Y.; Luu HT.; Sakata, SK.; Brown, EL.; Maldonado, FC.; Tuntland T.; Lee, CA.; Fuhrman, SA.; Zalman, LS.; Patick, AK.; Matthews, DA.; Wu, EY.; Guo M.; Borer, BC.; Nayyar, NK.; Moran, T.; Chen, L.; Rejto, PA.; Rose, PW.; Guzman, MC.; Dovalsantos, EZ.; Lee, S.; McGee, K.; Mohajeri, M.; Liese A.; Tao, J.; Kosa, MB.; Liu, B.; Batugo, MR.; Gleeson, JP., Wu, ZP.; Liu, J.; Meador, JW 3rd.; Ferre, RA. Structure-based design, synthesis, and biological evaluation of irreversible human rhinovirus 3C protease inhibitors. 8. Pharmacological optimization of orally bioavailable 2-pyridone-containing peptidomimetics. *J. Med. Chem.* **2003,** *46,* 4572-4585.
16. Verissimo, E.; Berry, N.; Gibbons, P.;. Cristiano, M. L; Rosenthal, P. J.; Gut, J.; Ward, S. A.; O'Neill, P. M. Design and synthesis of novel 2-pyridone peptidomimetic falcipain 2/3 inhibitors. *Bioorg. Med. Chem. Lett.* **2008,** 18*,* 4210-4214.
17. P. Sjö, *Fut. Med. Chem*. **2012**, *4*, 651–660.
18. Genin, E.; Reboud-Ravaux, M.; Vidal, J. Proteasome inhibitors: recent advances and new perspectives in medicinal chemistry. *Curr. Top. Med. Chem*. **2010**, *10*, 232-256.
19. Human African Trypanosomiasis; World Health Organization: Geneva, **2018**; https://www.who.int/trypanosomiasis_african/en/ (accessed March 20, 2019).

20. Bücher, P.; Cecchi, G.; Jamonneau, V.; Priotto, G. Human African Trypanosomiasis. *Lancet* **2017**, *390*, 2397−2409.
21. MacLean, L.; Reiber, H.; Kennedy, P.G.; Sternberg, JM. Stage progression and neurological symptoms in *Trypanosoma brucei rhodesiense* sleeping sickness: role of the CNS inflammatory response. *PLoS Negl. Trop. Dis.* **2012**; 6:e1857.
22. Mugnier, M. R. M; Cross, G. A. M.; Papavasiliou, F. N. The in Vivo Dynamics of Antigenic Variation in *Trypanosoma brucei*. *Science* **2015**, *347*; 1470–1473.
23. Babokhov, P.; Sanyaolu, A. O.; Oyibo, W. A.; Fagbenro-Beyioku, A. F.; Iriemenam, N. C. A Current Analysis of Chemotherapy Strategies for the Treatment of Human African Trypanosomiasis, *Pathog. Glob. Health* **2013**, *107*, 242-252.
24. a.) Priotto, G.; Kasparian, S.; Mutombo, W.; Ngouama, D.; Ghorashian, S.; Arnold, U.; Ghabri, S.; Baudin, E.; Buard, V.; Kazadi-Kyanza, S.; Ilunga, M.; Mutangala, W.; Pohlig, G.; Schmid, C.; Karunakara, U.; Torreele, E.; Kande, V. Nifurtimox Eflornithine Combination Therapy for Second-Stage African *Trypanosoma brucei gambiense* Trypanosomiasis: a Multicentre, Randomised, Phase III, Non-Inferiority Trial. *Lancet* **2009**, *374*, 56-64. b) Kansiime, F.; Adibaku S.; Wamboga C.; Idi F.; Kato C. D.; Yamuah L.; Vaillant M.; Kioy D.; Olliaro P.; Matovu E. A Multicentre, Randomised, Non-Inferiority Clinical Trial Comparing a Nifurtimox-Eflornithine Combination to Standard Eflornithine Monotherapy for Late Stage *Trypanosoma brucei gambiense* Human African Trypanosomiasis in Uganda. *Parasit. Vectors* **2018**, *11:105*.
25. a) Ettari, R.; Tamborini, L.; Angelo, I. C.; Micale, N.; Pinto, A.; De Micheli, C.; Conti, P. Inhibition of Rhodesain as a Novel Therapeutic Modality for Human African Trypanosomiasis. *J. Med. Chem.* **2013**, *56* , 5637–5658. (b) Ettari, R.; Previti, S.; Tamborini, L.; Cullia, G.; Grasso, S.; Zappalà M. The Inhibition of Cysteine Proteases *Rhodesain* and TbCatB: a Valuable Approach to Treat Human African Trypanosomiasis. *Mini Rev. Med. Chem.* **2016**, *16*, 1374-1391.
26. Steverding, D.; Sexton, D. W.; Wang, X.; Gehrke, S. S.; Wagner, G. K.; Caffrey, C. R. *Trypanosoma brucei*: Chemical evidence that cathepsin L is essential for survival and a relevant drug target. *Int. J. Parasitol.* **2012**, *42*, 481–488.

27. Nikolskaia, O. V.; de A Lima, A. P.; Kim, Y. V.; Lonsdale-Eccles, J. D.; Fukuma, T.; Scharfstein, J.; Grab, D. J. Blood-brain barrier traversal by African trypanosomes requires calcium signaling induced by parasite cysteine protease. *J. Clin. Invest.* **2006**, *116*, 2739–2747.

28. Triggs, V. P.; Bangs, J. D. Glycosylphosphatidylinositol-Dependent Protein Trafficking in Bloodstream Stage *Trypanosoma brucei*. *Eukaryotic Cell* **2003**, *2*, 76-83.

29. (a) Lalmanach, G.; Boulange, A.; Serveau, C.; Lecaille, F.; Scharfstein, J.; Gauthier, F.; Authie, E. Congopain from *Trypanosoma congolense*: Drug Target and Vaccine Candidate. *Biol. Chem.* **2002**, *383*, 739-749. (b) Santos, C. C.; Coombs, G. H.; Lima, A. P.; Mottram, J. C. Role of the *Trypanosoma brucei* natural cysteine peptidase inhibitor ICP in differentiation and virulence. *Mol. Microbiol.* **2007**, *66*, 991–1002.

30. Caffrey, C. R.; Hansell, E.; Lucas, K. D.; Brinen, L.S.; Hernandez, A. A.; Cheng, J.; Gwalteny, S. L.; Roush, W. R.; Stierhof, Y.-D.; Bogyo, M.; Steverding, D.; McKerrow, J. H. Active site mapping, biochemical properties and subcellular localization of rhodesain, the major cysteine protease of *Trypanosoma brucei rhodesiense*. *Mol. Biochem. Parasitol.,* **2001**, *118*, 61-73.

31. Previti, S.; Ettari, R.; Cosconati, S.; Amendola, G.; Chouchene, K.; Wagner, A.; Hellmich, U. A.; Ulrich, K.; Krauth-Siegel, R. L.; Wich, P. R.; Schmid, I.; Schirmeister, T.; Gut, J.; Rosenthal, P. J.; Grasso, S.; Zappalà M. Development of Novel Peptide-based Michael Acceptors Targeting Rhodesain and Falcipain-2 for the Treatment of Neglected Tropical Diseases (NTDs*). J. Med. Chem*. **2017**, *60*, 6911−6923.

32. Jaishankar, P.; Hansell, E.; Zhao, DM.; Doyle, PS. McKerrow, JH.; Renslo, AR. Potency and selectivity of P2/P3-modified inhibitors of cysteine proteases from trypanosomes. *Bioorg Med Chem Lett*. **2008**, *18*(2), 624-628.

33. Zwicker ,JD.; Diaz, NA.; Guerra, AJ.; Kirchhoff, PD.; Wen, B.; Sun, D.; Carruthers, VB.; Larsen, SD. Optimization of dipeptidic inhibitors of cathepsin L for improved Toxoplasma gondii selectivity and CNS permeability. *Bioorg Med Chem Lett*. **2018**, *28*(10), 1972-1980.

34. Borissenko, L.; Groll, M. 20S Proteasome and its inhibitors: crystallographic knowledge for drug development. *Chem. Rev.* **2007**, *107*, 687-717.

35. Micale, N.; Scarbaci, K.; Troiano, V.; Ettari, R.; Grasso, S.; Zappalà, M. Peptide-based proteasome inhibitors in anticancer drug design. *Medicinal Research Review* **2014**, *34*, 1001-1069.
36. Bellavista, E.; Santoro, A.; Galimberti, D.; Comi, C.; Luciani, F.; Mishto, M. Current understanding on the role of standard and immunoproteasomes in inflammatory/immunological pathways of multiple sclerosis. *Autoimmune Dis.* **2014**, 739705 10.1155/2014/739705.
37. Nandi, D.; Tahiliani, P.; Kumar, A.; Chandu, D. The ubiquitin-proteasome system. *J. Biosci.*, **2006**, *31*, 137-155.
38. Goldberg, A. L. Functions of the proteasome: From protein degradation and immune surveillance to cancer therapy. *Biochem. Soc. Trans.* **2007**, *35*, 12–17.
39. Fan, H.; Angelo, N. G.; Warren, J. D.; Nathan, C. F.; Lin, G. Oxathiazolones selectively inhibit the human immunoproteasome over the constitutive proteasome. *ACS Medicinal Chemistry Letters* **2014**, *5*, 405-410.
40. Groettrup, M.; Kirk, C. J.; Basler, M. Proteasomes in immune cells: more than peptide producers? *Nature Reviews Immunology* **2010**, *10*, 73-78.
41. Weissman, A. M.; Shabek, N.; Ciechanover, A. The predator becomes the prey: regulating the ubiquitin system by ubiquitylation and degradation. *Nature Reviews Molecular Cell Biology* **2011**, *12*, 605-620.
42. Zanker, D.; Weisan, C. Standard and immunoproteasomes show similar peptide degradation specificities. *European Journal of Immunology* **2014**, *44*, 3500-3503.
43. Kisselev, A. F.; Callard, A.; Goldberg, A. L. Importance of different active sites in protein breakdown by 26S proteasomes and the efficacy of proteasome inhibitors varies with the protein substrate. *J. Biol. Chem.* **2006**, *281*, 8582-8590.
44. Koroleva, O. N.; Pham, T. H.; Bouvier, D.; Dufau, L.; Qin, L.; Reboud-Ravaux, M.; Ivanov, A. A.; Zhuze, A. L.; Elizaveta S. Gromova, E. S.; Bouvier-Durand, M.. Bisbenzimidazole derivatives as potent inhibitors of the trypsin-like sites of the immunoproteasome core particle. *Biochimie* **2015**, *108*, 94-100.
45. Heinemeyer, W.; Fisher, M.; Krimmer, T.; Stachon, U.; Wolf, D.H. The active sites of the eukaryotic 20S proteasome and their involvement in subunit precursor processing. *J. Biol. Chem.*, **1997**, *272*, 25200-25209.

46. Groll, M.; Heinemeyer, W.; Jager, S.; Ullrich, T.; Botchler, M.; Wolf, D.H.; Huber, R. The catalytic sites of 20S proteasomes and their role in subunit maturation: A mutational and crystallographic study. *Proc. Natl, Acad. Sci. U.S.A.*, **1999**, *96*, 10976-10983.

47. Arciniega, M.; Beck, P.; Lange, O. F.; Groll, M.; Huber, R. Differential global structural changes in the core particle of yeast and mouse proteasome induced by ligand binding. *PNAS* **2014**, *111*, 9479-9484.

48. Murata, S.; Sasaki, K.; Kishimoto, T.; Niwa, S.; Hayashi, H.; Takahama, Y.; Tanaka, K. Regulation of CD8+ T cell development by thymus-specific proteasomes. *Science* **2007**, *316*, 1349-53.

49. Muchamuel, T.; Basler, M.; Aujay, M. A.; Suzuki, E.; Kalim, K. W.; Lauer, C.; Sylvain, C.; Ring, E. R.; Shields, J.; Jiang, J.; Shwonek, P.; Parlati, F.; Demo, S. D.; Bennett, M. K.; Kirk, C. J.; Groettrup, M. A selective inhibitor of the immunoproteasome subunit LMP7 blocks cytokine production and attenuates progression of experimental arthritis. *Nature medicine* **2009**, *15*, 781-787.

50. Xing, Y.; Jameson, S. C.; Hogquist, K. A. Thymoproteasome subunit-β5T generates peptide-MHC complexes specialized for positive selection. *Proc. Natl. Acad. Sci. USA* **2013**, *110*, 6979-6984.

51. Monaco, J. J. A molecular model of MHC class-I-restricted antigen processing. *Immunology today* **1992**, *13*, 173-179.

52. Ferrington, D. A.; Gregerson, D. S. Immunoproteasomes: structure, function, and antigen presentation. *Prog. Mol. Biol. Transl. Sci.* **2012**, *109*, 75-112.

53. Nandi, D.; Jiang, H.; Monaco, J. J. Identification of MECL-1 (LMP-10) as the third IFN-gammainducible proteasome subunit. *J. Immunol.* **1996**, *156*, 2361-2364.

54. Sijts, E. J. A. M.; Kloetzel P. M. The role of the proteasome in the generation of MHC class I ligands and immune responses. *Cell Mol Life Sci*, **2011**, *68*(9), 1491–1502.

55. Ebstein, F.; Kloetzel, P. M.; Krüger, E.; Seifert, U. Emerging roles of immunoproteasomes beyond MHC class I antigen processing. *Cell Mol Life Sci*, **2012**, *69*, 2543-2558.

56. Visekruna, A.; Slavova, N.; Dullat, S.; Grone, J.; Kroesen, A.; Ritz, J.; Buhr, H.; Steinhoff, U. Expression of catalytic proteasome subunits in the gut of patients with Crohn's disease. *Int J Colorect Dis*, **2009**, *10*, 1133–1139.

57. Basler, M.; Dajee, M.; Moll, C.; Groettrup, M.; Kirk, C. J. Prevention of experimental colitis by a selective inhibitor of the immunoproteasome. *J Immunol*, **2010**; *185*, 634–641.

58. Fitzpatrick, L. R.; Khare, V.; Small, J. S.; Koltun, W.A. Dextran sulfate sodium-induced colitis is associated with enhanced low molecular mass polypeptide 2 (LMP2) expression and is attenuated in LMP2 knockout mice. *Dig Dis Sci*. **2006**, *51*, 1269–1276.

59. Fitzpatrick, L. R.; Small, J. S.; Poritz, L. S.; McKenna, K. J.; Koltun, W. A. Enhanced intestinal expression of the proteasome subunit low molecular mass polypeptide 2 in patients with inflammatory bowel disease. *Dis Colon Rectum*, **2007**; *50*, 337–348.

60. McInnes, I. B.; Schett, G. The pathogenesis of rheumatoid arthritis. *N Engl J Med*, **2011**, *365*, 2205–2219.

61. Ichikawa, H. T.; Conley, T.; Muchamuel, T.; Jiang, J.; Lee, S.; Owen T.; Barnard, J.; Nevarez, S.; Goldman, B. I.; Kirk, C. J.; Looney, R. J.; Anolik, J. H. Beneficial effect of novel proteasome inhibitors in murine lupus via dual inhibition of type I interferon and autoantibody-secreting cells. *Arthritis Rheum,* **2012**, *64*, 493-503.

62. Cenci, S.; Oliva, L.; Cerruti, F.; Milan, E.; Bianchi, G.; Raule, M.; Mezghrani, A., Pasqualetto, E.; Sitia, R.; Cascio, P. Protein synthesis modulates responsiveness of differentiating and malignant plasma cells to proteasome inhibitors. *J Leukoc Biol*, **2012**, *92*, 921-931

63. Basler, M.; Mundt, S.; Muchamuel, T.; Moll, C.; Jiang, J.; Groettrup, M.; Kirk, C. J. Inhibition of the immunoproteasome ameliorates experimental autoimmune encephalomyelitis. *EMBO Mol Med*, **2014**, *6*, 226-238.

64. Ashton-Chess, J.; Mai, H. L.; Jovanovic, V.; Renaudin, K.; Foucher, Y.; Giral, M.; Moreau, A.; Dugast, E.; Mengel, M.; Racapé, M.; Danger, R.; Usal, C.; Smit, H.; Guillet, M.; Gwinner, W.; Le Berre, L.; Dantal, J.; Soulillou, J.-P., Brouard, S. Immunoproteasome beta subunit 10 is increased in chronic antibody-mediated rejection. *Kidney Int,* **2010**, *77*, 880-890.

65. Kuhn, D. J.; Hunsucker, S. A.; Chen, Q.; Voorhees, P. M.; Orlowski, M.; Orlowski, R. Z. Targeted inhibition of the immunoproteasome is a potent strategy against models of multiple myeloma that overcomes resistance to conventional drugs and nonspecific proteasome inhibitors. *Blood*, **2009**, *113*, 4667-4676
66. Chen, X.; Zhang, X.; Wang, Y.; Lei, H.; Su, H.; Zeng, J.; Pei, Z.; Huang, R. Inhibition of immunoproteasome reduces infarction volume and attenuates inflammatory reaction in a rat model of ischemic stroke. *Cell Death Dis*, **2015**, *6*, e1626.
67. Wojcik, C.; Di Napoli, M. Ubiquitin-proteasome system and proteasome inhibition: new strategies in stroke therapy. *Stroke*, **2004**, *35*, 1506-1518
68. Arastu-Kapur, S.; Anderl, J. L.; Kraus, M.; Parlati, F.; Shenk, K. D.; Lee, S. J.; Muchamuel, T.; Bennett, M. K.; Driessen, C.; Ball, A. J.; Kirk, C. J. Nonproteasomal targets of the proteasome inhibitors bortezomib and carfilzomib: a link to clinical adverse events. *Clin Cancer Res*; **2011**, *17*, 2734–2743.
69. Argyriou, A. A.; Iconomou, G.; Kalofonos, H. P. Bortezomib-induced peripheral neuropathy in multiple myeloma: a comprehensive review of the literature. *Blood*, **2008**, *112*, 1593-1599
70. Parlati, F.; Lee, S. J.; Aujay, M.; Suzuki, E.; Levitsky, K.; Lorens, J. B.; Micklem, D. R.; Ruurs, P.; Sylvain, C.; Lu, Y.; Shenk, K. D.; Bennett, M. K. Carfilzomib can induce tumor cell death through selective inhibition of the chymotrypsin-like activity of the proteasome. *Blood*, **2009**, 114, 3439-3447.
71. Roccaro, A. M.; Sacco, A.; Aujay, M.; Ngo, H. T.; Kareem Azab, A. , Azab, F.; Quang, P.; Maiso, P.; Runnels, J.; Anderson, K. C.; Demo, S.; Ghobrial, I. M. Selective inhibition of chymotrypsin-like activity of the immunoproteasome and constitutive proteasome in Waldenström macroglobulinemia. *Blood*, **2010**, *115*, 4051-4060.
72. Adams, J.; Behnke, M.; Chen, S.; Cruickshank, A. A.; Dick, L. R.; Grenier, L.; Klunder, J. M.; Ma, Y.-T.; Plamondon, L.; Stein, R. L. Potent and selective inhibitors of the proteasome: dipeptidyl boronic acids. *Bioorg. Med. Chem. Lett.*, **1998**, *8*, 333-338.
73. Richardson, P. G.; Sonneveld, P.; Schuster, M. W.; Irwin, D.; Stadtmauer, E. A.; Facon, T.; Harousseau, J.-L.; Ben-Yehuda, D.; Lonial, S.; Goldschmidt, H.; Reece,

D.; San-Miguel, J. F.; Blade, J.; Boccadoro, M.; Cavenaugh, J.; Dalton, W. S.; Boral, A. L.; Esseltine, D. L.; Porter, J. B.; Schenkein, D.; Anderson, K. C. Bortezomib or high-dose dexamethasone for relapsed multiple myeloma. *N. Engl. J. Med.*, **2005**, *352*, 2487-2498.

74. Adams, J.; Elliott, P. J.; Bouchard, P. Preclinical development of bortezomib (VELCADE): rationale for clinical studies. *Proteasome Inhibitors in Cancer Therapy*, **2004**, 233-269.
75. Orlowski, R. Z.; Zeger, E. L. Targeting the proteasome as a therapeutic strategy against haematological malignancies. *Expert Opin. Invest. Drugs*, **2006**, *15*, 117-130.
76. Groll, M.; Berkers, C. R.; Ploegh, H. L.; Ovaa, H. Crystal structure of the boronic acid-based proteasome inhibitor bortezomib in complex with the yeast 20S proteasome. *Structure*, **2006**, *14*, 451-456.
77. Berkers, C.R.; Verdoes, M.; Lichtman, E.; Fiebiger, E.; Kessler, B.M.; Anderson, K.C.; Ploegh, H.L.; Ovaa, H.; Galardy, P.J. Activity probe for in vivo profiling of the specificity of proteasome inhibitor bortezomib., *Nat Methods*. **2005**, *2*, 357-362.
78. Richardson, P.G.; Briemberg, H.; Jagannath, S.; Wen, P.Y.; Barlogie, B.; Berenson, J.; Singhal, S.; Siegel, D.S.; Irwin, D.; Schuster, M.; Srkalovic, G.; Alexanian, R.; Rajkumar, S.V.; Limentani, S.; Alsina, M.; Orlowski, R.Z.; Najarian, K.; Esseltine, D.; Anderson, K.C.; Amato, A.A. Frequency, characteristics, and reversibility of peripheral neuropathy during treatment of advanced multiple myeloma with bortezomib, *J Clin Oncol*. **2006**, *24*, 3113-3120.
79. Bo Kim, K.; Crews, C. M. From epoxomicin to carfilzomib: chemistry, biology, and medical outcomes. *Nat. Prod. Rep.*, **2013**, *30*, 600-604.
80. Hanada, M.; Sugawara, K.; Kaneta, K.; Toda, S.; Nishiyama, Y.; Tomita, K.; Yamamoto, H.; Konishi, M.; Oki, T., Epoxomicin, a new antitumor agent of microbial origin. *J. Antibiot.*, **1992**, *45*, 1746-1752.
81. Meng, L.; Mohan, R.; Kwok, B. H. B.; Elofsson, M.; Sin, N.; Crews, C. M. Epoxomicin, a potent and selective proteasome inhibitor, exhibits in vivo antiinflammatory activity. *Proc. Natl. Acad. Sci. U. S. A.*, **1999**, *96*, 10403-10408.
82. Meng, L.; Kwok, B. H. B.; Sin, N.; Crews, C. M. Eponemycin exerts its antitumor effect through the inhibition of proteasome function. *Cancer Res.,* **1999**, *59*, 2798-2801.

83. Groll, M.;Kim, K. B.; Kairies, N.; Huber, R.;Crews, C. M. Crystal Structure of Epoxomicin: 20S Proteasome Reveals a Molecular Basis for Selectivity of α‘,β‘-Epoxyketone Proteasome Inhibitors *J. Am. Chem. Soc.* **2000**, *122*, 1237–1238.

84. Demo, S. D.; Kirk, C. J.; Aujay, M. A.; Buchholz, T. J.; Dajee, M.; Ho, M. N.; Jiang, J.; Laidig, G. J.; Lewis, E. R.; Parlati, F.; Shenk, K. D.; Smyth, M. S.; Sun, C. M.; Vallone, M. K.; Woo, T. M.; Molineaux, C. J.; Bennett, M. K. Antitumor activity of PR-171, a novel irreversible inhibitor of the proteasome. *Cancer Res.*, **2007**, *67*, 6383–6391.

85. Kupperman, E.; Lee, E. C.; Cao, Y.; Bannerman, B.; Fitzgerald, M.; Berger, A.; Yu, J.; Yang, Y.; Hales, P.; Bruzzese, F.; Liu, J.; Blank, J.; Garcia, K.; Tsu, C.; Dick, .; Fleming, P.; Yu, L.; Manfredi, M.; Rolfe, M.; Bolen, J. Evaluation of the proteasome inhibitor MLN9708 in preclinical models of human cancer. *Cancer Res*, **2010**, *70*, 1970-1980

86. Ho, Y. K.; Bargagna-Mohan, P.; Wehenkel, M.; Mohan, R.; Kim, K. B. LMP2-specific inhibitors: chemical genetic tools for proteasome biology. *Chem Biol.*, **2007**; *14*, 419–430.

87. Sugawara, K.; Hatori, M.; Nishiyama, Y.; Tomita, K.; Kamei, H.; Konishi, M.; Oki, T. Eponemycin, a new antibiotic active against B16 melanoma. I. Production, isolation, structure and biological activity. *J. Antibiot.*, **1990**, *43*, 8-18.

88. Kim, K. B.; Myung, J.; Sin, N.; Crews, C. M. Proteasome inhibition by the natural products epoxomicin and dihydroeponemycin: insights into specificity and potency. *Bioorg Med Chem Lett.,* **1999**, *9*, 3335–3340.

89. Shenk, K. D.; Parlati, F.; Zhou, H.-J.; Sylvain, C.; Smyth, M. S.; Bennet, M. K.; Laidig, G. *J. Compounds for Enzyme Inhibition*. US20070293465, **2007**.

90. de Bruin, G.; Huber, E. M.; Xin, B.-T.; van Rooden, E. J.; Al-Ayed, K.; Kyung-Bo Kim, K.-B.; Kisselev, A. F.; Driessen, C.; van der Stelt, M.; van der Marel, G. A.; Groll, M.; Overkleeft, H. S. Structure-based design of β1i or β5i specific inhibitors of human immunoproteasomes. *J. Med. Chem.*, **2014**, *57*, 6197-6209.

91. Singh, A. V.; Bandi, M.; Aujay, M. A.; Kirk, C. J.; Hark, D. E.; Raje, N.; Chauhan, D.; Anderson, K. C. PR-924, a selective inhibitor of the immunoproteasome subunit LMP-7, blocks multiple myeloma cell growth both in vitro and in vivo. *Br J Haematol*, **2011**, *152*, 155–163.

92. Johnson, HWB.; Lowe, E.; Anderl, JL.; Fan A.; Muchamuel, T.; Bowers, S.; Moebius, DC.; Kirk, C.; McMinn, DL. Required Immunoproteasome Subunit Inhibition Profile for Anti-Inflammatory Efficacy and Clinical Candidate KZR-616((2S,3R)-N-((S)-3-(Cyclopent-1-en-1-yl)-1((R)-2-methyloxiran-2-yl)-1-oxopropan-2-yl)-3-hydroxy-3-(4-methoxyphenyl)-2-((S)-2-(2-morpholinoacetamido)propanamido)propenamide) *J. Med. Chem.* **2018**, *61*, 11127−11143.
93. Jones, G.; Willett, P.; Glen, RC.; Leach, AR.; Taylor, R. Development and validation of a genetic algorithm for flexible docking. *J. Mol. Biol.* **1997**, *267*, 727-748.
94. Schrader, J.; Henneberg, F.; Mata, RA.; Tittmann, K.; Schneider, TR.; Stark, H.; Bourenkov, G.; Chari, A. The inhibition mechanism of human 20S proteasomes enables next-generation inhibitor design. *Science* **2016**, *353*, 594-598.
95. Jeffrey, G. A. An introduction to hydrogen bonding, *Oxford University Press, New York,* **1997**.
96. Meye,r EA.; Castellano, RK.; Diederich, F. Interactions with aromatic rings in chemical and biological recognition. *Angew. Chem. Int. Ed.* **2003**, *42*, 1210–1250.
97. Persch, E.; Dumele, O.; Diederich, F. Molecular recognition in chemical and biological systems. *Angew. Chem. Int. Ed.* **2015**, *54*, 3290–3327.
98. Huber, EM.; Heinemeyer, W.; de Bruin, G.; Overkleeft, HS.; Groll, M. A humanized yeast proteasome identifies unique binding modes of inhibitors for the immunosubunit β5i. *EMBO J.* **2016**, *35*, 2602–2613
99. Verdonk, ML.; Chessari, G.; Cole, JC.; Hartshorn, MJ.; Murray, CW.; Nissink, JW.; Taylor, RD.; Taylor, R. Modeling water molecules in protein-ligand docking using GOLD. *J. Med. Chem.* **2005**, *48*, 6504–6515.
100. Verdonk, ML.; Cole, JC.; Hartshorn, MJ.; Murray, CW.; Taylor RD. Improved protein-ligand docking using GOLD. *Proteins* **2003**, *52*, 609–623.
101. Lonsdale-Eccles, J. D.; Grab, D. J. Trypanosome Hydrolases and the Blood-Brain Barrier. *Trends Parasitol.* **2002**, *18*, 17-19.
102. Rizzoli Larousse "Enciclopedia la biblioteca del sapere" Corriere della sera.

103. Ferguson, M. A. The structure, biosynthesis and functions of glycosylphosphatidylinositol anchors, and the contributions of trypanosome research. *J. Cell Sci.* **1999**, *112*, 2799-2809.
104. Barry, J. D.; McCulloch, R. Antigenic variation in trypanosomes: enhanced phenotypic variation in a eukaryotic parasite. *Adv. Parasitol.* **2001**, *49*, 1-70.
105. Matthews, K. R. The developmental cell biology of Trypanosoma brucei. *J. Cell Sci.* **2005**, *118*, 283-290.
106. https://www.msdmanuals.com/it/professionale/malattie-infettive/protozoi-extraintestinali/tripanosomiasi-africana
107. Turner, C. M. Antigenic variation in Trypanosoma brucei infections: an hostilic view. *J. Cell Sci.* **1999**, *112*, 3187-3192.
108. https://it.the-health-site.com/sleeping-sickness-5053#definizione
109. Büscher, P.; Cecchi, G.; Jamonneau, V.; Priotto, G. Human African trypanosomiasis. *The Lancet.* **2017**, DOI:10.1016/ S0140-6736(17)31510-6
110. https://www.focus.it/scienza/salute/che-cosa-e-la-malattia-del-sonno]
111. I protozoi patogeni per l'uomo In: La Placa M., Principi di Microbiologia Medica, XIII edizione. Bologna: Esculapio; **2012**. 431-479.
112. Brun, R.; Blum, J.; Chappuis, F.; Burri, C. Human african trypanosomiasis. *The Lancet* **2010**, *375*, 148-159.
113. http://www.dndi.org/diseases-projects/diseases/hat/target-product-profile.html.
114. Deborggraeve, S.; Büscher, P. Molecular diagnostics for sleeping sickness: what is the benefit for the patient? *Lancet Infect. Dis.* **2010**, *10*, 433–439.
115. Lemke Thomas L.; Farmaci antiparassitari In: Foye William O. Lemke Thomas L. Williams David A.; *Principi di chimica farmaceutica. V edizione italiana*. Padova: Piccin-Nuova Libraria. **2011**. 1182-1212.
116. Brun, R.; Don, R.; Jacobs, R. T.; Wang, M. Z.; Barrett, M. P. Development of novel drugs for human African trypanosomiasis. *Future Microbiol.* **2011**, *6*, 677-91.
117. Burri, C.; Brun, R. Eflornithine for the treatment of human African trypanosomiasis. *Parasitol. Res.* **2003**, *90* (Suppl. 1), S49-S52.
118. Delespaux, V.; de Koning, H. P. Drugs and drug resistance in African trypanosomiasis. *Drug Resist. Updates* **2007**, *10*, 30−50

119. Kennedy, P. G. Clinical features, diagnosis, and treatment of human African trypanosomiasis (sleeping sickness). *Lancet Neurol.* **2013**, *12*, 186-194.
120. Simarro, P. P.; Franco, J.; Diarra, A.; Postigo, J. A.; Jannin, J. Update on field use of the available drugs for the chemotherapy of human African trypanosomiasis. *Parasitology* **2012**, *139*, 842–46.
121. Coura, J. R.; de Castro, S. L. A critical review of Chagas disease chemotherapy. *Mem. Inst. Oswaldo Cruz* **2002**, *97*, 3−24.
122. Mdachi, R. E.; Thuita, J. K.; Kagira, J. M.; Ngotho, J. M.; Murilla, G. A.; Ndung'u, J. M.; Tidwell, R. R.; Hall, J. E.; Brun, R. Efficacy of the novel diamidine compound 2,5-bis(4-amidinophenyl)-furan-bis-O-methlylamidoxime (pafuramidine, DB289) against Trypanosoma brucei rhodesiense infection in vervet monkeys after oral administration. Antimicrob. *Agents Chemother.* **2009**, *53*, 953−957.
123. Deeks, ED. Fexinidazole: first global approval. *Drugs.* **2019**, *79*(2), 215-220.
124. Cox, F. E. History of sleeping sickness (African trypanosomiasis). *Infect Dis. Clin. N.Am.* **2004**, *18*, 231-245
125. de Koning, H. P.; Gould, M. K.; Sterk, G. J.; Tenor, H.; Kunz, S.; Luginbuehl, E.; Seebeck, T. Pharmacological validation of Trypanosoma brucei phosphodiesterases as novel drug targets. *J. Infect. Dis.* **2012**, *206*, 229-237.
126. Agbo, E. C.; Majiwa, P. A.; Büscher, P.; Claassen, E.; te Pas, M. F. W. Trypanosoma brucei genomics and the challenge of identifying drug and vaccine targets. *Trends Microbiol.* **2003**, *11*, 322-329.
127. Sajid, M.; McKerrow, J. H. Cysteine proteases of parasitic organisms. *Mol. Biochem. Parasitol.* **2002**, *120*, 1-21.
128. Turk, B. Targeting proteases: successes, failures and future prospects. *Nat. Rev. Drug Discovery* **2006**, *5*, 785−799.
129. Kerr, I. D.; Wu, P.; Marion-Tsukamaki, R.; Mackey, Z. B.;Brinen, L. S. Crystal structures of TbCatB and rhodesain, potentialchemotherapeutic targets and major cysteine proteases of Trypanosoma brucei. *PLoS Neglected Trop. Dis.* **2010**, *4*, e701. 23.
130. a) Mackey, Z. B.; O'Brien, T. C.; Greenbaum, D. C.; Blank, R. B.; McKerrow, J. H. A cathepsin B-like protease is required for host protein degradation in Trypanosoma brucei. *J. Biol. Chem.* **2004**, *279*, 48426−48433. b) Abdulla, M. H.;

O'Brien, T.; Mackey, Z. B.; Sajid, M.; Grab, D. J.; McKerrow, J. H. RNA interference of Trypanosoma brucei cathepsin B and L affects disease progression in a mouse model. *PLoS Neglected Trop. Dis.* **2008**, *2*, e298

131. Wheeler, R. J. The trypanolytic factor–mechanism, impacts and applications. *Trends Parasitol.* **2010**, *26*, 457-464
132. Overath, P.; Chaudhri, M.; Steverding, D.; Ziegelbauer, K. Invariant surface proteins in bloodstream forms of Trypanosoma brucei. *Parasitol. Today* **1994**, *10*, 53-58.
133. Kerr, I. D.; Lee, J. H.; Farady, C. J.; Marion, R.; Rickert, M.; Sajid, M.; Pandey, K. C.; Caffrey, C. R.; Legac, J.; Hansell, E.; McKerrow, J. H.; Craik, C. S.; Rosenthal, P. J.; Brinen, L. S. Vinyl sulfones as antiparasitic agents and a structural basis for drug design. *J. Biol. Chem.* **2009**, *284*, 25697−25703.
134. Ettari, R.; Nizi, E.; Di Francesco, M. E.; Dude, M. A.; Pradel, G.; Vicik, R.; Schirmeister, T.; Micale, N.; Grasso, S.; Zappalà, M. Development of Peptidomimetics with a Vinyl Sulfone Warhead as Irreversible Falcipain-2 Inhibitors. *J. Med. Chem.* **2008**, *51*, 988-996.
135. Schirmeister, T.; Kesselring, J.; Jung, S.; Schneider, T. H.; Weickert, A.; Becker, J.; Lee, W.; Bamberger, D.; Wich, P. R.; Distler, U.; Tenzer, S.; Johé, P.; Hellmich, U. A.; Engels, B. Quantum Chemical-Based Protocol for the Rational Design of Covalent Inhibitors. *J. Am. Chem. Soc.***2016**, *138*, 8332–8335.
136. Pandey, K. C.; Wang, S. X.; Sijwali, P. S.; Lau, A. L.; McKerrow, J. H.; Rosenthal, P. J. The Plasmodium falciparum Cysteine Protease Falcipain-2 Captures its Substrate, Haemoglobin, via a Unique Motif. *Proc. Natl. Acad. Sci. U.S.A.* **2005**, *102*, 9138-9143.
137. Morris, G. M.; Huey, R.; Lindstrom, W.; Sanner, M. F.; Belew, R. K.; Goodsell, D. S.; Olson, A. J. Autodock4 and AutoDockTools4: Automated Docking with Selective Receptor Flexibility. *J. Comput. Chem.* **2009**, *16*, 2785-2791.
138. Cosconati, S.; Forli, S.; Perryman, A. L.; Harris, R.; Goodsell, D. S.; Olson, A. J. Virtual Screening with AutoDock: Theory and Practice. *Expert Opin. Drug Discovery* **2010**, *5*, 597-607.

139. Bianco, G.; Forli, S.; Goodsell, D. S.; Olson, A. J. Covalent Docking Using Autodock: Two-Point Attractor and Flexible Side Chain Methods. *Protein Sci.* **2016**, *25*, 295-301.
140. Ahn, D.-S.; Park, S.-W.; Lee, S.; Kim, B. Effects of Substituting Group on the Hydrogen Bonding in Phenol−H_2O Complexes: Ab Initio Study. *J.Phys. Chem. A* **2003**, *107*, 131–139.
141. Schirmeister, T.; Schmitz, J.; Jung, S.; Schmenger, T.; Krauth-Siegel, R. L.; Gütschow, M. Evaluation of Dipeptide Nitriles as Inhibitors of Rhodesain, a Major Cysteine Protease of Trypanosoma brucei. *Bioorg. Med. Chem. Lett.* **2016**, *27*, 45-50.
142. Latorre, A; Schirmeister, T.; Kesselring, J.; Jung, S.; Johé, P.; Hellmich, U. A.; Heilos, A.; Engels, B.;Krauth-Siegel, R. L.; Dirdjaja, N.; Bou-Iserte, L.; Rodríguez, S.; González, F.V. Dipeptidyl Nitroalkenes as Potent Reversible Inhibitors of Cysteine Proteases Rhodesain and Cruzain, *ACS Med. Chem. Lett*. **2016**, *7*, 1073–1076.
143. Tian, W. X.; Tsou, C. L. Determination of the Rate Constant ofEnzyme Modification by Measuring the Substrate Reaction in the Presence of the Modifier. *Biochemistry* **1982**, *21*, 1028−1032.
144. GraFit, version 5.0.1.3; Erithacus Software Ltd.: London, **2006**.
145. Vicik, R.; Hoerr, V.; Glaser, M.; Schultheis, M.; Hansell, E.; McKerrow, J. H.; Holzgrabe, U.; Caffrey, C. R.; Ponte-Sucre, A.; Moll, H.; Stich, A.; Schirmeister, T. Aziridine-2,3-Dicarboxylate Inhibitors Targeting the Major Cysteine Protease of Trypanosoma brucei as Lead Trypanocidal Agents. *Bioorg. Med. Chem. Lett.* **2006**, *16*, 2753–2757.
146. Crouch, S. P.; Kozlowski, R.; Slater, K. J.; Fletcher, J. The Use ofATP Bioluminescence as a Measure of Cell Proliferation and Cytotoxicity. *J. Immunol. Methods* **1993**, *160*, 81−88.
147. Cunningham, M. P.; Vickerman, K. Antigenic Analysis in the Trypanosoma brucei Group, Using the Agglutination Reaction. *Trans.R. Soc. Trop. Med. Hyg.* **1962**, *56*, 48−59.
148. Schrödinger Maestro Release 2018-3, Schrödinger, LLC, New York, NY, **2018**.
149. AutoDock; Molecular Graphics Laboratory: La Jolla, CA, **2013**; http://autodock.scripps.edu/ . (January 13, **2016**).

150. UCSF Chimera: An Extensible Molecular Modeling System; University of California, San Francisco: San Francisco, **2017**; http://www.rbvi.ucsf.edu/chimera/. (September 13, **2016**).
151. https://themmrf.org/multiple-myeloma
152. Gerecke, C.; Fuhrmann, S.; Strifler, S.; Schmidt-Hieber, M.; Einsele, H.; Knop, S. The diagnosis and treatment of multiple myeloma. *Dtsch Arztebl Int*. **2016**, *113*, 470-6.
153. Tacar, O.; Sriamornsak, P.; Dass, CR. Doxorubicin: an update on anticancer molecular action, toxicity and novel drug delivery systems. *J Pharm Pharmacol*. **2013**, *65*, 157-70.
154. Bochet, C. G. Photolabile protecting groups and linkers. *J. Chem. Soc*., *Perkin Trans. 1*, **2002**, 125–142.
155. Hansen, MJ.; Velema, WA.; Lerch, MM.; Szymanski, W.; Feringa, BL. Wavelength-selective cleavage of photoprotecting groups: strategies and applications in dynamic systems. *Chem Soc Rev*. **2015**, *44*, 3358-77.
156. Knall, AC.; Slugovc, C. Inverse electron demand Diels–Alder (iEDDA)-initiated conjugation: a (high) potential click chemistry scheme. *Chem Soc Rev*. **2013**, *42,* 5131-42.
157. Neumann, K.; Jain, S.; Gambardella, A.; Walker, SE.; Valero, E.; Lilienkampf, A.; Bradley, M. Tetrazine-responsive self-immolative linkers. *Chembiochem*. **2017,** *18*, 91-95.
158. de Bruin G.; Xin, BT.; Kraus, M.; van der Stelt, M.; van der Marel, GA.; Kisselev, AF.; Driessen, C.; Florea, BI.; Overkleeft, HS. A set of Activity-Based Probes to visualize human (Immuno)proteasome activities. *Angew Chem Int Ed Engl*. **2016**, *55*, 4199-203.

11. ACKNOWLEDGEMENTS

I would like to thank my supervisor Prof. Maria Zappalà. Her suggestions and extensive medicinal chemistry knowledge helped me constantly, thanks for being caring and professional.

I would like to thank my co-supervisor, Prof. Roberta Ettari, who first encouraged me to pursue the scientific career. Her positivity and her wide expertises were fundamental for me during these three years.

I would like to thank my labmates Carla, Santo and Milad for the time, laughs and coffees spent together.

Thanks to my friends, flatmates and colleagues who believed and supported me in everyday life.

Thanks to my sister Grazia, for all the trips around the world between reactions and work-ups.

Last but not least, I would like to thank my parents, Maria and Sebastiano, who have always supported me and been by my side everyday.

The financial support of "Programma Operativo Fondo Sociale Europeo (FSE) Regione Siciliana 2014–2020 – Asse 3 Ob. 10.5" for the PhD fellowship is gratefully acknowledged.